PhD Thesis

PHOTOACTIVE MATERIALS BASED ON MOLYBDENUM CLUSTER SULFIDES

David Recatalá Ferrandis

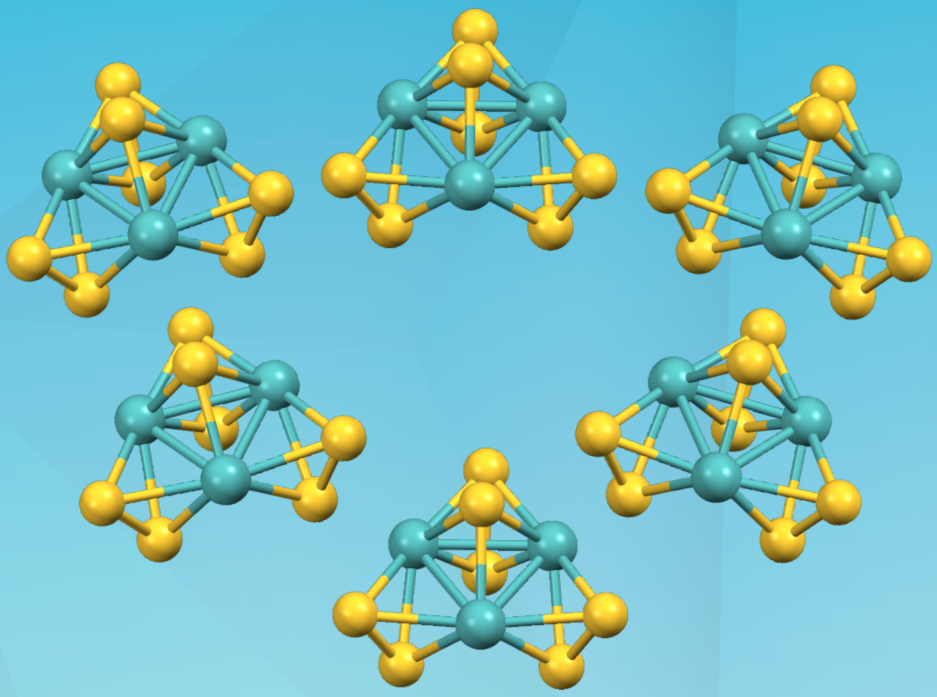

PhD Supervisor

Prof. Rosa Mª Llusar Barelles

CASTELLÓ DE LA PLANA, MAY 2015

UNIVERSITAT JAUME·I

DEPARTAMENT DE QUÍMICA FÍSICA I ANALÍTICA

ÀREA DE QUÍMICA FÍSICA

PHOTOACTIVE MATERIALS BASED ON MOLYBDENUM CLUSTER SULFIDES

David Recatalá Ferrandis

PhD THESIS

Supervised by:

Prof. Rosa Mª Llusar Barelles

CASTELLÓ DE LA PLANA, MAY 2015

ROSA Mª LLUSAR BARELLES, CATEDRÁTICA DEL ÁREA DE QUÍMICA FÍSICA DE LA UNIVERSITAT JAUME I

CERTIFICA: Que David Recatalá Ferrandis, licenciado en Ciencias Químicas por la Universitat Jaume I, ha realizado bajo su dirección, en el área de Química Física de esta universidad, el trabajo titulado: "Photoactive Materials Based on Molybdenum Cluster Sulfides", que constituye su memoria de Tesis Doctoral para optar al grado de Doctor en Ciencias Químicas, y que cumple los requisitos para la obtención de la Mención Internacional.

Y para que conste a los efectos oportunos, firmo el presente certificado en Castellón a 1 de Abril de 2015.

Dra. Rosa Mª Llusar Barelles

Universitat Jaume I
Departament de Química Física i Analítica
Telf.: 964728086, Fax: 964728066
Avda. de Vicent Sos Baynat, s/n
12071 Castelló de la Plana, España

Als meus pares

ABSTRACT

Coordination Chemistry deals with the synthesis and study of the physicochemical properties of metal complexes. Cluster Chemistry is a subfield of Coordination Chemistry, which focuses on the functionalization of complexes in which two or more metal atoms are directly bonded. Over the past few years, Cluster Chemistry has attracted a growing interest among scientists from diverse areas, mainly due to the fascinating properties of these compounds. A historical evolution of the term cluster, as well as an outline of the role of coordinated ligands and structural types in the final properties of metal clusters are provided in Chapter 1.

This PhD Thesis is devoted to the synthesis, characterization and applications of two families of group VI metal clusters containing dithiolene or diimine ligands, as detailed in Chapter 2. The synthetic approaches employed for the preparation of a series of dinuclear $M_2Q_2S_2$ cluster chalcogenides (M = Mo, W; Q = O, or S) bearing bifunctional dithiolene ligands are described in Chapter 3. These metal clusters present great potential for the design of heterometallic systems.

Chapter 4 is concerned with the preparation of an extensive family of mixed-ligand diimine-halide (or diimine-dithiolene) trinuclear molybdenum sulfides based on the Mo_3S_7 core. A great number of bipyridine and phenanthroline derivatives have been coordinated to these Mo_3S_7 units. The most important feature of the resulting cluster complexes of formula $Mo_3S_7X_4$(diimine), where X = Cl, or Br, is their crystallization as $[Mo_3S_7X_4(diimine)\cdot X]^-$ aggregates, in which the sulfur axial atoms participate in non-bonding interactions with halide anions.

The physicochemical properties of both series of metal clusters mentioned above are explored in Chapters 5 and 6. The luminescence properties of bis(dithiolene) $M_2Q_2S_2$ clusters (M = Mo, W; Q = O, or S), together with those of Mo_3S_7 clusters functionalized with imidazophenanthroline ligands are detailed in

Chapter 5. These diimine Mo_3S_7 complexes exhibit luminescent anion sensing behavior. The optical limiting capabilities of both series of compounds, namely $M_2Q_2S_2$- and Mo_3S_7-based clusters, are also described in Chapter 5 with the aim of finding correlations between molecular structures and third-order nonlinear optical functions.

Chapter 6 examines the electro- and photocatalytic activity of diimine Mo_3S_7 clusters immobilized on TiO_2 nanoparticles toward the hydrogen evolution reaction. This study has been stimulated by the analogy between the structure of Mo_3S_7 and the catalytic active sites of MoS_2 nanoparticles. The electrochemical properties of these TiO_2 electrodes are assessed in two different media, that is, aqueous perchloric acid and sulfide-sulfite mixtures. The role of the diimine ligands in the adsorption process is also described in this Chapter.

All experimental procedures employed in this work, together with the characterization of all compounds are presented in Chapter 7. Finally, the general conclusions of this PhD Thesis are provided in Chapter 8.

RESUM (ABSTRACT IN CATALAN)

La Química de Coordinació s'ocupa de la síntesi de complexos metàl·lics, així com de l'estudi de les seues propietats fisicoquímiques. La Química de Clústers és un subcamp de la Química de Coordinació, centrat en la funcionalització de complexos en els quals dos o més àtoms metàl·lics es troben enllaçats directament. En els darrers anys, la Química de Clústers ha tingut un interès creixent entre científics de diverses àrees, degut principalment a les fascinants propietats d'aquests compostos. L'evolució històrica del concepte de clúster, així com el paper que tenen els lligams i les estructures en les propietats finals dels clústers metàl·lics s'esmenten al Capítol 1.

Aquesta Tesi Doctoral s'ocupa de la síntesi, caracterització i aplicacions de dues famílies de clústers metàl·lics del grup VI funcionalitzats amb lligams diimina i ditiolè, tal i com es detalla al Capítol 2. Les estratègies sintètiques utilitzades per a la preparació d'una sèrie de calcogenurs clúster dinuclears de fórmula general $M_2Q_2S_2$ (M = Mo, W; Q = O, ó S), que contenen lligams ditiolè bifuncionals, es descriuen al Capítol 3. Aquests clústers metàl·lics presenten un gran potencial per al disseny de sistemes heterometàl·lics.

El Capítol 4 s'ocupa de la preparació d'una extensa família de sulfurs trinuclears de molibdè basats en el nucli Mo_3S_7 funcionalitzats amb lligams mixtes (diimina-halur o diimina-ditiolè). Un gran nombre de derivats de la bipiridina i de la fenantrolina s'han coordinat a aquestes unitats del tipus Mo_3S_7. La característica més important dels complexos preparats, de fórmula $Mo_3S_7X_4$(diimina), on X = Cl, ó Br, és la seua cristal·lització com a agregats del tipus $[Mo_3S_7X_4(\text{diimina})\cdot X]^-$, en els quals els àtoms de sofre axials participen en interaccions no enllaçants amb anions halur.

Les propietats fisicoquímiques d'ambdues sèries de clústers metàl·lics mencionades anteriorment s'estudien als Capítols 5 i 6. Les propietats luminiscents de clústers del tipus $M_2Q_2S_2(\text{ditiolè})_2$ (M = Mo, W; Q = O, ó S), juntament amb les

de clústers Mo_3S_7 funcionalitzats amb lligams imidazofenantrolina, es detallen al Capítol 5. Aquests complexos Mo_3S_7 amb diimines es comporten com a sensors luminiscents d'anions. La capacitat de limitació òptica de les dues sèries de compostos (clústers $M_2Q_2S_2$ i Mo_3S_7) també es descriu al Capítol 5, amb l'objectiu de trobar correlacions entre estructures moleculars i funcions d'òptica no lineal de tercer ordre.

El Capítol 6 examina el comportament electro- i fotocatalític de clústers Mo_3S_7 amb diimines, immobilitzats sobre TiO_2. Aquest estudi ha estat motivat per l'analogia descrita entre l'estructura del nucli Mo_3S_7 i els llocs catalíticament actius de les nanopartícules de MoS_2. Les propietats electroquímiques d'aquests elèctrodes de TiO_2 s'avaluen en dos medis diferents: àcid perclòric aquós i mescles sulfur-sulfit. El paper dels lligams diimina en el procés d'adsorció també es discuteix en aquest Capítol.

Tots els procediments experimentals emprats en aquest treball, juntament amb la caracterització dels compostos, es presenten al Capítol 7. Finalment, les conclusions generals d'aquesta Tesi Doctoral es troben al Capítol 8.

ABBREVIATIONS

et al.	*et alii* (and others)
vide supra	see above
vide infra	see below
i.e.	*id est* (that is)
ca.	*circa* (approximately)
Me	methyl
Et	ethyl
iPr	isopropyl
Bu	*n*-butyl
Ph	phenyl
PPN	bis(triphenylphosphine)iminium
DMSO	dimethyl sulfoxide
DMF	dimethylformamide
THF	tetrahydrofuran
RT	room temperature
HER	Hydrogen Evolution Reaction
UV/Vis	Ultraviolet/Visible
NMR	Nuclear Magnetic Resonance
XPS	X-ray Photoelectron Spectroscopy
ICPE	Incident Photon to Current Efficiency
ESI-MS	Electrospray Ionization Mass Spectrometry
m/z	mass/charge
IR	infrared
CV	Cyclic Voltammetry
TDDFT	Time-Dependent Density Functional Theory
ORTEP	Oak Ridge Thermal Ellipsoid Plot

ADP	Atom Displacement Parameters
GooF	Goodness of Fit
calcd.	calculated
CB	Conduction Band
VB	Valence Band
HOMO	Highest Occupied Molecular Orbital
LUMO	Lowest Unoccupied Molecular Orbital
MLCT	Metal to Ligand Charge Transfer
LMCT	Ligand to Metal Charge Transfer
ILCT	Intraligand Charge Transfer
met	*cis*-1,2-dicarbomethoxyethylene-1,2-dithiolate
Cl_2bdt	3,6-dichloro-1,2-benzenedithiolate
$BPyDTS_2$	2-bis-(2-pyridyl)methylene-1,3-dithiolene
pdt	2,3-pyrazinedithiolate
dmit	1,3-dithiole-2-thione-4,5-dithiolate
dtc	diethyldithiocarbamate
bpy	2,2'-bipyridine
dmbpy	4,4'-dimethyl-2,2'-bipyridine
dnbpy	4,4'-dinonyl-2,2'-bipyridine
dcbpy	2,2'-bipyridine-4,4'-dicarboxylic acid
dcmbpy	4,4'-dicarbomethoxy-2,2'-bipyridine
phen	1,10-phenanthroline
mphen	4-methyl-1,10-phenanthroline
dmphen	5,6-dimethyl-1,10-phenanthroline
tmphen	3,4,7,8-tetramethyl-1,10-phenanthroline
BPhen	4,7-diphenyl-1,10-phenanthroline
ppl	Pyrazino[2,3-f][1,10]phenanthroline
IPDOP	1H-Imidazo[4,5-f][1,10]phenanthroline-2-[3,4-bis(dodecyloxy)phenyl]

CONTENTS

Chapter 1. General Introduction **1**

1.1. An overview of metal clusters 3

1.2. Tuning the properties of molecular clusters 8

1.3. Dinuclear and trinuclear group VI clusters 10

1.4. References 12

Chapter 2. Objectives **17**

Chapter 3. Dinuclear and Trinuclear Molybdenum and Tungsten Cluster Complexes Containing Dithiolene Ligands **21**

3.1. Introduction 23

3.1.1. Dithiolene ligands containing nitrogen groups 23

3.1.2. Heterometallic structures based on bifunctional dithiolene ligands 25

3.1.3. Approach to the design of heterometallic molybdenum and tungsten dithiolene cluster complexes 30

3.2. Results and discussion 34

3.2.1. Synthesis and characterization 34

3.2.2. Reactivity of bis(dithiolene) dinuclear cluster complexes towards other metals 43

3.2.3. Crystal structure description 47

3.2.3.1. Bis(dithiolene) molybdenum and tungsten clusters 47

3.2.3.2. Tris(dithiolene) molybdenum clusters 50

3.3. Conclusions 53

3.4. References 54

Chapter 4. Heteroleptic Trinuclear Molybdenum Cluster Complexes Containing Diimine Ligands **59**

4.1. Introduction 61

4.1.1. Aplications of complexes containing diimine ligands 61

4.1.2. Non-bonding interactions in trinuclear molybdenum clusters 64

4.1.3. Heteroleptic trinuclear molybdenum clusters 69

4.2. Results and discussion 73
4.2.1. Synthesis and characterization 73
4.2.2. Reactivity of trinuclear diimine complexes towards sulfur donor ligands 86
4.2.3. Crystal structure description 90
4.3. Conclusions 98
4.4. References 99
Chapter 5. Optical Properties of Molybdenum Cluster Chalcogenides 105
5.1. Luminescence properties of dinuclear molybdenum clusters 107
5.1.1. Introduction 107
5.1.2. Results and discussion 110
5.2. Luminescence and anion sensing behavior of trinuclear molybdenum clusters 117
5.2.1. Introduction 117
5.2.2. Results and discussion 121
5.3. Optical nonlinearities of heteroleptic trinuclear molybdenum clusters 127
5.3.1. Introduction 127
5.3.2. Results and discussion 130
5.4. Conclusions 134
5.5. References 136
Chapter 6. Light-Driven Hydrogen Generation from Water Using Trinuclear Molybdenum Clusters 143
6.1. Introduction 145
6.2. Results and discussion 150
6.2.1. Spectroscopic and electrochemical studies 151
6.2.2. Photocatalytic behavior 160
6.3. Conclusions 163
6.4. References 164

Chapter 7. Experimental **169**

7.1. Synthesis and characterization 171

7.1.1. General procedures 171

7.1.2. Starting materials 172

7.1.2.1. Molecular clusters 172

7.1.2.2. Ligands 174

7.1.2.3. Bis(dithiolene) zinc and tin complexes 181

7.1.3. Dinuclear bis(dithiolene) molybdenum and tungsten clusters 184

7.1.4. Trinuclar tris(dithiolene) molybdenum clusters 192

7.1.5. Heteroleptic molybdenum clusters containing diimine ligands 194

7.1.6. Heteroleptic molybdenum clusters with diimine and sulfur donor ligands 205

7.2. Structural determination 209

7.2.1. General remarks 209

7.2.2. Structure of bis(dithiolene) molybdenum and tungsten clusters 211

7.2.2.1. Structure of $(Et_4N)_2[Mo_2O_2S_2(BPyDTS_2)_2]$, $((Et_4N)_2[4])$ 211

7.2.2.2. Structure of $(PPN)_2[Mo_2S_4(pdt)_2]$, $((PPN)_2[6])$ 215

7.2.2.3. Structure of $(Et_4N)_2[Mo_2O_2S_2(pdt)_2]$, $((Et_4N)_2[7])$ 219

7.2.2.4. Structure of $(PPN)_2[W_2S_4(pdt)_2]$, $((PPN)_2[8])$ 223

7.2.2.5. Structure of $(PPN)_2[W_2O_2S_2(pdt)_2]$, $((PPN)_2[9])$ 227

7.2.3. Structure of tris(dithiolene) molybdenum clusters 231

7.2.3.1. Structure of $(PPN)_2[Mo_3S_7(met)_3]$, $((PPN)_2[10])$ 231

7.2.3.2. Structure of $(Bu_4N)_2[Mo_3S_7(Cl_2bdt)_3]$, $((Bu_4N)_2[11])$ 237

7.2.4. Structure of heteroleptic molybdenum clusters containing diimine ligands 243

7.2.4.1. Structure of $(Bu_4N)[Mo_3S_7Br_4(BPhen)\cdot Br]$, $(Bu_4N)[14\cdot Br]$ 243

7.2.4.2. Structure of $(Bu_4N)[Mo_3S_7Cl_4(BPhen)\cdot Cl]$, $(Bu_4N)[15\cdot Cl]$ 249

7.2.4.3. Structure of $(Bu_4N)[Mo_3S_7Br_4(tmphen)\cdot Br]$, $(Bu_4N)[16\cdot Br]$ 255

7.2.4.4. Structure of $(Bu_4N)[Mo_3S_7Cl_4(tmphen)\cdot Cl]$, $(Bu_4N)[17\cdot Cl]$ 261

7.2.4.5. Structure of $(Bu_4N)[Mo_3S_7Cl_4(dmbpy)\cdot Cl]$, $(Bu_4N)[18\cdot Cl]$ 267
7.2.4.6. Structure of $(Bu_4N)[Mo_3S_7Br_4(dmbpy)\cdot Br]$, $(Bu_4N)[19\cdot Br]$ 273
7.2.4.7. structure of $(Bu_4N)[Mo_3S_7Br_4(bpy)\cdot Br]$, $(Bu_4N)[20\cdot Br]$ 279
7.2.4.8. Structure of $(Bu_4N)[Mo_3S_7Br_4(phen)\cdot Br]$, $(Bu_4N)[21\cdot Br]$ 285
7.2.4.9. Structure of $(Bu_4N)[Mo_3S_7Br_4(dcmbpy)\cdot Br]$, $(Bu_4N)[22\cdot Br]$ 291
7.2.4.10. Structure of $(Bu_4N)[Mo_3S_7Br_4(dcmphen)\cdot Br]$, $(Bu_4N)[24\cdot Br]$ 297
7.2.4.11. Structure of $(Bu_4N)[Mo_3S_7Cl_4(ppl)\cdot Cl]$, $(Bu_4N)[25\cdot Cl]$ 303
7.2.4.12. Structure of $(Bu_4N)[Mo_3S_7Cl_4(mphen)\cdot Cl]$, $(Bu_4N)[27\cdot Cl]$ 309
7.2.4.13. Structure of $(Bu_4N)[Mo_3S_7Br_4((CO_2Me)ppl)\cdot Br]$, $(Bu_4N)[28\cdot Br]$ 315
7.2.5. Structure of heteroleptic molybdenum clusters with diimine and sulfur donor ligands 321
7.2.5.1. Structure of $[Mo_3S_7(dmphen)(dtc)_2\cdot Br](PF_6)$, $([32\cdot Br](PF_6))$ 321
7.2.6. Structure of dialkyltin dithiolene complexes 327
7.2.6.1. Structure of $Me_2Sn(BPyDTS_2)$, (3) 327
7.3. Photophysical studies 331
7.3.1. Luminescent properties 331
7.3.2. Optical limiting behavior 332
7.3.3. Photocatalysis 333
7.3.4. Theoretical calculations 334
7.4. References 335
Chapter 8. Concluding Remarks **339**
Chapter 9. Publications **349**

1

GENERAL INTRODUCTION

"Nature uses only the longest threads to weave her patterns, so each small piece of her fabric reveals the organization of the entire tapestry."

Richard P. Feynman, *The Character of Physical Law*

1.1. AN OVERVIEW OF METAL CLUSTERS

The 50th anniversary of metal clusters was celebrated in 2014, coinciding with the 100th anniversary of Crystallography. The term "metal atom cluster" was first introduced by Cotton in 1964 to designate interactions between metal atoms. As the original paper reads:[1] "The term cluster seems an appropriate one for a finite group of metal atoms which are held together mainly, or at least to a significant extent, by bonds directly between the metal atoms, even though some nonmetal atoms may also be intimately associated with the cluster." This definition was broadened two years later "to include compounds in which the metal atoms are held together entirely by metal-metal bonds".[2] At the time when this definition was provided, only a few examples of clusters had been reported. However, research in this field has grown exponentially over the past decades, mainly stimulated by the development of X-ray crystallography, which allowed a profound insight into cluster chemistry.

Metal clusters have become attractive research targets in the fields of Coordination and Organometallic Chemistry, due to the fascinating electronic structures and physicochemical properties that can result upon functionalization of cluster cores with diverse ligands. Some examples of these properties include luminescence,[3] optical nonlinearities,[4] magnetism[5] or electrical conductivity.[6] Another noteworthy aspect of cluster chemistry is that an extremely large number of metal-metal bonds can be envisioned upon combination of transition metals, thus resulting in a wide range of structural types for these compounds.[7]

The first example of a metal cluster dates back to 1985 when C. Bloomstrand discovered a molybdenum compound which was supposed to contain two different types of halogen, since addition of silver ion only afforded the precipitation of one third of the halides present in that compound.[8] That observation led to postulate more than fifty years later that the molybdenum atoms would presumably be joined

together by bridging halide ligands. A $[Mo_3X_4]X_2$ formula (X = Cl, Br) was then proposed to explain the unusual behavior of that system.

Hexanuclear clusters of formula $[M_6X_{12}]X_2$ (M = Nb, Ta; X = Cl, or Br) were reported at the beginning of the twentieth century. These compounds were followed by molybdenum clusters based on octahedral Mo_6Cl_8 cores in which the metal atoms define the vertices of an octahedron, and each triangular face is capped with a μ_3-Cl atom. The first sixty decades of the 20th century have witnessed the advent of metal carbonyl clusters, being the trinuclear $Fe_3(CO)_{12}$ the first reported complex of this type. This trimetallic cluster was followed by the tetrametallic $Co_4(CO)_{12}$ and the hexametallic $Rh_6(CO)_{16}$ clusters. Finally, the triangular $[Re_3Cl_{12}]^{2-}$ cluster (Figure 1.1), which was reported in the 1960s coinciding with the coinage of the term cluster, is the first example of multiple bonds between metal atoms.[9,10]

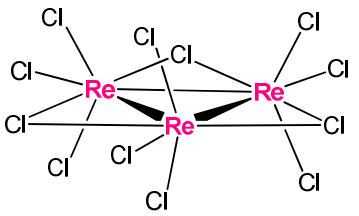

Figure 1.1. Structure of the $[Re_3Cl_{12}]^{2-}$ anion.

A large number of cluster compounds of different structural types have emerged since the term cluster was introduced. Although an exhaustive classification of them is not straightforward, molecular clusters can be classified into two major groups according to the nature of their constituent atoms, namely main-group elements clusters and transition metal clusters.[11] The former group encompasses clusters with elements from either the *s*- or the *p*- block, whereas the latter group is based on *d*-block metals. In this introduction we will focus on transition metal clusters, as they are more relevant to the topic of the present Thesis.

Two different types of transition metal clusters are known: electron-rich and electron-poor, also known as π-donor and π-acceptor, respectively. Electron-rich clusters contain early transition metals in low to medium oxidation states (generally, +2, +3, or +4) bound to π-donor ligands, such as halides, oxides or chalcogenides. Some examples of them include trinuclear M_3 (M = Mo, W, Re or Nb), or hexanuclear M_6 (M = Mo, Nb, Re), clusters featuring triangular or octahedral structures, such as those observed in Re_3Cl_9 and Mo_6Cl_8 cores, respectively. In contrast, electron-poor clusters are mainly based on late transition metals in very low (close to zero) oxidation states, which contain π-acceptor ligands (most commonly carbonyl, but also nitrosyl, phosphine, and others). These clusters form polyhedral structures with triangular faces, in which the metals occupy the vertices of the polyhedrons. The triangular $M_3(CO)_{12}$, (M = Ru, Os), and the tetrahedral $M_4(CO)_{12}$, (M = Co, Rh or Ir), metal carbonyls are representative examples of them (see Figure 1.2).[12,13]

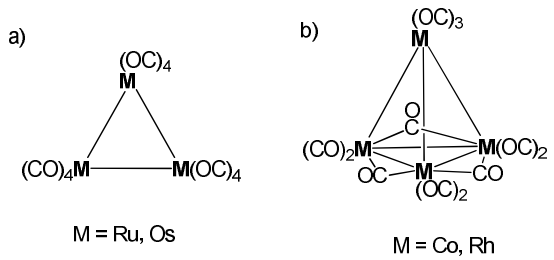

Figure 1.2. Structure of triangular $M_3(CO)_{12}$ (a) and tetrahedral $M_4(CO)_{12}$ (b) metal carbonyl clusters.

A combination of main group elements and transition metals is feasible in cluster chemistry. In particular, carbon and nitrogen have been incorporated into late transition metal clusters. This is exemplified in $RCCo_3(CO)_9$, (R = H, CH_3, C_6H_5, among others), wherein the carbon and cobalt atoms define a tetrahedral cluster.[14] Combining different metal atoms results in the formation of heterometallic bonds. For instance, the metal cluster $CuAg_3\{MoCp(CO)_3\}_4$ presents d^{10} - d^{10} heterometallic

interactions between its constituent atoms.[15] As shown in Figure 1.3, its peculiar structure contains a central square metal core formed by three silver(I) and one copper(I) ions in which each edge of the metal core is bridged by a $MoCp(CO)_3$ fragment.

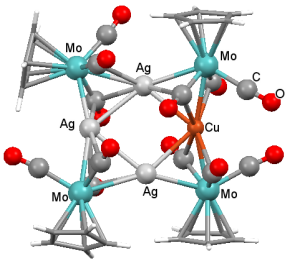

Figure 1.3. Crystal structure of the cluster complex $CuAg_3\{MoCp(CO)_3\}_4$.

Large clusters containing close-packed metal atoms have been gaining attention over the past decades. In this context, the mixed nickel-platinum cluster of formula $[Pd_{33}Ni_9(CO)_{41}(PPh_3)_6]^{4-}$ (see Figure 1.4) is notable for its large heterometallic $Pd_{33}Ni_9$ core bearing both carbonyl and triphenylphosphine ligands.[16] In this metal cluster, triphenylphosphine is bound to nickel, while the carbonyl ligands are coordinated to both nickel and palladium ions.

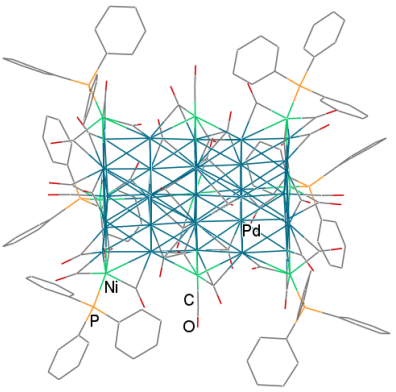

Figure 1.4. Crystal structure of the $[Pd_{33}Ni_9(CO)_{41}(PPh_3)_6]^{4-}$ anion.

Metal-metal bonding is not only restricted to molecular species. Bonds between metals have also been observed in solid state inorganic compounds, such as in Chevrel-type phases of formula $M_xMo_6Q_8$, were x can range from 1 to 4, M is a transition metal, and Q is a chalcogen (S, Se or Te).[17] These compounds have attracted a great deal of attention owing to their interesting structures and high-temperature superconductivity. In their crystal structure (see Figure 1.5), eight chalcogen atoms form a cube, and the six molybdenum atoms nearly occupy the center of its faces. This Mo_6Q_8 unit is inscribed in a larger cube defined by the heterometal atoms (M).

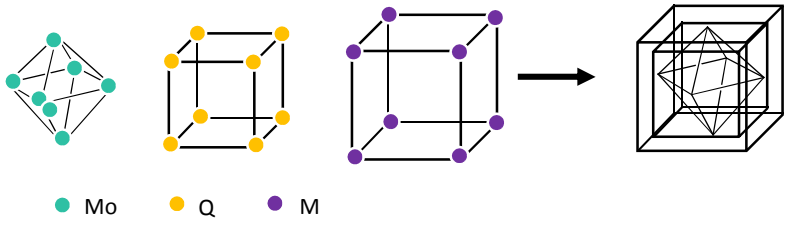

Figure 1.5. Schematic representation of a $M_xMo_6Q_8$ Chevrel phase (M = transition metal; x = 1 – 4; Q = S, Se, or Te). In the latter figure, the atoms in the vertices have been omitted for clarity.

The major classes of metal clusters have been presented herein, together with the most accepted definition of the term cluster, and a historic evolution of these compounds. The role of the outer ligands and structural types in the properties of molecular clusters will be discussed in the following sections. This discussion will be focused on dinuclear and trinuclear molybdenum cluster chalcogenides, as they are the cornerstone of this PhD thesis.

1.2. TUNING THE PROPERTIES OF MOLECULAR CLUSTERS

Transition metal complexes can be conveniently functionalized with a variety of ligands, with the aim of affording molecular materials with a number of properties and applications.[18–21] Metal cluster compounds offer more diversity of structural types than mononuclear complexes owing to the immense number of chemical bonds that can be envisioned upon combination of the existent transition metals. Furthermore, apart from the intrinsic properties that can emerge from intermetallic interactions in cluster units, their properties can still be tailored to meet the requirements of specific applications by means of ligands. In other words, the physicochemical properties of inorganic cluster compounds can be easily tuned by modification of the cluster core and outer ligands. For these reasons, cluster chemistry has engaged the interest not only of synthetic chemists, but also of scientists from other areas, such as medicine,[22] catalysis[23,24] and materials science.[25] Therefore, today a diversity of cluster complexes bearing different ligands, and either homometallic or heterometallic interactions can be found in the literature.[13,26]

Metal-metal interactions have been reported to confer intriguing photophysical properties to cluster complexes.[7] Incidentally, d^8 and d^{10} cluster compounds are frequently luminescent, being the emission dependent on the nature of the metals, ligands and their structural features.[27] However, luminescence properties in clusters is not only restricted to d^8 and d^{10} complexes. Octahedral molybdenum clusters of general formula $[Mo_6X_8Y_6]^n$, where X is an inner ligand (Cl, Br or I) and Y an outer ligand, have led to molecular materials exhibiting luminescence in both the visible and near-infrared regions, with high emission quantum yields and lifetimes.[28] The structure of the aforementioned octahedral clusters is illustrated in Figure 1.6 for the $[Mo_6I_8(OOCC_3F_7)_6]^{2-}$ cluster anion. In order to outline the role that ligand functionalization plays in cluster complexes, it is worth mentioning that the luminescence quantum yield of cluster

$(Bu_4N)_2[Mo_6I_8(OOCC_3F_7)_6]$ decreases from *ca.* 0.60 to a value of less than 0.01 upon replacement of iodide by chloride in its inner ligands.[29]

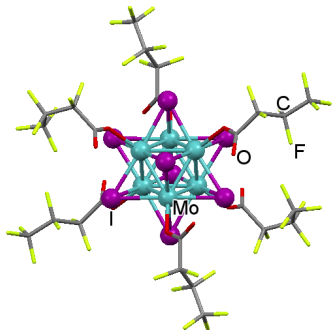

Figure 1.6. Structure of the $[Mo_6I_8(OOCC_3F_7)_6]^{2-}$ cluster anion.

Synthetic transition metal complexes containing sulfur are well-known to mimic the chemical behavior of certain biological systems.[30] In particular, redox-active iron-sulfur clusters of diverse nuclearities (typically, Fe_2S_2, Fe_3S_4 and Fe_4S_4) functionalized with alkylthiol or related ligands have been used as models for the active sites of a diverse family of metalloproteins which play essential roles in living organisms, such as in electron transfer chains, photosynthesis and nitrogen fixation.[31] Some examples of synthetic analogues of protein sites containing two, three and four iron atoms are depicted in Figure 1.7. The electronic and magnetic properties of these Fe-S systems have also been investigated in the past few decades.[32]

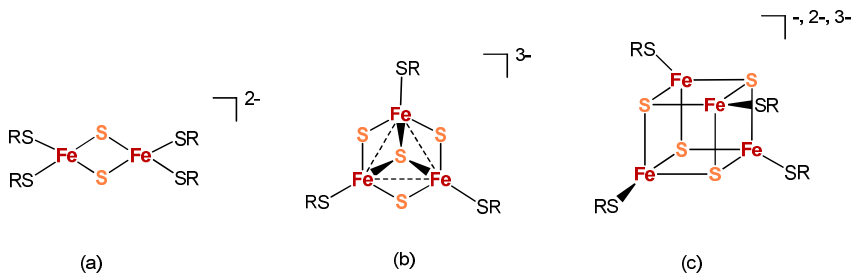

Figure 1.7. Iron cluster complexes which mimic protein sites containing two (a), three (b), and four (c) iron atoms. In all cases, R = methyl, ethyl, phenyl, or related groups.

1.3. DINUCLEAR AND TRINUCLEAR GROUP VI CLUSTERS

The research of the Molecular Materials group at Jaume I University is focused on the functionalization of dinuclear and trinuclear molybdenum and tungsten clusters with diverse ligands, with the aim of tuning the properties of the metal cores.[33–35] More specifically, dinuclear $M_2O_2(\mu\text{-}Q)_2$, and trinuclear $M_3(\mu_3\text{-}Q)(\mu\text{-}Q_2)_3$ and $M_3(\mu_3\text{-}Q)(\mu\text{-}Q)_3$ clusters, where M = Mo, or W, and Q = S, or Se, have attracted a wide interest in our group over the last few decades.

A family of bis(dithiolene) $Mo_2O_2(\mu\text{-}Q)_2$-based clusters (Q = S, Se) was prepared by simple ligand substitution in the $[Mo_2O_2S_2(DMF)_6]^{2+}$ cation.[36] The structure of the $M_2O_2(\mu\text{-}Q)_2$ core is depicted in Figure 1.8a. Their tungsten counterparts were prepared by treating the $\{W_3S_7Br_4\}_n$ polymeric phases with triphenylphosphine in the presence of oxygen and a dithiolene source.

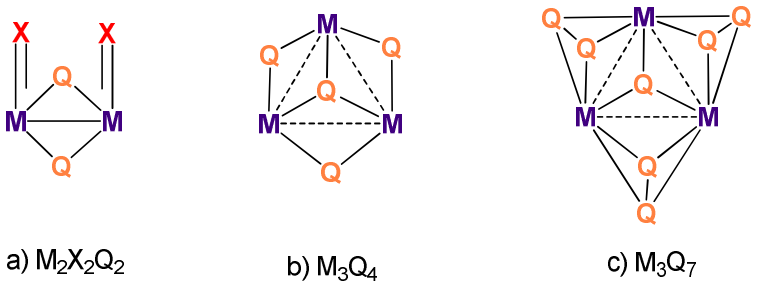

Figure 1.8. Structure of dinuclear and trinuclear group VI cluster chalcogenides (M = Mo, or W; X = O, or S; Q = S, or Se)

Much more attention was devoted to the functionalization of the triangular $M_3(\mu_3\text{-}Q)(\mu\text{-}Q)_3$ and $M_3(\mu_3\text{-}Q)(\mu\text{-}Q_2)_3$ cluster cores (M = Mo, W; Q = S, Se), their structures being depicted in Figures 1.8b and 1.8c, respectively. The difference between both cores arises from the nature of their brigding ligands: dichalcogenides ($\mu\text{-}Q_2$) *vs* chalcogenides ($\mu\text{-}Q$).[35] The M_3Q_4 core can be conveniently prepared by excision of $\{M_3Q_7X_4\}_x$ (X = Cl, Br) polymeric phases with diphosphine under

nitrogen atmosphere.[33] The resulting $[M_3Q_4X_3(diphosphine)_3]^+$ clusters were used for the synthesis of heterometallic $M_3M'Q_4$ cubane-like complexes, where M' is a heterometal (Cu, Co, and others).[37] These M_3Q_4 and $M_3M'Q_4$ compounds found applications in catalysis[38,39] and nonlinear optics.[40,41]

Regarding the M_3Q_7 core, a number of Mo_3S_7-based complexes were prepared in our group by ligand substitution in the $[Mo_3S_7X_6]^{2-}$ cluster anion, where X = Cl, or Br.[42] The functionalization of these Mo_3S_7 clusters with dithiolene ligands afforded a series of tris(dithiolene) molybdenum clusters with interesting redox, conducting and magnetic properties.[43,44] The use of a diversity of ligands, such as oxalate and thiocyanate afforded trinuclear molybdenum cluster sulfides with promising optical limiting capabilities.[45]

In the present PhD thesis, we have focused on the functionalization of the triangular Mo_3S_7 cluster unit with diimine ligands. The optical properties of the resulting compounds have been investigated, as well as their catalytic activity in the visible-light driven water splitting. The dinuclear $M_2Q_2(\mu\text{-}S)_2$ core (M = Mo, W; Q = O, or S) has been functionalized with dithiolene ligands bearing two coordination poles (S and N), aimed at the preparation of heterometallic complexes with luminescent properties. Further details about the objectives of this work will be provided in the following Chapter.

1.4. REFERENCES

(1) Cotton, F. A. *Inorg. Chem.* **1964**, *3*, 1217–1220.

(2) Cotton, F. A. *Q. Rev. Chem. Soc.* **1966**, *20*, 389.

(3) Goswami, N.; Baksi, A.; Giri, A.; Xavier, P. L.; Basu, G.; Pradeep, T.; Pal, S. K. *Nanoscale* **2014**, *6*, 1848–1854.

(4) Humphrey, M. G.; Schwich, T.; West, P. J.; Cifuentes, M. P.; Samoc, M. In *Comprehensive Inorganic Chemistry II*; Elsevier, 2013; pp. 781–835.

(5) Tirfoin, R.; Chamoreau, L.-M.; Li, Y.; Fleury, B.; Lisnard, L.; Journaux, Y. *Dalt. Trans.* **2014**, *43*, 16805–16817.

(6) Tabookht, Z.; Lõpez, X.; De Graaf, C.; Guihéry, N.; Suaud, N.; Benamor, N. *J. Comput. Chem.* **2012**, *33*, 1748–1761.

(7) Sculfort, S.; Braunstein, P. *Chem. Soc. Rev.* **2011**, *40*, 2741–2760.

(8) Blomstrand, C. W. *J. für Prakt. Chemie* **1857**, *71*, 449–471.

(9) Cotton, F. A.; Richard A. Walton. In *Multiple Bonds Between Metal Atoms*; Oxford University Press, 1993; pp. 1–26.

(10) Cotton, F. A. In *Metal Clusters in Chemistry*; P. Braunstein, L. A. Oro, P. R. R., Ed.; Wiley-VCH, 1999; Vol. 1, pp. 3–7.

(11) Michael, D.; Mingos, P. *Introduction to Cluster Chemistry*; Prentice-Hall, Inc., 1990.

(12) Michael, D.; Mingos, P.; Andrew S. May. In *The Chemistry of Metal Cluster Complexes*; Shriver, D. F.; Kaesz, H. D.; Adams, R. D., Eds.; VCH Publishers, Inc., 1990; pp. 11–114.

(13) Joan Ribas Gispert. In *Coordination Chemistry*; Wiley-VCH, Ed.; 2008; pp. 163–194.

(14) Miller, D. C.; Brill, T. B. *Inorg. Chem.* **1978**, *17*, 240–244.

(15) Sculfort, S.; Welter, R.; Braunstein, P. *Inorg. Chem.* **2010**, *49*, 2372–2382.

(16) Kawano, M.; Bacon, J. W.; Campana, C. F.; Dahl, L. F. *J. Am. Chem. Soc.* **1996**, *118*, 7869–7870.

(17) Burdett, J.; Lin, J. *Inorg. Chem.* **1982**, *21*, 5–10.

(18) Zhang, L.; Li, S.-Q.; Meng, X.-J.; Liao, D.-Z.; Jiang, Z.-H.; Wang, G.-L.; Shen, P.-W.; Zhao, Q.-H. *Transit. Met. Chem.* **1999**, *24*, 247–249.

(19) Zhu, H.-L.; Tong, Y.-X.; Chen, X.-M.; Ren, C.-X. *Transit. Met. Chem.* **2001**, *26*, 528–531.

(20) Yam, V. W.-W.; Ko, C.-C.; Zhu, N. *J. Am. Chem. Soc.* **2004**, *126*, 12734–12735.

(21) Eisenberg, R.; Gray, H. B. *Inorg. Chem.* **2011**, *50*, 9741–9751.

(22) Lin, X.; Zhang, Q.; Chen, J.; Kong, X.; Long, L.-S.; Wang, C.; Lin, W. *RSC Adv.* **2015**, *5*, 2914–2919.

(23) Buchwalter, P.; Rosé, J.; Braunstein, P. *Chem. Rev.* **2015**, *115*, 28–126.

(24) Puddephatt, R. J. In *Metal Clusters in Chemistry*; Braunstein, P.; Oro, L. A.; Raithby, P. R., Eds.; Wiley-VCH, 1999; pp. 603–613.

(25) Claridge, S. A.; Castleman, A. W.; Khanna, S. N.; Murray, C. B.; Sen, A.; Weiss, P. S. *ACS Nano* **2009**, *3*, 244–255.

(26) *Metal Clusters in Chemistry*; Braunstein, P.; Oro, L. A.; Raithby, P. R., Eds.; Wiley-VCH, 1999.

(27) Chen, Z. N.; Zhao, N.; Fan, Y.; Ni, J. *Coord. Chem. Rev.* **2009**, *253*, 1–20.

(28) Efremova, O. A.; Shestopalov, M. A.; Chirtsova, N. A.; Smolentsev, A. I.; Mironov, Y. V; Kitamura, N.; Brylev, K. A.; Sutherland, A. J. *Dalton Trans.* **2014**, *43*, 6021–6025.

(29) Sokolov, M. N.; Mihailov, M. A.; Peresypkina, E. V; Brylev, K. A.; Kitamura, N.; Fedin, V. P. *Dalton Trans.* **2011**, *40*, 6375–6377.

(30) *Transition Metal Sulfur Chemistry: Biological and Industrial Significance*; Stiefel, E. I.; Matsumoto, K., Eds.; ACS Symposium Series, 1996.

(31) Rao, P. V.; Rao, P. V.; Holm, R.; Holm, R. *Chem. Rev* **2004**, *104*, 527–560.

(32) Mouesca, J.; Lamotte, B. *Coord. Chem. Rev.* **1998**, *178-180*, 1573–1614.

(33) Shibahara, T. *Coord. Chem. Rev.* **1993**, *123*, 73–147.

(34) Llusar, R.; Uriel, S. *Eur. J. Inorg. Chem.* **2003**, *2003*, 1271–1290.

(35) Llusar, R.; Vicent, C. In *Inorganic Chemistry in Focus III*; G. Meyer, D. Naumann, L. W., Ed.; Wiley-VCH, 2006.

(36) Llusar, R.; Triguero, S.; Vicent, C.; Sokolov, M. N.; Domercq, B.; Fourmigué, M. *Inorg. Chem.* **2005**, *44*, 8937–8946.

(37) Feliz, M.; Llusar, R.; Uriel, S.; Vicent, C.; Coronado, E.; Gómez-García, C. J. *Chem. - A Eur. J.* **2004**, *10*, 4308–4314.

(38) Beltrán, T. F.; Feliz, M.; Llusar, R.; Mata, J. A.; Safont., V. S. *Organometallics* **2011**, *30*, 290–297.

(39) Sorribes, I.; Wienhöfer, G.; Vicent, C.; Junge, K.; Llusar, R.; Beller, M. *Angew. Chem. Int. Ed. Engl.* **2012**, *51*, 7794–7798.

(40) Feliz, M.; Garriga, J. M.; Llusar, R.; Uriel, S.; Humphrey, M. G.; Lucas, N. T.; Samoc, M.; Luther-Davies, B. *Inorg. Chem.* **2001**, *40*, 6132–6138.

(41) Feliz, M.; Llusar, R.; Uriel, S.; Vicent, C.; Humphrey, M. G.; Lucas, N. T.; Samoc, M.; Luther-Davies, B. *Inorganica Chim. Acta* **2003**, *349*, 69–77.

(42) Llusar, R.; Vicent, C. *Coord. Chem. Rev.* **2010**, *254*, 1534–1548.

(43) Llusar, R.; Uriel, S.; Vicent, C.; Clemente-Juan, J. M.; Coronado, E.; Gómez-García, C. J.; Braïda, B.; Canadell, E. *J. Am. Chem. Soc.* **2004**, *126*, 12076–12083.

(44) Llusar, R.; Triguero, S.; Polo, V.; Vicent, C.; Gómez-García, C. J.; Jeannin, O.; Fourmigué, M. *Inorg. Chem.* **2008**, *47*, 9400–9409.

(45) Garriga, J. M.; Llusar, R.; Uriel, S.; Vicent, C.; Usher, A. J.; Lucas, N. T.; Humphrey, M. G.; Samoc, M. *Dalt. Trans.* **2003**, 4546–4551.

2

OBJECTIVES

"I would like to live about three hundred years. I think I have ideas enough to keep me busy that long."

Thomas A. Edison

Cluster chemistry has arisen a great deal of interest among the scientific community, mainly due to the structural diversity and physicochemical properties of these compounds. This PhD thesis is devoted to the functionalization of molybdenum and tungsten clusters with different ligands, with the aim of tailoring their properties to specific applications. A large variety of ligands can be coordinated to cluster units. Among them, we have focused on diimines and dithiolenes. This choice of ligands has been stimulated by their non-innocent character, which results in transition metal complexes with fascinating properties. The specific objectives of this work are detailed herein:

1) Preparation of a series of $M_2Q_2(\mu\text{-}S)_2$-based dinuclear clusters, where M = Mo, or W, and Q = O, or S, functionalized with dithiolene ligands possessing two coordination poles with different chemical nature; sulfur and nitrogen.
2) Exploration of the reactivity of bis(dithiolene) dinuclear molybdenum and tungsten clusters toward other metals, with a view to the preparation of discrete and polymeric heterometallic compounds.
3) Synthesis and structural characterization of a family of triangular mixed-ligand diimine-halide $Mo_3(\mu_3\text{-}S)(\mu\text{-}S_2)_3$ clusters, and study of their reactivity toward sulfur donor ligands.
4) Study of the luminescence properties of bis(dithiolene) $Mo_2O_2S_2$ complexes, and also those of mixed-ligand diimine-halide Mo_3S_7 clusters.
5) Assessment of the optical limiting performance of homoleptic $Mo_2O_2S_2$ clusters containing dithiolene ligands, as well as that of heteroleptic Mo_3S_7 complexes functionalized with diimine ligands together with halides, or dithiolenes.
6) Immobilization of heteroleptic diimine-halide Mo_3S_7 clusters on TiO_2 nanoparticles, and investigation of their electro- and photocatalytic activity toward the hydrogen evolution reaction.

3

DINUCLEAR AND TRINUCLEAR MOLYBDENUM AND TUNGSTEN CLUSTER COMPLEXES CONTAINING DITHIOLENE LIGANDS

"I have no special talent. I am only passionately curious."

Albert Einstein

3.1. INTRODUCTION

3.1.1. DITHIOLENE LIGANDS CONTAINING NITROGEN GROUPS

Metal complexes containing non-innocent redox-active dithiolene ligands possess characteristic electronic structures which determine their electrical, magnetic and optical properties. Such complexes are usually notable for extensive ligand-metal mixing in their frontier orbitals, facile ligand-centered electron transfers and intense colors in solution. Several examples of mononuclear dithiolene complexes can be found in the literature, and typical coordination geometries are square planar and trigonal prismatic, although the latter are less frequent.[1–3]

Among the large number of dithiolene ligands reported, the most frequent contain a single coordination pole.[4] Nevertheless, in the past few years interesting examples of dithiolene ligands bearing both sulfur and nitrogen donor atoms have emerged. These ligands possess therefore two possible coordination poles with different chemical nature (S *vs* N) and charge (anionic *vs* neutral), which can be classified as primary and secondary, depending on the strength of the interaction with metal centers.[5] Some examples of dithiolene ligands containing nitrogen coordinating atoms are depicted in Figure 3.1.

Nitrogen coordinating groups may include cyano and pyridyl functionalities. The cyano group can be found to be appended directly to the C_2S_2 dithiolene group (mnt), or through a functionalized benzene ring (dcbdt). Moreover, it is possible to link a pyridyl group to the thiocarbonate ring by a methylene moiety ($BpyDTS_2$), or by an alkyl chain (dpesdt), which allows more flexibility to the nitrogen groups. Other moieties that have been traditionally used to functionalize dithiolene ligands are pyrazine (pdt), 1,10-phenanthroline (fendt) and 4,5-diazafluorene (DazDTS).

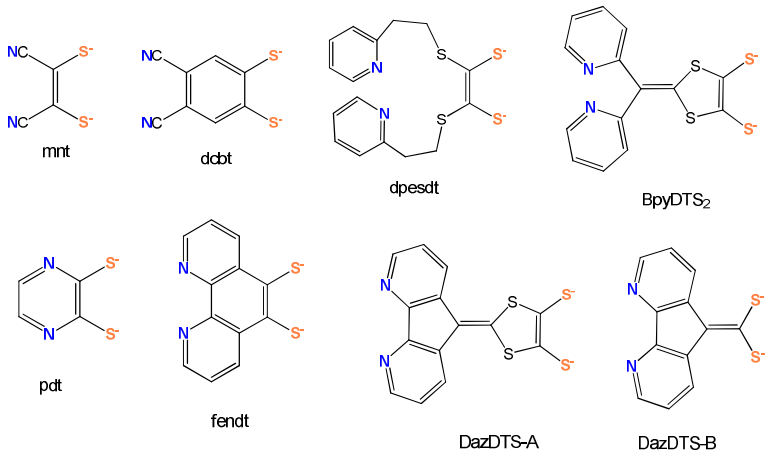

Figure 3.1. Dithiolene ligands containing nitrogen coordinating groups.

Dithiolene ligands bearing two coordination poles can selectively bind different metal ions, which may lead to a diversity of novel heterometallic coordination architectures. However, despite their potential, the coordination ability of dithiolene ligands containing nitrogen donor atoms has been so far much less explored than that of dithiolene ligands bearing only sulfur atoms.[5]

By an appropriate choice of auxiliary ligands, heterometallic discrete coordination or polymeric structures can be easily envisioned. A possible strategy for the preparation of the aforementioned structures is shown in Figure 3.2. Interaction of a bifunctional dithiolene ligand with a metal ion (metal 1) may afford a discrete complex. This unit possessing two identical coordination poles oriented in a divergent fashion represents a convenient building block, since in the presence of a second metal two different coordination structures can emerge. If a second metal ion (metal 2) is allowed to react with the building block, the iterative coordination processes taking place between metal centers and the secondary coordination poles (nitrogen groups) may lead to the formation of heterometallic coordination networks.

Nevertheless, reaction between the building block and a metal complex containing non-labile ligands (capped) would afford discrete trimetallic coordination complexes.[6]

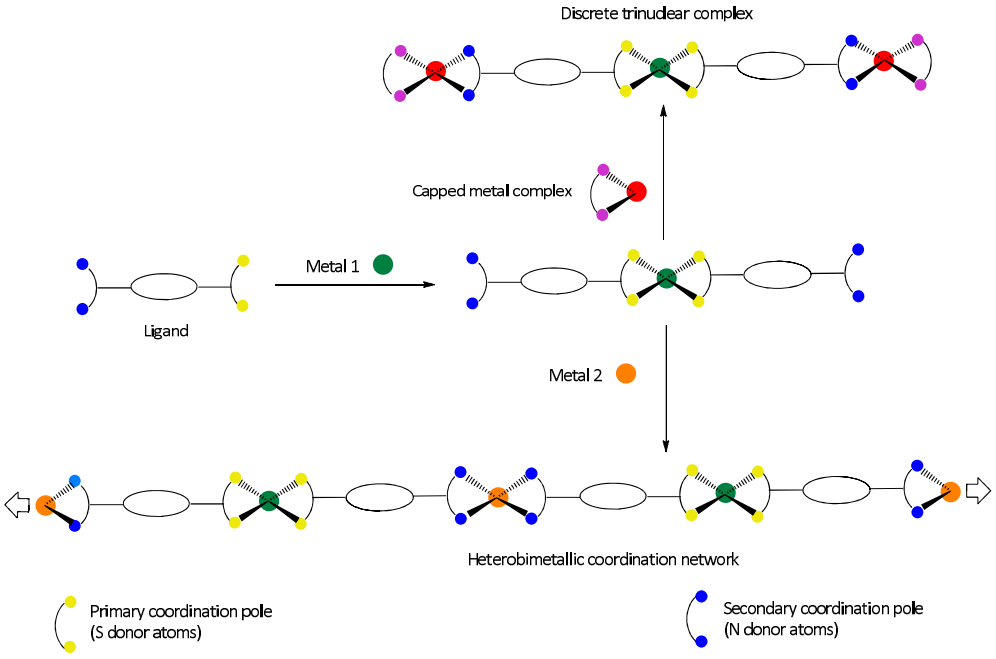

Figure 3.2. Stepwise approach to the design of heterometallic coordination architectures by using dithiolene ligands bearing two coordination poles.

3.1.2. HETEROMETALLIC STRUCTURES BASED ON BIFUNCTIONAL DITHIOLENE LIGANDS

In the past few years, the coordination ability through the nitrogen atoms of dithiolene ligands has been explored. Several ligands included in Fig. 3.1 have been used for these purposes. Regarding the use of mnt (mnt = maleonitriledithiolate), which bears a nitrile group, it is worth mentioning the heterobimetallic complex $[(CH_3CN)Ni(L)][Cu(mnt)_2]\cdot CH_3CN$, (L = tetrabenzo[b,f,j,n][1,5,9,13] tetra-azacyclohexadecine),[7] and the trimetallic compound $[K(DC18C6\text{-}B)]_2[Pd(i\text{-}mnt)_2]$, (DC18C6-B = *cis-anti-cis*-dicyclohexyl-18-crown-6; i-mnt =

isomaleonitriledithiolate).[8] The molecular structures of them are depicted in Figure 3.3. In the former, the copper(II) ion is coordinated by four sulfur atoms of the two mnt ligands, one of which is bound to a nickel(II) ion through the nitrogen atom, completing an octahedral coordination. In the latter, the mnt ligand is coordinated to palladium(II) and two coordinating nitrogen atoms in the ligand are bound to potassium cations.

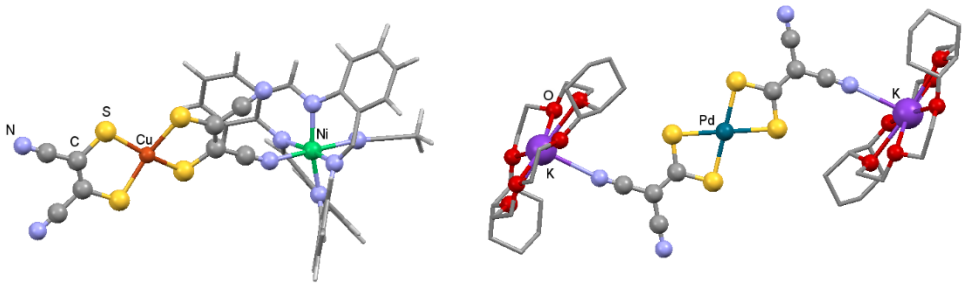

(a) (b)

Figure 3.3. Molecular structure of heterobimetallic (a) and trimetallic (b) complexes bearing dithiolene ligands with cyano functionalities.

It is also worth considering the work of Zuo *et al.*, who used the ligand $BPyDTS_2$ (see Fig. 3.1) to afford heterometallic luminescent materials upon coordination to rhenium(I) and other transitition metals, such as gold (I) and platinum(II).[9] This choice of metals was motivated by the interesting photophysical and photochemical properties of rhenium(I).[10–13]

Dithiolate-4,5-diazafluorene-like ligands have also been extensively used for the generation of both discrete heterotrinuclear complexes and coordination polymers. For instance, the group headed by S. A. Baudron prepared interesting examples of heterotrimetallic complexes by using the mononuclear compounds depicted in Figure 3.4 as building blocks.[6] In particular, such compounds containing

the bifunctional dithiolene ligand DazDTS-B (see Figure 3.1) have been used for further coordination to nickel complexes and sodium cations.

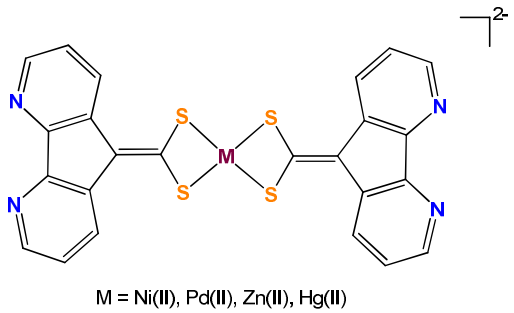

Figure 3.4. Mononuclear complexes containing a bifunctional dithiolene ligand with a 4,5-diazafluorene moiety.

The mononuclear dianionic palladium 1,1-bis(dithiolene)-4,5-diazafluorene complex represented in Figure 3.4 was used as a building block to prepare the trimetallic complex $[(Nicyclen)_2Pd(DazDTS\text{-}B)_2](BF_4)_2 \cdot 6DMF$, (cyclen = 1,4,7,10-tetracyclododecane; Fig. 3.5). This heterometallic complex contains two terminal nickel atoms capped by a cyclen ligand, which blocks the remaining coordination sites of the metal, and one central palladium atom. The two nickel(II) ions are paramagnetic with S = 1, while the palladium(II) ion is diamagnetic, and there is a weak antiferromagnetic coupling between the nickel centers.

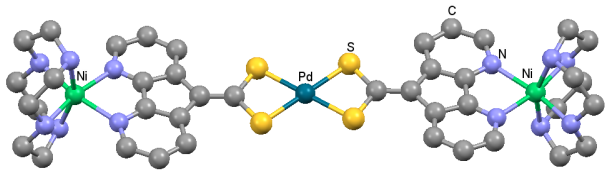

Figure 3.5. Molecular representation of the trimetallic complex $[(Nicyclen)_2Pd(DazDTS\text{-}B)_2](BF_4)_2$.

By using the same ligand, 1D coordination networks of formula $[M(DazDTS\text{-}B)_2Na_2(DMSO)_5]$ (M = Ni, Pd; for M = Pd, see Fig. 3.6) were obtained. In these

structures the dianionic complexes are bridged by sodium cation dimers bearing five dimethylsulfoxide molecules. Both coordination polymers are diamagnetic with a square-planar coordination for the central atoms.

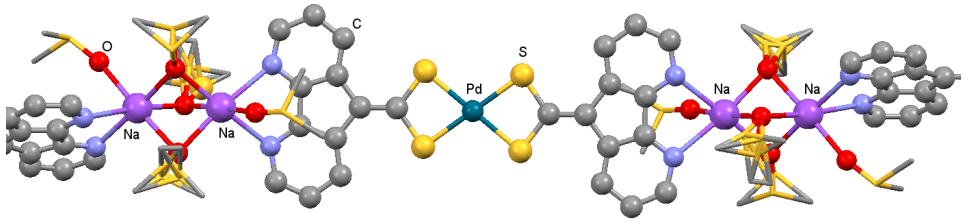

Figure 3.6. One-dimensional chains in complex $[Pd(DazDTS\text{-}B)_2Na_2(DMSO)_5]$.

The polymeric compound $(Et_4N)[Hg(DazDTS\text{-}B)_2Na(DMSO)](H_2O)_{0.5}$ (see Fig. 3.7) was obtained by using a similar strategy. In this complex, one tetraethylammonium cation is substituted by a sodium cation which acts as a bridging unit between adjacent $[Hg(DazDTS\text{-}B)_2]^{2-}$ dianions. The resulting 1D coordination network presents Hg-S short contacts between adjacent chains. Therefore, the overall arrangement can be described as a 2D network.

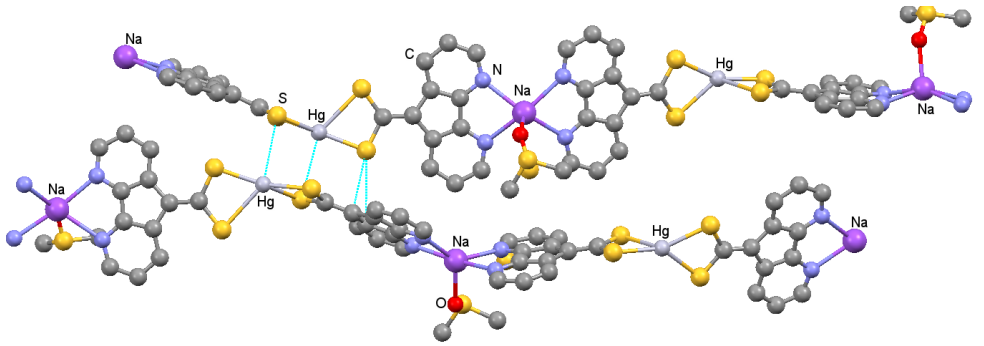

Figure 3.7. Two-dimensional networks in compound $(Et_4N)[Hg(DazDTS\text{-}B)_2Na(DMSO)](H_2O)_{0.5}$ (b). The Et_4N^+ cations have been omitted for clarity.

Complexes based on the pyrazine-like ligands pdt (pyrazine-2,3-diselenol) and pds (pyrazine-2,3-diselenol) show a remarkable ability to side coordinate alkaline metal ions, such as Li^+, Na^+ and Cu^+, generating 3D extended metal-organic frameworks (MOFs). Most examples of these MOFs were firstly published by C. Rovira *et al.*[5] Treatment of the ligand precursors with LiOH or NaOH, followed by addition of copper or nickel salts afforded the polymeric coordination compounds $M[Cu^{III}(pds)_2]\cdot xH_2O$ (M = Li, Na or Cu^I)[14,15] and $Na_2[Ni(pds)_2]\cdot 2H_2O$, among others.[16] A remarkable MOF, formulated as $Cu^I[Ni^{III}(pdt)_2]$, was published by the group headed by J. R. Long.[17] This heterometallic coordination polymer is isostructural with the previously reported $Cu^I[Cu^{III}(pdt)_2]$,[18] whose structure is depicted in Figure 3.8. The microporous network assembled from $Cu^I[Ni^{III}(pdt)_2]$ represents the first reported example of a MOF exhibiting electronic conductivity, doping capability and redox behavior at the same time.

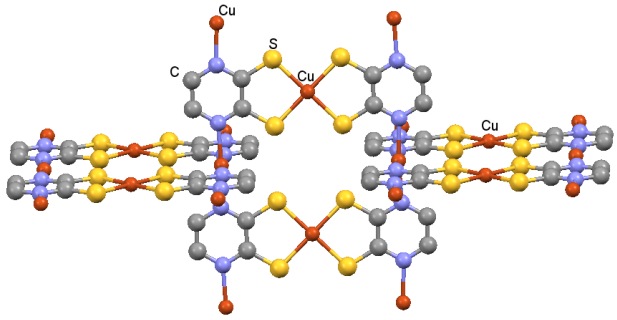

Figure 3.8. Crystal structure of $Cu^I[Cu^{III}(pdt)_2]$.

3.1.3. APPROACH TO THE DESIGN OF HETEROMETALLIC MOLYBDENUM AND TUNGSTEN DITHIOLENE CLUSTER COMPLEXES

The Molecular Materials group at Jaume I University is focused on the synthesis and characterization of dinuclear and trinuclear molybdenum and tungsten complexes functionalized with different ligands. In the past, interesting examples of cluster complexes containing dithiolene ligands and Mo_3S_7 and $Mo_2O_2S_2$ cores were published. For the trinuclear unit, either dialkyltin or zinc dithiolene complexes must be used as hidden forms of dithiolates, since the Mo_3S_7 core is not stable under the basic conditions which are usually required for the coordination of dithiolene ligands. In particular, the cluster $(Bu_4N)_2[Mo_3S_7(dmit)_3]$, prepared by the transmetallation reaction between $(Bu_4N)_2[Mo_3S_7Br_6]$[19] and $(Bu_4N)_2[Zn(dmit)_2]$, was used for the design of single component molecular conductors.[20–23] Despite the potential of these systems, the coordinative ability through the nitrogen groups of dithiolene ligands in molybdenum and tungsten complexes remain unexplored.

Motivated by the heterometallic coordination architectures reported in the literature,[5] we decided to study the reactivity of dithiolene ligands containing nitrogen groups towards molybdenum and tungsten cluster complexes. The resulting compounds could presumably open a new avenue in the search of heterometallic structures based on molybdenum and tungsten clusters. By following a similar approach to that described in Figure 3.2, should bis(dithiolene) dinuclear clusters be used as starting materials, either discrete tetrametallic complexes or 1D heterometallic networks could be achieved. The use of a tris(dithiolene) trinuclear complex would afford either an hexametallic complex or a 2D heterometallic layer instead. A schematic representation of such architectures is depicted in Figure 3.9.

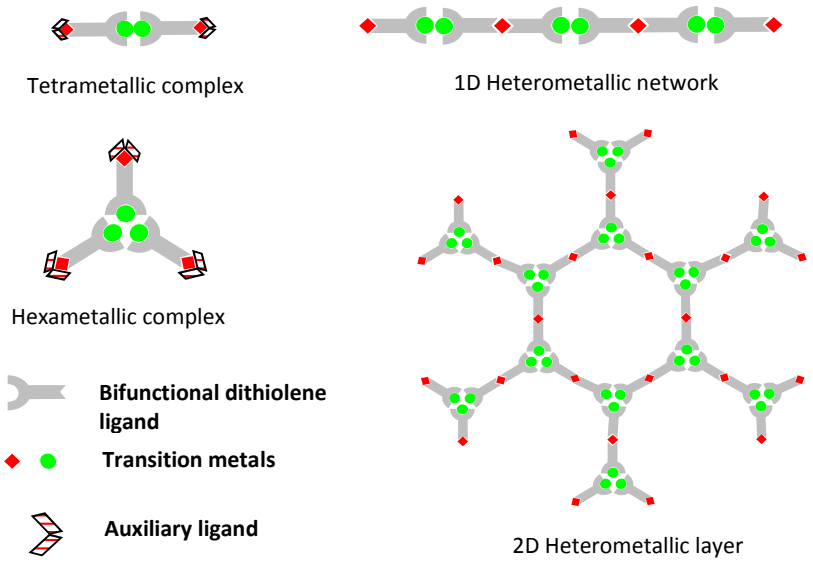

Figure 3.9. Schematic representation of possible coordination structures built from dinuclear and trinuclear clusters containing dithiolene ligands with nitrogen donor atoms.

A different strategy for the preparation of heterometallic dithiolene cluster complexes is depicted in Scheme 3.1. Three different synthetic routes are possible. Cubane-like clusters of formula $M_2M'M''S_4$, where M = Mo or W, and M and M' are heterometals (M' = M'' or M' ≠ M'') can be prepared by using a dinuclear M_2S_4 cluster as a starting material. By following the so-called [2 + 2] route, heterometallic cubane clusters with $M_2M'M''S_4$ (M' = M'') cores have been reported. By means of the [2 + 1 + 1] route, $M_2M'M''S_4$ (M' ≠ M') complexes containing three different metals can be envisaged, although no examples have been reported so far to the best of our knowledge. Finally, $M_3M'Q_4$ clusters (Q = S, Se) can be prepared in a similar fashion, by reacting a trinuclear cluster with a metal ion ([3 + 1] route).[24]

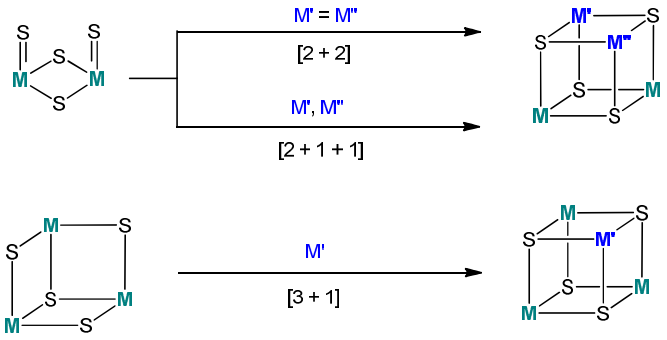

Scheme 3.1. Stepwise strategy for the design of heterometallic cubane-like clusters.

Several examples of heterobimetallic cubane-like $M_3M'Q_4$ clusters (M = Mo or W; Q = S or Se; M' = Fe, Ni, Cu, Co, Pd…) bearing aquo,[25,26] cyclopentadienyl[27–30] or diphosphine ligands[31–33] have been reported. However, the number of heterometallic cubane-type clusters containing sulfur-donor ligands is rather scarce, and date back to the late 80's and early 90's. All known examples contain dithiolate, dithiophosphate or dithiocarbamate ligands, and the most frequent building block is the *syn*-$M_2(\mu_2\text{-}S)_2S_2$ unit (M = Mo or W). In particular, the dinuclear molybdenum and tungsten clusters $M_2S_4(dtc)_2$ (dtc = diethyldithiocarbamate)[33,34] and $(Et_4N)_2[M_2S_4(edt)_2]$ (edt = 1,2-ehanedithiolate),[36] with two terminal and two μ_2-bridged sulfide ligands, have been used as precursors.[24]

Among the reported cubane-like clusters containing the ligands dtc or edt, it is worth mentioning the cluster $Mo_2Fe_2S_4(dtc)_5$, which was prepared in 18 % yield by a one-pot reaction in which the $[Mo_2S_4(dtc)_2]^{2-}$ precursor was prepared *in situ*.[37] The $M_2Co_2S_4$ (M = Mo or W) clusters $[M_2Co_2S_4(dtc)_2(CH_3CN)_2(CO)_2]$ were prepared by using the complex $Co_2(CO)_8$ as a cobalt source.[38] Scheme 3.2 shows a schematic representation of the approach followed in order to prepare $M_2Cu_xS_4$ (x = 1 or 2) cubane complexes. The incomplete cubane clusters $(Et_4N)[M_2CuS_4(edt)_2(PPh_3)]$ (M = Mo or W) were synthesized by reaction between $[M_2S_4(edt)_2]^{2-}$ and the copper

complex $Cu(PPh_3)_2(dtp)$.[39,40] The incorporation of two copper atoms in the cluster core was achieved by reacting $[W_2S_4(edt)_2]^{2-}$, $CuCl_2 \cdot H_2O$ and PPh_3, or CuCl in the presence of KSCN to afford $W_2Cu_2S_4(edt)_2(PPh_3)_2$ or $(Et_4N)_4[W_2Cu_2S_4(SCN)_8]$, respectively.[39,40] The molybdenum analogue cluster $Mo_2Cu_2S_4(edt)_2(PPh_3)_2$ was obtained by reaction with $Cu(PPh_3)_3Cl$.[41] Finally, the trinuclear clusters $[M_3S_4(dtp)_3(\mu_2\text{-}dtp)(L)]$ (dtp = diethyldithiophosphate, L = H_2O or CH_3CN) have also been employed to incorporate copper as heterometal, affording M_3CuS_4 cubane complexes.[43–45]

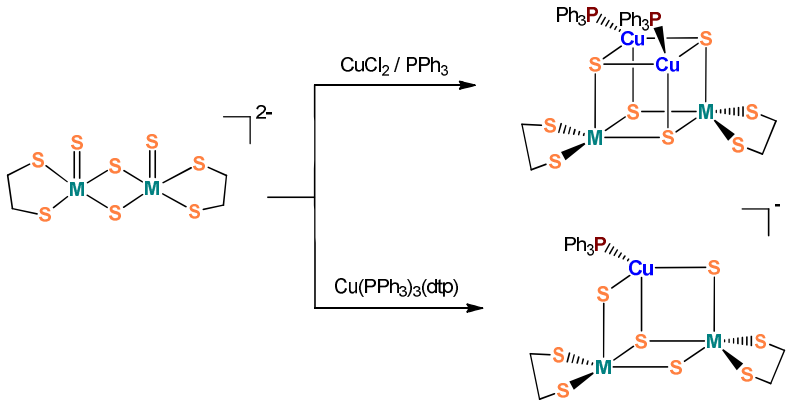

Scheme 3.2. Incorporation of one or two copper atoms into the dinuclear cluster $[M_2S_4(edt)]^{2-}$, (M = Mo, or W).

In this chapter, two dithiolene ligands containing nitrogen groups, namely 2-bis-(2-pyridyl)methylene-1,3-dithiolene ($BPyDTS_2$ in Figure 3.1) and 2,3-pyrazinedithiolate (pdt) have been coordinated to $M_2Q_2(\mu\text{-}S)_2$ dinuclear units (M = Mo or W; Q = O or S), and their reactivity towards other metals has been investigated by following the different strategies mentioned above. Furthermore, a novel dibutyltin dithiolate, $Me_2Sn(BPyDTS_2)$, and two zinc bis(dithiolene) complexes, *i.e.* $(Bu_4N)_2[Zn(met)_2]$ (met = *cis*-1,2-dicarbomethoxyethylene-1,2-dithiolate) and $(PPN)_2[Zn(Cl_2bdt)_2]$ (Cl_2bdt = 3,6-dichloro-1,2-benzenedithiol) have been prepared.

The reactions of the latter zinc and tin complexes towards the molybdenum cluster precursor $(Bu_4N)_2[Mo_3S_7Br_6]$[19] are also described herein.

3.2. RESULTS AND DISCUSSION

3.2.1. SYNTHESIS AND CHARACTERIZATION

In the past decades, several synthetic approaches were used for the preparation of molybdenum and tungsten dithiolene cluster complexes. One of these strategies consists in the fragmentation of clusters of higher nuclearity. Dithiolene cluster complexes of formula $[M_2O_2(\mu\text{-}Q)_2(\text{dithiolene})_2]^{2-}$ (M = Mo or W; Q = S or Se) were obtained by reaction between the trinuclear clusters $[M_3Q_4(\text{dppe})_3Br_3](PF_6)$, (dppe = 1,2-bis(diphenylphosphino)ethane) and the zinc complex $(Bu_4N)_2[Zn(\text{dmit})_2]$. Alternatively, $[M_2O_2(\mu\text{-}Q)_2(\text{dithiolene})_2]^{2-}$ clusters were obtained starting from the $\{M_3Q_7Br_4\}_n$ cluster polymers (M = Mo or W; Q = S or Se), although in the latter case longer reaction times were required (1 day *vs* 2 days). A schematic representation of the most common approaches to the preparation of bis(dithiolene) molybdenum and tungsten cluster complexes is depicted in Scheme 3.3. In all cases, the formation of the air-sensitive $[M_3Q_4(\text{dmit})_3]^{2-}$ complexes was observed, which in the presence of oxygen afforded the desired dinuclear clusters in low yields.[46]

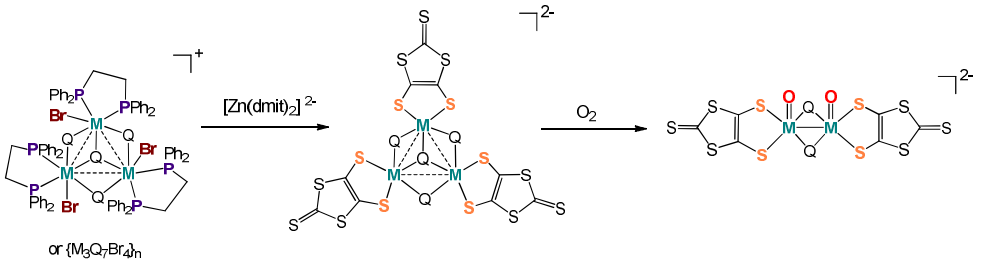

Scheme 3.3. Synthetic strategies employed for the preparation of $[M_2O_2(\mu\text{-}Q)_2(\text{dithiolene})_2]^{2-}$ cluster complexes (M = Mo or W; Q = S or Se).

The cluster $[Mo_2O_2(\mu\text{-}S)_2(\text{dmit})_2]^{2-}$ was also prepared in moderate yields by substitution of the labile dimethylformamide ligands in the $[Mo_2O_2(\mu\text{-}S)_2(DMF)_6](I_2)$

precursor. Apart from this complex, dinuclear molybdenum or tungsten cluster chalcogenides bearing labile ligands that could be easily replaced by dithiolates have not been reported. For this reason, we decided to investigate alternatives to the cluster complexes $[M_3Q_4(dppe)_3Br_3]^+$, (M = Mo, W; Q = S or Se), and to the polymers $\{M_3Q_7Br_4\}_x$, which allowed us to obtain bis(dithiolene) dinuclear clusters in high yields.

As mentioned earlier, dithiolene derivatives of the $Mo_2O_2(\mu\text{-}S)_2$ dinuclear unit can be conveniently prepared from the $[Mo_2O_2(\mu\text{-}S)_2(DMF)_6]^{2+}$ cation by simple ligand exchange reactions.[46] Nevertheless, its reactivity towards dithiolates is restricted to only a few examples, which include the use of dmit and dithiooxalate as ligands.[46,47] With the aim of extending this chemistry, we decided to synthesize and coordinate two dithiolene ligands containing nitrogen groups, namely 2-bis-(2-pyridyl)methylene-1,3-dithiolene (hereinafter, $BPyDTS_2$)[9] and 2,3-pyrazinedithiolate (pdt),[14,17] the molecular structure of them being represented in Figure 3.1. This choice of dithiolene ligands with two coordination poles would afford potential building blocks based on molybdenum dinuclear clusters which may be used for the construction of extended architectures, as envisioned in Figure 3.9.

Ligand $BPyDT(SCH_2CH_2CN)_2$ was prepared in *ca.* 50 % yields by the cross-coupling reaction between di(2-pyridyl)ketone and 4,5-bis(2-cyanoethylthio)-1,3-dithiole-2-thione[48] in the presence of $P(OEt)_3$, as reported in the literature.[9] In the step concerning the synthesis of 4,5-bis(2-cyanoethylthio)-1,3-dithiole-2-thione, the yield of the reaction was greatly increased with respect to the reported (90 % *vs* 66 %)[48] by increasing the quantity of 3-bromopropionitrile used. Deprotection of the dithiolene ligand was achieved with potassium *tert*-butoxide, a widely-used reagent for these purposes.[49] Compound 2,3-pyrazinedithiol was prepared by modifying the literature procedures.[14,17] This modification allowed us to prepare the ligand H_2pdt

in a significantly higher yield (72 % *vs* 43 %). Addition of a 2M sodium hydroxide solution in methanol afforded the deprotonation of the ligand.

As shown in Scheme 3.4, the *in situ* generated $BPyDTS_2^{2-}$ and pdt^{2-} dithiolates were reacted with the dinuclear molybdenum species $[Mo_2O_2(\mu\text{-}S)_2(DMF)_6](I_2)$ containing labile dimethylformamide ligands, which were easily replaced by the dithiolate to afford the desired $(Et_4N)_2[Mo_2O_2(\mu\text{-}S)_2(BPyDTS_2)_2]$, (hereinafter $(Et_4N)_2$[**4**]) and $(Et_4N)_2[Mo_2O_2(\mu\text{-}S)_2(pdt)_2]$, ($(Et_4N)_2$[**7**]), clusters respectively in *ca.* 80 % yields. The molybdenum precursor $[Mo_2O_2(\mu\text{-}S)_2(DMF)_6](I_2)$ was prepared by reaction of the cluster $(Et_4N)_2[Mo_2O_2S_8]$ with I_2 in DMF.[47]

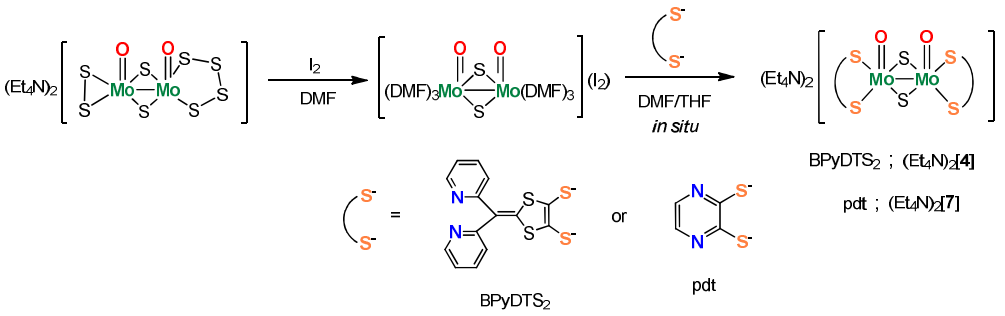

Scheme 3.4. Stepwise approach to the synthesis of bis(dithiolene) $Mo_2O_2(\mu\text{-}S)_2$ cluster complexes.

As mentioned in the introduction, molybdenum and tungsten cluster units containing $M_2S_2(\mu\text{-}S)_2$ cores (M = Mo or W) are very promising as they allow the synthesis of heterometallic structures based on cubane-like cluster units.[24] Since the number of dithiolene ligands coordinated to $M_2S_2(\mu\text{-}S)_2$ units is scarce, we decided to extend this chemistry by coordinating dithiolene ligands bearing nitrogen groups. For this purpose, we chose the ligand pdt due to its ability to side coordinate metal ions.

As shown in Scheme 3.5, for the synthesis of clusters $(PPN)_2[Mo_2S_2(\mu\text{-}S)_2(pdt)_2]$, ($(PPN)_2$[**6**]) and $(PPN)_2[W_2S_2(\mu\text{-}S)_2(pdt)_2]$, ($(PPN)_2$[**8**]), the ligand pdt was mixed with commercial ammonium tetrathiomolybdate or tetrathiotungstate,

respectively in the presence of dimethylformamide. Reddish-brown solutions were obtained upon heating for a few hours. Compound $(NH_4)_2[WS_4]$ is less reactive than $(NH_4)_2[MoS_4]$, and consequently higher temperatures and longer reaction times were required. Addition of PPNCl afforded the desired salts in *ca.* 60 % yields. The tetraethylammonium salts of complexes $[M_2S_2(\mu\text{-}S)_2(pdt)_2]^{2-}$ (M = Mo or W) were also obtained by using Et_4NBr instead of PPNCl. This convenient route is an adaptation of that proposed by Stiefel for the coordination of 1,2-ethanedithiol and o-aminobenzenethiol to molybdenum and tungsten dinuclear units.[36] In this synthetic approach, the anion precursors $[MS_4]^{2-}$ (M = Mo or W), in which the formal oxidation state for the metal is +6, are reduced to form dinuclear M(V), (M = Mo or W), cluster complexes. The reductant may be the pdt ligand or the sulfide which is present in the coordination sphere of the metals.

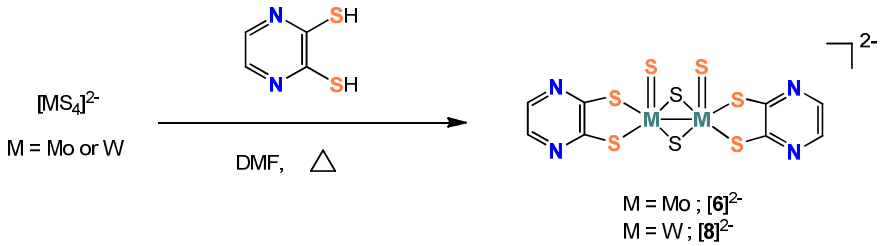

Scheme 3.5. Synthesis of bis(dithiolene) $Mo_2S_2(\mu\text{-}S)_2$ cluster complexes.

A tentative mechanism for the latter reaction was proposed by Stiefel and co-workers.[50] As shown in Scheme 3.6, the first step involves proton transfer from NH_4^+ to $[MS_4]^{2-}$, followed by expulsion of the HS^- anion and formation of the $[M_2S_7]^{2-}$ dimer.[51] The instability of the $[M_2S_7]^{2-}$ complex may lead to the formation of an isomeric intermediate. Reaction between the bidentate ligand (pdt) and the intermediate could replace the S_2^{2-} and S^{2-} sulfides present in the dimer in order to generate the species containing the $[M_2S_2(\mu\text{-}S)_2]^{2+}$ core.

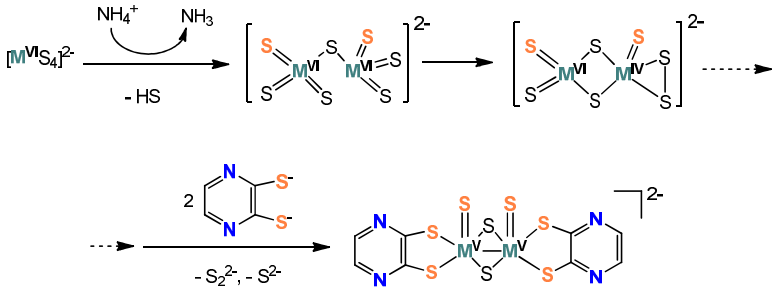

Scheme 3.6. Tentative mechanism for the synthesis of $[M_2S_2(\mu\text{-}S)_2(pdt)_2]^{2-}$ (M = Mo or W).

As mentioned in the Introduction, dithiolene ligands have been coordinated to trinuclear Mo_3S_7 and Mo_3S_4 cluster units by transmetallation starting either from tin or zinc dithiolene complexes to afford highly versatile redox active multifunctional cluster-based molecular conductors.[20–23] In order to provide further insight into the reactivity of Mo_3S_7 clusters towards dithiolene ligands, we decided to explore the coordinative abilities of dithiolates functionalized with several groups, namely carboxylates, chlorine and nitrogen. For this purpose, we chose four different ligands: *cis*-1,2-dicarbomethoxyethylene-1,2-dithiolate (met), 3,6-dichloro-1,2-benzenedithiolate (Cl_2bdt), and the aforementioned $BPyDTS_2$ and pdt. The ligands met and Cl_2bdt have the potential to generate complexes with interesting redox properties,[52] and in the former case, due to the presence of carboxylate groups in the ligand, the resulting clusters could be anchored onto semiconductor oxides.[53] On the other hand, the coordination of the nitrogen-containing ligands $BPyDTS_2$ and pdt to trinuclear molybdenum clusters could pave the way for the design of interesting heterometalic architectures based on transition metal clusters.

Since the Mo_3S_7 cluster unit is unstable under the basic conditions required for the deprotection of dithiolene ligands, we have used dialkyltin and zinc dithiolene complexes as hidden forms of dithiolates for the synthesis of tris(dithiolene) Mo_3S_7 clusters. Scheme 3.7 shows the synthetic procedures employed for the preparation of complexes $(Bu_4N)_2[Zn(met)_2]$, $((Bu_4N)_2[\mathbf{1}])$, and $(Bu_4N)_2[Zn(Cl_2bdt)_2]$, $((Bu_4N)_2[\mathbf{2}])$. Both compounds were prepared in moderate yields (40 % and 60 %, respectively) by reaction between $ZnCl_2$ and the corresponding dithiolates, which were generated *in situ*. The use of a 1:1 mixture of methanol and aqueous ammonia was required in order to dissolve the zinc chloride. The met ligand was obtained by treating dimethyl-2-oxo-1,3-dithiole-4,5-dicarboxylate[54] with a methanol solution of LiOH, whereas H_2Cl_2bdt was deprotonated with triethylamine. Complex $Me_2Sn(BPyDTS_2)$, (**3**), was prepared in 70 % yields by reacting the $BPyDTS_2^{2-}$ dithiolate with dimethyltin dichloride, since the reaction with zinc chloride did not afford the desired product. To date, all attempts to prepare tin or zinc derivatives containing the pdt ligand have been unsatisfactory. Further details about the preparation of these precursors can be found in the Experimental Section.

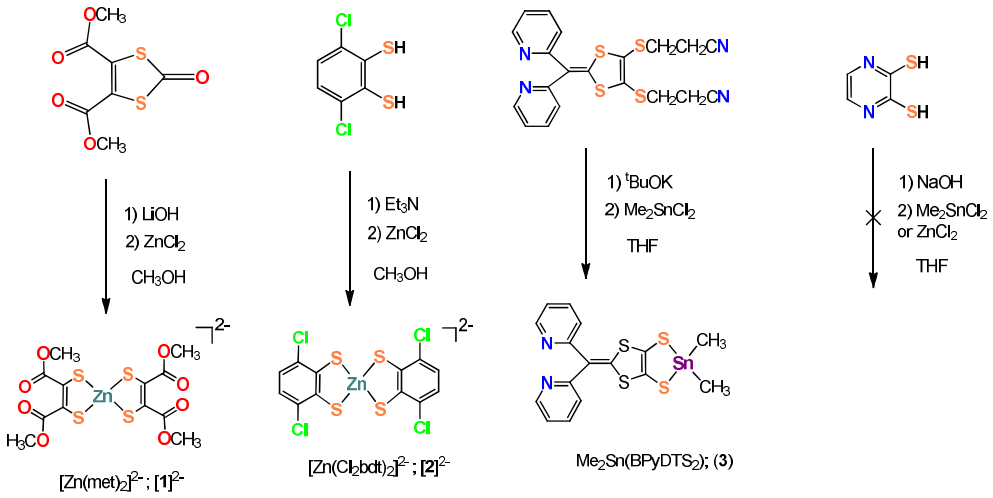

Scheme 3.7. Synthetic route for the preparation of zinc and tin dithiolene complexes.

The cluster complexes $(PPN)_2[Mo_3S_7(met)_3]$, ((PPN)$_2$[**10**]), and $(Bu_4N)_2[Mo_3S_7(Cl_2bdt)_3]$, ((Bu$_4$N)$_2$[**11**]), were prepared in moderate yields (*ca.* 70%) by reaction between the $[Mo_3S_7Br_6]^{2-}$ precursor[19] and $[Zn(met)_2]^{2-}$ or $[Zn(Cl_2bdt)_2]^{2-}$, respectively in acetonitrile at room temperature. Reaction of the tin complex $Me_2Sn(BPyDTS_2)$, (**3**), with $[Mo_3S_7Br_6]^{2-}$ under the same conditions afforded the $[Mo_2O_2(\mu\text{-}S)_2(BPyDTS_2)_2]^{2-}$, ([**4**]$^{2-}$), dinuclear cluster species upon oxidation of the trinuclear cluster core. Nevertheless, the presence of byproducts precluded the isolation of the dinuclear cluster compound [**4**]$^{2-}$ in its pure form. The molecular structures of complexes [**10**]$^{2-}$ and [**11**]$^{2-}$ are represented in Figure 3.10.

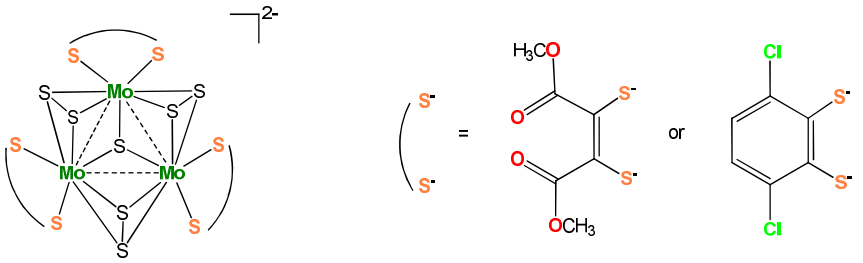

Figure 3.10. Molecular representation of the cluster anions [**10**]$^{2-}$ and [**11**]$^{2-}$.

The compounds presented in this section have been fully characterized by different techniques: NMR, mass spectrometry, IR, UV/Vis spectroscopy and elemental analysis, as described in detail in the Experimental Section. The crystal structures of compounds **3**, (Et$_4$N)$_2$[**4**], (PPN)$_2$[**6**], (Et$_4$N)$_2$[**7**], (PPN)$_2$[**8**–**10**] and (Bu$_4$N)$_2$[**11**] have been determined by using single crystal X-ray diffraction techniques, as detailed in a subsequent section. To our dismay, diffraction data for compounds (Bu$_4$N)$_2$[**1** – **2**] did not lead to a satisfactory refinement of the structures. All compounds are stable in both solid and solution phases with the exception of **3**, which decomposes in solution within few hours.

The electrochemical properties of $(PPN)_2[Mo_3S_7(met)_3]$, ($(PPN)_2$[**10**]), and $(Bu_4N)_2[Mo_3S_7(Cl_2bdt)_3]$, ($(Bu_4N)$[**11**]), were investigated by cyclic voltammetry. The cyclic voltammogram of $(PPN)_2$[**10**] in dichloromethane (Figure 3.11a) reveals three quasi-reversible oxidation waves at easily accessible potentials (0.38, 0.70 and 1.03 V ; *vs* Ag/AgCl). Cluster $(Bu_4N)_2$[**11**] exhibits one quasi-reversible oxidation wave at 0.55 V (*vs* Ag/AgCl) in acetonitrile solution (see Figure 3.11b). No reduction peaks were observed for both complexes within the solvent window.

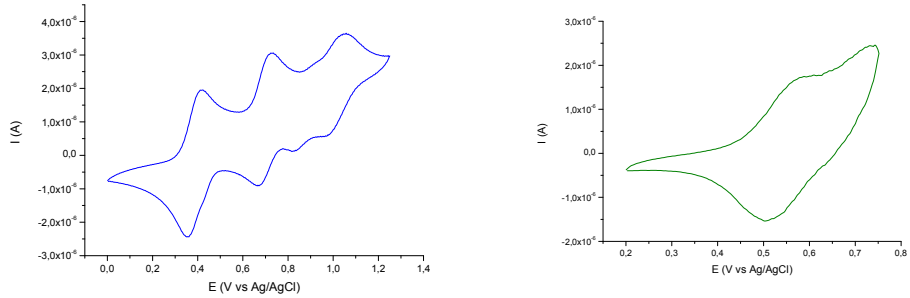

(a) (b)

Figure 3.11. Cyclic voltammograms of clusters $(PPN)_2[Mo_3S_7(met)_3]$ (a) and $(Bu_4N)_2[Mo_3S_7(Cl_2bdt)_3]$ (b) in solution, recorded at a scan rate of 100 mV/s (*vs* Ag/AgCl).

Table 3.1 lists the redox potentials of clusters $(PPN)_2$[**10**] and (Bu_4N)[**11**], together with those of related complexes. With the exception of $[\mathbf{10}]^{2-}$ and $[\mathbf{11}]^{2-}$, all Mo_3S_7 complexes show a reduction process which is associated to the reduction of the μ_2-bridged disulfide groups to sulfide, and implies transformation from the Mo_3S_7 to the Mo_3S_4 unit. Consequently, we conclude that the coordination of met and Cl_2bdt ligands to trinuclear molybdenum cluster units results in complexes which are more difficult to reduce than their bromide precursors or other tris(dithiolene) Mo_3S_7 complexes. As shown in Table 3.1, the oxidation potentials of compounds $(PPN)_2$[**10**] and $(Bu_4N)_2$[**11**] are in agreement with those reported for similar cluster complexes.

Table 3.1. Redox potentials (*vs* Ag/AgCl) measured at 100 mV/s in dichloromethane for several Mo_3S_7 dithiolene complexes.

Cluster Complex	Reduction, E_c / V	Oxidation, $E_{1/2}$ (ΔE) / V		
$(NH_4)_2[Mo_3S_{13}]$[55]	-1.03[a]	-	-	-
$(Bu_4N)_2[Mo_3S_7Br_6]$[56]	-1.15	-	-	-
$(PPN)_2$[**10**]	-	0.38 (0.07)	0.70 (0.08)	1.04 (0.09)
$(Bu_4N)_2$[**11**]	-	0.54 (0.07)[b]	-	-
$(Bu_4N)_2[Mo_3S_7(bdt)_3]$[21]	-1.26	0.23 (0.07)	0.41 (0.13)	-
$(Bu_4N)_2[Mo_3S_7(tfd)_3]$[21]	-1.22	0.51 (0.07)	0.89 (0.06)	-
$(Bu_4N)_2[Mo_3S_7(mnt)_3]$[56]	-1.04	0.77 (0.07)	1.16 (0.07)	-
$(Bu_4N)_2[Mo_3S_7(tdas)_3]$[57]	-1.31	0.72 (0.08)	-	-
$(Bu_4N)_2[Mo_3S_7(dmid)_3]$[21]	-1.27	0.36 (0.10)	-	-
$(Bu_4N)_2[Mo_3S_7(dmit)_3]$[20]	-1.20	0.38 (0.17)	-	-
$(Bu_4N)_2[Mo_3S_7(dsit)_3]$[21]	-1.69	0.34 (0.18)	-	-

$E_{1/2} = (E_a + E_c)/2$; $\Delta E = |E_a - E_c|$; [a] Data recorded in etanol ; [b] Data recorded in acetonitrile

Theoretical calculations show that the oxidation processes of $[Mo_3S_7(dithiolene)_3]^{2-}$ complexes are ligand centered.[20–23] In particular, the oxidation of the already reported $[Mo_3S_7(dmit)_3]^{2-}$ (dmit = 1,3-dithiole-2-thione-4,5-dithiolate) anion has been associated to a bielectronic process which affords neutral radical species, as shown in the following scheme:[20]

$$[Mo_3S_7L_3]^{2-} \underset{}{\overset{-2e^-}{\rightleftharpoons}} [Mo_3S_7L_3]^0$$

The shape of the oxidation waves of $[Mo_3S_7(dmit)_3]^{2-}$ suggests that insoluble species are formed at the electrode surface. This is not the case for the [**11**]$^{2-}$ cluster anion, for which similar intensities are observed in the cathodic and anodic peaks of the quasi-reversible redox wave registered at 0.54 V. With these data, it is not possible to assess whether the electron transfer corresponds to a mono- or bielectronic redox process. Nevertheless, the oxidation potential of [**11**]$^{2-}$ is in agreement with a ligand-

based oxidation (see Table 3.1). The presence of three reversible or quasi-reversible oxidation waves in the cyclic voltammogram of complex [**10**]$^{2-}$ can be explained by taking into consideration the ligand-based character of the HOMO orbitals in tris(dithiolene) Mo_3S_7 clusters.[21] In view of these redox waves, it can be postulated that the oxidation process observed in [**10**]$^{2-}$ occurs via a three-stepped one-electron mechanism, as follows:

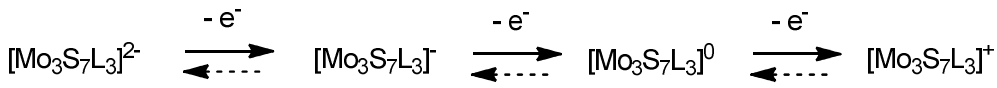

3.2.2. REACTIVITY OF BIS(DITHIOLENE) DINUCLEAR CLUSTER COMPLEXES TOWARDS OTHER METALS

As mentioned in the Introduction, dithiolene ligands bearing two coordination poles have given rise to a series of interesting heterometallic discrete complexes, or coordination polymers, in which a combination of physical properties is present.[5] With the aim of extending this chemistry to transition metal cluster complexes, we decided to use the dinuclear molybdenum cluster $[Mo_2O_2(\mu\text{-}S)_2(BPyDTS_2)_2]^{2-}$, ([**4**]$^{2-}$), as a building block for the formation of heterometallic structures in which the heterometals were bridged to the cluster unit by the nitrogen groups in the $BPyDTS_2$ dithiolene ligand. In the past, the ligand $BPyDTS_2$ was used by Zuo and co-workers for the preparation of luminescent heterometalic complexes containing rhenium(I) and other transition metals, such as platinum(II) and gold(I).[9]

Motivated by the reported photophysical properties of rhenium(I) tricarbonyl complexes with diimine ligands,[9,58] we focused our investigation on the reactivity of the molybdenum dimer $(Et_4N)_2[Mo_2O_2(\mu\text{-}S)_2(BPyDTS_2)_2]$ towards pentacarbonylchlororhenium(I), represented in Scheme 3.8. Optimum reaction conditions were achieved by using microwave irradiation (100 W) and a DMF/CH_3CN (1:4) mixture as a solvent. This mixture of solvents was crucial since it allowed the precipitation of impurities over the course of the reaction. The resulting

heterometallic cluster compound $(Et_4N)_2[Mo_2O_2S_2(BPyDTS_2)_2\{Re(CO)_3Cl\}_2]$, ($(Et_4N)_2$[**5**]), was isolated in 67 % yield and represents to the best of our knowledge, the first example of a discrete heteronuclear complex with two metal atoms (rhenium) connected to a molybdenum dinuclear cluster unit through a bridging ligand. As shown in Scheme 3.8, reaction between $[Mo_2O_2(\mu\text{-}S)_2(BPyDTS_2)_2]^{2-}$ and $Mn(CO)_5Br$ under analogous conditions did not afford the expected product.

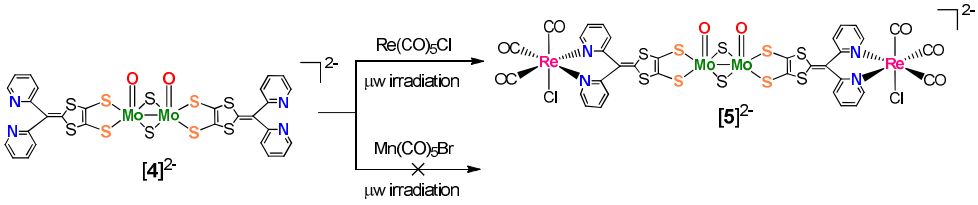

Scheme 3.8. Synthetic approach to the preparation of discrete heterometallic structures based on dinuclear $Mo_2O_2(\mu\text{-}S)_2$ clusters and rhenium(I).

The IR spectrum of complex $(Et_4N)_2$[**5**] shows the three typical bands found in the CO stretching region for Re(I) distorted octahedral complexes with three substituted positions (two nitrogen atoms and a halogen atom). These bands are consistent with a *facial* arrangement for the three coordinated C≡O ligands, and the infrared frequency values (2017, 1906 and 1891 cm^{-1}) are also in agreement with those reported previously.[9,58,59]

With the aim of constructing 1D polymeric coordination architectures, akin to those reported by Baudron and co-workers containing the ligand DazDTS-B (see Introduction for further details),[6] the cluster complex $[Mo_2O_2(\mu\text{-}S)_2(BPyDTS_2)_2]^{2-}$, ([**4**]$^{2-}$), was allowed to react with several transition metal ions bearing labile ligands, namely Cu(I), Ag(I), Pd(II) and Ni(II). For this purpose, a concentrated solution of $(Et_4N)_2$[**4**] in DMSO (*ca.* 3 mL) was prepared. Then 3 mL of a 1:2 DMSO/CH_3CN solution was carefully layered on the top of the dark brown solution containing the cluster. Finally, a solution of a transition metal source ($[Cu(CH_3CN)_4](PF_6)$,[60] AgOTf, $PdCl_2(CH_3CN)_2$ or $Ni(PPh_3)_2Cl_2$) in CH_3CN (*ca.* 3 mL) was layered on top of the

latter solvent mixture. Crystal formation was observed when solutions of complex $PdCl_2(CH_3CN)_2$ were layered. However, to our dismay, their quality was not good enough for X-ray structural analysis.

The ability of cluster complex $(Et_4N)_2[Mo_2O_2(\mu\text{-}S)_2(pdt)_2]$, ($(Et_4N)_2$[**7**]), to side-coordinate copper(I) through the nitrogen atoms contained in the 2,3-pyrazinedithiolate ligand[17,18] was also explored. Reaction between $[Mo_2O_2(\mu\text{-}S)_2(pdt)_2]^{2-}$ and 2 equivalents of CuBr in acetonitrile solution afforded the precipitation of a dark powder, insoluble in common organic solvents. All attempts to fully characterize the reaction product have to date been unsuccessful.

The reactivity of $[M_2S_2(\mu\text{-}S)_2(pdt)_2]^{2-}$, (M = Mo; [**6**]$^{2-}$, or W; [**8**]$^{2-}$), towards transition metals in order to obtain cubane-like clusters containing dithiolene ligands was also investigated. For this purpose, $(PPN)_2[M_2S_2(\mu\text{-}S)_2(pdt)_2]$ (M = Mo or W) was reacted with several metal complexes in dichloromethane, as summarized in Scheme 3.9. Copper(I) was used in the form of complex $Cu(PPh_3)_2(dtp)$, (dtp = diethyldithiophosphate).[40] When the compounds $(PPN)_2[M_2S_2(\mu\text{-}S)_2(pdt)_2]$ (M = Mo, W) were allowed to react with 1 or 2 equivalents of $Cu(PPh_3)_2(dtp)$ in dichloromethane under reflux conditions, the expected $M_2Cu_xS_4$ (x = 1 or 2) clusters bearing triphenylphosphine coordinated to the copper(I) atom[39,40] were not obtained, according to ^{31}P-NMR and ESI-MS techniques. Reaction of $(PPN)_2[M_2S_2(\mu\text{-}S)_2(pdt)_2]$ (M = Mo or W) with $FeCl_3$ (4 eq) in dichloromethane at room temperature led to the precipitation of a dark solid, insoluble in common organic solvents.

The reaction outcome between compound $(PPN)_2[M_2S_2(\mu\text{-}S)_2(pdt)_2]$ (M = Mo or W) and $Co_2(CO)_8$ was unexpected. Instead of affording the $M_2Co_2S_4$ cubane complexes,[38] substitution of sulfur by oxygen in the terminal M=S bonds was elucidated from the ESI-MS spectra (see Scheme 3.9). This unusual reactivity of $M_2S_2(\mu\text{-}S_2)$ complexes towards cobalt carbonyl is to the best of our knowledge, unprecedented. Addition of 1.1 equivalents of cobalt carbonyl to a dichloromethane

solution of $(PPN)_2[M_2S_2(\mu\text{-}S)_2(pdt)_2]$ (M = Mo, W) at room temperature replaces the terminal sulfide groups by oxygen, resulting in the formation of the $[M_2O_2(\mu\text{-}S)_2(pdt)_2]^{2-}$ clusters (M = Mo; **[7]**$^{2-}$, or W; **[9]**$^{2-}$). Nevertheless, when 0.5 equivalents of cobalt carbonyl were added, the partial substitution of the terminal sulfur was observed, leading to a mixture of species: $[M_2O_2(\mu\text{-}S)_2(pdt)_2]^{2-}$, $[M_2OS(\mu\text{-}S)_2(pdt)_2]^{2-}$ and $[M_2S_2(\mu\text{-}S)_2(pdt)_2]^{2-}$, where M = Mo or W. Addition of an excess of cobalt carbonyl (> 1.5 eq.) led to the precipitation of dark products, insoluble in common organic solvents. Interestingly, not only cobalt carbonyl was able to oxidize the metal-sulfur bond in the $M_2S_2(\mu\text{-}S)_2$ dinuclear cluster species, but also other metal carbonyl complexes, such as $M(CO)_4(piperidine)_2$ (M = Mo or W).[61] However, reactions between $[M_2S_2(\mu\text{-}S)_2(pdt)_2]^{2-}$ (M = Mo, W) and the latter carbonyl complexes under reflux conditions in CH_2Cl_2 led to the formation of more by-products and resulted in lower yields, as compared to reactions with $Co_2(CO)_8$.

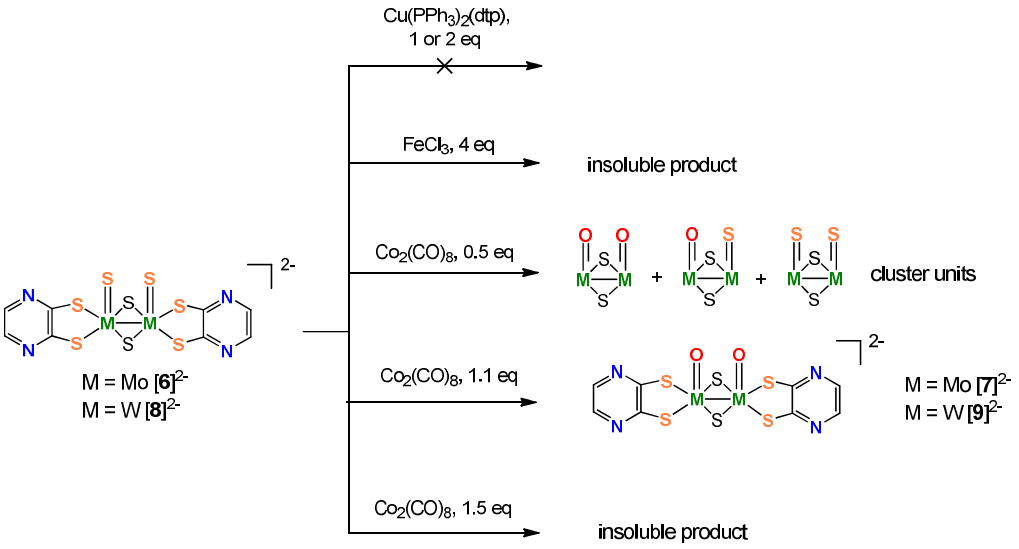

Scheme 3.9. Synthetic approach to the formation of heterometallic cubane-like complexes based on bis(dithiolene) $M_2S_2(\mu\text{-}S)_2$ cluster (M = Mo or W).

3.2.3. CRYSTAL STRUCTURE DESCRIPTION

3.2.3.1. BIS(DITHIOLENE) MOLYBDENUM AND TUNGSTEN CLUSTERS

Single crystals of compounds $(Et_4N)_2$[**4**], $(PPN)_2$[**6**], $(Et_4N)_2$[**7**], $(PPN)_2$[**8**] and $(PPN)_2$[**9**] were obtained by slow (or gas) diffusion methods, and their solid state structures were determined by X-ray diffraction. Figures 3.12 and 3.13 show the ORTEP representations of anions $[\mathbf{4}]^{2-}$ and $[\mathbf{7}]^{2-}$ with the atom numbering scheme. The crystallographic data collection parameters of all structures are given in the Experimental.

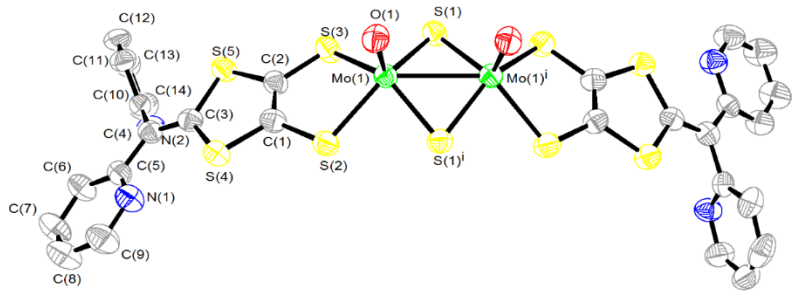

Figure 3.12. ORTEP representation (50 % probability ellipsoids) of the anionic dinuclear cluster $[\mathbf{4}]^{2-}$ with the atom numbering scheme.

All complexes contain the dinuclear cluster core $M_2Q_2(\mu\text{-}S)_2$, (M = Mo or W; Q = O or S), in which the two metal centers are connected through two doubly bridged sulfide ligands, and each metal atom is five-coordinated (if the metal-metal interaction is not considered). The remaining positions are occupied by the two sulfur atoms of the dithiolate ligand and a terminal chalcogenide atom (oxygen or sulfur) in a square pyramidal environment. The chalcogenide atoms of these cluster complexes are in a *syn* configuration. For all compounds, the metal atoms are located between 0.70 and 0.73 Å above the approximate square plane defined by the bridging chalcogenides and the sulfur atoms in the dithiolate ligand. Consequently, this

distance value remains relatively unchanged regardless of the nature of the metal, the dithiolene ligand, or the presence of M=S terminal bonds instead of M=O bonds.

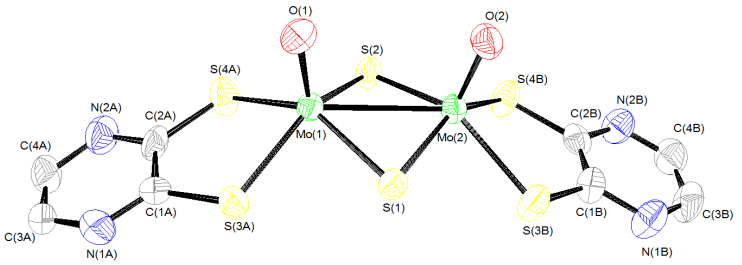

Figure 3.13. ORTEP representation (50 % probability ellipsoids) of the anionic dinuclear cluster [**7**]$^{2-}$ with the atom numbering scheme.

The arrangement of atoms described herein is typical for dinuclear clusters of general formula $M_2X_2(\mu\text{-}Q)_2L_2$, (M = Mo or W; X = O, S, or Se; Q = S or Se), in which L represents a variety of terminal ligands such as dithiocarbamates, maleonitriledithiolate, dithiophosphates, dithiolates, disulfide ligands or polyselenides.[14,46,62–67] Table 3.2 shows a list of selected bond lengths and angles for structures $(Et_4N)_2$[**4**], $(PPN)_2$[**6**], $(Et_4N)_2$[**7**], $(PPN)_2$[**8**] and $(PPN)_2$[**9**] together with those of other dinuclear complexes containing $M_2Q_2(\mu\text{-}S)_2$ (Q = O or S) cluster cores and dithiolene ligands. As can be seen in the Experimental Section, the cluster anions [**6**]$^{2-}$, [**8**]$^{2-}$ and [**9**]$^{2-}$, containing the ligand pdt, have similar structures to that of cluster [**7**]$^{2-}$. A dichloromethane molecule was found co-crystallized with clusters $(PPN)_2$[**6**] and $(PPN)_2$[**8**], whereas in structure $(PPN)_2$[**9**], two molecules of acetonitrile were observed.

The metal-metal bond distances in these clusters are consistent with those of an oxidation state of +5 for the metal, and the presence of a single metal-metal bond. For all complexes the metal-metal bond distances remain unchanged upon substitution of molybdenum by tungsten, and have a value of *ca.* 2.85 Å. Replacing molybdenum by tungsten, as also changing the outer ligands in $M_2Q_2(\mu\text{-}S)_2$ (Q = O or S) cluster complexes leaves the M-(μ-S) bond lengths unchanged, with a value of

ca. 2.33 Å. The metal-ligand distances (*ca.* 2.43 Å) do not vary significantly along the series of complexes, either. As expected, the most significant difference in bond length values is observed in terminal M=Q bonds (Q = O or S) when oxygen is replaced by sulfur, or *vice versa*. For instance, the M=S bond distances in cluster $(PPN)_2$[**8**] decrease by a factor of 0.40 upon replacement of sulfur by oxygen. In addition, the M=O bond lengths are slightly larger for the tungsten derivatives. This tendency is not unprecedented.[46]

Table 3.2. Selected average bond distances (Å) and angles (º) for clusters $(Et_4N)_2$[**4**], $(PPN)_2$[**6**], $(Et_4N)_2$[**7**], $(PPN)_2$[**8**] and $(PPN)_2$[**9**], and comparison with similar complexes (standard deviations are given in parentheses).

Cluster	M-M	M-(μ-S)	M=Q[a]	M-S_{ligand}	Π[b]	θ[c]
$(Et_4N)_2$[**4**]	2.8435(9)	2.3273(14)	1.687(3)	2.4315(14)	141.8	17.7
$(PPN)_2$[**6**]	2.8531(4)	2.3204(10)	2.1198(2)	2.4139(10)	148.4	19.6
$(Et_4N)_2$[**7**]	2.8622(9)	2.3258(2)	1.680(6)	2.4283(2)	146.1	19.1
$(PPN)_2$[**8**]	2.8504(2)	2.3278(9)	2.1344(9)	2.4115(9)	149.0	19.8
$(PPN)_2$[**9**]	2.84137(19)	2.3315(8)	1.737(3)	2.4183(8)	148.7	19.4
$(Bu_4N)_2[Mo_2O_2(\mu\text{-}S)_2(dmit)_2]$[46]	2.822(12)	2.316(2)	1.658(3)	2.432(2)	143.4	20.1
$(Bu_4N)_2[W_2O_2(\mu\text{-}S)_2(dmit)_2]$[46]	2.825(2)	2.323(6)	1.788(14)	2.432(6)	141.8	18.9
$(PPN)_2[W_2S_2(\mu\text{-}S)_2(edt)_2]$[36]	2.862(1)	2.328(2)	2.144(2)	2.404(2)	148.9	23.8

[a] Q = O or S. [b] Dihedral angle between the two M–(μ-S)$_2$ planes. [c] Folding angle in the metallacycle MS_2C_2.

In structure $(Et_4N)_2$[**4**] each pyridine ring connected to C(4) constitutes a plane which deviates from the plane defined by the adjacent pyridine ring. The dihedral angle between the two planes of the six-membered pyridyl moieties is 111.974(5)º. In all cluster complexes, the MS_2C_2 metallacycle is folded along the dithiolene S-S hinge. The folding angles (θ) observed in the salts of all cluster anions,

as also the dihedral angles (Π) between the two M-(μ-S)$_2$ planes are given in Table 3.2. No clear tendencies in the folding angle are observed upon substitution of the metal, terminal chalcogenide, or outer dithiolene ligands. However, counterion exchange in mononuclear titanium and molybdenum complexes containing dithiolene ligands has been reported to dramatically affect the folding angle along the dithiolene S-S hinge.[3] The M-(μ-S)$_2$ dihedral angles also seem to depend on the counterions rather than on the cluster anions themselves, and the larger Π angles in Table 3.2 correspond to the PPN^+ salts.

3.2.3.2. TRIS(DITHIOLENE) MOLYBDENUM CLUSTERS

Single crystals of compounds $(PPN)_2$[**10**] and (Bu_4N)[**11**] were obtained by slow diffusion methods, and the solid structure was determined by X-ray diffraction. The ORTEP representations of the cluster anions [**10**]$^{2-}$ and [**11**]$^{2-}$ with the atom numbering schemes are depicted in Figures 3.14 and 3.15, respectively.

Both structures contain an equilateral Mo_3 core capped by an apical μ_3-S^{2-} ligand (S(1) in the figures) which lies above the metallic plane. In addition, three bridging μ-S_2^{2-} groups connect adjacent metal atoms, with three sulfur atoms occupying an equatorial position (S_{eq}, labeled as S(2), S(4), and S(6)) essentially in the Mo_3 plane, and three axial sulfur atoms (S_{ax}, labeled as S(3), S(5) and S(7)) which are located out of the metal plane. The dithiolate groups fill the remaining two positions on the seven-coordinated molybdenum atoms, and are oriented almost perpendicular to the plane defined by the three molybdenum atoms in the Mo_3S_7 cluster core. A dichloromethane molecule was found co-crystallized with cluster (Bu_4N)[**11**].

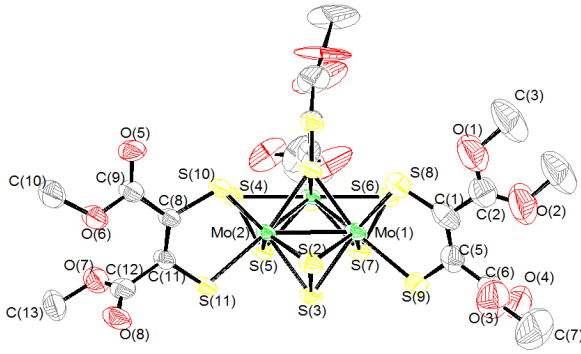

Figure 3.14. ORTEP representation (50 % probability ellipsoids) of the anionic trinuclear cluster [**10**]$^{2-}$ with the atom numbering scheme.

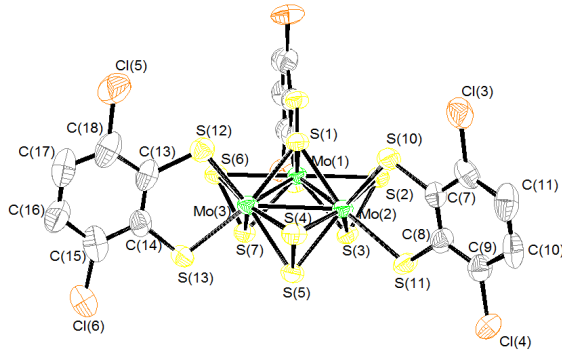

Figure 3.15. ORTEP representation (50 % probability ellipsoids) of the anionic trinuclear cluster [**11**]$^{2-}$ with the atom numbering scheme.

As shown in Table 3.3, the average bond lengths in clusters $(PPN)_2$[**10**] and $(PPN)_2$[**11**] are within the range of those reported for other Mo_3S_7 cluster complexes containing dithiolene ligands.[20,21] The average Mo-Mo bond distances in clusters $(PPN)_2$[**10 – 11**] of *ca.* 2.73 Å, as also the lengths between the molybdenum atoms and the bridging sulfide ligands, remain relatively unchanged regardless of the nature of the counterion and the outer dithiolate ligand.

Table 3.3. Selected average bond lengths (Å) for clusters $(PPN)_2$[**10**] and $(PPN)_2$[**11**], together with those of similar complexes (Q = S or Se).

Cluster	Mo-Mo	Mo-(μ_3-S)	Mo-S_{ax}	Mo-S_{eq}	Mo-Q_{ligand}
$(PPN)_2$[**10**]	2.7744(10)	2.372(2)	2.404(2)	2.529(2)	2.461(2)
$(Bu_4N)_2$[**11**]	2.7797(14)	2.368(4)	2.407(4)	2.523(4)	2.447(4)
$(Bu_4N)_2[Mo_3S_7(dmit)_3]$[20]	2.765(2)	2.367(3)	2.407(3)	2.508(4)	2.477(3)
$(Bu_4N)_2[Mo_3S_7(bdt)_3]$[21]	2.7859(8)	2.364(2)	2.415(2)	2.520(2)	2.466(2)
$(PPh_4)_2[Mo_3S_7(dmid)_3]$[21]	2.777(2)	2.376(3)	2.415(5)	2.514(5)	2.479(4)
$(Bu_4N)_2[Mo_3S_7(dsit)_3]$[21]	2.761(2)	2.373(4)	2.417(4)	2.511(4)	2.607(2)
$Mo_3S_7(dmit)_3$ [20]	2.772(3)	2.380(1)	2.413(5)	2.511(5)	2.476(4)

It is also worth remarking the existence of short S···H intermolecular contacts in the solid structure of complex $(Bu_4N)_2$[**11**], as shown in Figure 3.16. These contacts (2.838 – 2.961 Å) are given between two sulfide atoms in the cluster core (S3 and S5), a sulfur atom in the dithiolate (S11), and a hydrogen atom in the Cl_2bdt ligand contained in a neighboring cluster anion. For compound $(PPN)_2$[**10**], only intermolecular interactions between the cluster anion [**10**]$^{2-}$ and the phenyl groups contained in the PPN^+ counterion were observed. Intermolecular interactions between dithiolate Mo_3S_7 cluster units are not unprecedented.[20,56]

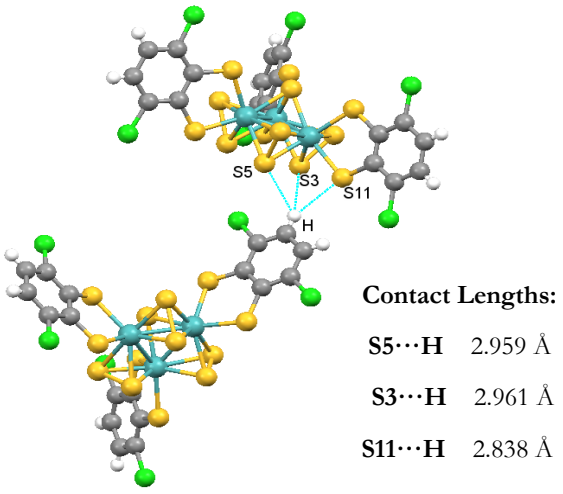

Figure 3.16. Crystal packing in structure $(Bu_4N)_2$[**11**] showing the intermolecular interactions between neighboring cluster anions.

3.3. CONCLUSIONS

A series of $M_2Q_2(\mu\text{-}S)_2$-based (M = Mo or W, Q = O or S) cluster complexes containing dithiolene ligands have been prepared. The ligands 2-bis-(2-pyridyl)methylene-1,3-dithiolene ($BPyDTS_2$) and 2,3-pyrazinedithiolate (pdt) have been employed for the coordination to these dinuclear units, resulting in the clusters anions [**4**]$^{2-}$, and [**6 – 9**]$^{2-}$, respectively. Reaction between compound [**4**]$^{2-}$ and $Re(CO)_5Cl$ affords the discrete heterometallic cluster [**5**]$^{2-}$, which represents to the best of our knowledge the first example of a discrete heteronuclear complex with two metal atoms (rhenium) connected to a molybdenum dinuclear cluster unit through a bridging ligand. The luminescence behavior of complexes [**4**]$^{2-}$ and [**5**]$^{2-}$ will be discussed in a subsequent chapter.

The reactivity of complexes [**6 – 9**]$^{2-}$ towards transition metal complexes to afford cubane-like clusters of formula $M_2M'_2S_4$ was also investigated. Surprisingly, the reaction of clusters $[M_2S_2(\mu\text{-}S)_2(pdt)]^{2-}$ (M = Mo or W) with metal carbonyls affords the substitution of the terminal sulfur atoms by oxygen, resulting in the formation of M=O bonds.

A series of trinuclear Mo_3S_7 clusters containing dithiolene ligands has also been prepared by using zinc dithiolene complexes as hidden forms of dithiolates. The resulting cluster complexes $(PPN)_2$[**10**] and $(Bu_4N)_2$[**11**] were obtained in high yields, and their electrochemical properties were investigated. Complex $(PPN)_2$[**10**] shows three quasi-reversible oxidation waves at easily accessible potentials in dichloromethane solution. The crystal packing in compound $(Bu_4N)_2$[**11**] reveals the existence of intermolecular interactions between neighboring cluster anions.

3.4. REFERENCES

(1) Eisenberg, R.; Gray, H. B. *Inorg. Chem.* **2011**, *50*, 9741–9751.

(2) Stielfel, E. I. Dithiolene Chemistry. *Progress in Inorganic Chemistry*, 2004, *52*.

(3) Fourmigué, M. *Acc. Chem. Res.* **2004**, *37*, 179–186.

(4) Robertson, N.; Cronin, L. *Coord. Chem. Rev.* **2002**, *227*, 93–127.

(5) Rabaça, S.; Almeida, M. *Coord. Chem. Rev.* **2010**, *254*, 1493–1508.

(6) Baudron, S. A.; Hosseini, M. W.; Kyritsakas, N.; Kurmoo, M. *Dalton Trans.* **2007**, 1129–1139.

(7) Zhong, Z. J.; Matsumoto, N.; Okawa, H.; Kida, S. *J. Chem. Soc. Dalt. Trans.* **1989**, 2095.

(8) Sun, Y. M.; Dong, F. Y.; Dou, J. M.; Li, D. C.; Gao, X. K.; Wang, D. Q. *J. Inorg. Organomet. Polym. Mater.* **2006**, *16*, 61–67.

(9) Liu, W.; Wang, R.; Zhou, X. H.; Zuo, J. L.; You, X. Z. *Organometallics* **2008**, *27*, 126–134.

(10) Cardinaels, T.; Ramaekers, J.; Nockemann, P.; Driesen, K.; Van Hecke, K.; Van Meervelt, L.; Lei, S.; De Feyter, S.; Guillon, D.; Donnio, B.; Binnemans, K. *Chem. Mater.* **2008**, *20*, 1278–1291.

(11) Gabrielsson, A.; Hartl, F.; Zhang, H.; Smith, J. R. L.; Towrie, M.; Vlček, A.; Perutz, R. N. *J. Am. Chem. Soc.* **2006**, *128*, 4253–4266.

(12) Wei, L.; Babich, J. W.; Ouellette, W.; Zubieta, J. *Inorg. Chem.* **2006**, *45*, 3057–3066.

(13) Yam, V. W.-W.; Ko, C.-C.; Zhu, N. *J. Am. Chem. Soc.* **2004**, *126*, 12734–12735.

(14) Ribas, X.; Dias, J. C.; Morgado, J.; Wurst, K.; Molins, E.; Ruiz, E.; Almeida, M.; Veciana, J.; Rovira, C. *Chem. - A Eur. J.* **2004**, *10*, 1691–1704.

(15) Ribas, X.; Dias, J.; Morgado, J.; Wurst, K.; Almeida, M.; Veciana, J.; Rovira, C. *CrystEngComm* **2002**, *4*, 564.

(16) Ribas, X.; Dias, J. C.; Morgado, J.; Wurst, K.; Santos, I. C.; Almeida, M.; Vidal-Gancedo, J.; Veciana, J.; Rovira, C. *Inorg. Chem.* **2004**, *43*, 3631–3641.

(17) Kobayashi, Y.; Jacobs, B.; Allendorf, M. D.; Long, J. R. *Chem. Mater.* **2010**, *22*, 4120–4122.

(18) Takaishi, S.; Hosoda, M.; Kajiwara, T.; Miyasaka, H.; Yamashita, M.; Nakanishi, Y.; Kitagawa, Y.; Yamaguchi, K.; Kobayashi, A.; Kitagawa, H. *Inorg. Chem.* **2009**, *48*, 9048–9050.

(19) Fedin, V. P.; Sokolov, M. N.; Mironov, Y. V.; Kolesov, B. A.; Tkachev, S. V.; Fedorov, V. Y. *Inorganica Chim. Acta* **1990**, *167*, 39–45.

(20) Llusar, R.; Uriel, S.; Vicent, C.; Clemente-Juan, J. M.; Coronado, E.; Gómez-García, C. J.; Braïda, B.; Canadell, E. *J. Am. Chem. Soc.* **2004**, *126*, 12076–12083.

(21) Llusar, R.; Triguero, S.; Polo, V.; Vicent, C.; Gómez-García, C. J.; Jeannin, O.; Fourmigué, M. *Inorg. Chem.* **2008**, *47*, 9400–9409.

(22) Llusar, R.; Vicent, C. *Coord. Chem. Rev.* **2010**, *254*, 1534–1548.

(23) Gushchin, A. L.; Llusar, R.; Vicent, C.; Abramov, P. A.; Gómez-Garcia, C. J. *Eur. J. Inorg. Chem.* **2013**, *2013*, 2615–2622.

(24) Llusar, R.; Uriel, S. *Eur. J. Inorg. Chem.* **2003**, 1271–1290.

(25) Hernandez-Molina, R.; Sykes, A. G. *Coord. Chem. Rev.* **1999**, *187*, 291–302.

(26) Hernandez-Molina, R.; Sokolov, M. N.; Sykes, A. G. *Acc. Chem. Res.* **2001**, *34*, 223–230.

(27) Rink, B.; Brorson, M.; Scowen, I. J. *Organometallics* **1999**, *18*, 2309–2313.

(28) Herbst, K.; Rink, B.; Dahlenburg, L.; Brorson, M. *Organometallics* **2001**, *20*, 3655–3660.

(29) Herbst, K.; Dahlenburg, L.; Brorson, M. *Inorg. Chem.* **2001**, *40*, 1989–1992.

(30) Curtis, M. D.; Riaz, U.; Curnow, O. J.; Kampf, J. W.; Rheingold, A. L.; Haggerty, B. S. *Organometallics* **1995**, *14*, 5337–5343.

(31) Llusar, R.; Sorribes, I.; Vicent, C. *Inorg. Chem.* **2009**, *48*, 4837–4846.

(32) Feliz, M.; Garriga, J. M.; Llusar, R.; Uriel, S.; Humphrey, M. G.; Lucas, N. T.; Samoc, M.; Luther-Davies, B. *Inorg. Chem.* **2001**, *40*, 6132–6138.

(33) Feliz, M.; Llusar, R.; Uriel, S.; Vicent, C.; Brorson, M.; Herbst, K. *Polyhedron* **2005**, *24*, 1212.

(34) Cohen, S. A.; Stiefel, E. I. *Inorg. Chem.* **1985**, *24*, 4657–4662.

(35) Miller, K. F.; Bruce, A. E.; Corbin, J. L.; Wherland, S.; Stiefel, E. I. *J. Am. Chem. Soc.* **1980**, *102*, 5102–5104.

(36) Pan, W. H.; Chandler, T.; Enemark, J. H.; Stiefel, E. I. *Inorg. Chem.* **1984**, *23*, 4265–4269.

(37) Xu, J.; Qian, J.; Wei, Q.; Hu, N.; Jin, Z.; Wei, G. *Inorganica Chim. Acta* **1989**, *164*, 55–58.

(38) Halbert, T. R.; Cohen, S. A.; Stiefel, E. I. *Organometallics* **1985**, *4*, 1689–1690.

(39) Zhu, N.; Zheng, Y.; Wu, X. *Inorg. Chem.* **1990**, *29*, 2705–2707.

(40) Zhu, N.; Zheng, Y.; Wu, X. *Polyhedron* **1991**, *10*, 2743–2755.

(41) Nianyong, Z.; Yifan, Z.; Xintao, W. *J. Chem. Soc. Chem. Commun.* **1990**, 780.

(42) Wu, J.; Zhu, N.; Du, S.; Wu, X.; Lu, J. *Inorganica Chim. Acta* **1991**, *185*, 181–185.

(43) Yifan, Z.; Huqiang, Z.; Xintao, W.; Jiaxi, L. *Transit. Met. Chem.* **1989**, *14*, 161–164.

(44) Zhan, H.; Zheng, Y.; Wu, X.; Lu, J. *Inorganica Chim. Acta* **1989**, *156*, 277–280.

(45) Wu, X.; Lu, S.; Zu, L.; Wu, Q.; Lu, J. *Inorganica Chim. Acta* **1987**, *133*, 39–42.

(46) Llusar, R.; Triguero, S.; Vicent, C.; Sokolov, M. N.; Domercq, B.; Fourmigué, M. *Inorg. Chem.* **2005**, *44*, 8937–8946.

(47) Coucouvanis, D.; Toupadakis, A.; Hadjikyriacou, A. *Inorg. Chem.* **1988**, *27*, 3272–3273.

(48) Kumasaki, M.; Tanaka, H.; Kobayashi, A. *J. Mater. Chem.* **1998**, *8*, 301–307.

(49) Chesneau, B.; Passelande, A.; Hudhomme, P. *Org. Lett.* **2009**, *11*, 649–652.

(50) Pan, W. H.; Leonowicz, M. E.; Stiefel, E. I. *Inorg. Chem.* **1983**, *22*, 672–678.

(51) Saxena, R.; Jain, M.; Mittal, M. *Aust. J. Chem.* **1968**, *21*, 91.

(52) Begum, A.; Moula, G.; Sarkar, S. *Chemistry* **2010**, *16*, 12324–12327.

(53) Galoppini, E. *Coord. Chem. Rev.* **2004**, *248*, 1283–1297.

(54) Parg, R. P.; Kilburn, J. D.; Petty, M. C.; Pearson, C.; Ryan, T. G. *Synthesis.* **1994**, *1994*, 613–618.

(55) Muller, A.; Jostes, R.; Jaegermann, W.; Bhattacharyya, R. G. *Inorganica Chim. Acta* **1980**, *41*, 259–263.

(56) Garriga, J. M.; Llusar, R.; Uriel, S.; Vicent, C.; Usher, A. J.; Lucas, N. T.; Humphrey, M. G.; Samoc, M. *Dalt. Trans.* **2003**, 4546–4551.

(57) Alberola, A.; Llusar, R.; Triguero, S.; Vicent, C.; Sokolov, M. N.; Gómez-García, C. *J. Mater. Chem.* **2007**, *17*, 3440–3450.

(58) Xiong, J.; Sun, L.; Kang, L. C.; Liu, W.; Zheng, Y. X.; Zuo, J. L.; You, X. Z. *Inorganica Chim. Acta* **2011**, *376*, 36–43.

(59) Wrighton, M.; Morse, D. L. *J. Am. Chem. Soc.* **1974**, *96*, 998–1003.

(60) Kubas, J. *Inorg. Synth.* **1990**, *28*, 68–70.

(61) Darensbourg, D. J.; Kump, R. L. *Inorg. Chem.* **1978**, *17*, 2680–2682.

(62) Gelder, J. I.; Enemark, J. H. *Inorg. Chem.* **1976**, *15*, 1839–1843.

(63) Howlader, N. C.; Haight, G. P.; Hambley, T. W.; Snow, M. R.; Lawrance, G. A. *Inorg. Chem.* **1984**, *23*, 1811–1815.

(64) Wardle, R. W. M.; Bhaduri, S.; Chau, C. N.; Ibers, J. A. *Inorg. Chem.* **1988**, *27*, 1747–1755.

(65) Lu, Y. J.; Ansari, M. A.; Ibers, J. A. *Inorg. Chem.* **1989**, *28*, 4049–4050.

(66) Drake, J. E.; Mislankar, A. G.; Ratnani, R. *Inorg. Chem.* **1996**, *35*, 2665–2673.

(67) Dessapt, R.; Simonnet-Jegat, C.; Marrot, J.; Secheresse, F. *Inorg. Chem.* **2001**, *40*, 4072–4074.

4

HETEROLEPTIC TRINUCLEAR MOLYBDENUM CLUSTER COMPLEXES CONTAINING DIIMINE LIGANDS

"One of the ways of stopping science would be only to do experiments in the region where you know the law. But experimenters search most diligently, and with the greatest effort, in exactly those places where it seems most likely that we can prove our theories wrong. In other words we are trying to prove ourselves wrong as quickly as possible, because only in that way can we find progress."

Richard P. Feynman, *The Character of Physical Law*

4.1. INTRODUCTION

4.1.1. APLICATIONS OF COMPLEXES CONTAINING DIIMINE LIGANDS

A great diversity of transition metal complexes reported in the literature contain diimine ligands such as phenanthroline and bipyridine derivatives (see Figure 4.1). These complexes have a great potential due to the phyisicochemical properties that can emerge. Their non-innocent redox character, as well as their ability to induce metal ligand charge transfers are the most notable features of complexes containing phenanthroline- and bipyridine-type ligands.[1,2] In particular, ruthenium bipyridyl complexes are characterized by their broad absorption spectra, long-lived excited-state lifetimes and good electrochemical stability. All these features make such complexes suitable in areas such as photocatalysis and photovoltaic cells.[3,4]

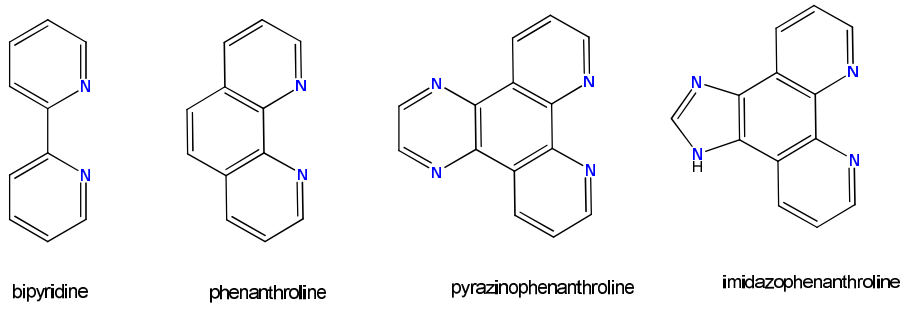

Figure 4.1. Examples of diimine ligands that have been coordinated to metal complexes.

Ruthenium(III) and iridium(III) polypyridyl complexes have been widely used as photoredox catalysts in a number of organic reactions which include the intra- and intermolecular addition of alkyl radicals to unsaturated carbon-carbon bonds.[5] One example of this type of reaction is the visible-light mediated halogenation of alcohols using $[Ru(bpy)_3]Cl_2$ as a catalyst.[6] The manganese complexes *cis*-$[MnL_2Cl_2]$ (L = 2,2'-bipyridine or 1,10-phenanthroline) have also been reported to efficiently

catalyze the disproportionation of hydrogen peroxide: $2H_2O_2 \rightarrow O_2 + 2H_2O$, an important reaction in cell detoxification.[7]

Ruthenium complexes containing bipyridyl ligands have been extensively used in the visible-light-driven water splitting reaction when anchored to semiconductor oxides, such as TiO_2.[3] In order to ensure a good anchoring, several functional groups have been appended to bipyridine and phenanthroline ligands, being phosphonic acids ($P(O)(OH)_2$), and carboxylic acids (COOH) the most common.[8] In addition, ruthenium complexes containing functionalized bipyridyl ligands have also been used in dye-sensitized photovoltaic cells.[4] In particular, complex $(Bu_4N)_2[Ru(dcbpy)_2(NCS)_2]$, (dcbpy = 2,2'-bipyridine-4,4'-dicarboxylic acid), has been reported to be an outstanding solar light harvester and charge-transfer sensitizer.[9]

Ruthenium is not the only metal employed for photocatalytic water splitting. In the recent past, Eisenberg and co-workers have reported that heteroleptic platinum(II) complexes, containing both diimine and dithiolene ligands, act as efficient catalysts for the reductive side of the water splitting reaction.[10] Representative examples include Pt(dcbpy)(met), (dcbpy = 2,2'-bipyridine-4,4'-dicarboxylic acid; met = *cis*-1,2-dicarbomethoxyethylene-1,2-dithiolate), and Pt(dcbpy)(bdt), (bdt = 1,2-benzenedithiol), depicted in Figure 4.2. Similar heteroleptic platinum(II) complexes have been employed as photosensitizers in TiO_2-based solar cells, showing conversion efficiencies close to 2.5 %.[11]

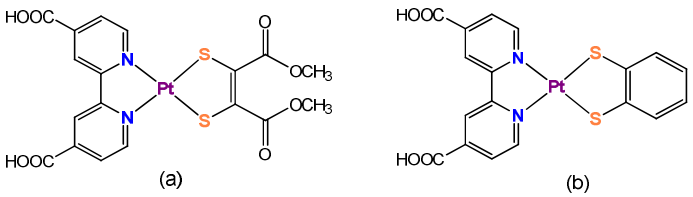

Figure 4.2. Molecular structure of complexes Pt(dcbpy)(met); (a) and Pt(dcbpy)(bdt); (b), reported by Eisenberg *et al.*

Transition metal complexes containing diimine ligands also find applications in Optics. In particular, heteroleptic nickel(II) complexes containing 1,10-phenanthroline and imidizaphenanthroline derivatives have been reported to exhibit third-order optical nonlinearities.[12] The luminescence and anion sensing properties of complexes derivatized with imidazophenanthroline-like ligands have also been investigated.[13] Finally, functionalization of imidazophenanthroline ligands with long alkyloxy chains has been explored with a view to the preparation of luminescent liquid crystals based on transition metal complexes.[14]

Regarding trinuclear clusters, a judicious choice of outer ligands in $M_3(\mu_3\text{-}Q)(\mu\text{-}Q_2)_3$ units (M = Mo or W; Q = S or Se) has resulted in homoleptic molybdenum and tungsten cluster chalcogenides exhibiting interesting physicochemical properties. Among all reported homoleptic M_3Q_7 complexes, to the best of our knowledge there are only two examples of M_3Se_7 clusters (M = Mo or W) functionalized with phenanthroline ligands.[15,16] As shown in Scheme 4.1, these complexes of formula $[M_3Se_7(phen)_3]Br_4$ (M = Mo or W; phen = 1,10-phenanthroline) were prepared in *ca.* 40 – 60 % yields by the solid state reaction between the $\{M_3Se_7Br_4\}_n$ coordination polymers and an excess of 1,10-phenanthroline at 250 ºC. Despite the potential of these systems, their physicochemical properties remain unexplored.

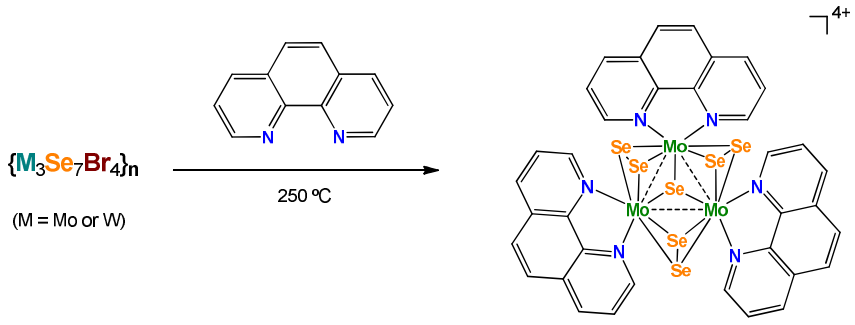

Scheme 4.1. Synthesis of $[M_3Se_7(phen)_3]^{4+}$ complexes (M = Mo or W).

Some examples of applications that result from homoleptic Mo_3S_7 complexes include non-linear optics,[17] magnetic conductivity,[18–21] or catalytic activity in the hydrogen evolution reaction (HER).[22] For instance, cluster $(Bu_4N)_2[Mo_3S_7(SCN)_6]$ is an efficient optical limiter.[17] Compound $Mo_3S_7(dmit)_3$, (dmit = 1,3-dithiole-2-thione-4,5-dithiolate), is a paramagnetic single-molecule molecular conductor which presents multiple sulfur-sulfur intermolecular contacts.[21] Finally, the $(NH_4)_2[Mo_3S_7(S_2)_3]$ cluster, bearing active sites that mimic those of MoS_2 nanomaterials, is a low-cost alternative to precious metal catalysts which efficiently electrocatalyzes the generation of hydrogen from water when adsorbed onto graphite surfaces.[22] Interesting properties have also emerged from functionalized M_3Q_4 cluster complexes (M = Mo or W; Q = S or Se), although these systems are not the object of study in the present thesis.[23–25]

4.1.2. NON-BONDING INTERACTIONS IN TRINUCLEAR MOLYBDENUM CLUSTERS

The crystal structure of Mo_3S_7 complexes is illustrated in Figure 4.3 for the $[Mo_3S_7Br_6]^{2-}$ cluster anion, a widely used starting material.[26] In trinuclear cluster chalcogenides containing the Mo_3S_7 core, the metal atoms are arranged in an equilateral triangle, which is capped by one apical μ_3-S^{2-} ligand (S_{ap} in Fig. 4.3). Additionally, the molybdenum(IV) ions are bridged by S_2^{2-} ligands, which results in a C_{3v} symmetry for the cluster core. The μ-S_2^{2-} disulfide bridging ligands are oriented perpendicularly to the Mo_3 triangle. One sulfur atom is lying on the metal plane (equatorial position; S_{eq}), whereas the other occupies an axial position (S_{ax}), out of the triangular metal plane. The coordination sphere of the molybdenum atoms is completed by peripheral ligands, which occupy *cis* and *trans* positions relative to the apical μ_3-S^{2-} ligand. The occupation of such coordination sites by ligands to afford homoleptic Mo_3S_7 clusters was discussed in the previous section.

A further remarkable feature of Mo_3S_7 systems is their ability to bind different anions to the sulfur atoms occupying axial positions (S_{ax}), owing to their electrophilic character.[27] Over the past 25 years, a great number of examples have been reported in which the axial sulfur atoms in Mo_3S_7 units are found to interact with a variety of anions and atoms. The distances of these $S_{ax}\cdots X$ contacts are smaller than the sum of the van der Waals radii of the involved atoms, and the three $S_{ax}\cdots X$ contacts present similar length values. As will be discussed later, these non-bonding interactions play a significant role in the formation of crystal structures, and they are crucial to understand the results presented in this chapter.

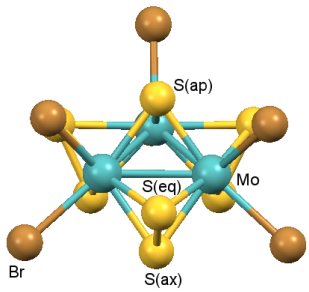

Figure 4.3. Crystal structure of the $[Mo_3S_7Br_6]^{2-}$ cluster anion.

Some examples of counterions which are known to interact with the axial sulfur atoms in Mo_3S_7 complexes include halides,[28–30] perchlorates,[31] nitrates,[31] sulfates,[31] sulfides[32] and dithiocarbamates.[30] The formation of anionic aggregates is clearly exemplified in the $[Mo_3S_7(dtc)_3]^+$ cluster cation (dtc = diethyldithiocarbamate), as summarized in Scheme 4.2. Reaction between the $[Mo_3S_7Br_6]^{2-}$ cluster and Na(dtc) afforded a solid identified as the $[Mo_3S_7(dtc)_3]\cdot Br$ aggregate by X-ray studies.[28] Under an excess of Na(dtc), the $[Mo_3S_7(dtc)_3]\cdot$dtc aggregate was prepared.[30] Compounds $[Mo_3S_7(dtc)_3]\cdot ClO_4$ and $[Mo_3S_7(dtc)_3]\cdot NO_3$ were obtained from cluster $[Mo_3S_7(dtc)_3]\cdot Br$ by counterion exchange on a Dowex column.[31] Replacing the Br^- ion in cluster $[Mo_3S_7(dtc)_3]\cdot Br$ by I^- resulted in a mixture of bromide and iodide

adducts.[31] Heating $[Mo_3S_7(dtc)_3]\cdot NO_3$ in DMF resulted in the formation of the tetrameric complex $[Mo_3S_7(dtc)_3]_4\cdot(SO_4)_2$, as revealed by X-ray structural determination.[31] The source of the sulfate anion is unclear in the latter case. The dimeric compound $[Mo_3S_7(dtc)_3]_2\cdot S$, and the chloride aggregate $[Mo_3S_7(dtc)_3]\cdot Cl$ were achieved by treating cluster $[Mo_3S_7(dtc)_3]\cdot dtc$ with aqueous potassium hydroxide, or by boiling it in 1,2-dichloroethane, respectively.[30,31]

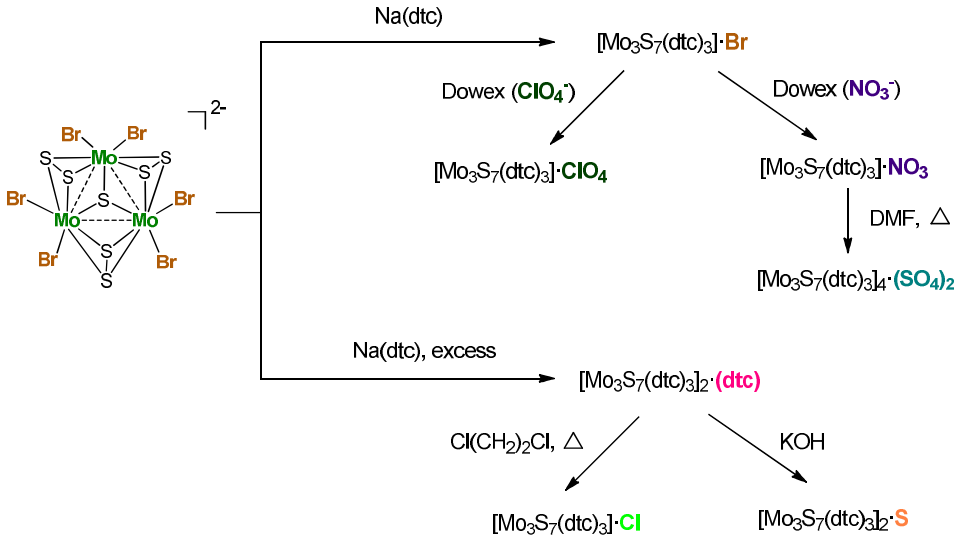

Scheme 4.2. Formation of aggregates in $[Mo_3S_7(dtc)_3]^+$ complexes.

The nature and charge of the counterion play a significant role in the crystal structure of these $[Mo_3S_7(dtc)_3]\cdot X$ aggregates. Structures containing monocharged anions form 1:1 adducts, whereas dimeric or tetrameric aggregates are obtained in the presence of dicharged anions such as sulfide or sulfate, respectively. The formation of 1:1 adducts is illustrated in Figure 4.4a for the $[Mo_3S_7(dtc)_3]\cdot I$ aggregate, which presents average $S_{ax}\cdots I$ contacts of *ca.* 3.30 Å. Figure 4.4b shows the formation of tetrameric aggregates in $[Mo_3S_7(dtc)_3]_4\cdot(SO_4)_2$. In this structure, one doubly charged sulfate anion is bound to four $[Mo_3S_7(dtc)_3]^+$ cluster entities, with $S_{ax}\cdots O$ contacts of

ca. 2.60 Å. This correlation between a higher anion charge and an increased number of interacting cluster entities around it is not a golden rule. In fact, in the structure of $\{[Mo_3S_7(dtp)_3]_4 \cdot I\}(HgI_3)_3\} \cdot 4H_2O$ (dtp = diethyl dithiophosphate), four $[Mo_3S_7(dtp)_3]^+$ cluster units were found to interact with a monocharged iodide anion through the axial sulfur atoms.[29]

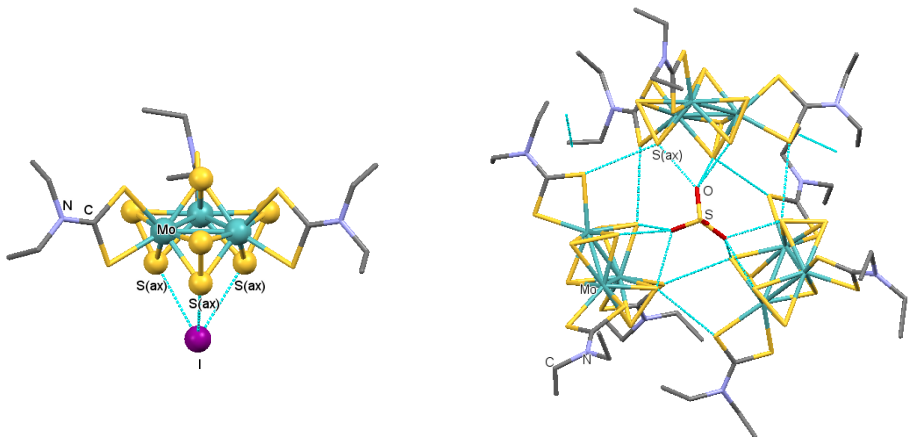

(a) (b)

Figure 4.4. Crystal structure of the $[Mo_3S_7(dtc)_3] \cdot I$ (a) and $[Mo_3S_7(dtc)_3]_4 \cdot (SO_4)_2$ (b), aggregates showing the $S_{ax} \cdots X$ interactions. For the latter, one of the sulfate anions has been omitted for clarity.

The axial sulfide atoms in Mo_3S_7 clusters can also interact with nucleophilic atoms contained in neighboring cluster complexes to afford supramolecular structures.[33–36] For instance, $S_{ax} \cdots S$ contacts (*ca.* 3.02 Å) involving the capping μ_3-S^{2-} ligand are observed in the structure of compound $(NH_4)_2[Mo_3S_7(S_2)_3]$.[37] These interactions result in the formation of a linear polymeric chain of anions. In contrast, the tetraphenylarsonium salt of cluster $[Mo_3S_7(S_2)_3]^{2-}$ does not present analogous non-bonding interactions. The formation of dimeric aggregates has been observed in the crystal structure of compound $(Bu_4N)_2[Mo_3S_7(tdas)_2]$ (tdas = 1,2,5-thiadiazole-3,4-dithiol). As shown in Figure 4.5, the axial sulfur atoms in the $[Mo_3S_7(tdas)_2]^{2-}$ cluster

anion interact with the dithiolene sulfur atoms from a neighboring cluster through two short $S_{ax}\cdots S_{ligand}$ contacts of *ca.* 3.30 and 3.40 Å.

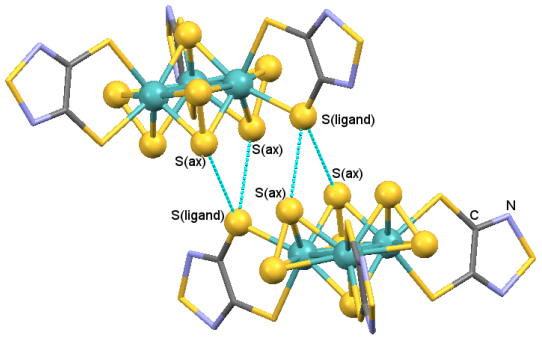

Figure 4.5. Crystal structure of the $\{[Mo_3S_7(tdas)_3]_2\}^{4-}$ dimeric anion.

Finally, non-bonding interactions can also arise between Mo_3S_7 cluster units and radical anions. In particular, the structure of $[Mo_3S_7(dtc)_3]_2(TCNQ)_2$ (dtc = diethyldithiocarbamate; TCNQ = 7,7,8,8-tetracyanoquinodimethane), depicted in Figure 4.6, presents short $S_{ax}\cdots N$ contacts of *ca.* 2.93 Å between the nitrogen atoms of the $TCNQ^-$ anion and the axial sulfur atoms in the $[Mo_3S_7(dtc)_3]^+$ cluster cation.

The $S_{ax}\cdots X$ interactions (X = Br, I…) in these $[Mo_3S_7(dtc)_3]\cdot X$ aggregates has been investigated by Hegetschweiler and co-workers.[31] Raman spectroscopy revealed that the force constants of the S_{eq}-S_{ax} bonds are rather sensitive to the nature of the anions interacting with the sulfur axial atoms. For hard anions, such as ClO_4^- or NO_3^- the stretching vibration frequencies proved to be higher than those for softer nucleophiles, such as I^- and S^{2-}. The decrease in the stretching vibration frequencies has been correlated with an elongation of the S_{eq}-S_{ax} bonds, which results in a higher force constant for the $S_{ax}\cdots X$ interactions, and therefore in a more covalent character for the non-bonding interactions in I^- and S^{2-} adducts, as compared to those of the harder anions ClO_4^- and NO_3^-. Theoretical calculations were used to confirm this interpretation.

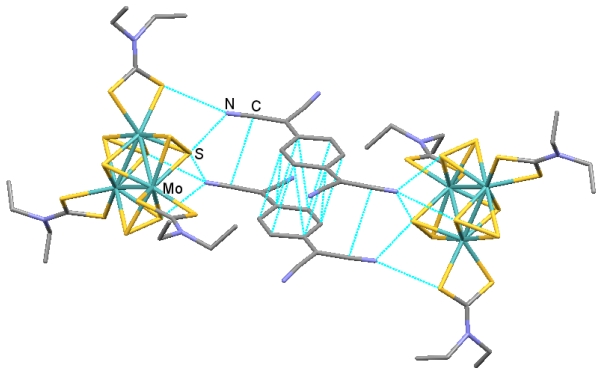

Figure 4.6. Crystal packing of $[Mo_3S_7(dtc)_3]_2(TCNQ)_2$, showing S···N non-bonding contacts.

4.1.3. HETEROLEPTIC TRINUCLEAR MOLYBDENUM CLUSTERS

Despite the large number of homoleptic complexes reported in the literature, the coordination of different ligands in order to afford heteroleptic compounds still remains a non-trivial task in coordination chemistry,[38] and cluster complexes are not an exception. The number of heteroleptic cluster compounds is rather scarce, as compared to their homoleptic analogues, mainly due to the difficulty involved in their synthesis. Attempts to coordinate two or more different ligands to a metal core usually afford mixtures of complexes which are very difficult to separate by traditional purification methods.[39]

The chemistry of transition metal clusters containing the $[Mo_3(\mu_3\text{-}S)(\mu_2\text{-}S_2)_3]^{4+}$ triangular core has been extensively developed over the past few decades.[40] Due to the lability of bromide ligands in the $[Mo_3S_7Br_6]^{2-}$ cluster precursor,[26] derivatives containing Mo_3S_7 units are readily accessible by simple ligand substitution reactions. Some examples of homoleptic Mo_3S_7-based cluster complexes contain a variety of charged ligands such as thiocyanate (NCS^-),[41] diethyl dithiocarbamate (dtc^-),[28,31] 8-hydroxyquinoline (oxq^-),[28] 2-thiopyridine (tpy^-),[28] catecholate (cat^{2-}),[28] imidodiphosphinochalcogenido ($[N(QPPh_2)_2]^-$, Q = S, Se),[42] mercapto succinate ($Hmsa^{2-}$),[43] and dithiolate (dt^{2-}),[19–21] among others. Unlike the straightforward

coordination of charged ligands to Mo_3S_7 units (Q = S or Se) to afford homoleptic complexes, the coordination of neutral ligands usually proceeds with great difficulty, and more often than not results in heteroleptic complexes. The formation of homoleptic trisubstituted phenanthroline clusters is exemplified in complex $[M_3Se_7(phen)_3]Br_4$ (M = Mo, W; phen = 1,10-phenanthroline), which was synthesized by a solid state reaction, as shown in Scheme 4.1.[15,16]

To date, only a limited number of heteroleptic Mo_3S_7 complexes have been reported. All known examples result from the partial substitution of chloride or bromide ligands in the $[Mo_3S_7X_6]^{2-}$ (X = Cl or Br) cluster precursors by solvent molecules, such as acetonitrile,[44] dimethylsulfoxide[45] or aniline.[46] These compounds containing labile monodentate ligands are attractive targets for the synthesis of other heteroleptic Mo_3S_7 clusters upon ligand exchange. Nevertheless, to the best of our knowledge the potential of these systems is yet to be explored.

Scheme 4.3 shows the synthetic approach used for the synthesis of heteroleptic Mo_3S_7 complexes. Compound $[Mo_3S_7Cl_6]^{2-}$ reacts with acetonitrile at 120 ºC leading to substitution of one chloride ligand by an acetonitrile molecule to afford $[Mo_3S_7Cl_5(CH_3CN)]^-$.[44] Crystallization of $[Mo_3S_7Br_6]^{2-}$ in DMSO/benzonitrile mixtures in the presence of $ThBr_4$ afforded compound $[Mo_3S_7Br_5(DMSO)]^-$, in which one bromide ligand in $[Mo_3S_7Br_6]^{2-}$ has been substituted by a dimethylsulfoxide molecule. The $[Mo_3S_7Br_5(DMSO)]^-$ heteroleptic compound was found co-crystallized with the $[Th_2(\mu\text{-}SO_4)_2(DMSO)_{12}]^{4+}$ dinuclear cluster.[45] Finally, reaction of the cluster precursor $[Mo_3S_7Br_6]^{2-}$ with an excess of aniline in hot acetonitrile afforded the heteroleptic complex $[Mo_3S_7(NH_2Ph)_3Br_3]^+$ in moderate yield.[46] It goes without saying that non-bonding interactions between cluster entities and counterions were observed in all the aforementioned heteroleptic complexes.

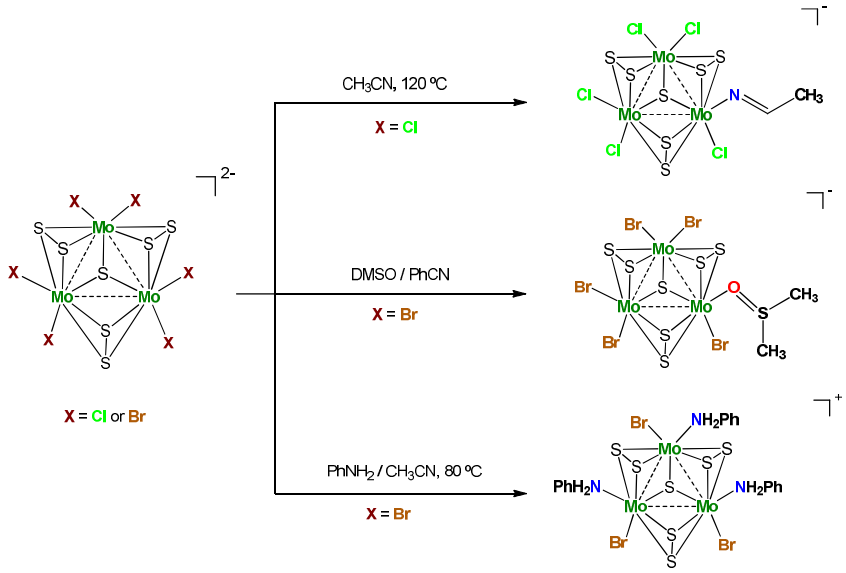

Scheme 4.3. Synthesis of heteroleptic Mo_3S_7 complexes containing neutral organic molecules.

As previously mentioned, a feature of the cluster precursors $[Mo_3S_7X_6]^{2-}$ (X = Cl or Br) is the non-equivalence of the halide ligands, since three of them are *cis* to the μ_3-S capping ligand, while the others are on the opposite side (*trans* position). In heteroleptic Mo_3S_7 complexes derivatized from $[Mo_3S_7X_6]^{2-}$ clusters (X = Cl or Br), the orientation of the neutral ligands relative to the trimetallic plane is unpredictable. In clusters $[Mo_3S_7Cl_5(CH_3CN)]^-$ (Fig. 4.7a) and $[Mo_3S_7Cl_5(DMSO)]^-$, the neutral ligands occupy the *trans* position, whereas in cluster $[Mo_3S_7Br_3(NH_2Ph)_3]^+$ (Fig. 4.7b), the aniline ligands are located in a *cis* position, relative to the apical sulfide ligand S_{ap}.

In this chapter, a series of heteroleptic $Mo_3S_7X_4$(diimine), (X = Cl or Br), complexes have been obtained by reacting bipyridine-, phenanthroline-, pyrazinophenanthroline- and imidazophenanthroline-like ligands (see Figure 4.1) with the $[Mo_3S_7X_6]^{2-}$, (X = Cl or Br)[26] cluster precursors. Further derivatization of these $Mo_3S_7X_4$(diimine) complexes with dithiolates afforded clusters bearing a mixture of diimine and dithiolene ligands. The optical properties, as also the potential

ability of the aforementioned cluster complexes to catalyze the hydrogen evolution reaction will be discussed in subsequent chapters.

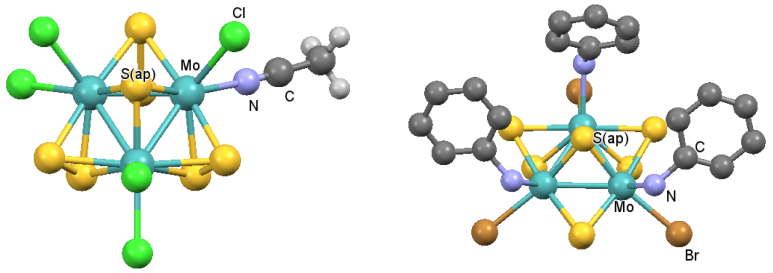

(a) (b)

Figure 4.7. Crystal structure of the heteroleptic cluster complexes $[Mo_3S_7Cl_5(CH_3CN)]^-$ (a) and $[Mo_3S_7Br_3(NH_2Ph)_3]^+$ (b). Hydrogen atoms have been omitted for clarity.

4.2. RESULTS AND DISCUSSION

4.2.1. SYNTHESIS AND CHARACTERIZATION

As mentioned in the Introduction, the lability of the bromide ligands in the $[Mo_3(\mu_3\text{-}S)(\mu_2\text{-}S_2)_3Br_6]^{2-}$ cluster complex[26] has led to the straightforward synthesis of a large number of Mo_3S_7-based homoleptic clusters containing a diversity of ligands.[17,19–21] The coordination of phenanthroline ligands to the Mo_3Se_7 core was explored by Sokolov and co-workers.[15] The trisubstituted $[Mo_3Se_7(phen)_3]^{4+}$ complex was achieved in 63 % yields by the solid state reaction between the $\{Mo_3Se_7Br_4\}_n$ coordination polymer and an excess of 1,10-phenantroline.

Motivated by the interesting properties that can emerge from transition metal complexes containing diimine ligands, such as photocatalysisis,[5,10] luminescence[13,14] and optical nonlinearities,[12] we decided to investigate the coordination of bipyridine, phenanthroline, and related ligands to trinuclear molybdenum clusters using mild reaction conditions. For this purpose we focused on the ligands depicted in Figure 4.8, which can be classified into four different groups, according to their nature:

Bipyridine-like ligands	2,2'-bipyridine (**bpy**)
	4,4'-dimethyl-2,2'-bipyridine (**dmbpy**)
	4,4'-dinonyl-2,2'-bipyridine (**dnbpy**)
	2,2'-bipyridine-4,4'-dicarboxylic acid (**dcbpy**)
	4,4'-dicarbomethoxy-2,2'-bipyridine (**dcmbpy**)

Phenanthroline-like ligands	1,10-phenanthroline (**phen**)
	4-methyl-1,10-phenanthroline (**mphen**)
	5,6-dimethyl-1,10-phenanthroline (**dmphen**)
	3,4,7,8-tetramethyl-1,10-phenanthroline (**tmphen**)
	4,7-diphenyl-1,10-phenanthroline (**BPhen**)

	4,7-dicarbomethoxy-1,10-phenanthroline (**dcmphen**)
Pyrazinophenanthroline-like ligands	Pyrazino[2,3-f][1,10]phenanthroline (**ppl**)
	2,3-dimethoxycarbonylpyrazino[2,3-f][1,10]phenanthroline (**(COOMe)$_2$ppl**)
Imidazophenanthroline-like ligands	1H-Imidazo[4,5-f][1,10]phenanthroline-2-[3,4-bis(dodecyloxy)phenyl] (**IPDOP**)

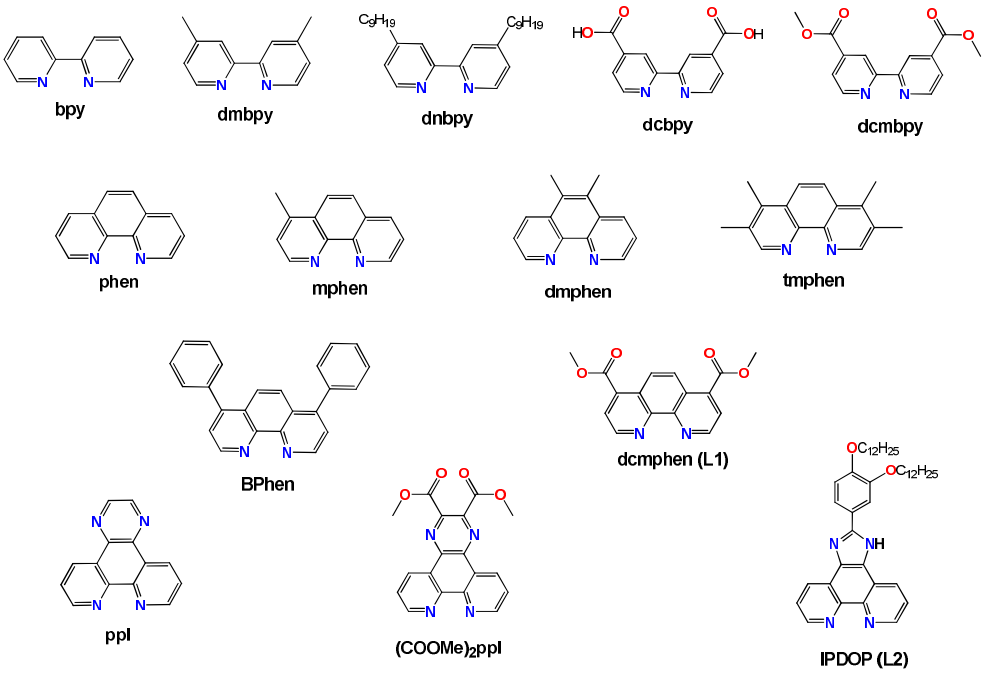

Figure 4.8. Molecular representation of selected diimine ligands.

Most ligands in Figure 4.8 were obtained from commercial sources. The ligands dcbpy and dcmbpy are not widely commercially available, and were therefore prepared according to literature procedures.[47,48] The novel ligands dcmphen (L1) and IPDOP (L2) were obtained by adapting synthetic methods previously reported for similar compounds.[49,50] The $(COOMe)_2$ppl ligand was kindly provided by the Novosibirsk Institute of Organic Chemistry (Russia). The synthetic pathways employed for the preparation of dcbpy, dcmbpy, dcmphen and IPDOP are shown in Schemes 4.4 – 4.6.

The ligand 2,2'-bipyridine-4,4'-dicarboxylic acid (dcbpy) was prepared in 85 % yield by oxidation of commercial 4,4'-dimethyl-2,2'-bipyridine (dmbpy), according to Scheme 4.4.[47] The sterification of dcbpy in methanol catalyzed by sulfuric acid afforded 4,4'-dicarbomethoxy-2,2'-bipyridine (dcmbpy) in 86 % yield.[48] These ligands were characterized by NMR techniques, and their spectra are in good agreement with the reported in the literature.

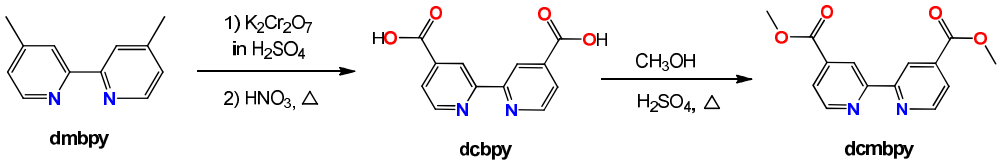

Scheme 4.4. Synthetic routes for the preparation of dcbpy and dcmbpy.

The novel ligand 4,7-dicarbomethoxy-1,10-phenanthroline (dcmphen) was prepared in two steps (see Scheme 4.5). The first step involves the oxidation of commercial 4,7-dimethyl-1,10-phenanthroline (4,7-dmbpy) to afford 1,10-phenanthroline-4,7-dicarboxylic acid (dcphen). All attempts to reproduce the already published reaction conditions for the oxidation of 4,7-dmbpy by nitric acid afforded the desired carboxylic acid in extremely low yields (< 10 %), and abundant emission of NO_2 was observed, presumably due to decomposition of the starting material.[49] Therefore, the reported conditions were modified in order to improve the reaction

yield (see Experimental Section). A decrease in the temperature from 120 ºC to 60 ºC, and an increase in the reaction time from 3 h to 4 h, afforded the dcphen ligand in 58 % yield, which is significantly higher than both the reported (43 %) and the reproduced in our laboratories (less than 10 %). The sterification of dcphen ligand with methanol to afford 4,7-dicarbomethoxy-1,10-phenanthroline (dcmphen) was carried out by adapting the reported procedure for the synthesis of dcmbpy (*vide supra*).[48] The dcmphen ligand was isolated as a white solid in 66 % yields, and it was fully characterized by different techniques to prove its purity. For instance, its ^{1}H-NMR spectrum in deuterated chloroform reveals the presence of three signals in the δ = 8.10 – 9.40 ppm region, corresponding to the aromatic ring, and one single signal at δ = 4.09 ppm, which can be assigned to the hydrogen atoms of the terminal methoxy groups in the ligand.

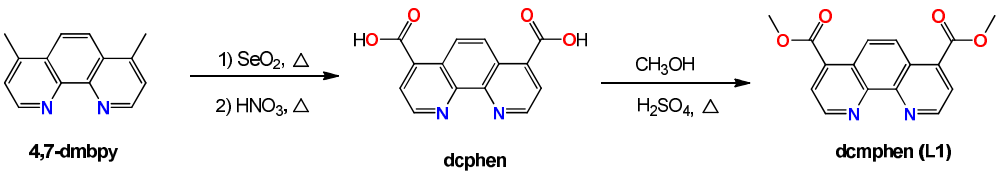

Scheme 4.5. Synthetic pathway for the preparation of dcmphen.

The novel IPDOP ligand was prepared by adapting the procedures described in the literature for similar compounds (see Scheme 4.6).[50] Reaction between 1,10-phenanthroline-5,6-dione (phendione) and 3,4-(didodecyloxy)benzaldehyde in the presence of glacial acetic acid and ammonium acetate afforded the desired imidazophenanthroline ligand as a yellowish solid in moderate yield (58 %). The ^{1}H-NMR spectrum of this compound in deuterated chloroform presents three groups of signals than can be clearly distinguished: a first group at δ = 0.86 – 3.91 ppm, corresponding to the long alkoxy chains, a second group in the δ = 7.06 – 9.23 ppm range, which can be assigned to the C – H aromatic protons, and finally a signal at δ = 14.86 ppm, corresponding to the NH group in the imidazole ring.

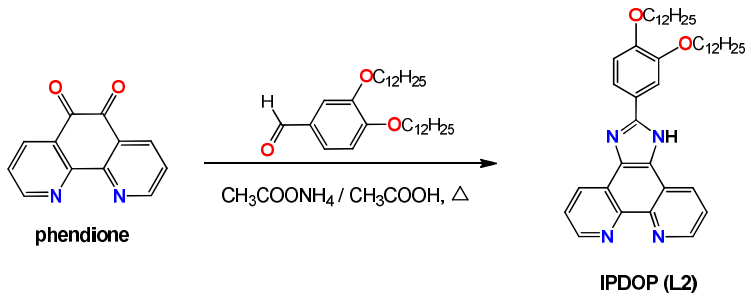

Scheme 4.6. Synthetic route for the preparation of IPDOP.

Coordination of the diimine ligands shown in Figure 4.8 to the Mo_3S_7 unit was carried out starting from the $(Bu_4N)_2[Mo_3S_7X_6]$ (X = Cl or Br) cluster precursors, and following the synthetic approach shown in Scheme 4.7. The starting material $(Bu_4N)_2[Mo_3S_7X_6]$ (X = Cl or Br) was mixed with an excess (3 – 5 equivalents) of the diimine ligand in dichloromethane. The substitution reaction in cluster $(Bu_4N)_2[Mo_3S_7Br_6]$ occurred at room temperature, while reflux conditions were needed to facilitate the substitution of the less labile chloride ligands of $(Bu_4N)_2[Mo_3S_7Cl_6]$. In all cases, color changing from orange to red was observed, due to the substitution of two halide ligands in $[Mo_3S_7X_6]^{2-}$ by the nitrogen atoms in the diimine ligand to afford $Mo_3S_7X_4$(diimine) complexes (X = Cl or Br). It is noteworthy that addition of a larger excess of diimine ligand equally led to the monosubstituted products.

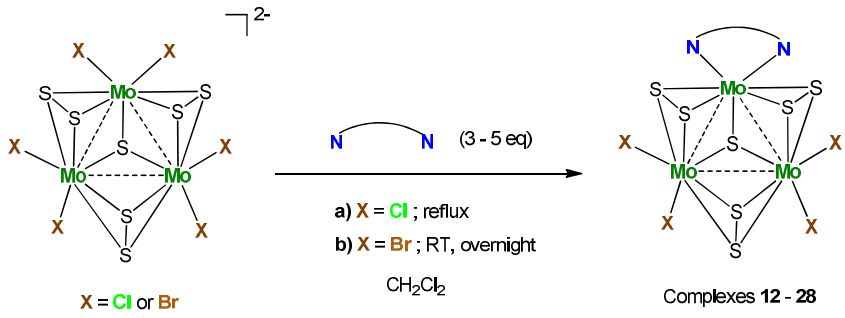

Scheme 4.7. General synthetic pathway for $Mo_3S_7X_4$(diimine) complexes (X = Cl or Br).

For the synthesis of $Mo_3S_7Br_4$(dcmbpy), (**22**), the reaction conditions were slightly modified owing to the particular solubility behavior of the ligand 4,4'-dicarbomethoxy-2,2'-bipyridine (dcmbpy). This ligand resulted to be extremely soluble in hot acetonitrile but exhibited a poor solubility in cold acetonitrile. Therefore, aimed at facilitating the removal of the excess ligand from the reaction mixture, complex $(Bu_4N)_2[Mo_3S_7Br_6]$ was reacted with the dcmbpy ligand in acetonitrile under reflux conditions. A change in the color of the solution (from orange to dark red) was observed after a few hours. Cooling this red solution afforded the complete precipitation of the dcmbpy ligand, which was removed by filtration, and hence the reaction product **22** could be purified in a straightforward fashion. The conditions for the reaction between the analogous ligand 2,2'-bipyridine-4,4'-dicarboxylic acid (dcbpy) and $[Mo_3S_7Br_6]^{2-}$ were also modified due to the low solubility of dcbpy in common organic solvents. Reaction between $[Mo_3S_7Br_6]^{2-}$ and *ca.* 5 equivalents of dcbpy in dimethylformamide at 130 ºC afforded an orange solid which was insoluble even in the most polar solvents, such as dimethylformamide and dimethylsulfoxide. The extremely low solubility of the resulting product precluded its characterization. Nevertheless, the reaction mixture containing the putative $(Bu_4N)[Mo_3S_7Br_4(dcbpy)\cdot Br]$ species (soluble in DMF) was used for the preparation of the dmit derivative (dmit = 1,3-dithiole-2-thione-4,5-dithiolate) of this diimino complex, as detailed in the following section.

In all cases, the reaction mixture was taken to dryness by rotary evaporation, and the solid residue was thoroughly washed with various solvents to afford reddish powders of formula $Mo_3S_7X_4$(diimine), (X = Cl or Br; complexes **12** – **28** in Table 4.1), in moderate to high yields (67 – 98 %). The most intriguing aspect of these $Mo_3S_7X_4$(diimine) complexes is their anomalous solubility behavior. Compounds **12** – **28** were completely soluble in the reaction mixture. However, after completing the purification process, the isolated solids became extremely insoluble in common organic solvents, the only exceptions being complexes **12**, **13** and **23**, which presented

an exceptional solubility in non-polar solvents owing to the long alkyl chains appended to their coordinated diimine ligands. To our astonishment, sonication of compounds **14** – **22** and **24** – **28** in dichloromethane in the presence of an excess of a tetrabutylammonium halide salt (either chloride or bromide) led to the complete dissolution of the cluster species. As will be detailed later in this chapter, toluene diffusion into the aforesaid solutions of complexes afforded red crystals whose X-ray diffraction studies revealed the formation of $[Mo_3S_7X_4(diimine)\cdot X]^-$ aggregates, (X = Cl or Br), containing $S_{ax}\cdots X$ non-bonding interactions between the three axial sulfur atoms in the cluster entity and a halide anion. As already mentioned in the Introduction, the formation of adducts between Mo_3S_7 clusters and halide anions is not unprecedented.[28–30] It is well established that the axial chalcogenide atoms in M_3Q_7 (M = Mo or W, Q = S, Se or Te) cluster complexes possess an electrophilic character, and can therefore interact with a variety of anions.[27,31,51,52]

Table 4.1. List of the $Mo_3S_7X_4(diimine)$ complexes (X = Cl or Br) obtained by reacting $(Bu_4N)_2[Mo_3S_7X_6]$ (X = Cl or Br) with the diimine ligands in Figure 4.8.

Complex	Nº	Complex	Nº
$Mo_3S_7Br_4(IPDOP)$	**12**	$Mo_3S_7Br_4(phen)$	**21**
$Mo_3S_7Cl_4(IPDOP)$	**13**	$Mo_3S_7Br_4(dcmbpy)$	**22**
$Mo_3S_7Br_4(BPhen)$	**14**	$Mo_3S_7Br_4(dnbpy)$	**23**
$Mo_3S_7Cl_4(BPhen)$	**15**	$Mo_3S_7Br_4(dcmphen)$	**24**
$Mo_3S_7Br_4(tmphen)$	**16**	$Mo_3S_7Cl_4(ppl)$	**25**
$Mo_3S_7Cl_4(tmphen)$	**17**	$Mo_3S_7Br_4(ppl)$	**26**
$Mo_3S_7Cl_4(dmbpy)$	**18**	$Mo_3S_7Cl_4(mphen)$	**27**
$Mo_3S_7Br_4(dmbpy)$	**19**	$Mo_3S_7Br_4((COOMe)_2ppl)$	**28**
$Mo_3S_7Br_4(bpy)$	**20**		

The red crystals corresponding to tetrabutylammonium salts of $[(\mathbf{14} – \mathbf{22})\cdot X]^-$ and $[(\mathbf{24} – \mathbf{28})\cdot X]^-$ anionic aggregates, where X = Cl or Br, readily dissolved in

dichloromethane, which contrasts with the insoluble character of the neutral cluster complexes **14** – **22** and **24** – **28**. Electrospray Ionization Mass Spectra revealed the presence of these aggregates in solution with the characteristic isotope pattern. This is illustrated in Figure 4.9 for the [**22**·Br]$^-$ anion, which presents a m/z ratio of 1183.5.

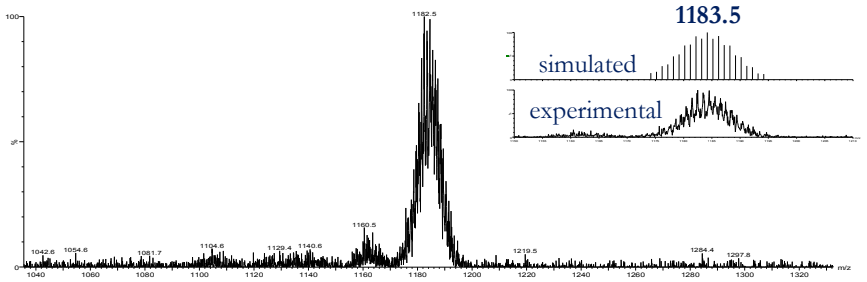

Figure 4.9. ESI-MS spectrum showing the simulated and experimental peaks corresponding to [**22**·Br]$^-$.

The use of Bu_4NCl as halide salts for the solubilization of neutral bromide $Mo_3S_7Br_4$(diimine) complexes led to halide scrambling. For instance, sonication of $Mo_3S_7Br_4$(bpy), (**20**) in dichloromethane in the presence of Bu_4NCl afforded a mixture of species of formulae $[Mo_3S_7Br_2Cl_3(bpy)]^-$, $[Mo_3S_7Br_3Cl_2(bpy)]^-$, $[Mo_3S_7Br_4Cl(bpy)]^-$ and $[Mo_3S_7Br_5(bpy)]^-$, as evidenced by their ESI-MS spectrum (Figure 4.10).

In general terms, these results can be summarized by saying that solubilization of neutral $Mo_3S_7X_4$(diimine) complexes (X = Cl or Br) in common organic solvents can only be achieved through formation of $[Mo_3S_7X_4(diimine)\cdot X]^-$ aggregates in which the halide anions participate in non-bonding interactions with the axial sulfur atoms in these cluster units. The purification process of these neutral clusters presumably breaks the weak $S_{ax}\cdots X$ interactions leading to insoluble powders. As previously mentioned, the only exceptions are the IPDOP derivatives **12** and **13**, and complex **23**, for which the long alkyl chains present in the ligands are responsible for their high solubility in non-polar solvents, even in their neutral forms.

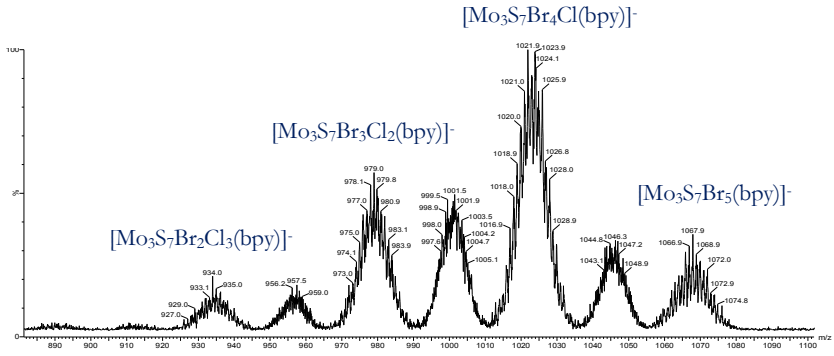

Figure 4.10. ESI-MS spectrum of complex $Mo_3S_7Br_4(bpy)$, (**20**), in the presence of an excess of Bu_4NCl.

Although the neutral character (and in general poor solubility) of the isolated complexes **12** – **28** led to certain difficulties in the characterization process, the reported compounds have been fully characterized by elemental analysis, UV-Vis and ^{1}H-NMR spectroscopies. In addition, with a few exceptions, the crystal structure of the $[Mo_3S_7X_4(diimine)\cdot X]^-$ aggregates (X = Cl or Br) was determined by X-ray structural analysis so that the composition of the neutral $Mo_3S_7X_4(diimine)$ clusters was confirmed. To our dismay all attempts to grow single crystals of compounds **12**, **13** and **23** have to date been unsuccessful due to the presence of long alkyl chains in the diimine ligand, which impede crystal packing, and therefore crystallization. For complex **26**, the obtained crystals did not have enough quality for X-ray diffraction, and hence its structure could not be determined. The mass/charge ratio of the neutral clusters **12** – **28** could not be elucidated from their ESI-MS spectra. Nevertheless, as mentioned earlier this technique was employed to confirm the formation of anionic aggregates when the complexes were crystallized in the presence of Bu_4NX salts (X = Cl or Br). The neutral complexes **12, 13** and **23** could not be elucidated by ESI-MS since they do not tend to form anionic aggregates, and furthermore cannot become ionized under typical electrospray ionization conditions.

The ^{1}H-NMR spectra of the current series of complexes, *i.e.* **12** – **28** were recorded in solution, with the limitation imposed by their low solubility in typical organic solvents. In all cases, the peaks corresponding to the hydrogen atoms adjacent to the chelating nitrogen groups in the ligand appear in their NMR spectra at different chemical shifts owing to the different electronic environment in the *cis* and *trans* positions relative to the capping sulfur atom in the cluster unit. As a representative example, the ^{1}H-NMR spectrum of complex $Mo_3S_7Br_4$(dcmbpy) (**22**; dcmbpy = 4,4'-dicarbomethoxy-2,2'-bipyridine) in deuterated acetonitrile is provided in Figure 4.11. This compound presents a doublet at δ = 4.04 ppm, corresponding to the hydrogen atoms of the terminal methoxy groups in the ligand, and four signals in the aromatic region at δ = 10.18 (1H), 9.68 (1H), 9.02 (2H) and 8.16 (2H) ppm, which can be assigned to the hydrogen atoms in the bipyridine ring, represented as H_a, H_b, H_c and H_d, respectively. As expected, in the free ligand (dcmbpy) only three signals in the aromatic region were observed, corresponding each of them to two protons.

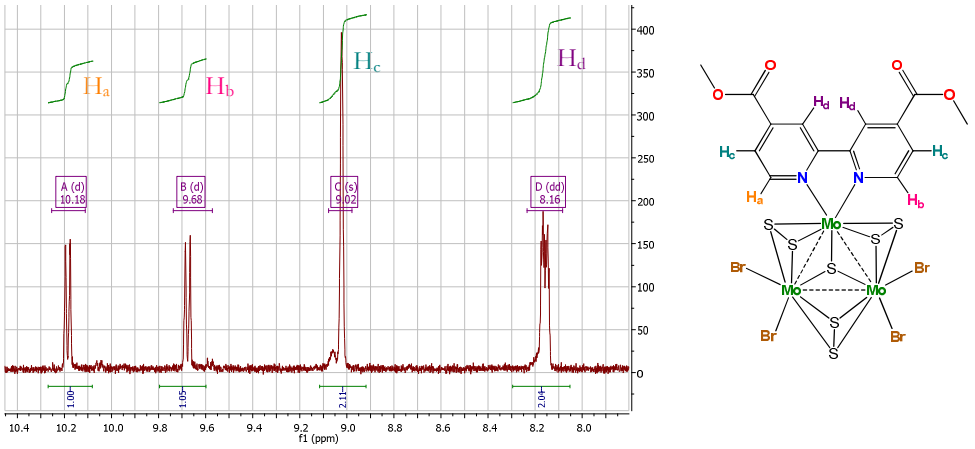

Figure 4.11. ^{1}H-NMR spectrum for **22** in deuterated acetonitrile. The doublet peak at δ = 4.04 ppm has been omitted for clarity.

The UV-Vis spectra of complexes **12** – **28** in dimethylsulfoxide solution reveal the existence of high intensity absorption bands in the UV region, and weaker bands in the 440 – 500 nm range, with ε values of *ca.* 1100 – 3900 M^{-1} cm^{-1}. The solubility behavior of the current series of complexes precluded a profound study of their absorption bands in different solvents. Nevertheless, in the cases where the readily soluble $(Bu_4N)[Mo_3S_7X_4(diimine)\cdot X]$ aggregates (X = Cl, Br) were isolated in high yields, the influence of the solvent on the absorption bands was investigated, and a marked negative solvatochromism was observed in the visible region of the spectra. This solvatochromic behavior is illustrated in Table 4.2 and Figure 4.12 for complex $(Bu_4N)[Mo_3S_7Br_4(dcmphen)\cdot Br]$, ($(Bu_4N)$[**24**·Br]).

The maximum absorption bands for cluster (Bu_4N)[**24**·Br] in various solvents, namely dichloromethane, acetonitrile, dimethylformamide and dimethylsulfoxide, shift towards the blue (hypsochromic shift) upon increasing the solvent polarity. In particular, a shift of *ca.* 44 nm towards shorter wavelength values was registered on proceeding from CH_2Cl_2 to DMSO or DMF (see Table 4.2 for further details). Analogous solvatochromic effects have already been reported in iron(II) complexes containing phenanthroline ligands.[53] More specifically, the solvatochromic shift observed in $Fe(phen)_2(CN)_2$ in acetonitrile and water solutions has been ascribed by DFT calculations to the stabilization of the HOMO orbital as a result of interactions between the cyanide ligands and solvent molecules. Solvatochromism is a very complex phenomenon in which a large number of interactions can play a role. Understanding the nature of the solvatochromic effect observed in $Mo_3S_7X_4(diimine)$ complexes would require complex theoretical calculations.[54] Therefore we are unable to comment further at present.

Table 4.2. UV/Vis absorption data for complex (Bu_4N)[**24**·Br] in different solvents.

Solvent	Polarity Index	Wavelength (nm)	ε ($M^{-1}cm^{-1}$)
CH_2Cl_2	3.1	532	3730
CH_3CN	5.8	493	3653
DMF	6.4	488	2729
DMSO	7.2	488	2995

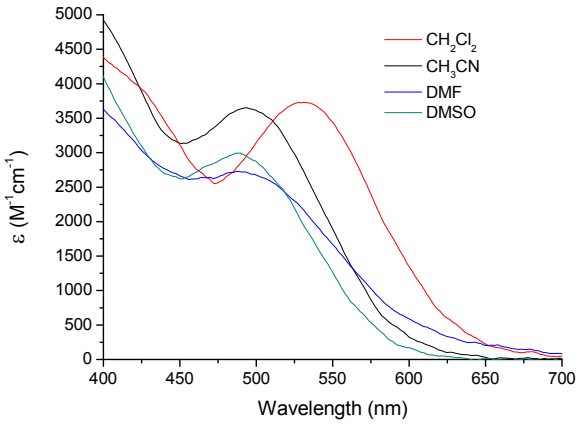

Figure 4.12. Absorption spectra of complex (Bu_4N)[**24**·Br] in different solvents.

Motivated by the non-innocent redox character of diimine ligands,[5,15,16,55] we decided to investigate the redox properties of the current series of $Mo_3S_7X_4$(diimine), (X = Cl, Br) cluster complexes. Once again, the poor solubility of the majority of these neutral compounds limited our study to a few complexes, and hence precluded a detailed analysis of the redox waves for all these clusters in solution. As illustrative examples, the electrochemical properties of $(Bu_4N)[Mo_3S_7Br_3$(dcmbpy)], ((Bu_4N)[**22**·Br]), and $Mo_3S_7Br_4$(dnbpy), (**23**) were investigated by cyclic voltammetry. These complexes present good solubility in acetonitrile and dichloromethane respectively, thus allowing the investigation of their redox behavior in solution in a wide range of easily accessible potentials. The cyclic voltammogram of complex

(Bu_4N)[**22**·Br] in acetonitrile (Figure 4.13a) presents one irreversible reduction peak at -0.83 V (*vs* Ag/AgCl), a quasi-reversible reduction wave at $E_{1/2}$ = -0.58 V ($E_{1/2}$ = (E_a+E_c)/2), and another irreversible peak in the oxidation region at 0.92 V. For compound **23**, its cyclic voltammogram recorded in dichloromethane reveals one irreversible reduction peak at -1.06 V (*vs* Ag/AgCl), and one irreversible peak at 0.74 V which is generated upon oxidation of the reduced species (Figure 4.13b).

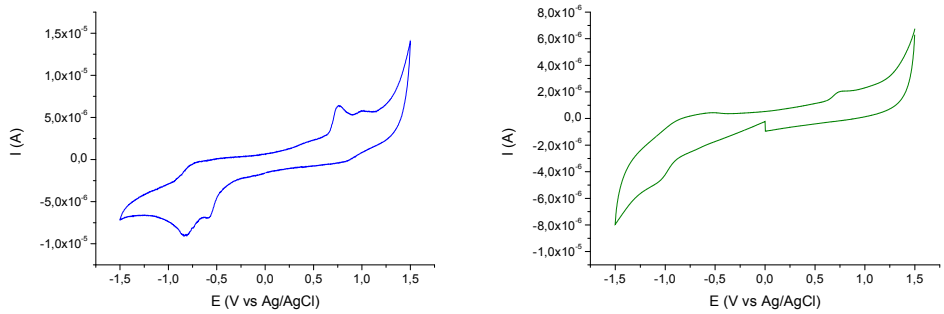

Figure 4.13. Cyclic voltammograms of clusters (Bu_4N)[**22**·Br] (a) and **23** (b) in solution, recorded at a scan rate of 100 mV/s (E *vs* Ag/AgCl).

Table 4.3 collects the reduction potentials (*vs* Ag/AgCl) for a series of homoleptic molybdenum and tungsten cluster chalcogenides bearing diimine ligands, together with those of complexes (Bu_4N)[**22**·Br] and **23**. The first reduction processes in ruthenium(III) and iridium(III) polypyridyl complexes have been ascribed to reduction of the ligands.[5,56,57] Analogous ligand-based reductions have also been postulated for homoleptic M_3Q_4 and M_3Q_7 (M = Mo, W; Q = S, Se) clusters containing bipyridine and phenanthroline derivatives.[15,55] In view of these redox behavior, the reduction processes observed in our complexes could also presumably be attributed to reduction of the diimine ligands. The reduction potentials for complexes (Bu_4N)[**22**·Br] and **23** present a cathodic shift with respect to other

homoleptic Mo_3S_4 and Mo_3S_7 clusters containing related ligands, thus indicating that our heteroleptic diimine-halide Mo_3S_7 clusters are more reluctant to be reduced.

Table 4.3. Reduction potentials (*vs* Ag/AgCl) for a series of diimino cluster complexes.

Cluster	Reduction, $E_{1/2}$ (V)	Reduction, E_c
(Bu_4N)[**22**·Br]	-0.58	-0.83
23	-	-1.06
$[Mo_3S_4Cl_3(phen)_3]Cl$	-0.090	-1.25
$[Mo_3S_4Cl_3(bpy)_3]Cl$	0.116	-
$[Mo_3Se_7(phen)_3]Br_4$	-0.086	-
$[W_3Se_7(phen)_3]Br_4$	-0.625	-

4.2.2. REACTIVITY OF TRINUCLEAR DIIMINE COMPLEXES TOWARDS SULFUR DONOR LIGANDS

In the recent past, interesting examples of platinum(II) complexes containing a mixture of diimine and dithiolate ligands have been reported. These complexes have proved to be very efficient as photosensitizers in photovoltaic cells, and also as catalysts for the photogeneration of hydrogen from water.[10,11] Motivated by the properties of platinum(II) complexes, as also with the aim of providing some insight into the chemical behavior of $Mo_3S_7X_4$(diimine) complexes (X = Cl or Br), we decided to prepare heteroleptic Mo_3S_7 clusters containing both diimine and dithiolate ligands. More specifically, we focused on 4,4'-dinonyl-2,2'-bipyridine (dnbpy), 4,4'-dicarbomethoxy-2,2'-bipyridine (dcmbpy), and 2,2'-bipyridine-4,4'-dicarboxylic acid (dcbpy) as examples of diimines (see Figure 4.8), and on dmit (1,3-dithiole-2-thione-4,5-dithiolate) as a dithiolate ligand. The approach used for the synthesis of the target molecules is depicted in Scheme 4.8.

The reaction between complex $Mo_3S_7Br_4$(dnbpy), (**23**), and one equivalent of $(Bu_4N)_2[Zn(dmit)_2]$, (dmit = 1,3-dithiole-2-thione-4,5-dithiolate)[58,59] in

dichloromethane at room temperature resulted in a deep purple solution, owing to the substitution of four bromide groups in compound **23** by two dmit ligands to afford the neutral cluster $Mo_3S_7(dnbpy)(dmit)_2$, (**29**), in almost quantitative yield. This strategy for the coordination of dithiolene ligands had previously been employed in our group for the preparation of trisubstituted Mo_3S_7 clusters containing dithiolenes.[19–21]

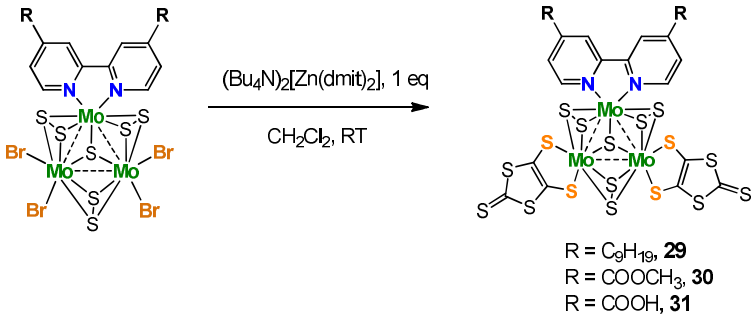

Scheme 4.8. Synthetic pathway for complexes **29** – **31**.

Complex $Mo_3S_7Br_4(dcmbpy)$, (**22**), proved not to be a convenient starting material due to its poor solubility in common organic solvents. Consequently, the bromide adduct $(Bu_4N)[Mo_3S_7Br_4(dcmbpy)\cdot Br]$, $(Bu_4N)[\mathbf{22}\cdot Br]$, was used as a source of the neutral cluster **22**. Reaction of $[\mathbf{22}\cdot Br]^-$ with $[Zn(dmit)_2]^{2-}$ under analogous conditions to those of compound **29** afforded $Mo_3S_7(dcmbpy)(dmit)_2$, (**30**), in high yield (82 %).

The application of the above procedures to the preparation of complex $Mo_3S_7(dcbpy)(dmit)_2$, (dcbpy = 2,2'-bipyridine-4,4'-dicarboxylic acid; **31**) was unsatisfactory owing to the insolubility of the $Mo_3S_7Br_4(dcbpy)$ precursor. As already stated in the previous section, all attempts to isolate complex $Mo_3S_7Br_4(dcbpy)$ resulted in orange solids which were insoluble even in dimethylformamide or dimethylsulfoxide. Consequently, an alternative procedure for the synthesis of the dmit derivative was developed. Complex $Mo_3S_7(dcbpy)(dmit)_2$, (**31**), was successfully

prepared by a one-pot procedure starting from $(Bu_4N)_2[Mo_3S_7Br_6]$ and dcbpy. Reaction between these precursors in dimethylformamide at 130 ºC afforded an orange solution from which the excess ligand precipitated upon cooling. After removing the excess ligand, the putative $Mo_3S_7Br_4$(dcbpy) species, which remained soluble in DMF, was reacted with one equivalent of $[Zn(dmit)_2]^{2-}$ *in situ* at room temperature to afford complex **31** in 74 % yield.

This chemistry could also be extended to other sulfur-donor ligands, such as diethyldithiocarbamate (dtc). As an illustrative example, we focused on 5,6-dimethyl-1,10-phenanthroline (dmphen) as a diimine ligand. The reaction between $(Bu_4N)_2[Mo_3S_7Br_6]$ and an excess of dmphen in dichloromethane afforded a red solution containing compound $(Bu_4N)[Mo_3S_7Br_4$(dmphen)]. As shown in Scheme 4.9, addition of Na(dtc)·$3H_2O$ to the latter solution resulted in color changing, owing to the formation of cluster $[Mo_3S_7$(dmphen)$(dtc)_2]$Br. Counterion exchange on silica gel column afforded the adduct complex $[Mo_3S_7$(dmphen)$(dtc)_2$·Br$](PF_6)$, ([**32**·Br$](PF_6)$), in 70 % yields. This strategy apparently seemed to be extremely convenient for the preparation of charged (and hence readily soluble) Mo_3S_7 complexes bearing diimine ligands. Nevertheless, to our dismay in most cases the dtc ligand was able to replace the diimine ligand, leading to the formation of trisubstituted $[Mo_3S_7(dtc)]^+$ complexes even when stoichiometric amounts of dtc were employed.

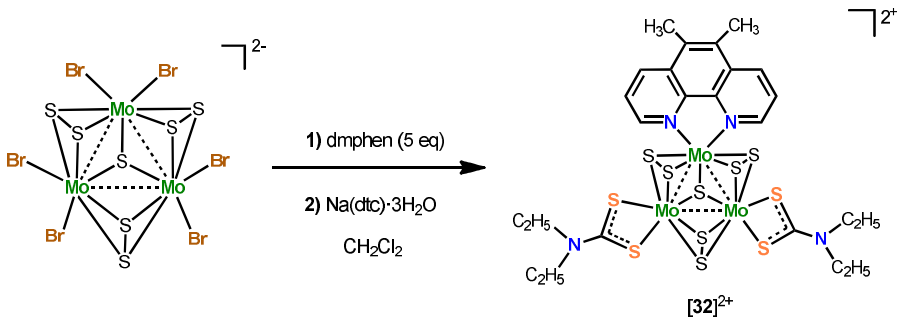

Scheme 4.9. Synthetic route for complex $[\mathbf{32}]^{2+}$.

Complexes **29** – **31** exhibit a poor solubility in common organic solvents due to their neutral nature; an analogous behavior to that observed in compounds **12** – **28**, presented in the previous section. Also in this case, the series of dmit derivatives (**29** – **31**) are dissolved upon sonication in dichloromethane in the presence of Bu_4NX salts (X = Cl, Br). Nevertheless, to our dismay all attempts to grow single crystals of these complexes suitable for X-ray structural analysis have to date been unsatisfactory. Crystal growing in the form of very fine needles of poor quality was observed for complex **31** by gas diffusion water/dimethylsulfoxide, although the characteristics of the obtained crystals precluded their analysis by X-ray diffraction. In contrast, the charged $[\mathbf{32}\cdot Br]^+$ complex exhibits good solubility in common solvents and its structure was obtained by the slow evaporation of a sample solution in chloroform.

Electrospray Ionization Mass Spectrometry was employed aimed at the determination of the m/z ratio in complexes **29** – **32**. However, the reluctance of complexes **29** – **31** to be ionized precluded their characterization by this technique. In the case of complex $[\mathbf{32}\cdot Br]^+$, the molecular peak at m/z = 1096 was observed, for which there is a good agreement between the experimental and simulated isotopic patterns.

Complexes **29** – **32** have been characterized by elemental analysis and infrared and UV/Vis spectroscopies. In all complexes, there is a good correlation between the calculated and experimental compositions for carbon, hydrogen, nitrogen and sulfur. The characteristic bands of the Mo_3S_7 units, as well as those of their outer diimine and dithiolene ligands were observed in the IR spectra of complexes **29** – **31**. These bands were identified on the basis of the stretching frequencies reported for similar cluster complexes.[15,20,21,55] In all cases, a weak band corresponding to the $S_{eq} - S_{ax}$ stretching vibration was observed at *ca.* 516 cm^{-1}. The vibrations of the Mo - μ_3S bonds were observed in the form of multiple bands in the

416 – 420 cm^{-1} range. The multiple signals corresponding to the C=C stretching vibrations of the bipyridine rings appear in the range of 1417 – 1613 cm^{-1}. The bands assigned to the C=S vibrations of the dmit ligand were found in all cases at 1053 cm^{-1}. In addition, further bands were observed due to the vibration of the atoms of the groups appended to the functionalized bipyridine ligands. For instance, in complex **29**, the Csp^3-H vibration bands of the long alkyl chains in the ligand were found in the range of 2849 – 2920 cm^{-1}. In complex **30** the vibrations of the C=O and C-O groups were observed as two single bands at 1732 cm^{-1} and 1267 cm^{-1}, respectively. Finally, in complex **31**, containing the analogous dcbpy ligand, apart from the C=O and C-S bands discussed for complex **30**, the vibrations of the terminal O-H groups were found as a broad band centered at 3446 cm^{-1}.

The UV/Vis absorption spectra of complexes **29** – **31** in dimethylsulfoxide exhibit high intensity bands in the 307 – 407 nm region, with molar extinction coefficients (ε) in the range of 7.4 – 27.7 × 10^3 M^{-1} cm^{-1}. In addition, weaker absorption bands can be found in the 450 – 500 nm region, presenting ε values which lie between 5.1 × 10^3 and 10.2 × 10^3 M^{-1} cm^{-1}. As will be more thoroughly discussed in Chapter 5, these mixed-ligand diimine-dithiolene complexes present absorption bands with higher molar extinction coefficients than those of their diimine-halide counterparts. To our dismay, the limited solubility of complexes **29** – **31** in common organic solvents prevented a deep study of their possible solvatochromism.

4.2.3. CRYSTAL STRUCTURE DESCRIPTION

Single crystals of compounds (Bu_4N)[(**14** – **22**)·X] and (Bu_4N)[(**24** – **28**)·X], where X = Cl or Br, were obtained by slow diffusion methods, and their solid structure was determined by X-ray diffraction. As illustrative examples, the ORTEP representations of the cluster anions $[Mo_3S_7Cl_4(dmbpy)\cdot Cl]^-$, [**18**·Cl]$^-$, and $[Mo_3S_7Br_4(dcmphen)\cdot Br]^-$, [**24**·Br]$^-$, with the atom numbering schemes are depicted in Figures 4.14 and 4.15, respectively.

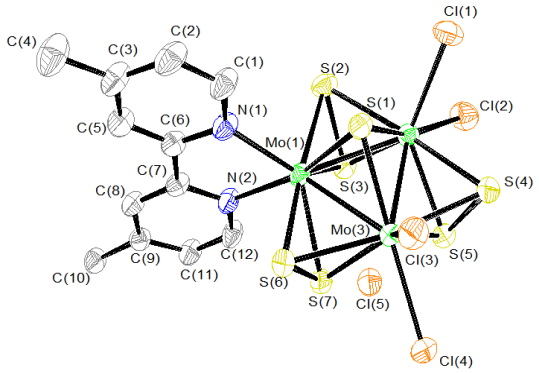

Figure 4.14. ORTEP representation (50 % probability ellipsoids) of the anionic trinuclear cluster [**18**·Cl]$^-$ with the atom numbering scheme.

The current series of clusters present similar structural features, crystallizing as tetrabutylammonium salts of anionic aggregates. In them, neutral cluster molecules of formula $Mo_3(\mu_3\text{-}S)(\mu_2\text{-}S_2)_3X_4$(diimine), (X = Cl or Br) participate in non-bonding interactions between the three sulfur axial atoms (S_{ax}) in the cluster, *i.e.* those labeled as S(3), S(5) and S(7), and a chloride or bromide anion, as depicted in Figures 4.14 and 4.15, respectively for complexes **18** and **24**. The Mo_3S_7 cluster core possess its usual geometry with one S_{ap} apical sulfur atom, S(1), bonded to the three metals which define an equilateral triangle. Each side of the metal triangle is bridged by a disulfide ligand with three S_{eq} equatorial sulfur atoms essentially located in the metal plane, S(2), S(4) and S(6), and three S_{ax} axial sulfur atoms placed out of the metal plane.[30,31,44–46,60,61] The two nitrogen atoms of the diimine ligand are coordinated to one of the molybdenum atoms in a chelating mode, and the plane defined by the ligand is oriented almost perpendicular to the trimetallic plane.

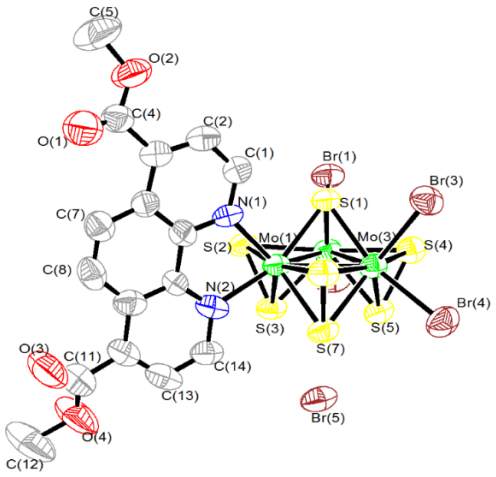

Figure 4.15. ORTEP representation (50 % probability ellipsoids) of the anionic trinuclear cluster [**24**·Br]$^-$ with the atom numbering scheme.

The average bond lengths for the series of complexes presented in this section together with those of other Mo_3S_7 clusters are collected in Table 4.4. In all compounds, the metal-metal bond distances (*ca.* 2.75 Å) are in agreement with an oxidation state of +4 for the molybdenum, and a single metal-metal bond. One diimine ligand binds to one molybdenum atom with an average Mo – N distance of *ca.* 2.22 Å. Furthermore, the bond lengths between metal atoms and the different sulfide ligands (S_{ap}, S_{eq} and S_{ax}) present similar values to those reported for other Mo_3S_7 complexes.[30,31,44–46,60,61] The distances between the molybdenum atoms and the halide ligands (Mo – X) follow the expected tendency based on ionic radii criteria, *i.e.* the Mo – Br lengths are *ca.* 0.15 Å longer than the Mo – Cl distances.[60,61] In addition, these Mo – X bond lengths depend on the nature of the coordinated diimine ligands. The Mo – Br distances are in the range of 2.5814(12) – 2.6277(5) Å, while the Mo – Cl bond lengths lie between 2.460(3) and 2.4708(3) Å. Nevertheless, no clear tendencies in Mo – X bond distances can be drawn from the data in Table 4.4.

Table 4.4. Selected average bond lengths (Å) for clusters (Bu_4N)[(**14** – **22**)·X], (Bu_4N)[(**24** – **28**)·X] and [**32**·Br](PF_6), together with those of similar complexes (X = Cl, Br or S_{lig}). Standard deviations for averaged values are given in square brackets.

Cluster	Mo-Mo	Mo-(μ_3-S)	Mo-S_{ax}	Mo-S_{eq}	Mo-N	Mo-X
$(Et_4N)_3[Mo_3S_7Cl_6]$[60]	2.758[2]	2.346[3]	2.391[3]	2.483[3]	-	2.478[3]
$(ET)_3[Mo_3S_7Br_6]$[61]	2.737[3]	2.344[6]	2.384[7]	2.466[7]	-	2.610[4]
(Bu_4N)[**14**·Br]	2.7478[4]	2.3593[10]	2.3912[10]	2.4837[10]	2.218[3]	2.6277[5]
(Bu_4N)[**15**·Cl]	2.7452[13]	2.3597[3]	2.3895[3]	2.4867[3]	2.2145[10]	2.4708[3]
(Bu_4N)[**16**·Br]	2.7480[8]	2.3601[18]	2.3811[16]	2.4848[16]	2.222[6]	2.5814[12]
(Bu_4N)[**17**·Cl]	2.7465[10]	2.3517[2]	2.3922[2]	2.4872[2]	2.209[7]	2.4605[2]
(Bu_4N)[**18**·Cl]	2.7502[6]	2.3531[12]	2.3852[13]	2.4861[14]	2.211[4]	2.4644[13]
(Bu_4N)[**19**·Br]	2.7502[11]	2.359[3]	2.393[3]	2.481[3]	2.211[8]	2.6172[14]
(Bu_4N)[**20**·Br]	2.7438[14]	2.3583[3]	2.391[3]	2.485[3]	2.225[10]	2.6212[17]
(Bu_4N)[**21**·Br]	2.7414[7]	2.3553[15]	2.3958[16]	2.4852[17]	2.216[5]	2.6083[9]
(Bu_4N)[**22**·Br]	2.7531[4]	2.3607[9]	2.3948[9]	2.4881[10]	2.229[3]	2.6259[5]
(Bu_4N)[**24**·Br]	2.7507[17]	2.358[3]	2.398[4]	2.486[4]	2.221[11]	2.6155[19]
(Bu_4N)[**25**·Cl]	2.7486[13]	2.357[3]	2.395[3]	2.485[3]	2.219[10]	2.460[3]
(Bu_4N)[**27**·Cl]	2.7461[10]	2.354[3]	2.388[2]	2.494[2]	2.213[7]	2.463[2]
(Bu_4N)[**28**·Br]	2.7448[4]	2.3628[10]	2.3908[11]	2.4831[11]	2.226[3]	2.6114[6]
$[Mo_3S_7(dtc)_3]\cdot Cl$[30]	2.721[2]	2.368[4]	2.409[4]	2.481[4]	-	2.499[4]
[**32**·Br](PF_6)	2.7248[7]	2.3735[16]	2.4021[16]	2.4869[17]	2.216[5]	2.4933[19]

dtc = diethyldithiocarbamate; ET = bis(ethylendithio)tetrathiafulvalene

Short intermolecular contacts between the axial sulfur atoms in the cluster unit and halide anions have also been observed in these series of complexes. For instance, the $S_{ax}\cdots Cl$ interactions in [**18**·Cl]$^-$ have a length of 2.896 – 2.910 Å, and are in the range of those reported for similar cluster complexes interacting with chlorides through the axial sulfur atoms.[44] The $S_{ax}\cdots Br$ contacts in complex [**24**·Br]$^-$ (2.969 – 3.146 Å) are also in agreement with previously reported analogous interactions.[45,46] For comparative purposes, Table 4.5 lists the length of the non-bonding interactions observed for the series of novel cluster complexes presented in this chapter, together with those reported previously. With the exception of complex (Bu_4N)[**27**·Cl], the $S_{ax}\cdots Cl$ contacts in $[Mo_3S_7X_4(diimine)\cdot X]^-$ clusters (X = Cl or Br) are slightly shorter than the $S_{ax}\cdots Br$ interactions, which is in agreement with the smaller ionic radii of chloride anions.

Table 4.5. Non-bonding $S_{ax}\cdots X$ (X = Cl or Br) contacts in heteroleptic Mo_3S_7 complexes, together with those of similar complexes.

Cluster	Interaction	Contact Length, Å
$(Et_4N)_3[Mo_3S_7Cl_6]$[60]	$S_{ax}\cdots Cl$	2.921 – 2.955
$(ET)_3[Mo_3S_7Br_6]$[61]	$S_{ax}\cdots Br$	2.985 – 3.120
(Bu_4N)[**14**·Br]	$S_{ax}\cdots Br$	2.944 – 3.020
(Bu_4N)[**15**·Cl]	$S_{ax}\cdots Cl$	2.829 – 2.973
(Bu_4N)[**16**·Br]	$S_{ax}\cdots Br$	2.991 – 3.156
(Bu_4N)[**17**·Cl]	$S_{ax}\cdots Cl$	2.841 – 2.931
(Bu_4N)[**18**·Cl]	$S_{ax}\cdots Cl$	2.896 – 2.910
(Bu_4N)[**19**·Br]	$S_{ax}\cdots Br$	3.004 – 3.108
(Bu_4N)[**20**·Br]	$S_{ax}\cdots Br$	3.030 – 3.058
(Bu_4N)[**21**·Br]	$S_{ax}\cdots Br$	2.991 – 3.134
(Bu_4N)[**22**·Br]	$S_{ax}\cdots Br$	2.959 – 3.020
(Bu_4N)[**24**·Br]	$S_{ax}\cdots Br$	2.970 – 3.146
(Bu_4N)[**25**·Cl]	$S_{ax}\cdots Cl$	2.863 – 2.967
(Bu_4N)[**27**·Cl]	$S_{ax}\cdots Cl$	2.912 – 2.933
(Bu_4N)[**28**·Br]	$S_{ax}\cdots Br$	2.936 – 3.092
$[Mo_3S_7(dtc)_3]\cdot Cl$[30]	$S_{ax}\cdots Cl$	2.969 – 3.051
[**32**·Br](PF_6)	$S_{ax}\cdots Cl$	2.949 – 3.009

Formation of additional $S_{eq}\cdots Br$ interactions connecting adjacent cluster units has been observed in the crystal structure of various $[Mo_3S_7X_4(diimine)\cdot X]^-$ complexes. As a representative example, the crystal packing of (Bu_4N)[**24**·Br] is depicted in Figure 4.16. In this structure, $S_{eq}\cdots Br$ interactions connect neighboring [**24**·Br]$^-$ aggregates, resulting in the formation of $\{[\mathbf{24}\cdot Br]_2\}^{2-}$ dimers. The formation of similar dimeric aggregates between neighboring cluster units is not unprecedented. Analogous intermolecular interactions have already been observed by Sokolov and co-workers in the heroleptic cluster compound $(Et_4N)[Mo_3S_7Cl_4(CH_3CN)\cdot Cl]$.[44]

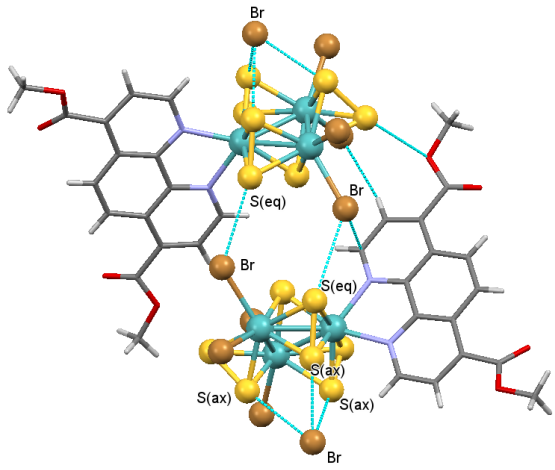

Figure 4.16. Crystal packing in the structure of (Bu_4N)[**24**·Br] showing the formation of $\{[\mathbf{24}\cdot Br]_2\}^{2-}$ dimers owing to intermolecular interactions between neighboring cluster anions.

The halide atoms in $[Mo_3S_7X_4(diimine)\cdot X]^-$ complexes can be easily replaced by sulfur donor ligands, as stated previously in Section 4.2.2. The structure of compound $[Mo_3S_7(dmphen)(dtc)_2\cdot Br](PF_6)$, [**32**·Br]$(PF_6)$, was obtained by slow evaporation methods, and again non-bonding contacts were observed in the crystal structure. The ORTEP representation of the $[\mathbf{32}]^{2+}$ cation is shown in Figure 4.17. The structure of [**32**·Br](PF_6) presents the characteristic Mo_3S_7 unit already observed in $[Mo_3S_7X_4(diimine)\cdot X]^-$ complexes (X = Cl, Br). Two diethyldithiocarbamate

ligands (dtc) are coordinated to two molybdenum atoms in a chelating mode, whereas the third molybdenum atom is bound to a chelating 5,6-dimethyl-1,10-phenanthroline ligand (dmphen), with an average Mo – N length of *ca.* 2.22 Å. This distance value is in good agreement to those observed in the mixed-ligand diimine-halide complexes, *i.e.* $(Bu_4N)[(\mathbf{14} – \mathbf{22})\cdot X]$ and $(Bu_4N)[(\mathbf{24} – \mathbf{28})\cdot X]$, (X = Cl, Br). The average Mo – S_{lig} bond length (roughly 2.49 Å) also correlates well with that reported for the trisubstituted $[Mo_3S_7(dtc)_3]\cdot Cl$ complex (see Table 4.4).[30]

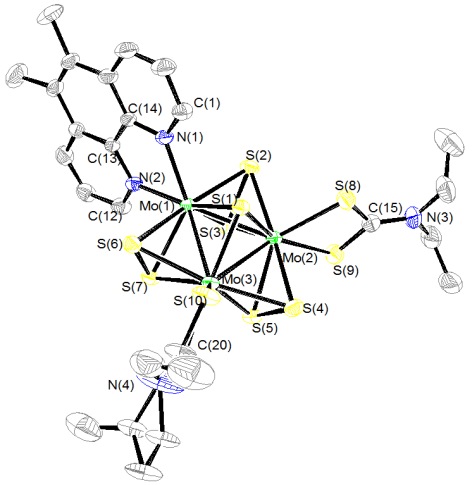

Figure 4.17. ORTEP representation (50 % probability ellipsoids) of the anionic trinuclear cluster $[\mathbf{32}]^{2+}$ with the atom numbering scheme.

The intermolecular interactions in $[\mathbf{32}\cdot Br](PF_6)$ are displayed in Figure 4.18. The crystal packing in the structure of $[\mathbf{32}\cdot Br](PF_6)$ reveals the presence of aggregates in which each $[\mathbf{32}]^{2+}$ cluster cation interacts with a bromide anion through the axial sulfur atoms, with $S_{ax}\cdots Br$ distances ranging from 2.949 to 3.009 Å. These contact distances are within the range of those reported for homoleptic Mo_3S_7 complexes containing diethyldithiocarbamate ligands (see Table 4.4).[27,28,30,31] Interestingly, the $[\mathbf{32}\cdot Br]^{+}$ adducts are connected via short S···S contacts between the apical or axial sulfur atoms in the cluster core, and the sulfur atoms in the dtc ligand. These contacts

have average lengths of *ca.* 3.491 Å ($S_{ap}\cdots Sl_{ig}$) and 3.577 Å ($S_{ax}\cdots S_{lig}$). Similar S···S non-bonding interactions have been observed in other Mo_3S_7 clusters containing sulfur donor ligands.[33–36] Nevertheless, compound [**32**·Br](PF_6) represents to the best of our knowledge the first example of a heteroleptic Mo_3S_7 cluster containing both diimine (dmphen) and sulfur donor ligands (dtc), in which short S···S and S···Br contacts are present at the same time.

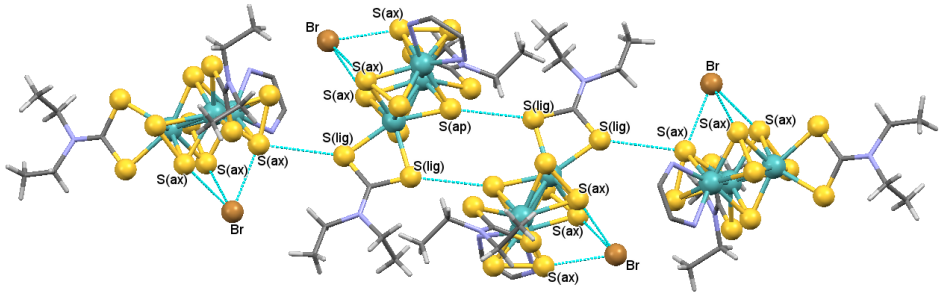

Figure 4.18. Crystal packing of [**32**·Br](PF_6) showing the intermolecular interactions between neighboring [**32**·Br]$^+$ cations.

4.3. CONCLUSIONS

A series of $Mo_3S_7X_4$(diimine) complexes (X = Cl or Br) containing a diversity of bipyridine-, phenanthroline-, imidazophenathroline- and pyrazinophenanthroline-like ligands have been prepared. The resulting complexes **12** – **28** have been characterized by different techniques. Crystallization of such compounds in the presence of Bu_4NX (X = Cl or Br) affords single crystals suitable for X-ray structural determination. The X-ray structure of the aforementioned clusters reveals the presence of $S_{ax}\cdots X$ (X = Cl or Br) interactions, which result in the formation of $[Mo_3S_7X_4(diimine)\cdot X]^-$ adducts. Additional interactions between equatorial sulfur atoms (S_{eq}) and halide ligands connect neighboring cluster adducts, resulting in the formation of $\{[Mo_3S_7X_4(diimine)\cdot X]_2\}^{2-}$ dimers.

Reaction of $Mo_3S_7X_4$(diimine) complexes (X = Cl or Br) with sulfur donor ligands yields clusters of formula $[Mo_3S_7(diimine)L_2]^{0,\,2+}$ (L = dmit or dtc). The neutral complexes **29** – **31** (bearing the dmit ligand) are highly insoluble in common organic solvents, which limits the number of techniques employed for their characterization to elemental analysis, and infrared and UV/Vis spectroscopy. In contrast, complex [**32**·Br](PF_6), containing the dtc ligand, exhibits good solubility in common organic solvents. Its crystal structure presents S···S interactions between neighboring cluster molecules giving rise to extended networks.

The optical properties of $Mo_3S_7X_4$(diimine) complexes, namely luminescence and optical nonlinearities will be discussed in Chapter 5. The ability of such complexes to photocatalyze the water splitting reaction will be investigated in Chapter 6.

4.4. REFERENCES

(1) Keniley, L. K.; Dupont, N.; Ray, L.; Ding, J.; Kovnir, K.; Hoyt, J. M.; Hauser, A.; Shatruk, M. *Inorg. Chem.* **2013**, *52*, 8040–8052.

(2) Maity, D.; Bhaumik, C.; Karmakar, S.; Baitalik, S. *Inorg. Chem.* **2013**, *52*, 7933–7946.

(3) Young, K. J.; Martini, L. A.; Milot, R. L.; Snoeberger, R. C.; Batista, V. S.; Schmuttenmaer, C. A.; Crabtree, R. H.; Brudvig, G. W. *Coord. Chem. Rev.* **2012**, *256*, 2503–2520.

(4) Grätzel, M. *Inorg. Chem.* **2005**, *44*, 6841–6851.

(5) Tucker, J. W.; Stephenson, C. R. J. *J. Org. Chem.* **2012**, *77*, 1617–1622.

(6) Dai, C.; Narayanam, J. M. R.; Stephenson, C. R. J. *Nat. Chem.* **2011**, *3*, 140–145.

(7) McCann, S.; McCann, M.; Casey, M. T.; Jackman, M.; Devereux, M.; McKee, V. *Inorganica Chim. Acta* **1998**, *279*, 24–29.

(8) Galoppini, E. *Coord. Chem. Rev.* **2004**, *248*, 1283–1297.

(9) Nakade, S.; Kubo, W.; Saito, Y.; Kanzaki, T.; Kitamura, T.; Wada, Y.; Yanagida, S. *J. Phys. Chem. B* **2003**, *107*, 14244–14248.

(10) Zhang, J.; Du, P.; Schneider, J.; Jarosz, P.; Eisenberg, R. *J. Am. Chem. Soc.* **2007**, *129*, 7726–7727.

(11) Islam, A.; Sugihara, H.; Hara, K.; Pratap Singh, L.; Katoh, R.; Yanagida, M.; Takahashi, Y.; Murata, S.; Arakawa, H. *New J. Chem.* **2000**, *24*, 343–345.

(12) Cai, Z.; Zhou, M.; Xu, J. *J. Mol. Struct.* **2011**, *1006*, 282–287.

(13) Zapata, F.; Caballero, A.; Espinosa, A.; Tárraga, A.; Molina, P. *J. Org. Chem.* **2008**, *73*, 4034–4044.

(14) Cardinaels, T.; Ramaekers, J.; Driesen, K.; Nockemann, P.; Van Hecke, K.; Van Meervelt, L.; Goderis, B.; Binnemans, K. *Inorg. Chem.* **2009**, *48*, 2490–2499.

(15) Gushchin, A. L.; Sokolov, M. N.; Peresypkina, E. V; Virovets, A. V; Kozlova, S. G.; Zakharchuk, N. F.; Fedin, V. P. *Eur. J. Inorg. Chem.* **2008**, *2008*, 3964–3969.

(16) Fedin, V. P.; Sokolov, M. N.; Geras'ko, O. A.; Virovets, A. V.; Podberezskaya, N. V.; Fedorov, V. Y. *Inorganica Chim. Acta* **1991**, *187*, 81–90.

(17) Garriga, J. M.; Llusar, R.; Uriel, S.; Vicent, C.; Usher, A. J.; Lucas, N. T.; Humphrey, M. G.; Samoc, M. *Dalt. Trans.* **2003**, 4546–4551.

(18) Gushchin, A. L.; Llusar, R.; Vicent, C.; Abramov, P. A.; Gómez-Garcia, C. J. *Eur. J. Inorg. Chem.* **2013**, *2013*, 2615–2622.

(19) Llusar, R.; Vicent, C. *Coord. Chem. Rev.* **2010**, *254*, 1534–1548.

(20) Llusar, R.; Triguero, S.; Polo, V.; Vicent, C.; Gómez-García, C. J.; Jeannin, O.; Fourmigué, M. *Inorg. Chem.* **2008**, *47*, 9400–9409.

(21) Llusar, R.; Uriel, S.; Vicent, C.; Clemente-Juan, J. M.; Coronado, E.; Gómez-García, C. J.; Braïda, B.; Canadell, E. *J. Am. Chem. Soc.* **2004**, *126*, 12076–12083.

(22) Kibsgaard, J.; Jaramillo, T. F.; Besenbacher, F. *Nat. Chem.* **2014**, *6*, 248–253.

(23) Feliz, M.; Llusar, R.; Uriel, S.; Vicent, C.; Humphrey, M. G.; Lucas, N. T.; Samoc, M.; Luther-Davies, B. *Inorganica Chim. Acta* **2003**, *349*, 69–77.

(24) Sorribes, I.; Wienhöfer, G.; Vicent, C.; Junge, K.; Llusar, R.; Beller, M. *Angew. Chemie Int. Ed.* **2012**, *51*, 7794–7798.

(25) Hou, Y.; Abrams, B. L.; Vesborg, P. C. K.; Björketun, M. E.; Herbst, K.; Bech, L.; Setti, A. M.; Damsgaard, C. D.; Pedersen, T.; Hansen, O.; Rossmeisl, J.; Dahl, S.; Nørskov, J. K.; Chorkendorff, I. *Nat. Mater.* **2011**, *10*, 434–438.

(26) Fedin, V. P.; Sokolov, M. N.; Mironov, Y. V.; Kolesov, B. A.; Tkachev, S. V.; Fedorov, V. Y. *Inorganica Chim. Acta* **1990**, *167*, 39–45.

(27) Virovets, A. V.; Podberezskaya, N. V. *J. Struct. Chem.* **1993**, *34*, 306–322.

(28) Zimmermann, H.; Hegetschweiler, K.; Keller, T.; Gramlich, V.; Schmalle, H. W.; Petter, W.; Schneider, W. *Inorg. Chem.* **1991**, *30*, 4336–4341.

(29) Chen, J.; Lu, S. F.; Huang, Z. X.; Yu, R. M.; Wu, Q. J. *Chemistry* **2001**, *7*, 2002–2006.

(30) Fedin, V. P.; Sokolov, M. N.; Geras'ko, O. A.; Virovets, A. V.; Podberezskaya, N. V.; Fedorov, V. Y. *Inorganica Chim. Acta* **1992**, *192*, 153–156.

(31) Mayor-López, M. J.; Weber, J.; Hegetschweiler, K.; Meienberger, M. D.; Joho, F.; Leoni, S.; Nesper, R.; Reiss, G. J.; Frank, W.; Kolesov, B. A.; Fedin, V. P.; Fedorov, V. E. *Inorg. Chem.* **1998**, *37*, 2633–2644.

(32) Meienberger, M. D.; Hegetschweiler, K.; Rüegger, H.; Gramlich, V. *Inorganica Chim. Acta* **1993**, *213*, 157–169.

(33) Hegetschweiler, K.; Keller, T.; Baumle, M.; Rihs, G.; Schneider, W. *Inorg. Chem.* **1991**, *30*, 4342–4347.

(34) Raymond, C. C.; Dorhout, P. K.; Miller, S. M. *Inorg. Chem.* **1994**, *33*, 2703–2704.

(35) Alberola, A.; Llusar, R.; Triguero, S.; Vicent, C.; Sokolov, M. N.; Gómez-García, C. *J. Mater. Chem.* **2007**, *17*, 3440–3450.

(36) Garriga, J. M.; Llusar, R.; Uriel, S.; Vicent, C.; Usher, A. J.; Lucas, N. T.; Humphrey, M. G.; Samoc, M. *Dalt. Trans.* **2003**, 4546–4551.

(37) Müller, A.; Wittneben, V.; Krickemeyer, E.; Bögge, H.; Lemke, M. *Zeitschrift für Anorg. und Allg. Chemie* **1991**, *605*, 175–188.

(38) Fallahpour, R.-A.; Neuburger, M.; Zehnder, M. *New J. Chem.* **1999**, *23*, 53–61.

(39) Sorribes, I.; Llusar, R.; Vicent, C. *Eur. J. Inorg. Chem.* **2013**, *2013*, 1418–1426.

(40) Shibahara, T. *Coord. Chem. Rev.* **1993**, *123*, 73–147.

(41) Fedin, V. P.; Sokolov, M. N.; Fedorov, V. Y.; Yufit, D. S.; Struchkov, Y. T. *Inorganica Chim. Acta* **1991**, *179*, 35–40.

(42) Béreau, V.; Pernin, C. G.; Ibers, J. A. *Inorg. Chem.* **2000**, *39*, 854–856.

(43) Hegetschweiler, K.; Keller, T.; Zimmermann, H.; Schneider, W.; Schmalle, H.; Dubler, E. *Inorganica Chim. Acta* **1990**, *169*, 235–243.

(44) Adonin, S. A.; Virovets, A. V.; Sokolov, M. N.; Fedin, V. P. *Russ. J. Coord. Chem.* **2010**, *36*, 871–875.

(45) Sokolov, M. N.; Gerasko, O. A.; Solodovnikov, S. F.; Fedin, V. P. *J. Struct. Chem.* **2004**, *45*, 490–495.

(46) Fedin, V. P.; Mironov, Y. V.; Virovets, A. V.; Podberezskaya, N. V.; Fedorov, V. Y. *Polyhedron* **1992**, *11*, 2083–2088.

(47) Schwalbe, M.; Schäfer, B.; Görls, H.; Rau, S.; Tschierlei, S.; Schmitt, M.; Popp, J.; Vaughan, G.; Henry, W.; Vos, J. G. *Eur. J. Inorg. Chem.* **2008**, *2008*, 3310–3319.

(48) Wiederholt, K.; Mclaughlin, L. W. *Nucleic Acids Res.* **1999**, *27*, 2487–2493.

(49) Yanagida, M.; Singh, L. P.; Sayama, K.; Hara, K.; Katoh, R.; Islam, A.; Sugihara, H.; Arakawa, H.; Nazeeruddin, M. K.; Grätzel, M. *J. Chem. Soc. Dalt. Trans.* **2000**, 2817–2822.

(50) Myśliwiec, D.; Donnio, B.; Chmielewski, P. J.; Heinrich, B.; Stępień, M. *J. Am. Chem. Soc.* **2012**, *134*, 4822–4833.

(51) Sokolov, M. N.; Abramov, P. A.; Gushchin, A. L.; Kalinina, I. V; Naumov, D. Y.; Virovets, A. V; Peresypkina, E. V; Vicent, C.; Llusar, R.; Fedin, V. P. *Inorg. Chem.* **2005**, *44*, 8116–8124.

(52) Virovets, A. V; Gushchin, A. L.; Abramov, P. A.; Alferova, N. I.; Sokolov, M. N.; Fedin, V. P. *J. Struct. Chem.* **2006**, *47*, 326–338.

(53) Georgieva, I.; Aquino, A. J. A.; Trendafilova, N.; Santos, P. S.; Lischka, H. *Inorg. Chem.* **2010**, *49*, 1634–1646.

(54) Marini, A.; Muñoz-Losa, A.; Biancardi, A.; Mennucci, B. *J. Phys. Chem. B* **2010**, *114*, 17128–17135.

(55) Gushchin, A. L.; Laricheva, Y. A.; Abramov, P. A.; Virovets, A. V.; Vicent, C.; Sokolov, M. N.; Llusar, R. *Eur. J. Inorg. Chem.* **2014**, *2014*, 4093–4100.

(56) Flamigni, L.; Barbieri, A.; Sabatini, C.; Ventura, B.; Barigelletti, F. *Top. Curr. Chem.* **2007**, *280*, 117–214.

(57) Flamigni, L.; Barbieri, A.; Sabatini, C.; Ventura, B.; Barigelletti, F. *Top. Curr. Chem.* **2007**, *281*, 143–203.

(58) Steimecke, G.; Sieler, H.-J.; Kirmse, R.; Hoyer, E. *Phosphorous Sulfur Relat. Elem.* **1979**, *7*, 49–55.

(59) Hansen, T. K.; Becher, J.; Jørgensen, T.; Varma, K. S.; Rajesh; Khedekar, M. P. C.; Hynes, J.; Smith, A. B. *Org. Synth.* **1996**, *73*, 270.

(60) Klingelhöfer, P.; Müller, U.; Friebel, C.; Pebler, J. *Zeitschrift für Anorg. und Allg. Chemie* **1986**, *543*, 22–34.

(61) Llusar, R.; Triguero, S.; Uriel, S.; Vicent, C.; Coronado, E.; Gomez-Garcia, C. J. *Inorg. Chem.* **2005**, *44*, 1563–1570.

5

OPTICAL PROPERTIES OF MOLYBDENUM CLUSTER CHALCOGENIDES

The results in this Chapter have been partly published as:

• "Dithiolene Dimetallic Molybdenum(V) Complexes Displaying Intraligand Charge Transfer (ILCT) Emission." David Recatalá, Artem L. Gushchin, Rosa Llusar, Francisco Galindo, Konstantin A. Brylev, Maxim R. Ryzhikov and Noboru Kitamura, *Dalton Transactions*, **2013**, 42, 12947 – 12955

(Content reproduced by permission of The Royal Society of Chemistry)

• "Heteroleptic Phenanthroline Complexes of Trinuclear Molybdenum Clusters with Luminescent Properties." David Recatalá, Rosa Llusar, Francisco Galindo, Konstantin A. Brylev and Artem L. Gushchin, *European Journal of Inorganic Chemistry*, **2015** (Article in press)

(Content reproduced by permission of John Wiley & Sons)

"There is always the possibility of proving any definite theory wrong; but notice that we can never prove it right."

Richard P. Feynman, *The Character of Physical Law*

5.1. LUMINESCENCE PROPERTIES OF DINUCLEAR MOLYBDENUM CLUSTERS

5.1.1. INTRODUCTION

Dithiolene complexes have been extensively studied since their early ages, stimulated by their potential applications in diverse areas such as light-energy conversion, hydrogen generation,[1] nonlinear optics[2] and biological models.[3] These applications mainly emerge from their interesting electronic structures, characterized by extensive ligand-metal mixing in their frontier orbitals.[4,5] In contrast, the extent of metal-ligand delocalization in other transition metal complexes containing non redox-active ligands is significantly lower. This difference is due to the π-delocalized electronic structure that results from coordination of dithiolate ligands to metal ions. For instance, the electronic structure of 1,2-dithiolene complexes containing unsaturated five-membered MS_2C_2 rings can be regarded as a resonance hybrid of the enedithiolate and the dithione forms (Figure 5.1), and therefore the metal oxidation states cannot be unequivocally assigned in these complexes.[6]

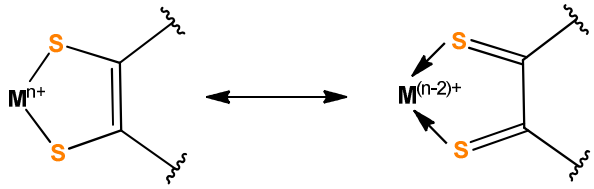

Figure 5.1. Delocalization in 1,2-dithiolene complexes.

In metal complexes, changes in electron distribution are commonly known as charge transfers (CT). Charge transfer can occur from metal to ligand (MLCT), from ligand to metal (LMCT), and even between two different ligands interacting via a metal center (LLCT). On the other hand, intraligand charge transfer (ILCT) occurs in ligands containing simultaneously a donor and an acceptor site. Therefore ILCT transitions are strictly ligand based, and can arise in free, as well as in coordinated

ligands. It is noteworthy that the emission energies that arise from MLCT, LMCT and LLCT excited states are strongly metal and ligand dependent, and are usually lower than those originating from ILCT transitions.[6]

In general, the most common dithiolene ligands are not notable for their emission. Nevertheless, luminescence properties have been reported in a significant number of square-planar homoleptic or heteroleptic complexes containing dithiolene ligands.[6] Heteroleptic complexes usually contain nonchromophoric or diimine ligands apart from dithiolenes, and exhibit stronger emission. Figure 5.2 shows the molecular structure of an homoleptic platinum(II) dithiolate complex, $[Pt(mnt)_2]^{2-}$ (mnt = 1,2-maleonitrile-1,2-dithiolate; Fig. 5.2a),[7] a heteroleptic iridium(I) compound containing carbonyl, cyanide and mnt ligands, $[Ir(CN)(CO)(mnt)]^-$ (Fig. 5.2b),[8] and a mixed-ligand diimine-dithiolene complex, Pt(dmbpy)(bdt), (dmbpy = 4,4'-dimethyl-2,2'-bipyridine; bdt = toluene-3,4-dithiolate; Fig. 5.2c).[9] In these systems, the luminescence arises from charge transfers either between the metal centers and the ligands, or between the two different ligands.

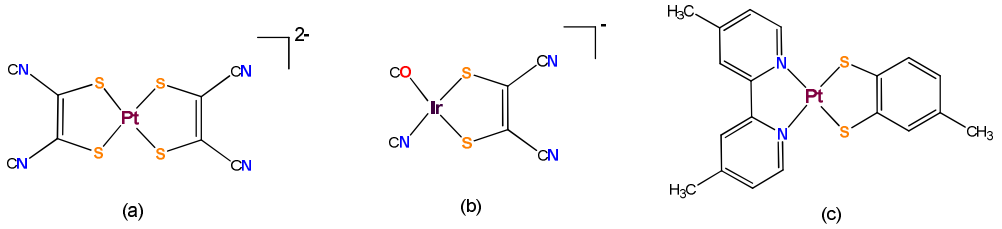

Figure 5.2. Molecular structure of $[Pt(mnt)_2]^{2-}$; (a), $[Ir(CN)(CO)(mnt)]^-$; (b), and Pt(dmbpy)(tdt); (c).

In homoleptic dithiolene complexes, the luminescence can be explained by a charge transfer from either the metal or the mixed metal-dithiolene orbitals to the π^* orbitals of the dithiolate ligand. On the other hand, in heteroleptic complexes containing dithiolene ligands, the origin of the charge transfer depends on the relative energy of the π^* orbitals of the coordinated ligands. For instance, the presence of

both diimine and dithiolene ligands in a metal complex leads to charge transfer from dithiolene π (or metal-dithiolene) to diimine π* orbitals, due to the lower energy of the π* diimine LUMO, as compared to that of the corresponding dithiolene π* orbitals.[6,10,11]

In contrast to the vast majority of dithiolene ligands, the N-heterocyclic-substituted 1,2-enedithiolates reported by Pilato's group are emissive in their non-coordinated forms. Interestingly, the coordination of such ligands to platinum(II) affords room temperature dual emitters.[12] The origin of the dual emission has been ascribed to ^{3}ILCT* (phosphorescence) and ^{1}ILCT* (fluorescence) excited states.[13]

As mentioned in Chapter 3, a great many examples of dithiolene ligands containing nitrogen donor atoms have been reported.[14] In particular, the coordination of 2-bis-(2-pyridyl)-methylene-1,3-dithiolene (hereinafter, $BPyDTS_2$) to gold(I) and platinum(II) has been explored by Zuo and co-workers (see Fig. 5.3).[15] The preparation of heterometallic complexes containing rhenium(I) coordinated through the terminal nitrogen groups in the complexes depicted in Figure 5.3 was motivated by the interesting photophysical and photochemical properties reported in rhenium(I) complexes with diimine ligands.[16–19]

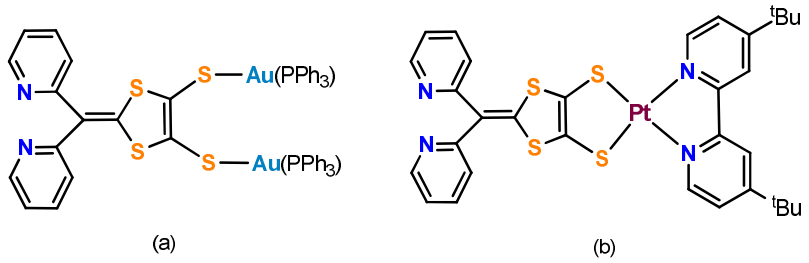

Figure 5.3. Molecular structure of $Au_2(PPh_3)_2(BPyDTS_2)$, (a; PPh_3 = triphenylphosphine, $BPyDTS_2$ = 2-bis-(2-pyridyl)-methylene-1,3-dithiolene), and Pt(dbbpy)($BPyDTS_2$), (b; dbpy = 4,4'-di-*tert*-butyl-2,2'-bipyridine).

The coordination of the aforementioned $BPyDTS_2$ ligand to the $Mo_2O_2(\mu\text{-}S)_2$ cluster unit to afford compound $(Et_4N)_2[Mo_2O_2S_2(BPyDTS_2)_2]$, ($(Et_4N)$[**4**]), was described in Chapter 3. Herein, we present the luminescence properties of ((Et_4N)[**4**]), as well as those of the heterometallic complex that results from the coordination of $(Et_4N)_2$[**4**] to rhenium(I) through the nitrogen atoms in the $BPyDTS_2$ ligand, namely $(Et_4N)_2[Mo_2O_2S_2(BPyDTS_2)_2\{Re(CO)_3Cl\}_2]$, ($(Et_4N)_2$[**5**]). The emission of the organotin complex $Me_2Sn(BPyDTS_2)$, (**3**), has also been studied for comparative purposes. Density Functional Theory (DFT) calculations have been performed in order to provide further insight into the origin of the emission in these complexes. The molecular structures of complexes **3**, $[\mathbf{4}]^{2-}$ and $[\mathbf{5}]^{2-}$ are depicted in Figure 5.4. Details about the synthesis and structural characterization of these compounds are provided in Chapters 3 and 7.

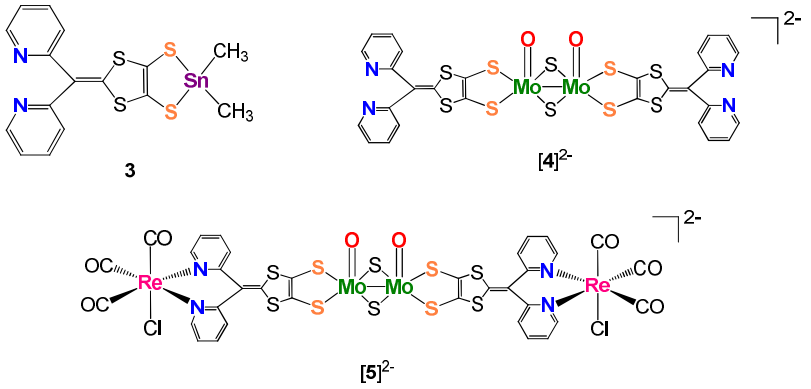

Figure 5.4. Molecular structures of complexes **3**, $[\mathbf{4}]^{2-}$ and $[\mathbf{5}]^{2-}$.

5.1.2. RESULTS AND DISCUSSION

The absorption and emission properties of complexes **3**, $(Et_4N)_2$[**4**] and $(Et_4N)_2$[**5**], containing the $BPyDTS_2$ ligand, have been investigated both in solution and in the solid state in collaboration with Dr. K. Brylev and Prof. N. Kitamura at Hokkaido University (Sapporo, Japan). The UV/Vis electronic spectra of these complexes in

acetonitrile, as well as that of the protected form of the dithiolene ligand, *i.e.* BPyDT(SCH$_2$CH$_2$CN)$_2$.[15] are shown in Figure 5.5. The absorption bands of the three complexes present similar shape but different intensities and wavelengths of maximum absorption. The molar extinction coefficient for all the absorption maxima are listed in Table 5.1.

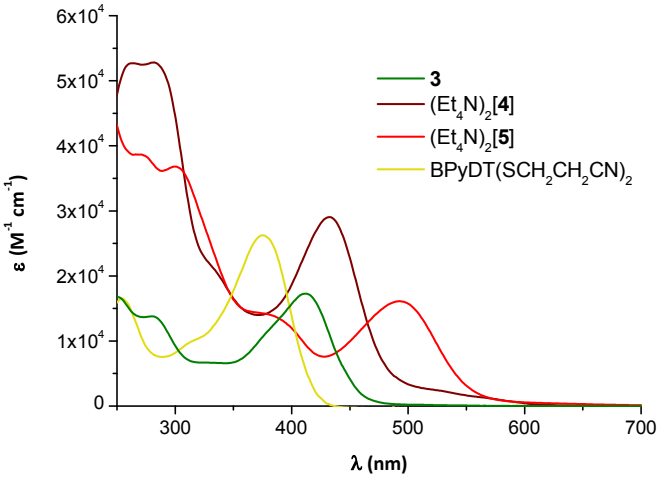

Figure 5.5. UV/Vis absorption spectra of complexes **3**, (Et$_4$N)$_2$[**4**], (Et$_4$N)$_2$[**5**] and ligand BPyDT(SCH$_2$CH$_2$CN)$_2$.

Complexes **3**, (Et$_4$N)$_2$[**4**] and (Et$_4$N)$_2$[**5**] exhibit intense absorption bands in the 250 – 310 nm wavelength region, and the molar absorption coefficients lie between 1 × 10^4 and 5 × 10^4 M^{-1} cm^{-1}. These bands can be ascribed to intraligand π-π* transitions, since the protected BPyDT(SCH$_2$CH$_2$CN)$_2$ ligand exhibits analogous transitions when coordinated to a series of metal ions, which include platinum(II), gold(I) and rhenium(I).[15,20] All three complexes present absorption bands in the visible region of the spectrum. The absorption band at *ca.* 435 nm observed for complex (Et$_4$N)$_2$[**4**] has been investigated by TDDFT calculations (*vide infra*). This band can be ascribed to an intraligand charge transfer (ILCT) transition, whereby the

dithiolate moiety acts as an electron donor, and the bis(2-pyridyl) subunits as electron acceptors.

In complex $(Et_4N)_2$[**4**], the ILCT band appears at longer wavelengths, as compared to the free ligand, BPyDT$(SCH_2CH_2CN)_2$. More specifically, this band is red-shifted by 60 nm. Analogously, in complexes **3** and $(Et_4N)_2$[**5**] similar shifts to longer wavelengths have been registered, being more pronounced in $(Et_4N)_2$[**5**] (*ca.* 117 nm, as compared to the free ligand) than for compound **3** (*ca.* 36 nm). Displacements of the ILCT absorption bands towards longer wavelengths (bathochromic shifts) have also been reported in platinum(II) and gold(I) complexes containing the $BPyDTS_2$ ligand.[15] These results prove that coordination of the $BPyDTS_2$ ligand to transition metals results in longer absorption wavelengths, and therefore in lowering the absorption energy. It is also noteworthy that the coordination of rhenium(I) to cluster $(Et_4N)_2$[**4**] through the nitrogen atoms in the $BPyDTS_2$ ligand results in increasing the maximum absorption wavelength by a factor of 57 nm, in comparison with complex $(Et_4N)_2$[**4**].

Table 5.1. Absorption data for compounds **3**, $(Et_4N)_2$[**4**], $(Et_4N)_2$[**5**], and BPyDT$(SCH_2CH_2CN)_2$ in acetonitrile solution at 298 K.

Compound	λ_{abs} (nm)	ε (M^{-1} cm^{-1})
BPyDT$(SCH_2CH_2CN)_2$	254, 310 sh, 375	16 545, 9 701, 26 250
3	251, 281, 411	16 788, 13 859, 17 384
$(Et_4N)_2$[**4**]	267, 283, 338 sh, 435	52 715, 52 880, 20 451, 29 035
$(Et_4N)_2$[**5**]	266, 299, 388, 492	38 682, 36 811, 13 578, 16 111

Quantum-chemical calculations have been performed for cluster $(Et_4N)_2$[**4**], aimed at providing insight into the nature of the ILCT band which is observed at 435 nm in acetonitrile solution. Such theoretical studies have been carried out in collaboration with M. Ryzhikov from the Nikolaev Institute of Inorganic Chemistry

(Novosibirsk, Russia). According to TDDFT calculations, the highest intensity dipole-allowed excitation occurs at 432 nm. As shown in Figure 5.6, the calculated band at 432 nm has its origin in an electronic transition arising from the HOMO-6 to the LUMO +3, and these orbitals are mainly located on the coordinated $BPyDTS_2$ ligand (*ca.* 100 % electron distribution). The energy of the calculated transition is 2.87 eV (432 nm), which is in close agreement with the experimental value (435 nm), obtained from the UV/Vis spectrum of complex $(Et_4N)_2$[**4**] (see Figure 5.5 and Table 5.1). It is noteworthy that the electronic distribution on the HOMO-6 is located on the dithiolate moiety of the ligand, and has π-donor character (60 %). In contrast, the electron distribution on the LUMO+3 is located on the pyridyl moieties, and presents π-acceptor character (70 %).

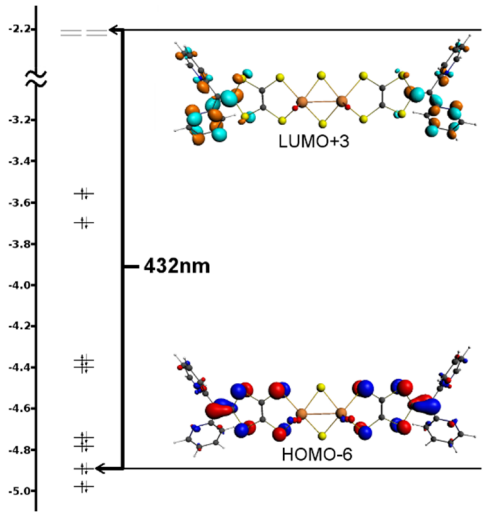

Figure 5.6. Molecular orbital scheme and graphical representation of the HOMO-6 and LUMO+3 orbitals for complex $(Et_4N)_2$[**4**].

The photophysical data for complexes **3**, $(Et_4N)_2$[**4**] and $(Et_4N)_2$[**5**] in acetonitrile at room temperature are listed in Table 5.2. Compound $(Et_4N)_2$[**4**] exhibits emission in the 600 – 800 nm wavelength region upon excitation at 532 nm

(see Figure 5.7). For this complex, the maximum emission intensity is observed at 628 nm, and the emission quantum yield (ϕ_{em}, relative to $[Ru(bpy)_3](BF_4)_2$) has a value of 0.092. Complex $(Et_4N)_2$[**5**], which results from the coordination of rhenium(I) through the nitrogen groups in complex $(Et_4N)_2$[**4**], presents a similar emission band shape, although the emission quantum yield is reduced by a factor of 4.6, as compared to that of $(Et_4N)_2$[**4**]. The dialkyltin dithiolene complex, **3**, presents a quantum yield value which lies between those of complexes $(Et_4N)_2$[**4**] and $(Et_4N)_2$[**5**], and its emission band coincides in shape and position with those of the dinuclear molybdenum clusters, *i.e.* $[\mathbf{4}]^{2-}$ and $[\mathbf{5}]^{2-}$.

Table 5.2. Luminescence data for compounds **3**, $(Et_4N)_2$[**4**] and $(Et_4N)_2$[**5**] in acetonitrile solution at 298 K.

Compound	λ_{em} (nm)	ϕ_{em}[a]
3	628	0.038
$(Et_4N)_2$[**4**]	628	0.092
$(Et_4N)_2$[**5**]	628	0.020

[a] Relative quantum yield using $[Ru(bpy)_3](BF_4)_2$ as a standard.

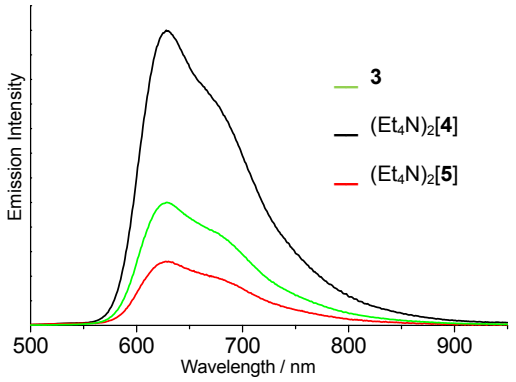

Figure 5.7. Emission spectra for complex **3**, $(Et_4N)_2$[**4**] and $(Et_4N)_2$[**5**] in acetonitrile at 298 K.

The analogous shape and position of the emission spectra of complexes **3**, $(Et_4N)_2$[**4**] and $(Et_4N)_2$[**5**] indicates that the observed emission can be ascribed to ILCT* excited states. This observation is in good agreement with the TDDFT calculations performed for compound $(Et_4N)_2$[**4**], and for other transition metal complexes containing the same ligand.[15,20] Analogous ILCT transitions have been reported in a number of transition metal complexes containing a diversity of ligands with both π-donor and π-acceptor sites.[21–25] In particular, an azobenzene-conjugated dithiolate platinum(II) complex presents electronic bands that can be attributed to π-π* ILCT transitions from the dithiolene to the azobenzene moiety.[23] A series of complexes of formula (dppe)M{S_2C_2(heterocycle)(H)}, (dppe = 1,2-bis(diphenylphosphino)ethane; M = Ni, Pd, and Pt; heterocycle = pyridine, pyrazine or quinoxaline derivatives), reported by Pilato and co-workers are notable for their ILCT absorption and emission transitions.[13,26–29] For instance, complex (dppe)Pt{S_2C_2(2-quinoxaline)(H)} presents two ILCT transitions arising from ^{1}ILCT* and ^{3}ILCT* excited states. For this complex, the maxima absorption and ^{1}ILCT* emission wavelengths in dichloromethane were observed at 442 nm and 636 nm, respectively.[27] These values are in good agreement with those listed in Tables 5.1 and 5.2 for complexes **3**, $(Et_4N)_2$[**4**] and $(Et_4N)_2$[**5**]. The absorption and emission bands in the aforementioned platinum(II) complexes have been ascribed to an ILCT from the 1,2-enedithiolate (π) to the N-heterocycle (π*). This explanation gives support to our description about the nature of the emission bands in complexes **3**, $(Et_4N)_2$[**4**] and $(Et_4N)_2$[**5**].

Despite the luminescence behavior exhibited by reported molybdenum clusters, the emission of clusters $(Et_4N)_2$[**4**] and $(Et_4N)_2$[**5**] is not directly related to the dinuclear molybdenum core, since the emission band of the tin complex **3** presents identical shape and λ_{em} to those of [**4**]$^{2-}$ and [**5**]$^{2-}$ (see Fig. 5.7). Nevertheless, the $Mo_2O_2S_2$ core seems to play a significant role in the emission quantum yield, as

the ϕ_{em} value for complex [**4**]$^{2-}$ is almost 2.5 times that of the tin complex **3**. The emission quantum yield values obtained for the series of complexes in Table 5.2 are significantly higher than those reported for transition metal complexes of formula (dppe)M{S_2C_2(heterocycle)(H)}, presenting intraligand charge transfers.[13,26–29] In these complexes the ϕ_{em} values typically lie between less than 0.01 and 0.03. The emission lifetime of complexes **3**, $(Et_4N)_2$[**4**] and $(Et_4N)_2$[**5**] in acetonitrile resulted to be extremely short (< 10 ns), and therefore they could not be determined with the equipment employed. This short emission lifetime agrees well with the τ_{em} values for the systems reported by Pilato, which present analogous ILCT transitions to the series of complexes investigated in this chapter.[13,26–29] The lower quantum yield in the heterometalic complex [**5**]$^{2-}$ in comparison to [**4**]$^{2-}$ could be tentatively ascribed to fast charge separation in the excited state, since it is well stablished that rhenium tricarbonyl polypyridine complexes can act as electron acceptors.[17,30] Finally, it is also worth mentioning that powdered samples of compounds **3**, $(Et_4N)_2$[**4**] and $(Et_4N)_2$[**5**] did not display emission at room temperature, presumably due to self-quenching processes in the solid state.

5.2. LUMINESCENCE AND ANION SENSING BEHAVIOR OF TRINUCLEAR MOLYBDENUM CLUSTERS

5.2.1. INTRODUCTION

Imidazo[4,5-f]-1,10-phenanthroline ligands have the ability to form stable complexes with a diversity of transition metals, which include zinc, platinum, rhenium, ruthenium, lanthanides, and even uranium.[16,31–33] The extensively investigated coordination of imidazophenanthroline-like ligands to transition metals has been motivated by the interesting properties of these compounds.[31–45] More specifically, imidazophenanthrolines have been used for the design of metallomesogens,[33,45] anion sensors,[32,34] nonlinear optical materials,[44] and electroluminescent devices,[36,38] among other applications. Additionally, the luminescent character of substituted imidazophenanthroline ligands allows the synthesis of multifunctional materials, in which a combination of physical properties can be present.[33,45]

Cardinaels and co-workers have developed a series of imidazophenanthrolines substituted with long alkyl chains, and their coordination to different metals has been investigated.[33,45] In particular, the ruthenium(II) complex depicted in Figure 5.8 presents liquid crystalline properties with smectic A phases, and the transition temperature strongly depends on the counterion.[33] In addition, this complex is luminescent in both chloroform solution and in the solid state, with an emission maximum located at 630 nm, which can be assigned to π^*(ligand)←d_π(Ru) MLCT transitions.

An interesting imidazophenanthroline ligand containing a ferrocenyl group has been employed by Tárraga *et al.* for the preparation of iridium(III) and ruthenium(II) complexes. For instance, the trisubstituted iridium(III) complex in Figure 5.9 is a reversible redox-luminescent switch, in which the fluorescence intensity is enhanced upon addition of a chemical oxidant.[37] The ruthenium(II)-ferrocene heterobimetallic system in Figure 5.9 exhibits a high anion sensing

selectivity towards chloride.[34] A dramatic increase in the fluorescence intensity and in the emission quantum yield was registered in acetonitrile solutions of this complex upon addition of Cl^-. This increase was attributed to the formation of a hydrogen-bonded adduct in which the chloride anion interacts with the imidazophenanthroline ligand. The formation of this aggregate was not observed in other anions.

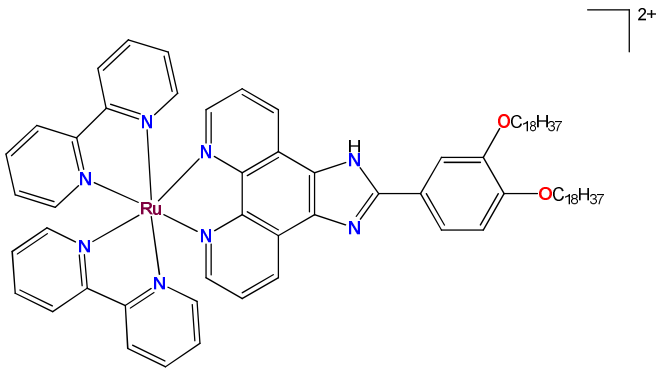

Figure 5.8. Molecular structure of a ruthenium(II) complex exhibiting simultaneously liquid crystalline and luminescence properties.

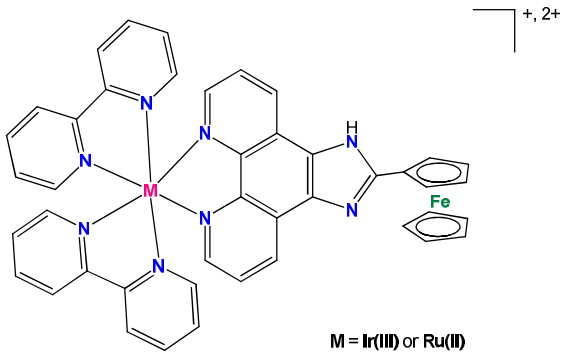

Figure 5.9. Molecular structure of iridium(III) and ruthenium(II) complexes containing an imidazophenanthroline ligand with a ferrocenyl subunit.

Raposo and co-workers have developed a series of π–conjugated imidazophenanthroline derivatives containing thiophene moieties.[44] These compounds exhibit a strong solvatochromic effect and luminescence properties. In

addition, they present a modest second-order nonlinear optical response. These properties make these compounds suitable for the preparation of optical materials based on transition metals, and also for the development of solvent polarity probes.

Another noteworthy aspect of imidazophenanthroline ligands is their relatively straightforward preparation, as well as their versatility. To illustrate this, the synthetic pathway for 2-phenylimidazo[4,5-f]-1,10-phenanthroline (PIP) is provided in Scheme 5.1. These types of ligands can be conveniently prepared by following an adaptation of the method reported by Steck and Day for the synthesis of 2-substitued phenanthrimidazoles.[46] Reaction between 1,10-phenanthroline-5,6-dione (abbreviated as phendione) and an aldehyde (benzaldehyde in this case) in the presence of ammonium acetate and glacial acetic acid affords the desired imidazopheanthroline ligand in good yields.[47] In this way, a judicious choice of benzaldehyde precursor can afford a diversity of imidazophenanthroline derivatives.

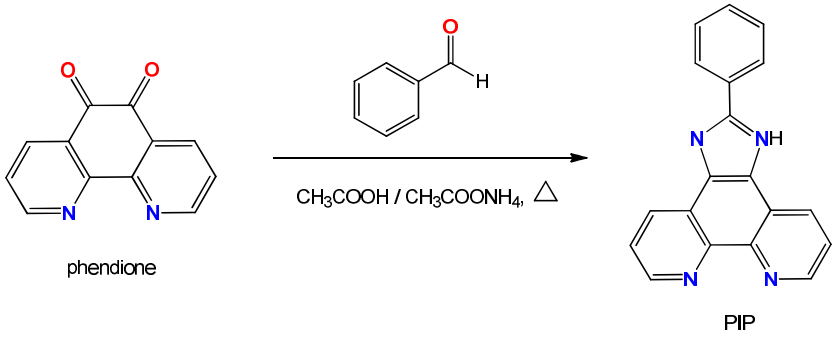

Scheme 5.1. Synthetic approach to the preparation of imidazophenanthroline ligands.

Motivated by the interesting properties that can emerge from transition metal complexes functionalized with imidazophenanthroline ligands,[31–45] as well as by their relatively simple and convenient synthetic procedures,[47] we decided to explore the preparation and further coordination of such ligands to Mo_3S_7 cluster units. As already mentioned in Chapter 4, the coordination of diimine ligands to $[Mo_3S_7X_6]^{2-}$ cluster precursors (X = Cl or Br)[48] results in the partial substitution of two bromide

ligands by the nitrogen groups in the diimine to afford neutral cluster complexes of formula $Mo_3S_7X_4$(diimine), where X = Cl or Br.[48] The luminescence properties of complexes $Mo_3S_7X_4$(IPDOP) (X = Br; **12**, or Cl; **13**), obtained by coordination of the novel ligand 1H-Imidazo[4,5-f]-1,10-phenanthroline-2-[3,4-bis(dodecyloxy)phenyl] (IPDOP) to the Mo_3S_7 unit (see Scheme 5.2) are investigated herein. Moreover, the potential ability of complexes **12** and **13** to detect halide ions in solution, as well as the study of their liquid-crystalline properties are also presented in this chapter.

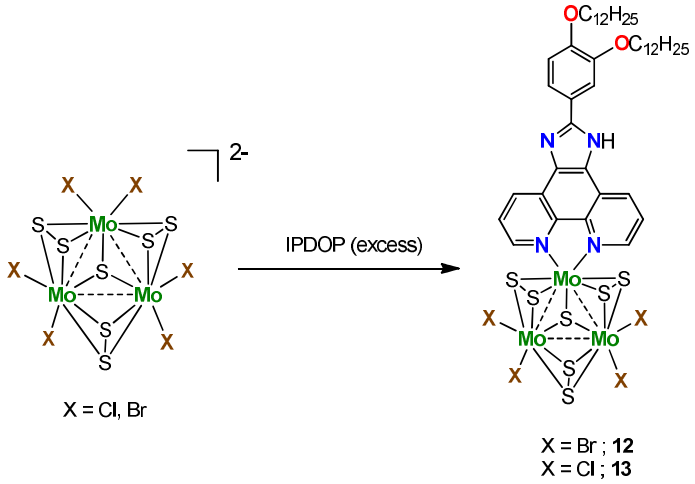

Scheme 5.2. Synthetic pathway for complexes **12** and **13**.

5.2.2. RESULTS AND DISCUSSION

Complexes **12** and **13** represent the first examples of molybdenum clusters derivatized with imidazophenanthroline ligands, and hence could lead to potential optical materials.[32–34,44,45] The photophysical behavior of complexes **12**, **13**, as well as that of the free ligand, IPDOP, was investigated by steady-state and time-resolved fluorescence spectroscopy at Universitat Jaume I (Castelló, Spain) in collaboration with Prof. F. Galindo. As a representative example, the normalized absorption and emission spectra of complex **12** in both dichloromethane and dimethylformamide are depicted in Figure 5.10. For all compounds, the emission spectra were recorded upon excitation at 330 nm.

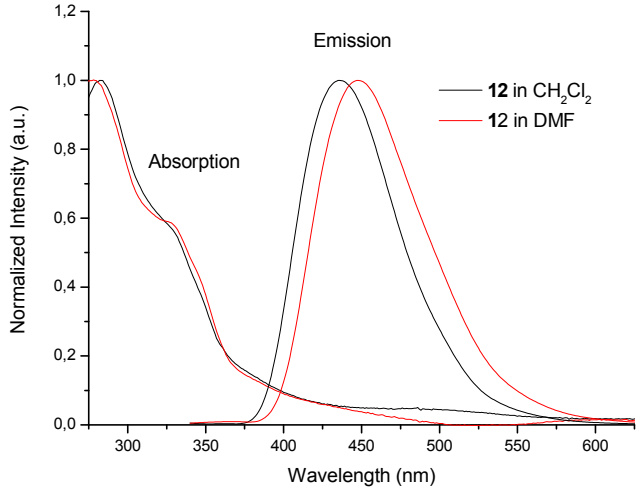

Figure 5.10. Absorption and emission spectra of 5 μM solutions of complex **12** in dichloromethane and dimethylformamide. The emission spectra were recorded upon excitation at 330 nm.

The UV/Vis spectra of complexes **12** and **13** present high intensity absorption bands in the 275 – 375 nm range, and low intensity bands in the visible range, the latter leading to reddish-colored solutions in CH_2Cl_2 and DMF. These bands may be assigned to charge-transfer transitions, as reported for transition metal

complexes containing phenanthroline derivatives.[49] The steady-state emission spectra of complexes **12** and **13** in CH_2Cl_2 present maxima at 436 nm. These spectra coincide in shape and position with that of the free ligand, IPDOP, which exhibits an emission maximum intensity at 435 nm in the same solvent. As listed in Table 5.3, the emission maxima of complexes **12** and **13** in DMF (448 nm and 451 nm, respectively) also coincide with that of IPDOP ligand in this solvent (450 nm).

The emission quantum yields (ϕ_{em}) of the samples were calculated according Equation 5.1, using quinine sulfate as a standard (ϕ_{em} = 0.546 in 0.5 M H_2SO_4).[50]

$$\phi_s = (\phi_r \cdot A_r \cdot I_s \cdot n_s^2)/(A_s \cdot I_r \cdot n_r^2) \quad \textbf{(5.1)}$$

where A_s and A_r are the absorbance of the sample and the reference; I_s and I_r are the corresponding integrated emissions, and n_s and n_r are the refractive indexes of the solvent of the sample, and the reference. In both solvents, the emission quantum yield (ϕ_{em}) for the free ligand is higher than those of complexes **12** and **13**. For instance, the emission quantum yield of IPDOP in DMF (0.29) decreases three-fold in complex **12**, and is roughly reduced by *ca.* a factor of 2 in complex **13**. An analogous tendency was observed for the same compounds in CH_2Cl_2. The difference between the emission quantum yield for complexes **12** and **13** indicates that the value of ϕ_{em} strongly depends on the halide groups coordinated to the Mo_3S_7 cluster. On the other hand, the coincidence in the positions of the emission maxima in complexes **12** and **13**, and in the free ligand IPDOP suggest that the nature of the emission in these imidazophenanthroline-based clusters can be ascribed to intraligand charge-transfer (ILCT) transitions.[51] As a matter of fact, unsubstituted 1H-imidazo[4,5-f]-1,10-phananthroline has been reported to emit at 460 nm in methanol, with a quantum yield of 0.25 and a lifetime of 2.5 ns.[35] These values are in good agreement with the fluorescence data listed in Table 5.3 for the ligand IPDOP and for complexes **12** and

13, and therefore give support to our description of the ligand-based emission in these clusters.

Table 5.3. Fluorescence data for the free ligand IPDOP, and for complexes **12** and **13**, recorded upon excitation at 330 nm.

Solvent	Compound	ϕ_{em}[a]	τ, ns	k_r, s^{-1}	k_{nr}, s^{-1}	λ_{em}, nm
CH_2Cl_2	IPDOP	0.21	5.5	3.8×10^7	1.4×10^8	435
	12	0.06	5.4	1.1×10^7	1.7×10^8	436
	13	0.11	5.5	2.0×10^7	1.6×10^8	436
DMF	IPDOP	0.29	7.5	3.9×10^7	9.5×10^7	450
	12	0.10	7.6	1.3×10^7	1.2×10^8	448
	13	0.15	7.5	2.0×10^7	1.1×10^8	451

[a] relative to quinine sulfate

The emission behavior of complexes **12** and **13** sharply contrasts with that of other transition metal complexes. For instance, the solid state emission spectrum of an imidazophenanthroline cadmium(II) complex described by Wang *et al.* has been ascribed to ligand to metal charge-transfer (LMCT) transitions.[52] It is also noteworthy the solvent dependency found in the emission maxima of complexes **12** and **13**, as well as in that of the free ligand IPDOP (see Table 5.3). The most dramatic shift was registered for complex **13**. The emission spectrum of this complex in dimethylformamide is red-shifted by 15 nm, as compared to that of the same compound in dichloromethane. This bathochromic effect is not unprecedented, since it has already been reported in analogously functionalized imidazophenanthroline ligands.[44]

In order to determine the emission lifetimes (τ) of the free ligand IPDOP and complexes **12** and **13**, time-resolved emission measurements were carried out, and the decays fitted to a monoexponential model (see Equation 5.2). All three compounds present virtually identical τ values, which strictly depend on the solvent (*ca.* 5.5 ns in CH_2Cl_2 *vs* 7.5 ns in DMF). These low τ values indicate that the emission originates from a ^{1}ILCT* excited state (fluorescence).

$$I(t) = A \cdot e^{-t/\tau} \quad \textbf{(5.2)}$$

Aimed at providing further insight into the quenching processes associated to the emission of our compounds, the radiative (k_r) and non-radiative (k_{nr}) rate constants were calculated according to Equations 5.3 and 5.4.

$$k_r = \phi_{em}/\tau \quad \textbf{(5.3)}$$

$$k_{nr} = (1 - \phi_{em})/\tau \quad \textbf{(5.4)}$$

As can be seen in Table 5.3, the singlet excited state of the free ligand IPDOP is radiatively deactivated at a rate of 3.8×10^7 s^{-1} in dichloromethane solution, whereas for complexes **12** and **13**, k_r is significantly lower. On the other hand, the non-radiative processes are enhanced in the complexes, as compared to the free ligand. More specifically, k_{nr} increases from 1.4×10^8 to *ca.* 1.7×10^8 s^{-1} upon coordination of the IPDOP ligand. The same tendencies in k_r and k_{nr} were observed when the measurements were carried out in dimethylformamide (see Table 5.3). These decrease in k_r and increase in k_{nr} (relative to the free ligand) for complexes **12** and **13** indicate that the singlet excited state is deactivated by non-radiative processes. As shown in the simplified Jablonski diagram for the free ligand IPDOP (Figure 5.11), there are four non-radiative processes that may participate in the deactivation of a singlet excited state, namely internal conversion (IC), intersystem crossing (ISC) to the triplet state, electron transfer (eT), or energy transfer (ET). Further studies would be required to discern between IC, ISC, eT and ET as the main cause of the deactivation process. Nevertheless, it can be concluded that coordination of imidazophenanthrolines to molybdenum clusters has a significant effect on the photophysical properties. These results pave the way to a new series of photoactive materials based on Mo_3S_7 cluster units.

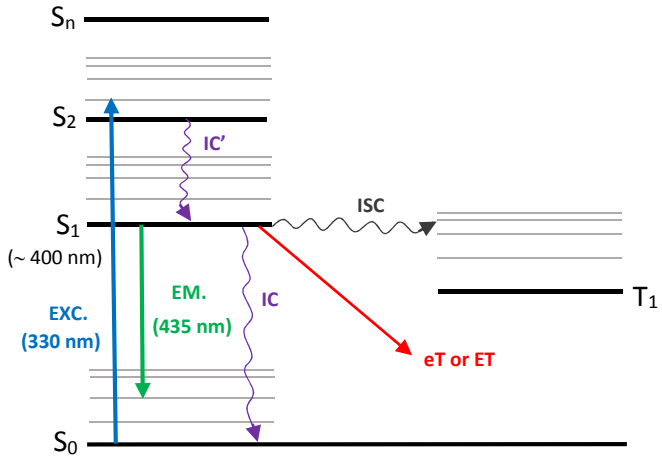

Figure 5.11. Simplified Jablonski diagram for IPDOP in CH_2Cl_2. Note that according to Palit *et al.*, the $S_1 \leftarrow S_0$ transition must be observed at *ca.* 400 nm, corresponding to a n-π^* forbidden excitation.[35]

An important aspect of the fluorescence behavior of complexes **12** and **13** is the striking changes in their emission spectra upon addition of various anions. As depicted in Figure 5.12, in the presence of anionic species such as F^-, OH^- and AcO^- in their tetrabutylammonium forms, the emission band of complex **12** in DMF undergoes a dramatic red-shift of roughly 92 nm (from 448 to ~540 nm). Nevertheless, addition of Cl^-, Br^- or SCN^- do not have any effect on the emission spectrum of complex **12**. A similar behavior was observed for complex **13** in the same solvent. This intriguing phenomenon can be presumably attributed to charge redistributions within the IPDOP ligand originated by hydrogen bonding interactions between the NH group of the imidazole ring and certain anions, as already observed by Liu *et al.* for a calix[4]arene compound containing imidazophenanthroline groups.[53] Analogous emission shifts induced by anions have been recently reported in a number of transition metal complexes bearing imidazole moieties, which serve as chemosensors for the selective detection of anions.[54–59] For instance, Zheng and co-workers have described a lanthanide complex containing a 2-(3,4,5-

trimethoxyphenyl)imidazo[4,5-f]-1,10-phenanthroline ligand, which displays a red shift in its emission spectrum of *ca.* 50 nm (from roughly 450 to 500 nm) upon interaction with acetate anions in dimethylsulfoxide solution.[32]

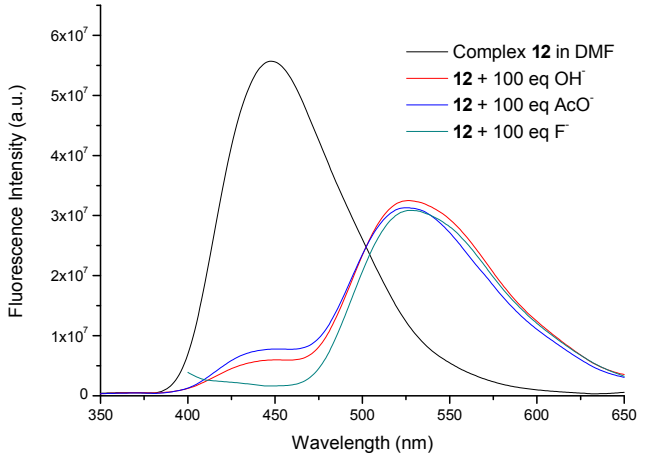

Figure 5.12. Emission spectra of 5 μM complex **12** in DMF in the presence of different anions: a) 100 eq OH^-, b) 100 eq CH_3COO^- and c) 100 eq F^-. The emission spectra were recorded upon excitation at 330 nm.

The liquid-crystalline phases observed by Cardenaels *et al.* in ruthenium complexes containing imidazophenanthroline ligands with long alkoxy chains led us to investigate the liquid-crystalline character of complexes **12** and **13**.[33,45] This property was studied in collaboration with Dr. Y. Molard from the Institut de Sciences Chimiques de Rennes (France) by Temperature Dependent Polarized Optical Microscopy. To our dismay, both of these compounds decomposed upon heating to temperatures above the boiling point (> 240ºC), and neither isotropic states nor clear birefringence were observed. Nevertheless, the complexes presented in this section, *i.e.* **12** and **13**, represent to the best of our knowledge the first examples of Mo_3S_7 clusters containing imidazophenanthroline ligands which exhibit dramatic shift in their emission spectra upon interaction with anionic species, and hence open

new avenues in the search for anion probes based on transition metal complexes.[54–59]

5.3. OPTICAL NONLINEARITIES OF HETEROLEPTIC TRINUCLEAR MOLYBDENUM CLUSTERS

5.3.1. INTRODUCTION

In the digital era, electronic devices are taken for granted without considering the limitations of electronics, such as limits in the operational speed which are intrinsic to the electric circuits, and the existence of electromagnetic interferences. Photonics has emerged as a new field which uses photons instead of electrons to acquire, store, process and transmit information, overcoming in this way the drawbacks of traditional electrical devices.[60]

Nonlinear optics is a cornerstone in photonics. When light propagates on a material, its electrons oscillate in response to the external electromagnetic field. At low light intensities, the induced electrical polarization is proportional to the amplitude of the electrical field, *E*. However, if the light intensity is high, a non-linear response to the electric field may emerge. This phenomenon is commonly known as nonlinear optics (NLO), and in such a case the dipole moment (μ) can be determined by Equation 5.5.

$$\mu_i = \mu_i^0 + \alpha_{ij}E_j + \beta_{ij}E_jE_k + \gamma_{ijkl}E_jE_kE_l + \cdots \quad \textbf{(5.5)}$$

In the latter expression, μ_i^0 is the permanent dipolar moment in the *i* direction, α represents the linear polarizability, while β and γ are the second-order and third-order polarizabilities, respectively. $E_{j,k,l}$ refers to the electrical field inside the material in the different directions, *i.e.* j, k, and l.[61–63]

One important aspect in nonlinear optics is optical limiting (OL). This physical phenomenon consists in a decrease in the transmittance of a material when the incident light intensity increases. An ideal optical limiter should become

transparent at low light intensity, and opaque at high intensity. Moreover, it should be able to present reversibility between these two states, as well as fast responses to external optical stimuli. This behavior is opposite to that of most materials, which become more transparent upon irradiation with high-intensity light. Some applications of optical limiters include the protection of human eyes and optical devices from high intensity lasers.[64,65]

Inorganic materials have been widely used in optics and electronics for a long time. The development of microelectronics has led to a growing demand of novel compounds able to meet the demands of technology. In this context, the search for materials presenting optical nonlinearities is of outmost importance these days, motivated by their use in communications and information storage devices, among other fields.[66–68]

Over the past few decades, a great deal of effort has been devoted to the development of third-order nonlinear optical materials based on inorganic semiconductors, organic polymers, and fullerenes.[60] A diversity of transition metal complexes exhibiting optical nonlinearities have also been developed as potential photonic materials.[61] Nevertheless, inorganic cluster compounds have been far less explored for these purposes mainly due to two reasons: their usual deep color, which makes them unsuitable for most NLO applications, and their frequent instability when exposed to high-intensity light.[60]

Despite the apparent limitations of metal clusters in the field of nonlinear optics, they present a number of advantages over other inorganic/organic compounds traditionally used in nonlinear optics. Firstly, their constituent heavy atoms introduce more energy sublevels, and thus more allowed transitions and larger NLO effects, as compared to organic molecules. Secondly, the NLO properties of metal clusters can be easily tailored to specific application requirements by changing the constituent elements, oxidation state, structural type and/or outer ligands.[60]

Furthermore, the photochemical stability of metal clusters can be enhanced with bridging sulfide groups which reinforce the metal-metal bonds. Incidentally, M/Q/M' (M = Mo, W; Q = S, Se; M' = Cu, Ag) heterometallic clusters have attracted significant interest in the search for novel materials with strong third-order optical nonlinearities and good optical limiting performance.[69,70] It is noteworthy that a series of reported heterometallic cubane-like clusters present great stability toward light irradiation, and exhibit superior optical limiting capabilities to fullerene C_{60}, a well-known optical limiter.[71–73]

The nonlinear optical performance of a series of trinuclear and tetranuclear cluster chalcogenides of formulae $[M_3(\mu_3\text{-}Q)(\mu_2\text{-}Q)_3X_3(\text{diphosphine})_3]^+$ and $[M_3Cu(\mu_3\text{-}Q)(\mu_2\text{-}Q)_3X_3(\text{diphosphine})_3]^+$, respectively (M = Mo or W; Q = S or Se; X = Cl or Br) have been investigated in the past few years.[74,75] These compounds are efficient optical limiters, and their optical limiting merit decrease on proceeding from the tetranuclear to the trinuclear core, and upon replacing tungsten by molybdenum. Optical power limiting has also been found in $Mo_3(\mu_3\text{-}S)(\mu_2\text{-}S_2)_3$ cluster sulfides bearing maleonitriledithiolate, oxalate or thiocyanate ligands, although no clear tendencies in the effect of the outer ligand on the NLO properties could be drawn from these results.[76]

In our search for better NLO materials, in this Section we have investigated the nonlinear optical properties of a series of heteroleptic Mo_3S_7 clusters containing either mixed diimine-halide, $Mo_3S_7X_4(\text{diimine})$, (X = Cl, Br; complexes **18** – **21**), or diimine-dithiolene ligands, $Mo_3S_7(\text{dithiolene})_2(\text{diimine})$, (complexes **29** – **31**). This choice of outer ligands was motivated by the nonlinear optical behavior reported in transition metal complexes with diimine ligands.[77,78] Furthermore, dithiolene π-extended systems are well-known to enhance the NLO properties of a material.[79,80] Complexes **18** – **21** and **29** – **31** (see Figure 5.13) represent to the best of our knowledge the first examples of heteroleptic trinuclear molybdenum cluster

exhibiting third-order NLO effects. The NLO behavior of the dinuclear cluster $(Et_4N)_2[Mo_2O_2S_2(BPyDTS_2)_2]$, ($(Et_4N)_2$[**4**]; $BPyDTS_2$ = 2-bis-(2-pyridyl)methylene-1,3-dithiolene; Fig. 5.4), whose luminescent properties were studied in Section 5.1, has also been investigated, with the aim of finding correlations between nuclearity and third-order nonlinear optical functions.

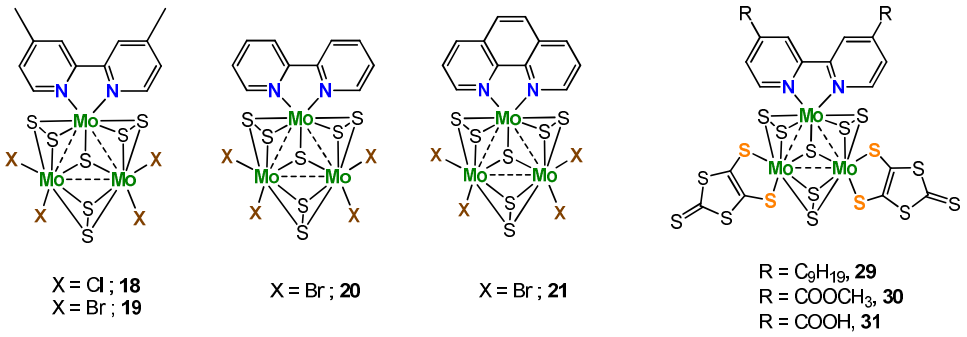

Figure 5.13. Molecular structure of complexes **18** – **21** and **29** – **31**.

5.3.2. RESULTS AND DISCUSSION

The linear and non-linear optical properties of clusters **18** – **21** and **29** – **31** were assessed by the group of Prof. M. Humphrey at the Research School of Chemistry (Australian National University), and compared to those exhibited by the dinuclear cluster $(Et_4N)_2$[**4**]. All measurements were carried out in dimethylformamide, owing to the limited solubility of the samples in less polar solvents.

Table 5.4 lists the UV/Vis absorption wavelengths for complexes **18** – **21**, bearing both diimine and halide ligands. All complexes present high intensity bands in the 300 – 375 nm region, with molar extinction coefficients lying between 5.2 × 10^3 and 21.1 × 10^3 M^{-1} cm^{-1}. The absorption bands for the mixed-ligand diimine-dithiolene complexes **29** – **31** are in general more intense than those for the diimine-bromide derivatives, and present molar extinction coefficients in the range of 7.4 – 27.7 × 10^3 M^{-1} cm^{-1} between 307 and 407 nm. In addition, weaker absorption bands

have been found in the 450 – 500 nm region for both series of complexes. The molar absorption coefficients for complexes **29** – **31** (5.1 – 10.2 × 10^3 M^{-1} cm^{-1}) in this region are again higher than those for compounds **18** – **21** (1.9 – 3.7 × 10^3 M^{-1} cm^{-1}). Remarkably, the highest energy maximum in the 450 – 500 nm region has been observed for the chloro-ligated cluster **18**, whereas the lowest energy maxima have been registered for complexes **29** – **31**, containing the dmit (1,3-dithiole-2-thione-4,5-dithiolate) ligand.

The cluster $(Et_4N)_2[Mo_2O_2S_2(BPyDTS_2)_2]$, ($(Et_4N)_2$[**4**]) is structurally distinct, possessing a $Mo_2O_2(\mu\text{-}S)_2$ core, in contrast to the other Mo_3S_7-based heteroleptic complexes. The absorption bands in this complex present the lowest energy values in the series. Interestingly, the linear optical spectra of the eight metal clusters present low-intensity absorption bands in the visible region of the spectrum, a requisite for the design of broad-band optical limiters.[75]

Table 5.4. Linear optical data for $(Et_4N)_2$[**4**], **18** – **21** and **29** – **31**.

Cluster	λ_{abs}/nm ($10^{-3}\cdot\varepsilon$ / M^{-1} cm^{-1})		
$(Et_4N)_2$[**4**]	341 (32)	423 (sh, 10.1)	525 (2.4)
18	320 (sh, 11.1)	370 (sh, 5.3)	450 (2.3)
19	313 (sh, 21.1)	375 (sh, 7.5)	461 (3.7)
20	313 (sh, 16.5)	370 (sh, 5.2)	471 (sh, 2.4)
21	304 (sh, 14.9)	352 (sh, 6.1)	493 (sh, 1.9)
29	307 (sh, 27.7)	-	497 (5.1)
30	332 (sh, 17.1)	407 (sh, 7.4)	493 (10.2)
31	311 (sh, 24.8)	335 (sh, 17)	500 (9.7)

Relevant data for the optical limiting merit of the di- and trinuclear complexes investigated in this chapter are collected in Table 5.5. The optical limiting power was assessed by the Z-scan technique at 570 nm,[81] where the absorption of all eight clusters is rather low (ε = 310 – 4 410 M^{-1} cm^{-1}). This technique has already been employed in previous studies on trinuclear molybdenum and tungsten chalcogenides.[74–76] The data from the power limiting curves was converted into transmittance-fluence plots assuming a Gaussian character for the laser beam, and the effective cross-sections were calculated.[82]

Table 5.5. Optical limiting data for $(Et_4N)_2$[**4**], **18** – **21** and **29** – **31**.

Cluster	ε_{570} (M^{-1} cm^{-1})[a]	$F_{15\%}$ (J cm^{-2})[b]	Cross Section ($\times 10^{-18}$ cm^2)	
			Ground State, σ_0	Excited State, σ_{eff}
$(Et_4N)_2$[**4**]	1590	0.32	6.1	5.5
18	310	0.25	1.2	2.1
19	830	0.14	3.2	3.4
20	790	0.13	3.0	3.2
21	820	0.20	3.2	3.9
29	4410	0.05	16.9	21.3
30	1790	0.07	13.6	16.8
31	3060	0.20	11.7	12.7

[a] Molar extinction coefficient at the measurement wavelength (570 nm). [b] Incident fluence required to reduce the transmittance through the sample by 15 %

A representative transmission *vs* fluence (energy of laser/unit area) plot (that of complex **20**) is displayed in Figure 5.14. For comparative purposes, a threshold limiting fluence $F_{15\%}$ was used to assess the relative optical limiting merit of the current clusters. This value represents the incident fluence required to reduce the

transmittance through a sample by 15 %. The threshold limiting fluence $F_{15\%}$ for our series of complexes increases on decreasing the nuclearity (see Table 5.5). In other words, the optical limiting merit increases on proceeding from the dinuclear ($(Et_4N)_2$[**4**]) to the trinuclear (**18** – **21** and **29** – **31**) clusters. The skeletal structure and metal nuclearity have been reported to have a strong impact on the NLO properties of transition metal complexes.[69,83] In particular, in cluster chalcogenides of formula $[M_3(\mu_3\text{-}Q)(\mu_2\text{-}Q)_3X_3(diphosphine)_3]^+$ (M = Mo, W; Q = S, Se; X = Cl, Br), the threshold limiting fluence has been found to decrease upon insertion of copper into the trinuclear core to afford tetranuclear $[M_3Cu(\mu_3\text{-}Q)(\mu_2\text{-}Q)_3X_3(diphosphine)_3]^+$ complexes.[74]

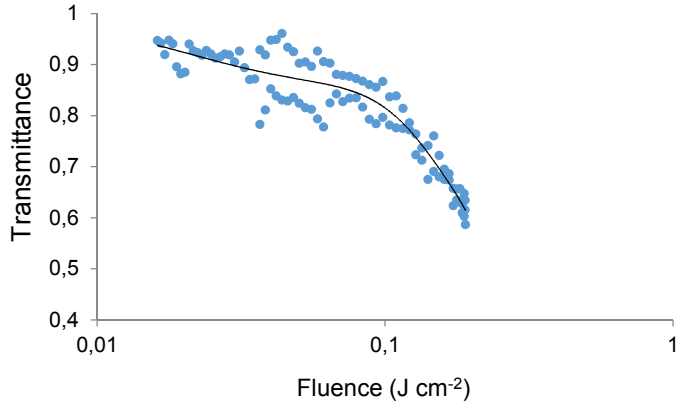

Figure 5.14. Optical limiting behavior of complex **20** in dimethylformamide.

Values of the excited-state cross section (σ_{eff}) for all eight clusters are given in Table 5.5. With the exception of the dinuclear cluster $(Et_4N)_2$[**4**], the σ_{eff} values are larger than those of the corresponding ground-state cross section, σ_0, that is to say, all heteroleptic trinuclear clusters in the series (*i.e.* **18** – **21** and **29** – **31**) are efficient optical limiters. The mixed-ligand diimine-dithiolene complexes **29** – **31** present larger σ_{eff} values than those of complexes **18** – **21** bearing both diimine and halide

ligands. This fact suggests that π-delocalization induced by dmit ligands enhances the optical limiting performance of the trinuclear clusters. This is not unexpected, since it is well established that the presence of dithiolene ligands has a dramatic effect in the NLO responses of transition metal complexes.[80,84,85] Moreover, mixed-ligand diimine-dithiolene complexes analogous to compounds **29** – **31** have attracted a great deal of interest due to the NLO effects that can derive from the different character of the ligands; acceptor for the diimine, and donor for the dithiolate.[86] In these push-pull complexes, the HOMO is formed by a mixture of metal and dithiolate orbitals, while the diimine orbitals contribute predominantly to the LUMO. It is noteworthy that the effective excited state cross section, σ_{eff}, should be regarded as only a measure of the power limiting ability of a material under certain experimental conditions, and therefore comparison between σ_{eff} values obtained in different experiments should be circumspect.[74–76]

5.4. CONCLUSIONS

The luminescent properties of a novel dinuclear cluster complex, *i.e.* $(Et_4N)_2$[$Mo_2O_2(\mu\text{-}S)_2(BPyDTS_2)_2$], ($(Et_4N)_2$[**4**]), have been investigated. This complex exhibits fluorescence in acetonitrile solution with an emission maximum at 628 nm and a quantum yield of *ca.* 0.10. According to TDDFT calculations, the emission in $(Et_4N)_2$[**4**] arises from an ILCT transition from the dithiolene (π) to the pyridyl moieties (π*). Insertion of two terminal $Re(CO)_3Cl$ fragments into complex $(Et_4N)_2$[**4**] through the outer nitrogen atoms in the $BPyDTS_2$ ligand leads to a decrease in the emission quantum yield by a factor of *ca.* 4.6, as compared to that of $(Et_4N)_2$[**4**]. The emission behavior of a tin complex containing the $BPyDTS_2$ ligand, namely $Me_2Sn(BPyDTS_2)$, (**3**), has also been investigated for comparative purposes. The coincidence in shape and position of the emission spectra in all three complexes indicates that the emission arises in all cases from an ILCT* excited state.

Two novel heteroleptic Mo_3S_7 complexes bearing imidazophenanthroline ligands, *i.e.* $Mo_3S_7X_4$(IPDOP), (X = Br; **12**, or Cl; **13**) exhibit luminescence in the 375 – 600 nm region in both dichloromethane and dimethylformamide solutions. The maximum quantum yield and emission lifetime were achieved for complex **13** in DMF, with ϕ_{em} = 0.15 and τ = 7.5 ns. The emission spectrum of this complex in dimethylformamide is red-shifted by 15 nm, as compared to that of the same compound in dichloromethane. It is also noteworthy that the non-radiative processes are enhanced in complexes **12** and **13**, in comparison with those of the free ligand IPDOP. A dramatic shift towards longer emission wavelengths was observed in the emission spectra of complexes **12** and **13** in solution upon addition of proton-abstractor anions (F^-, OH^- or AcO^-). These results envisage the potential of these systems for metal-cluster-based halide sensors, as long as they are tailored to the specific sensitivity and selectivity requirements of a given application.

The optical power limiting of a series of mixed-ligand diimine-halide or diimine-dithiolene Mo_3S_7 cluster complexes (*i.e.* **18** – **21** and **29** – **31**) has been assessed by Z-scan techniques in dimethylformamide solution. The threshold limiting fluence and effective cross section values for the aforementioned series of trinuclear complexes were compared to those of the dinuclear complex $(Et_4N)_2[Mo_2O_2(\mu\text{-}S)_2(BPyDTS_2)_2]$, ($(Et_4N)_2$[**4**]). All trinuclear clusters are efficient optical limiters with $\sigma_{eff} > \sigma_0$. The optical limit merit increases on increasing the metal nuclearity and upon replacing the halides by dmit ligands. These results contribute to the search for better molecular materials presenting third-order NLO properties.

5.5. REFERENCES

(1) Zarkadoulas, A.; Koutsouri, E.; Mitsopoulou, C. A. *Coord. Chem. Rev.* **2012**, *256*, 2424–2434.

(2) Mitra, J.; Pal, K.; Sarkar, S. *Dalton Trans.* **2013**, *42*, 13905–13911.

(3) Davies, E. S.; Beddoes, R. L.; Collison, D.; Dinsmore, A.; Docrat, A.; Joule, J. A.; Wilson, C. R.; Garner, C. D. *J. Chem. Soc. Dalt. Trans.* **1997**, 3985–3996.

(4) Eisenberg, R.; Gray, H. B. *Inorg. Chem.* **2011**, *50*, 9741–9751.

(5) Fourmigué, M. *Acc. Chem. Res.* **2004**, *37*, 179–186.

(6) Cummings, S. D.; Eisenberg, R. In *Dithiolene Chemistry: Synthesis, Properties, and Applications*; Stiefel, E. I., Ed.; John Wiley & Sons, Inc., 2004; Vol. 52, pp. 315–367.

(7) Persaud, L.; Sharma, D. K.; Langford, C. H. *Inorganica Chim. Acta* **1986**, *114*, L5–L6.

(8) Johnson, C. E.; Eisenberg, R.; Evans, T. R.; Burberry, M. S. *J. Am. Chem. Soc.* **1983**, *105*, 1795–1802.

(9) Bevilacqua, J. M.; Eisenberg, R. *Inorg. Chem.* **1994**, *33*, 1886–1890.

(10) Sakamoto, R.; Kume, S.; Sugimoto, M.; Nishihara, H. *Chem. Eur. J.* **2009**, *15*, 1429–1439.

(11) Makedonas, C.; Mitsopoulou, C. A.; Lahoz, F. J.; Balana, A. I. *Inorg. Chem.* **2003**, *42*, 8853–8865.

(12) Pilato, R. S.; Van Houten, K. A. In *Dithiolene Chemistry: Synthesis, Properties, and Applications*; Stiefel, E. I., Ed.; John Wiley & Sons, Inc., 2004; Vol. 52, pp. 369–397.

(13) Kaiwar, S. P.; Hsu, J. K.; Liable-Sands, L. M.; Rheingold, A. L.; Pilato, R. S. *Inorg. Chem.* **1997**, *36*, 4234–4240.

(14) Rabaça, S.; Almeida, M. *Coord. Chem. Rev.* **2010**, *254*, 1493–1508.

(15) Liu, W.; Wang, R.; Zhou, X. H.; Zuo, J. L.; You, X. Z. *Organometallics* **2008**, *27*, 126–134.

(16) Cardinaels, T.; Ramaekers, J.; Nockemann, P.; Driesen, K.; Van Hecke, K.; Van Meervelt, L.; Lei, S.; De Feyter, S.; Guillon, D.; Donnio, B.; Binnemans, K. *Chem. Mater.* **2008**, *20*, 1278–1291.

(17) Gabrielsson, A.; Hartl, F.; Zhang, H.; Smith, J. R. L.; Towrie, M.; Vlček, A.; Perutz, R. N. *J. Am. Chem. Soc.* **2006**, *128*, 4253–4266.

(18) Wei, L.; Babich, J. W.; Ouellette, W.; Zubieta, J. *Inorg. Chem.* **2006**, *45*, 3057–3066.

(19) Yam, V. W.-W.; Ko, C.-C.; Zhu, N. *J. Am. Chem. Soc.* **2004**, *126*, 12734–12735.

(20) Liu, W.; Chen, Y.; Wang, R.; Zhou, X. H.; Zuo, J. L.; You, X. Z. *Organometallics* **2008**, *27*, 2990–2997.

(21) Vogler, A.; Kunkely, H. *Coord. Chem. Rev.* **2007**, *251*, 577–583.

(22) Singh, B.; Drew, M. G. B.; Kociok-Kohn, G.; Molloy, K. C.; Singh, N. *Dalton Trans.* **2011**, *40*, 623–631.

(23) Sakamoto, R.; Kume, S.; Sugimoto, M.; Nishihara, H. *Chem. - A Eur. J.* **2009**, *15*, 1429–1439.

(24) Michalec, J. F.; Bejune, S. A.; Cuttell, D. G.; Summerton, G. C.; Gertenbach, J. A.; Field, J. S.; Haines, R. J.; McMillin, D. R. *Inorg. Chem.* **2001**, *40*, 2193–2200.

(25) Le Bozec, H.; Renouard, T. *Eur. J. Inorg. Chem.* **2000**, *2000*, 229–239.

(26) Kaiwar, S. P.; Vodacek, A.; Blough, N. V; Pilato, R. S. *J. Am. Chem. Soc.* **1997**, *119*, 9211–9214.

(27) Kaiwar, S. P.; Vodacek, A.; Blough, N. V.; Pilato, R. S. *J. Am. Chem. Soc.* **1997**, *119*, 3311–3316.

(28) Van Houten, K. A.; Heath, D. C.; Barringer, C. A.; Rheingold, A. L.; Pilato, R. S. *Inorg. Chem.* **1998**, *37*, 4647–4653.

(29) Van Houten, K. A.; Walters, K. A.; Schanze, K. S.; Pilato, R. S. *J. Fluoresc.* **2000**, *10*, 35–40.

(30) Shih, C.; Museth, A. K.; Abrahamsson, M.; Blanco-Rodriguez, A. M.; Di Bilio, A. J.; Sudhamsu, J.; Crane, B. R.; Ronayne, K. L.; Towrie, M.; Vlcek, A.; Richards, J. H.; Winkler, J. R.; Gray, H. B. *Science* **2008**, *320*, 1760–1762.

(31) Yang, Z. H.; Xiong, X. F.; Hu, H. M.; Luo, Y.; Zhang, L. H.; Bao, Q. H.; Shang-Guan, Y. Q.; Xue, G. L. *Inorg. Chem. Commun.* **2011**, *14*, 1406–1409.

(32) Zheng, Y.; Tan, C.; Drummen, G. P. C.; Wang, Q. *Spectrochim. Acta - Part A Mol. Biomol. Spectrosc.* **2012**, *96*, 387–394.

(33) Cardinaels, T.; Ramaekers, J.; Driesen, K.; Nockemann, P.; Van Hecke, K.; Van Meervelt, L.; Goderis, B.; Binnemans, K. *Inorg. Chem.* **2009**, *48*, 2490–2499.

(34) Zapata, F.; Caballero, A.; Espinosa, A.; Tárraga, A.; Molina, P. *J. Org. Chem.* **2008**, *73*, 4034–4044.

(35) Mondal, J. A.; Ramakrishna, G.; Singh, A. K.; Ghosh, H. N.; Mariappan, M.; Maiya, B. G.; Mukherjee, T.; Palit, D. K. *J. Phys. Chem. A* **2004**, *108*, 7843–7852.

(36) Wang, R. Y.; Jia, W. L.; Aziz, H.; Vamvounis, G.; Wang, S.; Hu, N. X.; Popović, Z. D.; Coggan, J. A. *Adv. Funct. Mater.* **2005**, *15*, 1483–1487.

(37) Zapata, F.; Caballero, A.; Espinosa, A.; Tárraga, A.; Molina, P. *Dalton Trans.* **2009**, 3900–3902.

(38) Lee, J. F.; Chen, Y. C.; Lin, J. T. S.; Wu, C. C.; Chen, C. Y.; Dai, C. A.; Chao, C. Y.; Chen, H. L.; Liau, W. Bin. *Tetrahedron* **2011**, *67*, 1696–1702.

(39) Gan, G. L.; Chao, H.; Ji, S. B.; Chen, L. L.; Li, H. *Spectrochim. Acta - Part A Mol. Biomol. Spectrosc.* **2012**, *97*, 297–305.

(40) Andersson, J.; Lincoln, P. *J. Phys. Chem. B* **2011**, *115*, 14768–14775.

(41) Chen, H.; Lee, J.; Tseng, S.; Lin, M.; Liau, W. *J. Lumin.* **2012**, *132*, 2182–2187.

(42) Bao, Q. H.; Chen, Q.; Hu, H. M.; Ren, Y. L.; Xu, B.; Dong, F. X.; Yang, M. L.; Xue, G. L. *Inorganica Chim. Acta* **2013**, *405*, 51–57.

(43) Banik, B.; Somyajit, K.; Hussain, A.; Nagaraju, G.; Chakravarty, A. R. *Dalton Trans.* **2014**, *43*, 1321–1331.

(44) Batista, R. M. F.; Costa, S. P. G.; Belsley, M.; Lodeiro, C.; Raposo, M. M. M. *Tetrahedron* **2008**, *64*, 9230–9238.

(45) Cardinaels, T.; Ramaekers, J.; Nockemann, P.; Driesen, K.; Van Hecke, K.; Van Meervelt, L.; Lei, S.; De Feyter, S.; Guillon, D.; Donnio, B.; Binnemans, K. *Chem. Mater.* **2008**, *20*, 1278–1291.

(46) Steck, E. A.; Day, A. R. *J. Am. Chem. Soc.* **1943**, *65*, 452–456.

(47) Wu, J.-Z.; Ye, B.-H.; Wang, L.; Ji, L.-N.; Zhou, J.-Y.; Li, R.-H.; Zhou, Z.-Y. *J. Chem. Soc. Dalt. Trans.* **1997**, 1395–1402.

(48) Fedin, V. P.; Sokolov, M. N.; Mironov, Y. V.; Kolesov, B. A.; Tkachev, S. V.; Fedorov, V. Y. *Inorganica Chim. Acta* **1990**, *167*, 39–45.

(49) Mayoh, B.; Day, P. *Theor. Chim. Acta* **1978**, *49*, 259–275.

(50) Brouwer, A. M. *Pure Appl. Chem.* **2011**, *83*, 2213–2228.

(51) Shi, X.; Zhu, G.; Wang, X.; Li, G.; Fang, Q.; Zhao, X.; Wu, G.; Tian, G.; Xue, M.; Wang, R.; Qiu, S. *Cryst. Growth Des.* **2005**, *5*, 341–346.

(52) Wang, X. L.; Chen, Y. Q.; Liu, G. C.; Zhang, J. X.; Lin, H. Y.; Chen, B. K. *Inorganica Chim. Acta* **2010**, *363*, 773–778.

(53) Liu, Y.; Li, Z.; Zhang, H.-Y.; Wang, H.; Li, C.-J. *Supramol. Chem.* **2008**, *20*, 419–426.

(54) Mo, H. J.; Shen, Y.; Ye, B. H. *Inorg. Chem.* **2012**, *51*, 7174–7184.

(55) Das, S.; Saha, D.; Karmakar, S.; Baitalik, S. *J. Phys. Chem. A* **2012**, *116*, 5216–5226.

(56) Saha, D.; Das, S.; Karmakar, S.; Dutta, S.; Baitalik, S. *RSC Adv.* **2013**, *3*, 17314–17334.

(57) Maity, D.; Bhaumik, C.; Mondal, D.; Baitalik, S. *Inorg. Chem.* **2013**, *52*, 13941–13955.

(58) Das, A.; Agarwala, H.; Kundu, T.; Ghosh, P.; Mondal, S.; Mobin, S. M.; Lahiri, G. K. *Dalt. Trans.* **2014**, *43*, 13932–13947.

(59) Satheshkumar, A.; Manivannan, R.; Elango, K. P. *J. Organomet. Chem.* **2014**, *750*, 98–106.

(60) Shi, S. In *Optoelectronic Properties of Inorganic Compounds*; Roundhill, D. M.; Fackler, J. P., Eds.; Springer US, 1999; p. 412.

(61) Humphrey, M. G.; Schwich, T.; West, P. J.; Cifuentes, M. P.; Samoc, M. In *Comprehensive Inorganic Chemistry II*; Elsevier, 2013; pp. 781–835.

(62) Boyd, R. W. *Nonlinear Optics*; Elsevier, 2008.

(63) A. Miller, K.R. Welford, B. D. *Nonlinear Optical Materials and Devices for Applications in Information Technology*; Springer Netherlands, 1995.

(64) Chen, Y.; Lin, Y.; Liu, Y.; Doyle, J.; He, N.; Zhuang, X.; Bai, J.; Blau, W. J. *J. Nanosci. Nanotechnol.* **2007**, *7*, 1268–1283.

(65) Shi, S.; Ji, W.; Tang, S. H.; Lang, J. P.; Xin, X. Q. *J. Am. Chem. Soc.* **1994**, *116*, 3615–3616.

(66) Stegeman, G. I.; Stegeman, R. A. *Nonlinear Optics: Phenomena, Materials and Devices*; John Wiley & Sons, Inc., 2012.

(67) Haurylau, M.; Zhang, J.; Weiss, S. M.; Fauchet, P. M.; Martyshkin, D. V.; Rupasov, V. I.; Krivoshlykov, S. G. *J. Photochem. Photobiol. A Chem.* **2006**, *183*, 329–333.

(68) Innocenzi, P.; Lebeau, B. *J. Mater. Chem.* **2005**, *15*, 3821.

(69) Zhang, C.; Song, Y.; Wang, X. *Coord. Chem. Rev.* **2007**, *251*, 111–141.

(70) Li, J.; Zhang, J.; Humphrey, M. G.; Zhang, C. *Eur. J. Inorg. Chem.* **2013**, *2013*, 328–346.

(71) Shi, S.; Ji, W.; Tang, S. H.; Lang, J. P.; Xin, X. Q. *J. Am. Chem. Soc.* **1994**, *116*, 3615–3616.

(72) Shi, S.; Ji, W.; Lang, J. P.; Xin, X. Q. *J. Phys. Chem.* **1994**, *98*, 3570–3572.

(73) Zhang, W.; Jiao, W.; Shi, G.; Song, Y.; Wang, Y.; Liu, D.; Chang, Q.; Zhang, C.; Xin, X. *Opt. Mater. (Amst).* **2008**, *31*, 218–222.

(74) Feliz, M.; Garriga, J. M.; Llusar, R.; Uriel, S.; Humphrey, M. G.; Lucas, N. T.; Samoc, M.; Luther-Davies, B. *Inorg. Chem.* **2001**, *40*, 6132–6138.

(75) Feliz, M.; Llusar, R.; Uriel, S.; Vicent, C.; Humphrey, M. G.; Lucas, N. T.; Samoc, M.; Luther-Davies, B. *Inorganica Chim. Acta* **2003**, *349*, 69–77.

(76) Garriga, J. M.; Llusar, R.; Uriel, S.; Vicent, C.; Usher, A. J.; Lucas, N. T.; Humphrey, M. G.; Samoc, M. *Dalt. Trans.* **2003**, 4546–4551.

(77) Coe, B. J.; Fielden, J.; Foxon, S. P.; Brunschwig, B. S.; Asselberghs, I.; Clays, K.; Samoc, A.; Samoc, M. *J. Am. Chem. Soc.* **2010**, *132*, 3496–3513.

(78) Cai, Z.; Zhou, M.; Xu, J. *J. Mol. Struct.* **2011**, *1006*, 282–287.

(79) Dai, J.; Bian, G.-Q.; Wang, X.; Xu, Q.-F.; Zhou, M.-Y.; Munakata, M.; Maekawa, M.; Tong, M.-H.; Sun, Z.-R.; Zeng, H.-P. *J. Am. Chem. Soc.* **2000**, *122*, 11007–11008.

(80) Chatzikyriakos, G.; Papagiannouli, I.; Couris, S.; Anyfantis, G. C.; Papavassiliou, G. C. *Chem. Phys. Lett.* **2011**, *513*, 229–235.

(81) Sheik-Bahae, M.; Said, A. A.; Wei, T. H.; Hagan, D. J.; Van Stryland, E. W. *IEEE J. Quantum Electron.* **1990**, *26*, 760–769.

(82) Sutherland, R. L. *Handbook of Nonlinear Optics*; Marcel Dekker, Inc., 1996.

(83) Niu, Y.; Zhang, N.; Song, Y.; Hou, H.; Fan, Y.; Zhu, Y. *Inorg. Chem. Commun.* **2005**, *8*, 495–499.

(84) Romaniello, P.; D'Andria, M. C.; Lelj, F. *J. Phys. Chem. A* **2010**, *114*, 5838–5845.

(85) Dai, J.; Bian, G. Q.; Wang, X.; Xu, Q. F.; Zhou, M. Y.; Munakata, M.; Maekawa, M.; Tong, M. H.; Sun, Z. R.; Zeng, H. P. *J. Am. Chem. Soc.* **2000**, *122*, 11007–11008.

(86) Deplano, P.; Pilia, L.; Espa, D.; Mercuri, M. L.; Serpe, A. *Coord. Chem. Rev.* **2010**, *254*, 1434–1447.

6

LIGHT-DRIVEN HYDROGEN GENERATION FROM WATER USING TRINUCLEAR MOLYBENUM CLUSTERS

The results in this Chapter have been partly published as:

- "Photogeneration of Hydrogen from Water by Hybrid Molybdenum Sulfide Clusters Immobilized on Titania." David Recatalá, Rosa Llusar, Artem L. Gushchin, Ekaterina A. Kozlova, Yuliya A. Laricheva, Pavel A. Abramov, Maxim N. Sokolov, Roberto Gómez and Teresa Lana-Villarreal, *ChemSusChem*, **2015**, 8, 148 – 157

"The only source of knowledge is experience."

Albert Einstein

6.1. INTRODUCTION

Nowadays, the world energy demand is mainly supplied by fossil fuels, which are known to increase carbon dioxide levels, and hence to have a profound impact on global climate. Another major drawback of fossil fuels is that they are an exhaustible resource, and consequently a hike in fuel prices seems likely in the future. Despite the growing effort devoted over the past few years to the discovery and development of efficient, abundant and renewable sources of energy, to date none of them have been able to replace or significantly reduce fossil fuels consumption.[1]

Light energy from the sun would vastly exceed our current power demand. However, sunlight is intermittent and diffuse, and thus its substantial use as a source of energy would require energy storage in chemical bonds. In this context, the use of hydrogen as a fuel has been widely investigated.[2] The combustion of hydrogen presents the highest enthalpy of all existent chemical fuels. In addition, water is the only product of this reaction, making the process environmentally benign. For these reasons, the use of hydrogen as a fuel using water as a feedstock has emerged as one of the best alternatives to petroleum-based fuels.[3–5] Nevertheless, water splitting is energetically demanding, and the efficient generation of hydrogen from water still remains one of the major challenges in the use of hydrogen as a fuel.

The past four decades have witnessed significant progress in the development of solar energy conversion systems that to some extent mimic natural photosynthesis, and this interest has led to the emergence of Artificial Photosynthesis. In contrast to naturally occurring photosynthesis, in which the solar energy is stored in the form of chemical bonds in NADPH (nicotinamide adenine dinucleotide phosphate), in artificial systems, sunlight is employed for the generation of hydrogen and oxygen by water splitting.[1,4,6]

Artificial photosynthetic systems usually employ semiconductor oxides in order to enhance the water splitting process.[2,7] In the presence of an electron donor,

this species is oxidized, and hence the oxidation of water to produce oxygen is blocked. Focusing on the reductive side of water splitting, visible-light driven hydrogen evolution systems involve three basic steps (see Figure 6.1):[8]

(1) Absorption of sunlight by a photosensitizer (PS), such as $[Ru(bpy)_3]^{2+}$ (bpy = 2,2'-bipyridine) anchored onto the surface of a wide band gap semiconductor, most commonly titanium dioxide.

(2) Electron injection from the chromophore into the conduction band of the semiconductor to generate a long-lived excited state.

(3) Transfer of the photogenerated electrons to water molecules by a catalyst adsorbed over the semiconductor surface, and concomitant regeneration of the photosensitizer by a sacrificial electron donor (ED), such as triethanolamine (TEOA), ethylenediaminetetraacetic acid (EDTA) or the S^{2-}/SO_3^{2-} system.

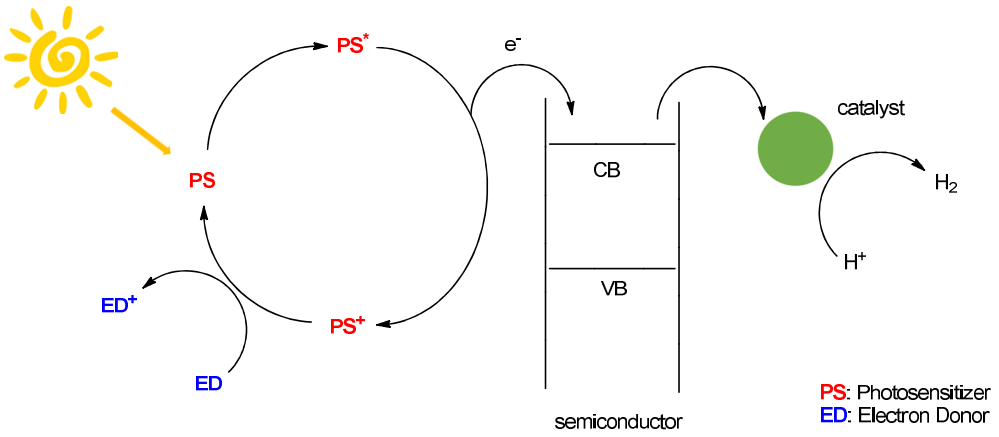

Figure 6.1. Schematic representation of a hydrogen evolution system employing a photosensitizer and an oxide semiconductor. CB: conduction band; VB: valence band.

The use of photosensitizers in systems commonly employed for the hydrogen evolution reaction (HER) is not strictly necessary if the semiconductor

presents a visible light response, hence being able to generate electrons and holes upon absorption of sunlight.[9–11] In these systems, the sacrificial agent is still required to avoid recombination of electrons and holes in the semiconductor, and it is well known that a cocatalyst adsorbed over the semiconductor surface improves the HER rate, since it participates in transferring the photogenerated electrons to water. A schematic representation of these types of systems is depicted in Figure 6.2.

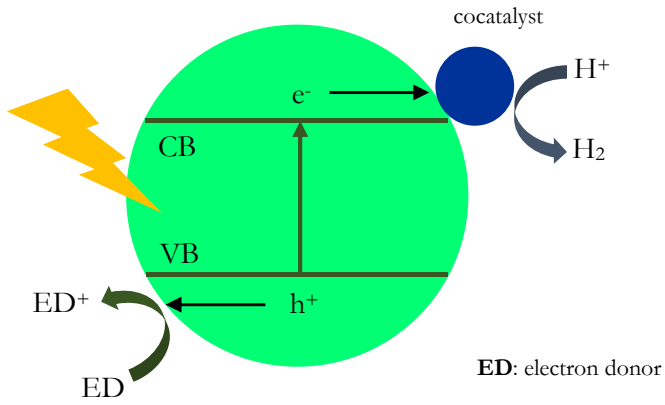

Figure 6.2. Schematic representation of a visible-light induced hydrogen evolution system based on a semiconductor photocatalyst. CB: conduction band; VB: valence band.

Over the past decades, colloidal platinum has been widely investigated as a catalyst (or cocatalyst) in the hydrogen evolution reaction (HER).[1] Nevertheless, its use in water splitting systems presents a major drawback: the high cost of this metal, which renders it problematic for use on a large scale. Recently, molybdenum sulfide (MoS_x) materials have emerged as low-cost alternatives to platinum and other precious metals for the photo- and electrocatalytic reduction of water.[12] Electrocatalysis, in which the electrons are generated by an electrochemical process, usually serves as an inspiration to the design of photocatalysts, owing to the electrochemical nature of most of the steps involved in a photocatalytic process. Molybdenum sulfide, MoS_2, is a well-known catalyst for the hydrodesulfurization

reaction.[13] However, it was not until MoS_2 nanoparticles were employed instead of bulk material that molybdenum sulfides began to be considered as attractive research targets for the hydrogen evolution reaction.[14]

Since the catalytically active sites in MoS_2 nanocrystals were identified to have a triangular geometry with sulfur edges, these materials have opened new avenues in the search for photo- and electrocatalysts based on molecular molybdenum sulfides presenting similar structural motifs to those of MoS_2 nanocrystals. For instance, Jaramillo *et al.* have shown that incomplete cubane-type complexes of formula $[Mo_3S_4(H_2O)_9]^{4+}$, containing three bridging μ-S^{2-} sulfides, when supported on highly oriented pyrolytic graphite (HOPG) possess a similar electrocatalytic activity in the HER to that of the edge sites of MoS_2 nanoparticles.[15] These electrocatalytic studies have also been extended to molybdenum clusters containing both three bridging (μ-S_2^{2-}) and three terminal (S_2^{2-}) sulfide ligands. In particular, adsorption of $[Mo_3S_7(S_2)_3]^{2-}$ over graphite has resulted in an excellent performance in the hydrogen evolution reaction.[16] The highest electrocatalytic activity of the $[Mo_3S_7(S_2)_3]^{2-}$ system, as compared to that of the Mo_3S_4-based cluster, has been attributed to the presence of more catalytically active edge sites in the Mo_3S_7 complex. Mononuclear molybdenum sulfides have also been investigated for the HER. For instance, a molecular poly(pyridyl) molybdenum sulfide complex containing a terminal S_2^{2-} ligand has been reported to be an efficient electrocatalyst for water reduction under acidic conditions.[17]

A significant number of molybdenum sulfides which serve as catalysts or co-catalysts for light-driven water splitting have also emerged.[12] For instance, trinuclear Mo_3S_4 clusters are efficient catalysts for the HER when coupled to a p-type silicon semiconductor which harvests sunlight.[18] The photocatalytic water splitting performance of $NaTaO_3$ has been significantly enhanced by using a molecular Mo_3S_4 complex as a co-catalyst.[19] In addition, a number of publications describe an

increased catalytic activity towards the hydrogen evolution reaction upon modification of the surface of TiO_2,[20,21] CdS,[22] Si[23,24] and copper oxide[25] with MoS_2 nanoparticles of different morphologies.

Over the past decades, the Molecular Materials group at Jaume I University has developed a series of functionalized molecular molybdenum(IV) clusters based on Mo_3S_7 and Mo_3S_4 cores, which only differ in the nature of their bridging ligands: disulfides *vs* sulfides.[26] In the case of the Mo_3S_7 cluster unit, the metal atoms define a triangle with a capping sulfur and three bridging S_2^{2-} ligands; an ideal topology to mimic the active edge sites of MoS_2.[14,17] This analogy between the structural motifs of both materials is illustrated in Figure 6.3.

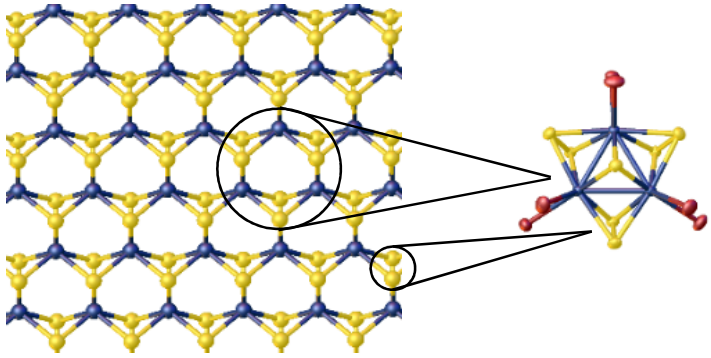

Figure 6.3. Representation of the analogy between the topology of the Mo_3S_7 cluster unit and the catalytically active sites of MoS_2.

As mentioned above, molecular molybdenum clusters containing Mo_3S_4 and Mo_3S_7 cores have been employed to modify the surface of semiconductors, thus enhancing the hydrogen evolution reaction.[15,16,18,19] Motivated by these results, and also by the widespread use of transition metal polypyridyl complexes as sensitizers in artificial photosynthesis systems,[1] we decided to investigate the electro- and photocatalytic activity of mixed-ligand diimine-halide Mo_3S_7 clusters adsorbed over titanium dioxide. More specifically, we focused on complexes

$(Bu_4N)[Mo_3S_7Br_4(dcmbpy)\cdot Br]$, ($(Bu_4N)$[**22**·Br]; dcmbpy = 4,4'-dicarbomethoxy-2,2'-bipyridine), and $Mo_3S_7Br_4(dnbpy)$, (**23**; dnbpy = 4,4'-dinonyl-2,2'-bipyridine), which can be obtained from the $[Mo_3S_7Br_6]^{2-}$ cluster precursor[27] by simple ligand substitution. Further details about the preparation of $Mo_3S_7X_4(diimine)$, (X = Cl, Br) complexes are provided in Chapter 4. A representation of the molecular structure of compounds (Bu_4N)[**22**·Br] and **23** is depicted in Figure 6.4.

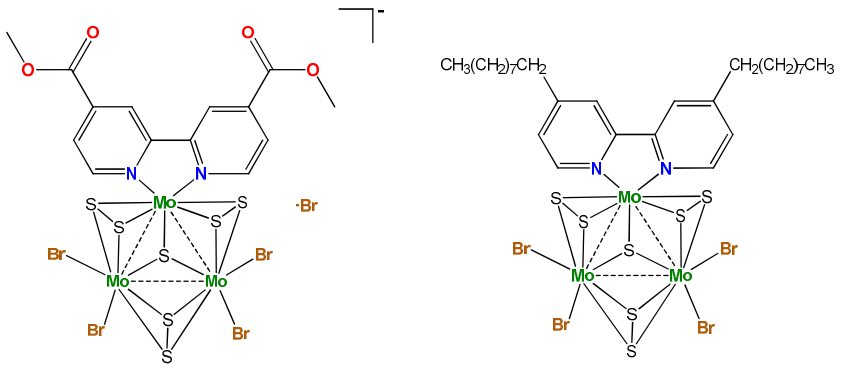

Figure 6.4. Molecular structure of complexes [**22**·Br]$^-$ and **23**.

6.2. RESULTS AND DISCUSSION

The trinuclear clusters (Bu_4N)[**22**·Br] and **23** were adsorbed from acetone solutions over nanoporous TiO_2 thin films deposited on FTO (fluorine-doped tin oxide), and their electrocatalytic activity toward hydrogen evolution was investigated. The chemical nature of the resulting molybdenum species was studied by UV/Vis and X-ray photoelectron spectroscopies. The electrochemical experiments, as well as the characterization of the resulting materials, were carried out in collaboration with Prof. T. Lana and Prof. R. Gómez at University of Alacant (Spain). The photocatalytic activity of complex (Bu_4N)[**22**·Br] adsorbed over TiO_2 was investigated in collaboration with Dr. E. A. Kozlova at Boreskov Institute of Catalysis (Novosibirsk, Russia).

6.2.1. SPECTROSCOPIC AND ELECTROCHEMICAL STUDIES

The UV/Vis diffuse reflectance spectra for the TiO_2 electrodes before and after adsorption of (Bu_4N)[**22**·Br] from acetone solutions are shown in Figure 6.5. It is noteworthy that the TiO_2 electrodes (initially white) became pink after adsorption of the complex, and this fact is reflected by a shoulder in their diffuse reflectance spectra at roughly 500 nm. The intensity of this band varies depending on the solution concentrations and adsorption time, thus indicating different cluster loadings. In contrast, the absorption spectrum of complex (Bu_4N)[**22**·Br] in acetone (see inset in Fig. 6.5) presents a band at 525 nm. This solvatochromic effect can be ascribed to a change in the environment of complex (Bu_4N)[**22**·Br] upon adsorption over TiO_2.

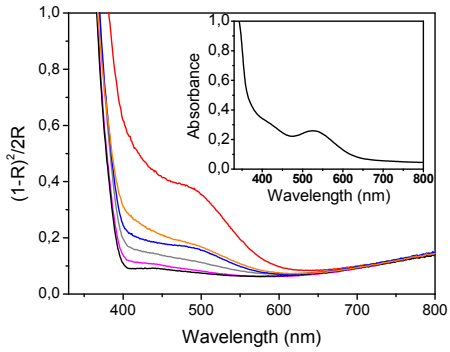

Figure 6.5. UV/Vis diffuse reflectance spectra (in Kubelka Munk units) for TiO_2 electrodes (2 μm) before (black line) and after immersion in acetone solutions of (Bu_4N)[**22**·Br] for different periods of time (5 min (pink), 15 min (grey), 1 hour (blue, orange, red) with different concentrations (18 μM (pink and grey), 72 μM (blue), 172 μM (orange), 290 μM (red)). The inset shows the UV/Vis absorption spectrum for a 72 μM solution of (Bu_4N)[**22**·Br] in acetone

The Cyclic Voltammograms (CVs) for the TiO_2 electrodes were recorded under nitrogen atmosphere before and after modification with (Bu_4N)[**22**·Br]. For this purpose, the electrodes were immersed either in a 0.1 M Na_2S/0.02 M Na_2SO_3 mixture, or in a 0.1 M $HClO_4$ solution. The resulting CVs are depicted in Figures 6.6a and 6.6c, respectively. A clear change in the shape of the CVs occurs

upon adsorption of (Bu_4N)[**22**·Br]. The electrochemical behavior of TiO_2 supported on FTO has previously been reported. When the potential is scanned toward negative values, electron transfer from the FTO substrate to the TiO_2 nanoparticles occurs, and hence electrons are accumulated in the TiO_2.[28] This accumulation is reflected in the blue curves in Figures 6.6a and 6.6c. A fast electron transfer from the modified TiO_2 to the molybdenum species, which results in their reduction (see below), is observed in both media (either Na_2S/Na_2SO_3 or $HClO_4$ aqueous solutions). The as-generated species behave as efficient electrocatalysts for the HER, precluding electron accumulation in TiO_2. This is evidenced by the Faradaic currents observed in both media (red curves in Figures 6.6a and 6.6c) instead of the typical accumulation region of TiO_2 (blue curves in Figures 6.6a and 6.6c).

Complex (Bu_4N)[**22**·Br] was also reduced when adsorbed over bare FTO, although the total contribution to the current can be regarded as negligible since the FTO surface is blocked by the TiO_2 nanoparticles, and furthermore the measured current densities for FTO electrodes are one order of magnitude lower than those of TiO_2 electrodes. The enhancement of the activity of (Bu_4N)[**22**·Br]/TiO_2 toward hydrogen evolution was assessed by comparing the overpotential values of the modified TiO_2 electrodes with those of bare TiO_2 supported either on FTO or titanium. In this context, the overpotential is regarded as the difference between the observed and the theoretical reduction potential for the H^+/H_2 conversion.[29] It is noteworthy that the use of titanium as a substrate instead of FTO permits to avoid the contribution of FTO to hydrogen evolution. In both materials, the HER electrocatalytic activity is significantly enhanced upon modification of TiO_2 with (Bu_4N)[**22**·Br]. More specifically, the overpotential for a current density of 1 $mA \cdot cm^{-2}$ (with respect to the geometric electrode area) decreased by roughly 0.30 V (in Na_2S/Na_2SO_3 mixtures) and 0.40 V (in aqueous $HClO_4$) in the presence of the cluster complex, as compared to that of bare TiO_2 supported on titanium (see Figure 6.6).

In addition, the overpotentials observed for the modified TiO_2 electrodes supported on FTO presented values of -0.16 and -0.35 V, in 0.1 M $HClO_4$ and in 0.1 M Na_2S + 0.02 M Na_2SO_3, respectively.

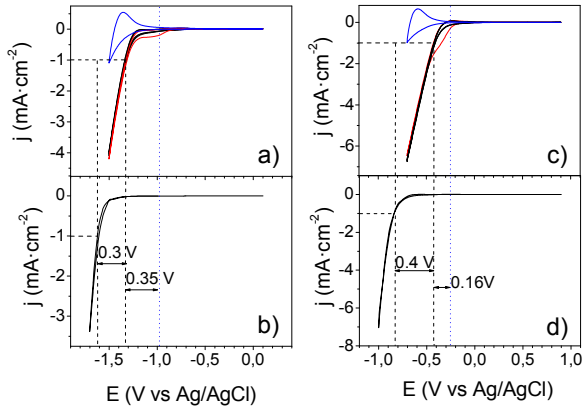

Figure 6.6. Stationary cyclic voltammograms for TiO_2 electrodes (≈ 3 μm in thickness) before (blue line) and after immersion in a 72 μM (Bu_4N)[**22**·Br] acetone solution for 1 hour. The red and black lines display the first and subsequent cycles, respectively. Scan rate: 20 mV s^{-1} in both cases. The CVs for TiO_2 nanoporous films deposited on titanium are presented in panels b) and d) using scan rates of 0.2 and 2 mV s^{-1}, respectively. Panels a) and b) correspond to N_2-purged 0.1 M Na_2S + 0.02 M Na_2SO_3, while panels c) and d) correspond to N_2-purged 0.1 M $HClO_4$. The vertical blue dashed line indicates the value of E_{eq} (H^+/H_2) at the corresponding pH.

The overpotential at a specific current density is not commonly used to make comparisons between different electrocatalysts, owing to differences in the experimental conditions, such as the nature of the support and electrocatalyst coverage. As an alternative, the onset potential for the hydrogen evolution reaction is usually regarded as the basis for comparison. The TiO_2 electrodes modified with complex (Bu_4N)[**22**·Br] present low onset overpotentials, with values of -0.05 V in 0.1M $HClO_4$ and -0.26 V in 0.1 M Na_2S/0.02 M Na_2SO_3 mixtures. The previously reported onset overpotentials for MoS_2 adsorbed over a variety of substrates are in good agreement with those registered for our

systems, and lie in the range between -0.15 and -0.20 V.[30–34]

As mentioned earlier in this Section, the chemical nature of (Bu_4N)[**22**·Br] adsorbed over TiO_2 changes upon electrochemical reduction. Furthermore, the modified TiO_2 electrodes (initially pink) became brownish upon immersion in the Na_2S/Na_2SO_3 mixture. This color changing was not observed when the modified TiO_2 electrodes were soaked in the $HClO_4$ solution. Nevertheless, in both media electrochemical reduction led to gray electrodes (see Figure 7.23 in Chapter 7). The color changing upon electrochemical reduction of the (Bu_4N)[**22**·Br]/TiO_2 system in Na_2S/Na_2SO_3 is illustrated in the UV/Vis diffuse reflectance spectra for the modified electrodes before and after the CV experiments (see Figure 6.7). The shape of the spectra for the modified TiO_2 after the electrochemical experiments sharply contrasts with those of the electrodes before the CV studies, which suggests that the as-generated molybdenum species are not well-defined molybdenum cluster sulfides.

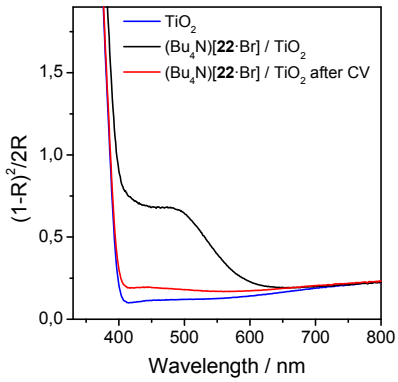

Figure 6.7. UV/Vis diffuse reflectance spectra for a TiO_2 electrode before and after modification with (Bu_4N)[**22**·Br], and after the electrochemical experiments shown in Figure 6.6a in Na_2S/Na_2SO_3 mixtures.

The difference between the first (red curve in Fig. 6.6a and c) and subsequent cycles (black lines in Fig. 6.6a and c) in the cyclic voltammograms for the electrodes in either Na_2S/Na_2SO_3 or $HClO_4$ solutions reveals that during electrochemical

experiments, an irreversible reduction occurs in both media. Remarkably, although the electrodes that correspond to Figures 6.6a and c are virtually identical in terms of film thickness and cluster loading, the charge difference between the first and further scans is significantly larger in acidic media (Fig. 6.6c). This result is in good agreement with the fact that the reduction of (Bu_4N)[**22**·Br] in aq. $HClO_4$ occurs only during the electrochemical experiments, whereas in the presence of Na_2S/Na_2SO_3 mixtures, presumably an initial reduction of the complex occurs concomitantly upon immersion of the electrode in the sulfide-sulfite media. The charge required to complete the reduction of complex (Bu_4N)[**22**·Br] in acidic media is thus larger than in aq. Na_2S/Na_2SO_3 due to the higher stability of the (Bu_4N)[**22**·Br]/TiO_2 system in aq. $HClO_4$. As will be discussed later, XPS studies reveal that the electrogenerated species in both media (aq. Na_2S/Na_2SO_3 and aq. $HClO_4$) are virtually identical.

A number of metal complexes containing diimine ligands functionalized with anchoring groups, such as carboxylic acids, act as sensitizers when anchored onto TiO_2.[2] These diimine ligands are usually bipyridine and phenanthroline derivatives, which are well-known to undergo one-electron reduction processes.[35] Moreover, it is well established that $Mo_3(\mu_3\text{-}S)(\mu\text{-}S_2)_3$ clusters can undergo reduction of the μ-S_2 ligands to generate incomplete cubane-like $Mo_3(\mu_3\text{-}S)(\mu\text{-}S)_3$ complexes.[36] Incidentally, these Mo_3S_4 clusters are good electro- and photocatalysts for the HER.[15,18,19] These facts lead to two questions. Firstly, whether the reduction of (Bu_4N)[**22**·Br] occurs mainly on the metal core or on the diimine ligand, and secondly which is the role of the diimine ligand in the adsorption of (Bu_4N)[**22**·Br] over TiO_2. To answer these questions, we decided to adsorb and perform electrochemical measurements in other closely related Mo_3S_7 clusters. We chose compound $Mo_3S_7Br_4$(dnbpy), (**23**; dnbpy = 4,4'-dinonyl-2,2'-bipyridine), bearing long alkyl chains appended to the bipyridine ligand, and complex $(Bu_4N)_2[Mo_3S_7Br_6]$, which is not functionalized with diimine ligands. To our astonishment, complex **23** adsorbed over nanoporous TiO_2 despite having no anchoring groups. The resulting yellow electrodes underwent color

changing after immersion in the 0.1M Na_2S + 0.02 M Na_2SO_3 solution, and also upon the CV experiments in both media (aq. $HClO_4$ and aq. Na_2S/Na_2SO_3). In addition, the electrochemical behavior of TiO_2 modified with complex **23** was identical to that of (Bu_4N)[**22**·Br]/TiO_2. These results indicate that bipyridine-like ligands do not play a key role in the electrochemical behavior of $Mo_3S_7X_4$(diimine) complexes (X = Cl, Br), and hence the reduced Mo_3S_7 core is responsible for the electrocatalytic activity toward HER. Nevertheless, it is noteworthy that in the absence of diimine ligands, Mo_3S_7 complexes do not adsorb over TiO_2. All attempts to adsorb complex $(Bu_4N)_2[Mo_3S_7Br_6]$ from acetone solutions were unsatisfactory, which proves that the diimine ligand plays a crucial role in the immobilization of the $Mo_3S_7X_4$(diimine) complexes on TiO_2.

The CV scans in aq. Na_2S/Na_2SO_3 for different cluster loadings, as well as the turnover frequency (TOF) at an overpotential of -0.53 V *versus* the cluster coverage are displayed in Figures 6.8a and b, respectively. The TOF (number of H_2 molecules generated per second and per molybdenum atom) has been calculated by taking into account that each (Bu_4N)[**22**·Br] molecule adsorbed over TiO_2 contains three molybdenum atoms. As expected, the currents associated with the HER strongly depend on the cluster loading: higher loadings result in higher current densities at a given potential (Fig. 6.8a). In contrast, as the coverage increases, the TOF is progressively reduced (Fig. 6.8b), presumably due to the generation of Mo-based aggregates. The calculated TOF values for our (Bu_4N)[**22**·Br]/TiO_2 systems are in good agreement with those reported by Jaramillo *et al.* for amorphous molybdenum sulfide, which lie in the 0.03 – 3 s^{-1} range for an overpotential of -0.20 V and a current density of 10 $mA \cdot cm^{-2}$.[34]

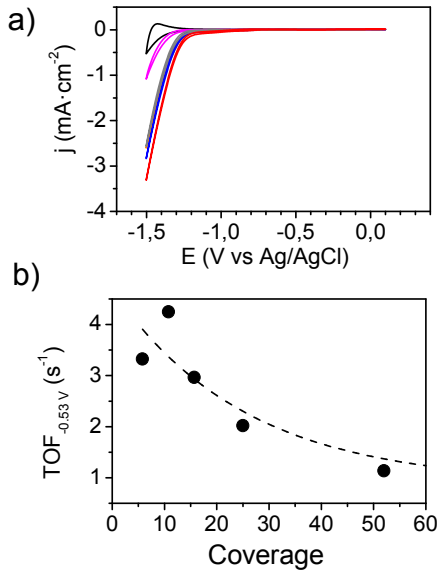

Figure 6.8. a) Cyclic voltammograms for nanoporous TiO_2 electrodes (2 μm in thickness) in N_2-purged 0.1 M Na_2S + 0.02 M Na_2SO_3 before (black line) and after immersion in acetone solutions of (Bu_4N)[**22**·Br] for different periods of time (5 min (pink), 15 min (grey), 1 hour (blue, orange, red) and different concentrations (18 μM (pink and grey), 72 μM (blue), 172 μM (orange), 290 μM (red)). Scan rate: 20 mV s^{-1}. b) Turnover frequency at an overvoltage of -0.53 V as a function of the (Bu_4N)(**22**·Br) coverage.

With the aim of providing some insight into the nature of the as-generated Mo-based catalyst, the Mo 3d and S 2p high-resolution XPS spectra for (Bu_4N)[**22**·Br] were recorded before and after the CV experiments in aq. Na_2S/Na_2SO_3 (see Figure 6.9). The Mo 3d XPS spectrum (Fig. 6.9a) is characterized by two peaks: Mo $3d_{5/2}$ at a binding energy (BE) of 229.8 eV, and Mo $3d_{3/2}$ at 232.8 eV. These energy values are in agreement with a formal oxidation state of +4 for the molybdenum, as already reported in the literature.[37,38] A broad shoulder at approximately 226 eV can also be observed, which has been ascribed to the S 2s contribution. After the CV experiments, the peak intensities diminish, presumably due to partial desorption of the complex. In addition, the peaks shift toward slightly lower binding energy values (Mo $3d_{5/2}$

at 229.1 eV, and Mo $3d_{3/2}$ at 232.6 eV). This shift can be attributed either to the partial reduction of the molybdenum ions or to a change in their chemical environment.

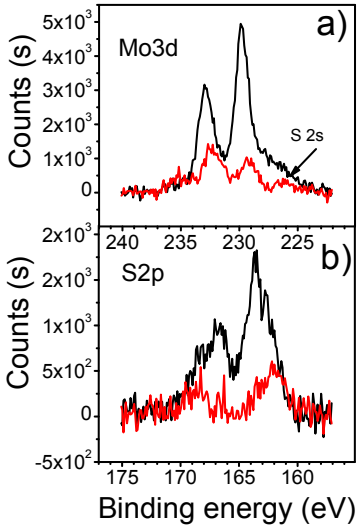

Figure 6.9. XPS spectra for (Bu_4N)[**22**·Br] adsorbed on TiO_2 before (black line) and after (red line) the CV experiments: a) Mo 3d and S 2s peaks; b) S 2p peaks.

The XPS spectra for the (Bu_4N)[**22**·Br]/TiO_2 system before the CV experiments in Na_2S/Na_2SO_3 reveal two peaks at binding energies of 163.4 and 166.7 eV, corresponding to S 2p contributions (Fig. 6.9b). The first peak can be assigned to two different types of sulfide ligands: S_2^{2-} and S^{2-}.[37] After the experiments, the peak at 163.4 eV shifts to 161.9 eV, indicating reduction of the S_2^{2-} ligands to S^{2-}.[39] To our astonishment, the peak at 166.7 eV is absent in the XPS spectrum reported for complex $(Et_4N)_2[Mo_3S_7Cl_6]$.[37] This binding energy value agrees well with that reported for thiosulfate-like species,[40] and the intensity of the S 2p peaks decreases upon CV measurements. The lack of strong anchoring groups in the 4,4'-dicarbomethoxy-2,2'-bipyridine ligand suggests that the

(Bu_4N)[**22**·Br] clusters are adsorbed over the TiO_2 surface in a flat-lying geometry, thus allowing interaction between the Mo_3S_7 core and the oxide semiconductor surface. This direct interaction could presumably lead to decomposition of the cluster core, and hence to the generation of thiosulfate-like structures. The decrease in the intensity of the S 2p peaks at 166.7 eV would be thus explained by the high solubility of the thiosulfate-type species in water. Furthermore, it is well established that bipyridine ligands are able to interact with TiO_2 surfaces through the nitrogen atoms.[41] Interestingly, the species generated upon CV measurements in 0.1 M $HClO_4$ present an analogous chemical nature to those obtained in Na_2S/Na_2SO_3 mixtures, as revealed by the UV/Vis diffuse reflectance spectra and XPS analysis of the modified TiO_2 electrodes. The only difference is the absence of the peak at 166.7 eV in the S 2p XPS spectrum.

The results presented so far reveal that the as-generated electrocatalyst contains molybdenum atoms in a formal oxidation state of +4, mainly in a S^{2-} environment. This species exhibit greatly enhanced catalytic activity toward HER, as compared to that of bare TiO_2, with overpotential values in the range of 0.3 – 0.4 V. Incidentally, MoS_2 nanoparticles have been reported to efficiently sensitize TiO_2 to visible light.[42] The question that now arises is whether the electrogenerated molybdenum species could also act as sensitizers (by injecting electrons into the semiconductor). Although it seems unlikely that the clusters themselves act both as sensitizers and catalysts, the answer to that question has been provided by comparing the photocurrent response of the modified (Bu_4N)[**22**·Br]/TiO_2 electrodes with that of bare TiO_2. The photocurrent response was measured at -0.40 V in a N_2-purged 0.1 M Na_2S/0.02 M Na_2SO_3 mixture, and the Incident Photon to Current Efficiency (IPCE) was plotted *versus* wavelength (see Figure 6.10). No response was registered in the visible region of the spectra ($\lambda > 420$ nm), and the same IPCE onset was observed for both bare and modified TiO_2 electrodes, which indicates that TiO_2 is not sensitized to

visible light by the as-generated molybdenum sulfide species.

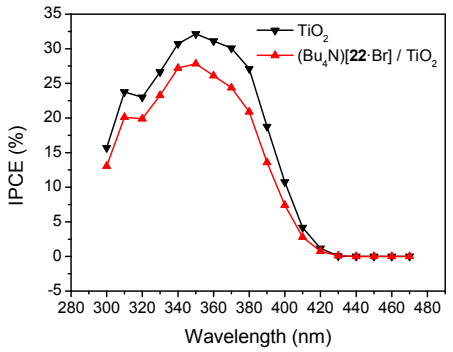

Figure 6.10. IPCE spectra in a N_2-purged 0.1 M Na_2S/0.02 M Na_2SO_3 mixture for a TiO_2 electrode before and after modification with (Bu_4N)[**22**·Br].

The fact that the Mo-based catalyst does not act as a sensitizer indicates that the function of these species is to extract electrochemically generated electrons from the semiconductor, and transfer them to water molecules. The ability of these molybdenum sulfides to transfer electrons in the presence of visible light is discussed in the following section.

6.2.2. PHOTOCATALYTIC BEHAVIOR

The photocatalytic activity of the (Bu_4N)[**22**·Br]/TiO_2 system was assessed in collaboration with Dr. E.A. Kozlova at Boreskov Institute of Catalysis. The samples were prepared by sonicating the TiO_2 nanoparticles in acetone solutions of the complex, followed by evaporation of the acetone. The resulting pink powder contained 5 wt. % of (Bu_4N)[**22**·Br]. The photocatalytic experiments were carried out under analogous conditions to those of the electrochemical measurements presented in the previous section in this chapter, that is to say, a 0.1 M Na_2S/0.02 M Na_2SO_3 mixture was used as a sacrificial donor, and the studies were carried out under an

argon atmosphere. All samples were irradiated with visible light by using a previously described setup.[43]

The photocatalytic activity of modified TiO_2 was compared to that of bare TiO_2, and also to those of complexes (Bu_4N)[**22**·Br] and $(Bu_4N)_2[Mo_3S_7Br_6]$. The latter complex was also adsorbed over TiO_2 for comparative purposes. The rate of hydrogen generation for (Bu_4N)[**22**·Br]/TiO_2, together with that of complex (Bu_4N)[**22**·Br] alone under different conditions is represented in Figure 6.11.

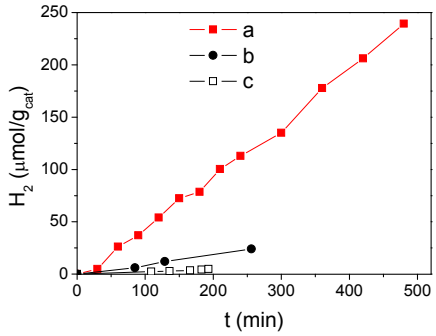

Figure 6.11. Kinetic curves for hydrogen generation in an Ar-purged 0.1 M Na_2S/0.02 M Na_2SO_3 mixture in the presence of: a) 1 g L^{-1} of 5 wt. % (Bu_4N)[**22**·Br]/TiO_2; b) 0.31 g L^{-1} suspension of (Bu_4N)[**22**·Br]; c) 0.77 g L^{-1} suspension of (Bu_4N)(**22**·Br) in a water/acetone mixture.

The (Bu_4N)[**22**·Br]/TiO_2 system presents a TOF of 8×10^{-5} s^{-1} (per Mo atom), whereas the hydrogen evolution activity for (Bu_4N)[**22**·Br] suspended either in water or in water/acetone mixtures is almost negligible. No hydrogen evolution was observed for bare TiO_2 or for TiO_2 modified with $(Bu_4N)_2[Mo_3S_7Br_6]$ under the same conditions. The obtained TOF value for $(Bu_4N)_2$[**22**·Br]/TiO_2 is significantly lower than that obtained in the electrocatalytic studies, due to the fact that in the electrochemical experiments the injection of electrons into TiO_2 is favored by FTO. Furthermore, the different catalyst loadings used in the electro- and photocatalytic experiments can have a strong influence on hydrogen evolution owing to differences

in catalyst aggregation. The as-generated molybdenum sulfide cocatalyst presents a remarkably high stability, since the hydrogen evolution rate remains constant throughout the 8 h experiment. Incidentally, hydrogen generation was found to cease completely in the dark. However, hydrogen evolution was observed again when the sample was irradiated after a brief period of darkness (*ca.* 20 min).

The energy levels for the (Bu_4N)[**22**·Br]/TiO_2 system immersed in a 0.1 M Na_2S/0.02 M Na_2SO_3 mixture before and after irradiation with visible light are depicted in Figure 6.12. This diagram includes the presence of surface state distribution (SS) below the conduction band (CB), and monoenergetic trap states ascribed to grain boundaries (GB), as reported in the literature for anatase.[44] The energy of the (Bu_4N)[**22**·Br] level corresponds to the potential value in which the irreversible reduction is observed in the CV experiments. The levels for the species in solution have been assumed to correspond to their redox potentials.

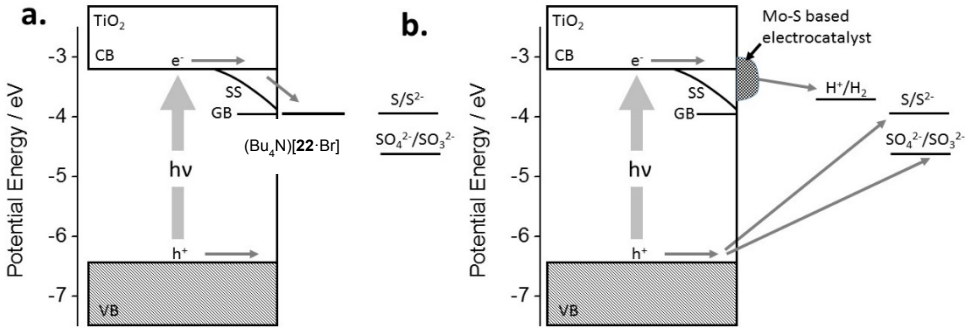

Figure 6.12. Energy band diagram for the (Bu_4N)[**22**·Br]/TiO_2 system in contact with an Ar-purged 0.1 M Na_2S/0.02 M Na_2SO_3 mixture a) when the illumination starts b) during the photocatalytic measurements. The position of the energy levels for TiO_2 anatase has been obtained from the literature.[44] SS stands for surface states whereas GB indicates grain boundary traps.

As previously mentioned, the (Bu_4N)[**22**·Br] complex can be reduced by the sulfide-sulfide species. In addition, upon illumination the TiO_2

photogenerated electrons are presumably transferred to the molybdenum species, thus generating an analogous species to that of the CV experiments (see Section 6.2.1). The as-generated electrocatalyst favors the funneling of the photogenerated electrons to water molecules to produce hydrogen. The absence of photocatalytic activity upon substitution of (Bu_4N)[**22**·Br] by $(Bu_4N)_2[Mo_3S_7Br_6]$ can be explained by the fact that the latter complex cannot be adsorbed over the TiO_2 surface, thus resulting in the formation of aggregates which are difficult to reduce. As already mentioned in the Introduction, the necessity of modifying semiconductors with co-catalysts in order to enhance the visible-light driven water splitting has been reported in a number of recent publications, and our results represent a significant contribution to this field.[45–48]

6.3. CONCLUSIONS

The electro- and photocatalytic activity toward HER of a diimino molybdenum cluster, namely $(Bu_4N)[Mo_3S_7Br_4(dcmbpy)\cdot Br]$, ($(Bu_4N)$[**22**·Br]; dcmbpy = 4,4'-dicarbomethoxy-2,2'-bipyridine) adsorbed over TiO_2 has been investigated. The electrocatalytic activity of TiO_2 modified with $Mo_3S_7Br_4$(dnbpy) (**23**; dnbpy = 4,4'-dinonyl-2,2'-bipyridine) has also been studied with the aim of analyzing the role of the diimine ligands in the adsorption and reduction processes. The diimine ligand has been found to be crucial for the adsorption of Mo_3S_7 complexes over TiO_2 nanoparticles. Complex (Bu_4N)[**22**·Br] is a precatalyst, which evolves to generate molybdenum(IV) sulfide species. The as-generated Mo-S species show superior electro- and photocatalytic activity for hydrogen evolution to bare TiO_2 due to the efficient interfacial electron transfer from TiO_2 to the Mo-S species, and the decrease in the hydrogen reduction overpotential by 0.3 – 0.4 V. These results pave the way for the design of novel photocathodes for hydrogen generation based on molybdenum sulfides.

6.4. REFERENCES

(1) Eckenhoff, W. T.; Eisenberg, R. *Dalt. Trans.* **2012**, *41*, 13004–13021

(2) Young, K. J.; Martini, L. A.; Milot, R. L.; Snoeberger, R. C.; Batista, V. S.; Schmuttenmaer, C. A.; Crabtree, R. H.; Brudvig, G. W. *Coord. Chem. Rev.* **2012**, *256*, 2503–2520.

(3) Teets, T. S.; Nocera, D. G. *Chem. Commun.* **2011**, *47*, 9268–9274.

(4) Gust, D.; Moore, T. A.; Moore, A. L. *Acc. Chem. Res.* **2009**, *42*, 1890–1898.

(5) Ardo, S.; Meyer, G. J. *Chem. Soc. Rev.* **2009**, *38*, 115–164.

(6) Ka, M. D.; Verho, O.; Johnston, E. V; Åkermark, B. *Chem. Rev.* **2013**, *114*, 11863–12001.

(7) Youngblood, J. W.; Lee, S. H. A.; Kobayashi, Y.; Hernandez-Pagan, E. A.; Hoertz, P. G.; Moore, T. A.; Moore, A. L.; Gust, D.; Mallouk, T. E. *J. Am. Chem. Soc.* **2009**, *131*, 926–927.

(8) Zhang, J.; Du, P.; Schneider, J.; Jarosz, P.; Eisenberg, R. *J. Am. Chem. Soc.* **2007**, *129*, 7726–7727.

(9) Chen, X.; Shen, S.; Guo, L.; Mao, S. S. *Chem. Rev.* **2010**, *110*, 6503–6570.

(10) Kudo, A.; Miseki, Y. *Chem. Soc. Rev.* **2009**, *38*, 253–278.

(11) Maeda, K.; Domen, K. *J. Phys. Chem. Lett.* **2010**, *1*, 2655–2661.

(12) Laursen, A. B.; Kegnæs, S.; Dahl, S.; Chorkendorff, I. *Energy Environ. Sci.* **2012**, *5*, 5577–5591.

(13) Prins, R.; De Beer, V. H. J.; Somorjai, G. A. *Catal. Rev.* **1989**, *31*, 1–41.

(14) Merki, D.; Hu, X. *Energy Environ. Sci.* **2011**, *4*, 3878–3888.

(15) Jaramillo, T. F.; Bonde, J.; Zhang, J.; Ooi, B. L.; Andersson, K.; Ulstrup, J.; Chorkendorff, I. *J. Phys. Chem. C* **2008**, *112*, 17492–17498.

(16) Kibsgaard, J.; Jaramillo, T. F.; Besenbacher, F. *Nat. Chem.* **2014**, *6*, 248–253.

(17) Karunadasa, H. I.; Montalvo, E.; Sun, Y.; Majda, M.; Long, J. R.; Chang, C. J. *Science.* **2012**, *335*, 698–702.

(18) Hou, Y.; Abrams, B. L.; Vesborg, P. C. K.; Björketun, M. E.; Herbst, K.; Bech, L.; Setti, A. M.; Damsgaard, C. D.; Pedersen, T.; Hansen, O.; Rossmeisl, J.; Dahl, S.; Nørskov, J. K.; Chorkendorff, I. *Nat. Mater.* **2011**, *10*, 434–438.

(19) Seo, S. W.; Park, S.; Jeong, H.-Y.; Kim, S. H.; Sim, U.; Lee, C. W.; Nam, K. T.; Hong, K. S. *Chem. Commun.* **2012**, *48*, 10452–10454.

(20) Liu, Q.; Pu, Z.; Asiri, A. M.; Qusti, A. H.; Al-Youbi, A. O.; Sun, X. *J. Nanoparticle Res.* **2013**, *15*, 1–7.

(21) Zhou, W.; Yin, Z.; Du, Y.; Huang, X.; Zeng, Z.; Fan, Z.; Liu, H.; Wang, J.; Zhang, H. *Small* **2013**, *9*, 140–147.

(22) Zong, X.; Yan, H.; Wu, G.; Ma, G.; Wen, F.; Wang, L.; Li, C. *J. Am. Chem. Soc.* **2008**, *130*, 7176–7177.

(23) Tran, P. D.; Pramana, S. S.; Kale, V. S.; Nguyen, M.; Chiam, S. Y.; Batabyal, S. K.; Wong, L. H.; Barber, J.; Loo, J. *Chem. - A Eur. J.* **2012**, *18*, 13994–13999.

(24) Laursen, A. B.; Pedersen, T.; Malacrida, P.; Seger, B.; Hansen, O.; Vesborg, P. C. K.; Chorkendorff, I. *Phys. Chem. Chem. Phys.* **2013**, *15*, 20000–20004.

(25) Morales-Guio, C. G.; Tilley, S. D.; Vrubel, H.; Grätzel, M.; Hu, X. *Nat. Commun.* **2014**, *5*, 3059.

(26) Llusar, R.; Vicent, C. In *Inorganic Chemistry in Focus III*; G. Meyer, D. Naumann, L. W., Ed.; Wiley-VCH, 2006.

(27) Fedin, V. P.; Sokolov, M. N.; Mironov, Y. V.; Kolesov, B. A.; Tkachev, S. V.; Fedorov, V. Y. *Inorganica Chim. Acta* **1990**, *167*, 39–45.

(28) Berger, T.; Monllor-Satoca, D.; Jankulovska, M.; Lana-Villarreal, T.; Gómez, R. *ChemPhysChem* **2012**, *13*, 2824–2875.

(29) Bard, A. J.; Faulkner, L. R. *Electrochemical Methods: Fundamentals and Applications*; Wiley, Ed.; 2001.

(30) Jaramillo, T. F.; Jørgensen, K. P.; Bonde, J.; Nielsen, J. H.; Horch, S.; Chorkendorff, I. *Science* **2007**, *317*, 100–102.

(31) Bonde, J.; Moses, P. G.; Jaramillo, T. F.; Nørskov, J. K.; Chorkendorff, I. *Faraday Discuss.* **2008**, *140*, 219–231.

(32) Wang, D.; Pan, Z.; Wu, Z.; Wang, Z.; Liu, Z. *J. Power Sources* **2014**, *264*, 229–234.

(33) Chen, Z.; Cummins, D.; Reinecke, B. N.; Clark, E.; Sunkara, M. K.; Jaramillo, T. F. *Nano Lett.* **2011**, *11*, 4168–4175.

(34) Benck, J. D.; Chen, Z.; Kuritzky, L. Y.; Forman, A. J.; Jaramillo, T. F. *ACS Catal.* **2012**, *2*, 1916–1923.

(35) Tucker, J. W.; Stephenson, C. R. J. *J. Org. Chem.* **2012**, *77*, 1617–1622.

(36) Hegetschweiler, K.; Keller, T.; Baumle, M.; Rihs, G.; Schneider, W. *Inorg. Chem.* **1991**, *30*, 4342–4347.

(37) Muijsers, J. C.; Weber, T.; van Hardeveld, R. M.; Zandbergen, H. W.; Niemantsverdriet, J. W. *J. Catal.* **1995**, *157*, 698–705.

(38) Weber, T.; Muijsers, J. C.; Niemantsverdriet, J. W. *J. Phys. Chem.* **1995**, *99*, 9194–9200.

(39) Castner, D. G.; Hinds, K.; Grainger, D. W. *Langmuir* **1996**, *12*, 5083–5086.

(40) Lindberg, B. J.; Hamrin, K.; Johansson, G.; Gelius, U.; Fahlman, A.; Nordling, C.; Siegbahn, K. *Phys. Scr.* **1970**, *1*, 286–298.

(41) Bagshaw, S. A.; Cooney, R. P. *J. Mater. Chem.* **1994**, *4*, 557–563.

(42) Kiesewetter, T.; Tomm, Y.; Turrión, M.; Tributsch, H. *Sol. Energy Mater. Sol. Cells* **1999**, *59*, 309–323.

(43) Kozlova, E. A.; Vorontsov, A. V. *Int. J. Hydrogen Energy* **2010**, *35*, 7337–7343.

(44) Jankulovska, M.; Berger, T.; Lana-Villarreal, T.; Gómez, R. *Electrochim. Acta* **2012**, *62*, 172–180.

(45) Wang, G.; Ling, Y.; Wang, H.; Xihong, L.; Li, Y. *J. Photochem. Photobiol. C Photochem. Rev.* **2014**, *18*, 35–51.

(46) Zhou, H.; Qu, Y.; Zeid, T.; Duan, X. *Energy Environ. Sci.* **2012**, *5*, 6732–6743.

(47) Li, Z.; Luo, W.; Zhang, M.; Feng, J.; Zou, Z. *Energy Environ. Sci.* **2013**, *6*, 347–370.

(48) Joya, K. S.; Joya, Y. F.; Ocakoglu, K.; Van De Krol, R. *Angew. Chemie - Int. Ed.* **2013**, *52*, 10426–10437.

7

EXPERIMENTAL

"If science is to progress, what we need is the ability to experiment, honesty in reporting results […], and finally – an important thing – the intelligence to interpret the results."

Richard P. Feynman, *The Character of Physical Law*

7.1. SYNTHESIS AND CHARACTERIZATION

7.1.1. GENERAL PROCEDURES

Infrared spectra were recorded in the 400–4000 cm^{-1} range on a Jasco FT/IR 6200 spectrometer using KBr pellets. Characteristic IR bands were assigned on the basis of those of previously reported complexes. ^{1}H, ^{13}C and ^{31}P NMR spectra were recorded either on a Varian Mercury Vx 300 MHz or a Varian VNMR System 500 MHz using deuterated solvents. For ^{1}H-NMR and ^{13}C-NMR, tetramethylsilane was used as an internal reference. Electronic spectra in the different solvents were recorded either on an Agilent Cary 60 UV/Vis spectrophotometer or on a Hewlett-Packard UV/Vis 8453 over the spectral range 200-800 nm.

Elemental analysis was performed on a Euro EA 3000 CHN analyzer. Electrospray ionization mass spectra were recorded on a triple quadrupole mass spectrometer (Micromass Quattro LC). The chemical composition of each peak in the scan mode was assigned by comparing the isotope experimental pattern with that calculated using the MassLynx 4.1 program.

Cyclic voltammetry experiments were performed with an Echochemie PGSTAT20 electrochemical analyzer. All measurements were carried out with a conventional three-electrode configuration consisting of glassy carbon working and platinum auxiliary electrodes and an Ag/AgCl reference electrode. The solvent used in all experiments was acetonitrile or dichloromethane (HPLC grade), which was deoxygenated before use. Tetrabutylammonium hexafluorophosphate (0.1 M solution) was used as a supporting electrolyte. Redox potentials values ($E_{1/2}$) were determined as $\frac{1}{2}(E_a + E_c)$, where E_a and E_c are anodic and cathodic peak potentials, respectively. The microwave-assisted synthetic reactions were carried out with a CEM Discover microwave system.

Unless otherwise stated, all synthetic reactions were carried out under nitrogen-gas atmosphere using standard Schlenk techniques. Air and moisture

sensitive compounds were handled inside a gloves box. High-purity solvents for synthesis were used. Dichloromethane, acetonitrile, tetrahydrofuran and toluene were further purified by using an MBRAUN SPS-800 system. Dimethylformamide (DMF) was degassed *in vacuo*. Methanol was dried over molecular sieves (4 Å), and deaerated by bubbling a N_2-gas stream for 30 min prior to use.

7.1.2. STARTING MATERIALS

The syntheses and characterization of metal precursors and ligands are described below. Commercially available starting materials were obtained from several sources, and used as received without further purification. Some compounds were prepared according to literature procedures with modifications. Numbers between brackets are used to indicate novel metal compounds. Novel ligands are indicated by the combination of the letter "L" and a number, *e.g.* L1.

7.1.2.1. MOLECULAR CLUSTERS

$(Et_4N)_2[Mo_2O_2S_8]$ [1]

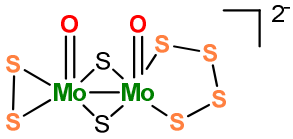

The synthesis of this compound was carried out with a modification of the reported procedure. Commercial $(NH_4)_2Mo_7O_{24}{\cdot}4H_2O$ (10 g, 8.1 mmol) was dissolved in 400 mL of water. A polysulfide ammonium solution obtained by mixing 20 % purity $(NH_4)_2S$ (65 mL, 0.19 mol) and elemental sulfur (15 g, 0.47 mol) was added to the solution. The mixture was briefly stirred for 24 h in air, and then Et_4NBr (10.7 g, 50 mmol) dissolved in 150 mL of water was added. The orange-brown precipitate was filtered and washed with EtOH, CS_2 and Et_2O. Further purification was achieved by recrystallization from DMF/isopropanol mixtures. Yield: 14.00 g, (67 %).

ESI(-) MS (CH_3CN, 5V): m/z = 240.0 $[M]^{2-}$.

$(NH_4)_2[Mo_3S_{13}]\cdot nH_2O$ (n = 0 - 2) [2]

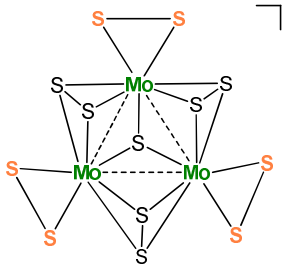

Elemental sulfur (27 g, 0.84 mmol) was dissolved in 120 mL of $(NH_4)_2S$ (20 % purity). The solution turned reddish. Separately, $(NH_4)_6[Mo_7O_{24}]\cdot 4H_2O$ (4 g, 3.24 mmol) was dissolved in water (20 mL) in a 250 mL Erlenmeyer flask. The ammonium molybdate solution was warmed, and then the ammonium polysulfide solution was slowly added. The flask was covered with a watch glass and the dark red mixture was heated to 82 – 85 ºC for 5 days without stirring. After cooling to room temperature, the red microcrystalline solid formed was filtered off. The product was thoroughly washed with water, ethanol, carbon disulfide and diethyl ether. Yield: 5.05 g (88 %).

Elemental analysis (%) calcd. for $H_8Mo_3N_2S_{13}\cdot H_2O$: H, 1.33; N, 3.69; S, 54.93; found H, 1.10; N, 3.35; S, 55.80.

$(Bu_4N)_2[Mo_3S_7Cl_6]$ [3]

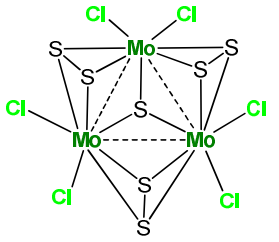

The thiocluster $(NH_4)_2[Mo_3S_{13}]\cdot H_2O$ (5 g, 6.59 mmol) was mixed with 37 % purity HCl (250 mL), and heated to *ca.* 80 ºC overnight under air. Precipitation of elemental sulfur was observed. The dark orange solution was filtered, and an excess of Bu_4NCl was added to the filtrate. After standing at 2 ºC for a few hours, the microcrystalline orange solid was filtered off and thoroughly washed with water, methanol and diethyl ether. The reaction is almost quantitative. Yield: 7.90 g (99 %).

ESI(-) MS (CH_3CN, 20V): m/z = 690.4 $[M - Cl]^-$, 362.7 $[M]^{2-}$.

$(Bu_4N)_2[Mo_3S_7Br_6]$ [3]

This compound was prepared in a similar fashion to $(Bu_4N)_2[Mo_3S_7Cl_6]$. The cluster compound $(NH_4)_2[Mo_3S_{13}]\cdot H_2O$ (5 g, 6.59 mmol) and 48 % purity HBr (350 mL) were gently refluxed overnight. An excess of tetrabuthylammonium bromide was used to afford the complete precipitation of the product. Yield: 9.10 g (94 %).

ESI(-) MS (CH_3CN, 20V): m/z = 912.1 $[M - Br]^-$, 495.2 $[M]^{2-}$.

7.1.2.2. LIGANDS

4,5-Bis(2-cyanoethylthio)-1,3-dithiole-2-thione [4]

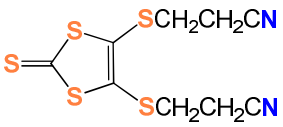

Freshly prepared $(Et_4N)_2[Zn(dmit)_2]$ [5] (10 g, 0.014 mol) was dissolved in 80 mL of CH_3CN, and 3-bromopropionitrile (7.5 g, 0.056 mol) was added. The mixture was refluxed for 1h. After filtration, the solution was concentrated by rotary evaporation. Then 125 mL of CH_2Cl_2 were added, and the white precipitate was removed by filtration. The solution was washed with water (3 x 100 mL), and the organic extracts were combined and dried with anhydrous $MgSO_4$. Ethanol was slowly added and the mixture was cooled overnight in the freezer. The brown needle crystals formed were washed with EtOH and Et_2O. Yield: 7.70 g (90 %).

^{1}H-NMR (300 MHz, $CDCl_3$): δ = 2.80 (t, 4H), 3.16 ppm (t, 4H).

4,5-Bis(2-cyanoethylthio)-2-bis(2-pyridyl)methylene-1,3-dithiole, BPyDT$(SCH_2CH_2CN)_2$ [6]

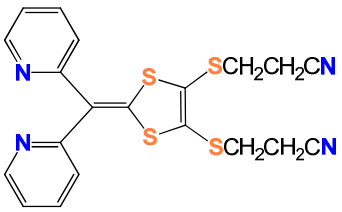

Under a nitrogen atmosphere, a mixture of di(2-pyridyl)ketone (2.76 g, 15 mmol) and 4,5-bis(2-cyanoethylthio)-1,3-dithiole-2-thione (4.57 g, 15 mmol) was dissolved in 40 mL of toluene. Then triethyl phosphite, $P(OEt)_3$ (15 mL) was added

dropwise. The mixture turned reddish. After heating to reflux for 4 h, a dark green solution was observed. After cooling to -20 ºC overnight, a green solid precipitated. The product was collected by filtration and washed with cold toluene and diethyl ether. Then it was redissolved in CH_2Cl_2 in the presence of activated charcoal. After filtration, the yellow solution was layered with Et_2O. Needle-like crystals were obtained after cooling to -20 ºC overnight. The solid was kept at 2 ºC protected from sunlight. Yield: 3.19 g (48 %).

^{1}H-NMR ($CDCl_3$, 300 MHz): 2.71 (t, 4H), 3.09 (t, 4H), 7.12 (d, 2H), 7.19 (m, 2H), 7.68 (t, 2H), 8.75 ppm (d, 2H).

ESI(+) MS (CH_3CN, 20V): 441.1 $[M+H]^+$.

IR (KBr, cm^{-1}): 2247 (m, ν (C≡N)), 1582 (s), 1527 (m), 1459 (s, ν (C=C)), 1278 (m), 784 (m), 671 (m), 621 (m), 502 (w, ν (C-S)), 407 (m).

UV/Vis (CH_3CN): λ_{max} (ε)= 254 (16 545), 310 sh (9701), 375 (26 250) nm ($M^{-1}cm^{-1}$)

Pyrazine-2,3-dithiol (pdt) [7,8]

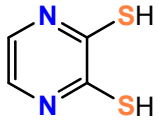

2,3-dichloropyrazine (1.5 mL, 13.7 mmol) was slowly mixed with a yellow solution of $NaHS{\cdot}xH_2O$ (3.93 g, 35.7 mmol assuming trihydrate) in 15 mL of water, which was degassed by bubbling N_2 for 30 min. The mixture was refluxed under vigorous stirring for 3 h. The color of the solution turned orange-red and a small amount of a yellow precipitate was observed. The precipitate was filtered off the solution, and the filtrate was exactly adjusted to pH 7.5 with HCl 1.8 M. The abundant brown precipitate formed was filtered and washed thoroughly with water, cold methanol and diethyl ether. The solid was dried *in vacuo* at 50 ºC overnight. Yield: 1.42 g (72 %)

^{1}H-NMR (d_6-DMSO, 300 MHz): δ = 6.88 (s, 2H), 13.70 ppm (s, 2H).

^{13}C-NMR (d_6-DMSO, 300 MHz): 117.43, 180.05 ppm.

2,2'-Bipyridine-4,4'-dicarboxylic acid (dcbpy) [9]

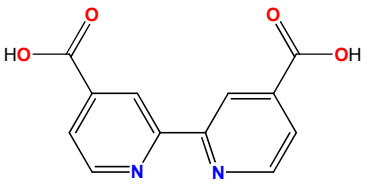

Commercial 4,4'-dimethyl-2,2'-bipyridine (2.70 g, 15 mmol) was dissolved in concentrated sulfuric acid (70 mL). The mixture was cooled to 0 ºC and then an excess of $K_2Cr_2O_7$ (17.6 g, 60 mmol) was added in small portions. After heating to 50 ºC for 1 h, the dark green mixture was poured onto water-ice (*ca.* 300 mL). The light yellow solid was filtered off, and thoroughly washed with water. After drying, the solid was mixed with 50 % nitric acid (70 mL), and refluxed for 4 h. The solution was then poured again over water-ice (*ca.* 300 mL). The precipitated white solid was filtered off, washed with water and acetone, and dried *in vacuo* overnight. The afforded product is insoluble in common organic solvents. Yield: 3.12 g (85 %).

^{1}H-NMR (d_6-DMSO, 300 MHz): δ = 7.91 (d, 2H), 8.85 (s, 2H), 8.92 ppm (d, 2H).

4,4'-Dicarbomethoxy-2,2'-bipyridine (dcmbpy) [10]

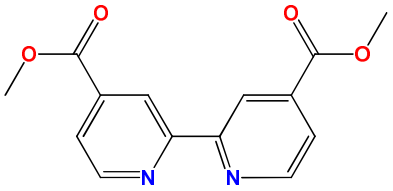

The ligand 2,2'-bipyridine-4,4'-dicarboxylic acid (1.71 g, 7 mmol) was suspended in CH_3OH (25 mL). Concentrated H_2SO_4 (3.5 mL) was slowly added while stirring. The mixture was heated to reflux for 8 h. The slightly reddish solution was then poured onto water-ice (75 mL), resulting in a white slurry. The pH was adjusted to 8 with 25 % NaOH, and the product was extracted with CH_2Cl_2 (3 × 100 mL). The organic extracts were dried over anhydrous $MgSO_4$, and taken to dryness by rotary evaporation. The solid residue was recrystallized from hot toluene to afford white crystals. Yield: 1.65 g (86 %).

^{1}H-NMR (CD_2Cl_2, 300 MHz): δ = 3.99 (s, 6H), 7.89 (dd, 2H), 8.85 (d, 2H), 8.95 ppm (s, 2H).

1,10-Phenanthroline-4,7-dicarboxylic acid, (dcphen) [11]

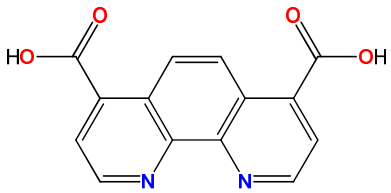

This compound was prepared by modifying the reported procedure. Commercial 4,7-dimethyl-1,10-phenanthroline (1.97 g, 9.27 mmol) and SeO_2 (5 g, 45 mmol) were mixed with 130 mL of dioxane:water (96:4, v/v). The suspension was refluxed for 2 h. Abundant precipitation of selenium was observed. The mixture was filtered over Celite while hot. The filtrate was then cooled to 2 ºC for a few hours. The solid was filtered off and recrystallized from tetrahydrofuran to afford yellow crystals. Yield: 1.88 g (76 %). This solid was identified as 4,7-diformyl-1,10-phenanthroline, and used in the next step without further purification.

Compound 4,7-diformyl-1,10-phenanthroline (0.95 g, 3.54 mmol) was mixed with 70 % HNO_3 (20 mL) and heated to 60 ºC for 4 h. Emission of nitrogen dioxide was observed. Then the yellow solution was cooled to 0 ºC, and water was slowly added until the complete precipitation of a white solid. The powder was filtered off, and washed with water, isopropanol and diethyl ether. The afforded white product is insoluble in common organic solvents. Yield: 0.63 g (58 %).

^{1}H-NMR (d_6-DMSO, 300 MHz): δ = 8.15 (d, 2H), 8.77 (s, 2H), 9.26 ppm (d, 2H).

4,7-Dicarbomethoxy-1,10-phenanthroline, (dcmphen, L1)

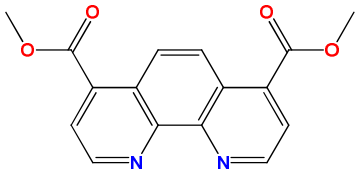

Compound 1,10-phenanthroline-4,7-dicarboxylic acid (1.63 g, 6.1 mmol) was suspended in CH_3OH (35 mL), and concentrated H_2SO_4 (3.5 mL) was slowly added while stirring. The mixture was heated to reflux overnight. The resulting solution was then poured onto water-ice (175 mL). The pH was adjusted to 9 with 25 % NaOH, and a copious white precipitate was observed. The product was extracted with CH_2Cl_2 (3 × 150 mL), dried with

anhydrous $MgSO_4$, and taken to dryness by rotary evaporation. The white solid was recrystallized from toluene to afford a slightly pink solid. White needles appeared from the filtrate after cooling to - 30 ºC overnight. Yield: 1.19 g (66 %).

^{1}H-NMR ($CDCl_3$, 500 MHz): δ = 4.09 (s, 6H), 8.17 (d, 2H), 8.91 (s, 2H), 9.34 ppm (s, 2H).

ESI(+) MS (CH_2Cl_2/CH_3CN, 20V): m/z = 297.1 $[M + H]^+$.

Elemental analysis (%) calcd. for $C_{16}H_{12}N_2O_4$: C, 64.86; H, 4.08; N, 9.46; found C, 64.10; H, 4.70; N, 8.85.

1,10-Phenanthroline-5,6-dione (dipyridobenzoquinone, dpq)[12]

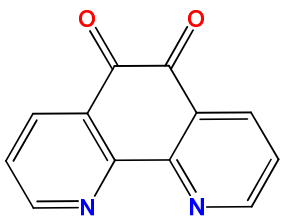

An ice cold mixture of concentrated H_2SO_4 (40 mL) and HNO_3 (20 mL) was added to 1,10-phenanthroline (4 g, 22.2 mmol) and KBr (4 g, 33.6 mmol). The mixture was heated to reflux for 3 h. Abundant emission of Br_2 was observed. The yellow solution was poured over water-ice (500 mL), and neutralized carefully with NaOH until pH=7. The product was extracted with $CHCl_3$ (3 × 200 mL) and dried over anhydrous Na_2SO_4. After taking to dryness by rotary evaporation, the yellow solid was further purified by recrystallization from ethanol. Small yellow needles were obtained. Yield: 3.04 g (65 %).

^{1}H-NMR ($CDCl_3$, 300 MHz): δ = 7.58 (ddd, 2H), 8.46 (dd, 2H), 9.06 ppm (dd, 2H).
ESI(+) MS (CH_3CN, 20V): m/z = 211.2 $[M+H]^+$.

3,4-(Didodecyloxy)benzaldehyde.[13]

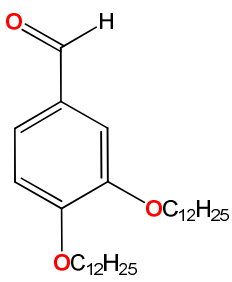

Commercial 3,4-dihydroxybenzaldehyde (4 g, 28.9 mmol) and 1-bromododecane (16 mL, 66 mmol) were dissolved in dry DMF (140 mL). The solution was purged with nitrogen for 15 minutes, and then anhydrous K_2CO_3 (15.9 g, 15.6 mmol) was added. The mixture was stirred at 60 ºC for 16 h. After cooling to room temperature, the mixture was poured onto ice-water (*ca.* 400 mL). A white precipitate formed, which was filtered under reduced pressure, and washed several times with water. The crude product was crystallized twice from *ca.* 1 L of acetone to afford off-white crystals. Yield: 9.73 g (71 %).

^{1}H-NMR ($CDCl_3$, 300 MHz): δ = 0.88 (t, 6H), 1.26 – 1.32 (m, 32H), 1.45 (m, 4H), 1.84 (m, 4H), 4.06 (q, 4H), 6.94 (d, 1H), 7.39 (m, 1H), 7.42 (m, 1H), 9.82 ppm (s, 1H).

1H-Imidazo[4,5-f][1,10]phenanthroline-2-[3,4-bis(dodecyloxy)phenyl], (IPDOP, L2)

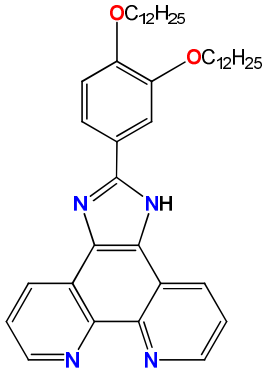

Compound 3,4-(didodecyloxy)benzaldehyde (0.95 g, 2 mmol) was added to a warm solution of 1,10-phenanthroline-5,6-dione (0.42 g, 2 mmol) and ammonium acetate (1.34 g, 1.70 mmol) in glacial acetic acid (20 mL). The mixture was heated to 85 ºC in air for 5 h and then allowed to cool to room temperature overnight. The orange suspension was poured onto water (100 mL) and neutralized to pH 7 with 25% NH_4OH. The orange precipitate was filtered off, washed with water, acetone and diethyl ether. Then the solid was dried *in vacuo* at 50 ºC. The product was purified on a silica column with $CHCl_3$/hexane/MeOH (50:50:10) as the eluent. After taking to dryness, a sticky yellowish solid was obtained. Since the compound holds solvents firmly, it was dried in a vacuum oven at 50 ºC. Yield: 0.77 g (58 %).

^{1}H-NMR ($CDCl_3$, 300 MHz): δ = 0.86 (m, 6H, CH_3-), 0.90-1.80 (m, 40H, -CH_2-), 3.24 (t, 2H, -CH_2-O-), 3.91 (t, 2H, -CH_2-O-), 6.78 (d, 1H, Ar-H), 7.06, (br. s, 1H, Ar-H), 7.70, (br. s, 1H, Ar-H), 7.85-8.05, (m, 2H, Ar-H), 8.60 (br. s, 2H, Ar-H), 8.91 (br. s, 1H, Ar-H), 9.23 (br. s, 1H, Ar-H), 14.86 ppm (br. s, 1H, N-H).

ESI(+) MS (CH_3CN, 20V): m/z = 665.5 $[M+H]^+$, 687.4 $[M+Na]^+$.

Elemental analysis (%) calcd. for $C_{43}H_{60}O_2N_4$: C, 77.67; H, 9.09; N, 8.43; found C, 76.67; H, 8.52; N, 6.96.

UV/Vis (CH_2Cl_2): λ_{max} (ε) = 280 (26 308), 328 sh (27 524) nm ($M^{-1}cm^{-1}$).

Dimethyl 2-oxo-1,3-dithiole-4,5-dicarboxylate.[14]

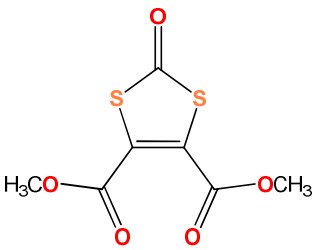

Commercial dimethyl 2-thioxo-1,3-dithiole-4,5-dicarboxylate (2.79 g, 0.011 mmol) was dissolved in CH_2Cl_2 (140 mL) and glacial acetic acid (70 mL). Then solid mercury (II) acetate, $Hg(OAc)_2$, (4.20 g, 0.013 mmol) was added in one portion. The mixture was stirred at 50 ºC for 24 h. The black precipitate was filtered through Celite / activated charcoal, and the filtrate was concentrated up to *ca.* 50 mL by rotary evaporation. The yellow solution was washed three times with a saturated aqueous $NaHCO_3$ solution. The organic extract was dried over anhydrous $MgSO_4$, and taken to dryness by rotary evaporation. The yellow residue was mixed with hexane, and a yellow precipitate was observed. The solid was filtered off and recrystallized from ethyl acetate / hexane. Yellow needles were observed after cooling to - 30 ºC overnight. Yield: 0.93 g (36 %).

^{1}H-NMR ($CDCl_3$, 300 MHz): δ = 3.88 ppm (s, 6H).

^{13}C-NMR ($CDCl_3$, 300 MHz): δ = 53.84, 129.47, 159.54, 186.71 ppm.

7.1.2.3. BIS(DITHIOLENE) ZINC AND TIN COMPLEXES

$(Et_4N)_2[Zn(dmit)_2]$ and $(Bu_4N)_2[Zn(dmit)_2]$ [5]

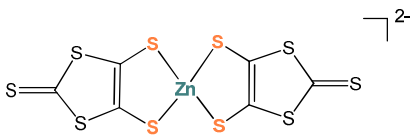

Under a nitrogen atmosphere, carbon disulfide (90 mL, 1.5 mol) and dimethylformamide (200 mL) were mixed and cooled to 0 ºC. Sodium (11.5 g, 0.5 mol) was added in small portions over a period of 4 h. The mixture was allowed to warm to room temperature overnight with continuous stirring. Then the deep red solution containing residual sodium was cooled to 0 ºC again. Methanol (25 mL) was slowly added, followed by a mixture of methanol (250 mL) and water (250 mL). A solution of zinc chloride, $ZnCl_2$, (10 g, 0.073 mol) in a mixture of concentrated aqueous ammonium hydroxide (250 mL) and methanol (250 mL) was then added to the red solution while stirring. After a brief period of time, tetraethylammonium bromide (26.5 g, 0.13 mol) or tetrabuthylammonium bromide (40.3 g, 0.13 mol), dissolved in deionized water (125 mL) was added. The mixture was allowed to stir for a few hours. The abundant precipitate was collected by filtration, and thoroughly washed with water (250 mL), isopropanol (*ca.* 400 mL; until the filtrate became colourless), and finally with diethyl ether (100 mL). The tetraethylammonium or tetrabutylammonium zincates were obtained as red or purple powders respectively, depending on the salt employed for the precipitation. Yield: $(Et_4N)_2[Zn(dmit)_2]$ (33.0 g, 63 %) ; $(Bu_4N)_2[Zn(dmit)_2]$ (52.1 g, 69 %).

ESI(-) MS (CH_3CN, 20V): m/z = 229.0 $[M]^{2-}$.

$(Bu_4N)_2[Zn(met)_2]$, $((Bu_4N)_2[1])$

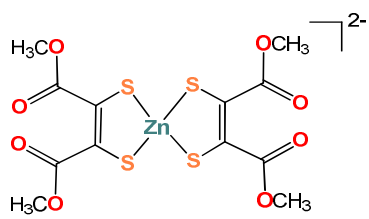

Dimethyl 2-oxo-1,3-dithiole-4,5-dicarboxylate (440 mg, 1.88 mmol) was dissolved in dry and degassed methanol (50 mL). A solution of lithium methoxide (164 mg, 4.23 mmol) in methanol (20 mL) was added dropwise. The yellow solution was allowed

to stir for 20 minutes at room temperature. $ZnCl_2$ (128 mg, 0.94 mmol) was dissolved in 20 mL of a CH_3OH : 25 % NH_4OH solution (1:1, v/v), and added to the latter mixture. There was a slight change in the colour of the solution. Then solid Bu_4NBr (691 mg, 2.1 mmol) was added in one portion, and the mixture was stirred overnight at room temperature. The solution was filtered, and the filtrate was concentrated to *ca.* 5 - 10 mL by rotary evaporation. The yellow solid was filtered off and washed with water, isopropanol and diethyl ether. Single pale yellow crystals were obtained from CH_2Cl_2/toluene mixtures. Yield: 0.73 g (40 %).

^{1}H-NMR (CD_2Cl_2, 300 MHz): δ = 0.99 (t, 24H), 1.41 (m, 16H), 1.62 (m, 16H), 3.19 (m, 16H), 3.62 ppm (s, 12H).

^{13}C-NMR (CD_2Cl_2, 300 MHz): δ = 14.05, 20.30, 24.65, 51.94, 59.43, 137.15, 171.00 ppm.

ESI(-) MS (CH_3CN, 20V): m/z = 238.0 $[M]^{2-}$.

Elemental analysis (%) calcd. for $C_{44}H_{84}N_2O_8S_4Zn$: C, 54.89; H, 8.79; N, 2.91; S, 13.32; found: C, 53.90; H, 8.50; N, 2.77; S, 12.70.

$(Bu_4N)_2[Zn(Cl_2bdt)_2]$, $((Bu_4N)_2[2])$

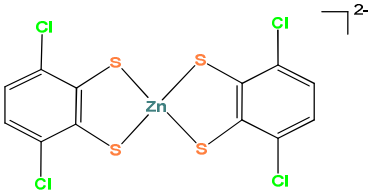

Compound 3,6-dichloro-1,2-benzenedithiol (250 mg, 1.13 mmol) was dissolved in dry and degassed methanol (75 mL), affording a reddish solution. Then 2.5 equivalents of triethylamine (400 µL, 2.83 mmol) were added, and the mixture was stirred for 10 minutes at room temperature. The solution turned yellowish. Zinc chloride (80 mg, 0.55 mmol) was dissolved in 20 mL of a CH_3OH : 25 % NH_4OH solution (1:1, v/v), and added to the latter mixture. After stirring overnight at room temperature the solution became slightly darker. The mixture was filtered, and the filtrate was concentrated up to *ca.* 20 mL by rotary evaporation. Solid Bu_4NBr (405 mg, 1.25 mmol) was added to the concentrated

solution while stirring vigorously. An abundant yellow precipitate was observed. The solid was filtered off and washed with methanol (*ca.* 3 mL), ethanol, water, isopropanol, and finally with diethyl ether. A yellow powder was obtained. Crystals were obtained by slow diffusion Et_2O/CH_3CN. Yield: 325 mg (61 %).

^{1}H-NMR (CD_3CN, 300 MHz): δ = 0.96 (t, 24H), 1.34 (m, 16H), 1.58 (m, 16H), 3.08 (m, 16H), 6.71 ppm (s, 4H).

^{13}C-NMR (d_6-DMSO, 300 MHz): δ = 13.43, 19.16, 23.05, 57.50, 120.09, 131.14, 149.78 ppm.

ESI(-) MS (CH_3CN, 20V): m/z = 242.0 $[M]^{2-}$.

Elemental analysis (%) calcd. for $C_{44}H_{76}Cl_4N_2S_4Zn$: C, 54.56; H, 7.91; N, 2.89; S 13.24; found: C, 54.41; H, 7.62; N, 2.70; S, 12.72

$Me_2Sn(BPyDTS_2)$, (3)

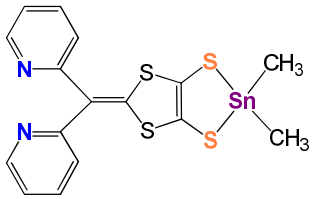

$BPyDT(SCH_2CH_2CN)_2$ (0.30 g, 0.68 mmol) was dissolved in 60 mL of dry THF. Then solid potassium *tert*-butoxide (0.16 g, 1.36 mmol) was added to the yellow solution with vigorous stirring. A red precipitate was formed. Stirring was continued for 30 min. Then dimethyltin dichloride (0.23 g, 1.02 mmol) dissolved in 20 mL of THF was added dropwise for 5 min to the red mixture containing the dithiolate. The solution turned orange, and a suspension was formed. After 2 h of stirring at room temperature, it was immediately filtered and concentrated by rotary evaporation. Hexane (*ca.* 20 mL) was slowly added to the solution, and after standing for some minutes, the yellow-brown solid was filtered off and washed with warm hexane, iPrOH, H_2O, again with iPrOH, and finally with Et_2O. Yield: 0.23 g (70 %).

^{1}H-NMR (d_6-DMSO, 300 MHz): δ = 0.95 (s, 6H), 7.04 (dt, 2H), 7.23 (ddd, 2H), 7.75 (m, 2H), 8.69 ppm (ddd, 2H).

ESI(-) MS (CH_3CN, 20V): 516.9 $[MCl]^-$.

Elemental analysis (%) calcd. for $C_{16}H_{14}N_2S_4Sn$: C, 39.9; H, 2.9; N, 5.8; S, 26.7; found: C, 40.3; H, 3.1; N, 6.1; S, 26.6.

IR (KBr, cm^{-1}): 1585 (m), 1570 (m), 1492 (s), 1458 (s, C=C), 782 (m), 670 (m), 468 (m), 420 (m).

UV/Vis (CH_3CN): λ_{max} (ε) = 251 (16 788), 281 (13 859), 411 (17 384) nm ($M^{-1}cm^{-1}$)

7.1.3. DINUCLEAR BIS(DITHIOLENE) MOLYBDENUM AND TUNGSTEN CLUSTERS

Dinuclear molybdenum and tungsten cluster complexes containing dithiolene ligands were synthesized starting either from the $[Mo_2O_2S_8]^{2-}$ species or commercial ammonium tetrathiomolybdates or tetrathiotungstates, $[MS_4]^{2-}$, where M = Mo or W. The synthetic procedure and characterization of the compounds are described below.

$(Et_4N)_2[Mo_2O_2S_2(BPyDTS_2)_2]$, $((Et_4N)_2[4])$

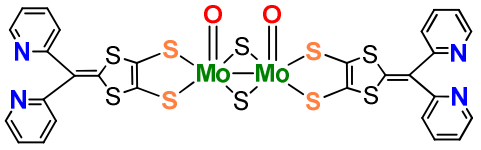

Compound BPyDT$(SC_2H_4CN)_2$ (0.71 g, 1.62 mmol) was dissolved in 30 mL of dry THF. Solid potassium *tert*-butoxide (0.38 g, 3.28 mmol) was added to the yellow solution rapidly and in one portion under vigorous stirring. A copious red solid precipitate corresponding to the potassium salt of the dithiolate ligand was observed. The mixture was further stirred for 30 min. Separately, $(Et_4N)_2[Mo_2O_2S_8]$ (0.6 g, 0.81 mmol) was dissolved in 30 mL of degassed DMF, and 5 mL of a I_2 solution in DMF (0.41 g, 1.62 mmol) were added while stirring to the latter brown-orange solution to generate the species $(Et_4N)_2[Mo_2O_2S_2(DMF)_6]$.[1]

Stirring was continued for 15 min, and the precipitation of elemental sulfur was observed. This mixture was added without filtering to the red solution containing the dithiolate. The precipitate dissolved, and the solution turned brown. After 2 h of stirring at room temperature, the solution was concentrated by removing the THF in a rotary evaporator. Diethyl ether (*ca.* 150 mL) was slowly added to the DMF solution and the mixture was cooled to -20 °C overnight. The solution was decanted, and the brown solid was washed with Et_2O, iPrOH, H_2O, EtOH, CS_2, and finally dried with Et_2O (0.82 g). The product obtained in this way was almost pure. Further purification was achieved by slowly diffusing Et_2O (*ca.* 150 mL) into a solution of the compound in DMF (*ca.* 25 mL). A crystalline dark brown solid was obtained. Yield: 0.75 g (77 %).

^{1}H-NMR (CD_3CN, 300 MHz): δ = 1.14 (t, 24H), 3.09 (q, 16H), 7.09 (d, 2H), 7.19 (dd, 2H), 7.71 (td, 2H), 8.73 ppm (d, 2H).

ESI(-) MS (CH_3CN, 20V): m/z = 477.0 $[M]^{2-}$.

Elemental analysis (%) calcd for $C_{44}H_{56}N_6Mo_2O_2S_{10}$: C, 43.5; H, 4.7; N, 6.9; found: C, 42.7; H, 4.6; N, 6.95.

IR (KBr, cm^{-1}): 1580 (s), 1522 (w), 1457 (s, ν (C=C)), 1271 (w), 944 (m, ν (Mo=O)), 785 (m), 670 (w), 619 (w), 503 (w, ν (C-S)), 469 (w, ν (Mo-S_{ligand})), 408 (w).

UV/Vis (CH_3CN): λ_{max} (ε) = 267 (52 715), 283 (52 880), 338 sh (20 451), 435 (29 035) nm ($M^{-1}cm^{-1}$).

CV (in CH_3CN, vs Ag/AgCl): $E_{1/2}$ = 0.43 V.

$(Et_4N)_2[Mo_2O_2S_2(BPyDTS_2)_2\{Re(CO)_3Cl\}_2]$, ($(Et_4N)_2$[5])

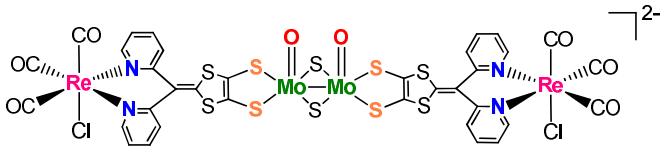

Compound $(Et_4N)_2[Mo_2O_2S_2(BPyDTS_2)_2]$ (50 mg, 0.041 mmol) and fresh $Re(CO)_5Cl$ (45 mg, 0.12 mmol) were mixed with DMF (1 mL) and CH_3CN (4 mL). The mixture was heated in a microwave system (110 ºC, 100 W, 25 min). After cooling to room temperature, the dark red solution was cooled to -20 ºC for some hours. Then it was immediately filtered using a 0.2 µm nylon syringe filter. Diethyl ether was added to the filtrate until the complete precipitation of a red solid, which after standing for 10 minutes was filtered and washed with toluene and Et_2O. Yield: 50 mg (67 %).

^{1}H-NMR (d_6-DMSO, 300 MHz): δ = 1.15 (t, 24H), 3.18 (q, 16H), 7.56 (m, 2H), 8.13 (m, 4H), 8.88 ppm (m, 2H).

ESI(-) MS (CH_3CN, 20V): 782.9 $[M]^{2-}$, 737.9 $[M - 3CO]^{2-}$, 694.9.

Elemental analysis (%) calcd. for $C_{50}H_{56}Cl_2Mo_2N_6O_8Re_2S_{10}$: C, 32.9; H, 3.1; N, 4.6; S, 17.6; found C, 31.2; H, 2.8; N, 5.1; S, 17.7

IR (KBr, cm^{-1}): 2017 (s, ν (C≡O)), 1906 (s, ν (C≡O)), 1891 (s, ν (C≡O)), 948 (w, ν (Mo=O)), 536 (w, (C–S)), 458 (w, $\nu(Mo–S_{ligand})$).

UV/Vis (CH_3CN): λ_{max} (ε) = 266 (38 682), 299 (36 811), 388 (13 578), 492 (16 111) nm ($M^{-1}cm^{-1}$).

$(PPN)_2[Mo_2S_4(pdt)_2]$, $((PPN)_2[6])$

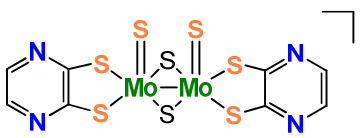

Ammonium tetrathiomolybdate (100 mg, 0.38 mmol) and 1.5 equivalents of 2,3-pyrazinedithiol (83 mg, 0.58 mmol) were dissolved in dry and degassed DMF (5 mL). The reddish-brown mixture was heated to 90 °C for 1 h. After cooling to room temperature, 2.5 equivalents of PPNCl (560 mg, 0.95 mmol) were added. After stirring for 30 minutes, the mixture was filtered. Diethyl ether (*ca.* 50 mL) was added to the filtrate, and the mixture was cooled to 2 °C for 2 - 3 days. The brown precipitate was redissolved in acetonitrile (*ca.* 50 mL), and filtered. The afforded brown microcrystalline precipitate was washed with acetonitrile, isopropanol, water, again with isopropanol, and finally with diethyl ether. The product is soluble in dichloromethane and methanol. Yield: 193 mg (60 %).

^{1}H-NMR (d_6-DMSO, 300 MHz): δ = 7.50 – 7.57 (m, 60H), 8.04 ppm (s, 2H).

^{13}C-NMR (d_6-DMSO, 300 MHz): δ = 126.03 (2), 127.48 (2), 129.46 (3), 131.92 (3), 133.60, 136.09, 164.47 ppm.

^{31}P-NMR (d_6-DMSO, 300 MHz): δ = 20.57 ppm.

ESI(-) MS (CH_3CN, 20V): m/z = 302.0 $[M]^{2-}$.

Elemental analysis (%) calcd. for $C_{80}H_{64}Mo_2N_6P_4S_8$: C, 57.14; H, 3.84; N, 5.00; S, 15.25; found: C, 55.28; H, 3.75; N, 5.55; S, 14.86.

$(Et_4N)_2[Mo_2S_4(pdt)_2]$, $((Et_4N)_2[6])$

This compound was prepared in a similar fashion to $(PPN)_2[Mo_2S_4(pdt)_2]$, but using Et_4NBr (200 mg, 0.95 mmol) instead of PPNCl as a precipitation salt. After stirring for some minutes at room temperature, the mixture was filtered. Diethyl ether (*ca.* 50 mL) was added to the filtrate, and the mixture was cooled to 2 °C for 2 – 3 days. A brown precipitate was obtained. The solid was redissolved in acetonitrile (*ca.* 50 mL)

and the mixture was filtered. The filtrate was layered with diethyl ether (*ca.* 100 mL). After cooling to 2 ºC overnight, the brown solid was collected by filtration and washed with ethanol and diethyl ether. Yield: 105 mg (64 %).

^{1}H-NMR (d_6-DMSO, 300 MHz): δ = 1.10 (t, 24H), 3.12 (q, 16H), 8.09 ppm (s, 4H).

^{13}C-NMR (d_6-DMSO, 300 MHz): δ = 7.04, 51.43 (3), 136.20, 164.39 ppm.

ESI(-) MS (CH_3CN, 20V): m/z = 302.1 $[M]^{2-}$.

Elemental analysis (%) calcd. for $C_{24}H_{44}Mo_2N_6S_8$: C, 33.32; H, 5.13; N, 9.72; found: C, 34.95; H, 6.16; N, 8.45.

$(Et_4N)_2[Mo_2O_2S_2(pdt)_2]$, ($(Et_4N)_2$[7])

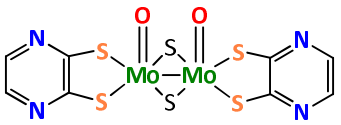

Pyrazine-2,3-dithiol (137 mg, 0.94 mmol) was suspended in 5 mL of degassed methanol. A 2 M solution of NaOH in CH_3OH (1 mL, 2 mmol) was slowly added. The mixture was stirred for 10 min, and then the yellow solution was diluted with 15 mL of THF. Separately, compound $(Et_4N)_2[Mo_2O_2S_8]$ (350 mg, 0.47 mmol) was dissolved in 20 mL of degassed DMF, and I_2 (240 mg, 0.94 mmol) dissolved in 5 mL of DMF was added to the cluster solution to generate the species $(Et_4N)_2[Mo_2O_2S_2(DMF)_6]$.[1] After stirring for 15 min, the orange-brown mixture was slowly added (without filtering) to the yellow solution containing the dithiolate ligand. The solution turned reddish-orange. The mixture was stirred for 100 min at room temperature. Then the lowest boiling point solvents (THF and CH_3OH) were removed by rotary evaporation. The DMF solution containing the final product was layered with 100 mL of Et_2O and cooled to 2 ºC for 2 - 3 days. A crystalline yellow solid was observed. After filtration, the product was washed with iPrOH, H_2O, EtOH, Et_2O, CS_2 and again with Et_2O. Yield: 0.31 g (80 %).

^{1}H-NMR (d_6-DMSO, 300 MHz): δ = 1.11 (t, 24H), 3.15 (q, 16H), 7.99 ppm (s, 4H).

^{13}C-NMR (d_6-DMSO, 300 MHz): δ = 7.03, 51.40 (3), 135.96, 163.67 ppm.

ESI(-) MS (CH_3CN, 20V): m/z = 286.0 $[M]^{2-}$.

Elemental analysis (%) calcd. for $C_{24}H_{44}Mo_2N_6O_2S_6$: C, 34.61; H, 5.32; N, 10.09; found: C, 34.25; H, 5.25; N, 9.70.

IR (KBr, cm^{-1}): 1480 (m), 1329 (s), 1294 (m), 1185 (m), 1151(s), 1051 (w), 948 (s, Mo=O), 536 (w, C-S), 446 (m, Mo-S_{ligand}).

UV/Vis(CH_3CN): λ_{max} (ε)= 238 (48 756), 310 sh (18 611), 357 nm (33 595 $M^{-1}cm^{-1}$).

CV (in CH_3CN, vs Ag/AgCl): $E_{1/2}$ = 1.18 V.

$(PPN)_2[Mo_2O_2S_2(pdt)_2]$, ($(PPN)_2$[7])

Compound $(PPN)_2[Mo_2S_4(pdt)_2]$ (50 mg, 0.030 mmol) and cobalt carbonyl, $Co_2(CO)_8$, (11 mg, 0.033 mmol) were dissolved in dry dichloromethane (10 mL), and stirred overnight at room temperature. A dark brown solution was observed together with a black precipitate, which was removed by filtration. The filtrate was concentrated up to *ca.* 5 mL by rotary evaporation. Then diethyl ether was slowly added while stirring to afford the precipitation of a brown solid. After filtration, the solid was washed with toluene and diethyl ether. A dark brown powder, soluble in dichloromethane was obtained. Yield. 36 mg (73 %).

^{1}H-NMR (d_6-DMSO, 300 MHz): δ = 7.45 – 7.75 (m, 60H), 8.0 ppm (s, 4H).

^{31}P-NMR (d_6-DMSO, 300 MHz): δ = 20.56 ppm.

ESI(-) MS (CH_2Cl_2/CH_3CN, 20V): m/z = 286.0 $[M]^{2-}$.

Elemental analysis (%) calcd. for $C_{80}H_{64}Mo_2N_6O_2P_4S_6$: C, 58.25; H, 3.91; N, 5.09; S, 11.66; found: C, 58.10; H, 3.75; N, 5.05; S, 12.16.

$(PPN)_2[W_2S_4(pdt)_2]$, $((PPN)_2[8])$

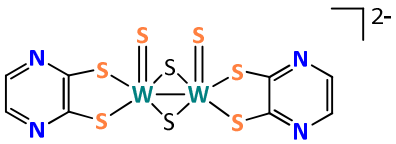

Ammonium tetrathiotungstate (100 mg, 0.29 mmol) and 2,3-pyrazinedithiol (65 mg, 0.45 mmol) were mixed with dry and degassed DMF (5 mL). The mixture was heated to 140 ºC for 2h. After cooling to room temperature, 2.5 equivalents of PPNCl (432 mg, 0.73 mmol) were added, and the mixture was further stirred for 30 minutes. Then the brown solution was filtered. After filtration, the solution was flooded with diethyl ether, and cooled to 3 ºC for 2 – 3 days. The mother liquor was decanted, and the sticky solid was suspended in acetonitrile (*ca.* 50 mL), and sonicated for a few minutes. The orange powder was filtered off and washed with acetonitrile, isopropanol, water, ethanol, methanol, and finally with diethyl ether. An orange solid, soluble in dichloromethane was obtained. Yield: 168 mg (62 %).

^{1}H-NMR (d_6-DMSO, 300 MHz): δ = 7.48 – 7.75 (m, 60H), 8.00 ppm (s, 4H).

^{13}C-NMR (d_6-DMSO, 300 MHz): δ = 126.03 (2), 127.47 (2), 129.45 (3), 131.91 (3), 133.59, 136.42, 165.66 ppm.

^{31}P-NMR (d_6-DMSO, 300 MHz): 20.59 ppm.

ESI(-) MS (CH_3CN, 20V): m/z = 389.7 $[M]^{2-}$.

Elemental analysis (%) calcd. for $C_{80}H_{64}N_6P_4S_8W_2$: C, 51.73; H, 3.47; N, 4.52; S, 13.81; found: C, 50.53; H, 3.45; N, 4.90; S, 13.76.

$(Et_4N)_2[W_2S_4(pdt)_2]$, $((Et_4N)_2[8])$

This compound was prepared in a similar fashion to $(PPN)_2[W_2S_4(pdt)_2]$, but using Et_4NBr (153 mg, 0.73 mmol) instead of PPNCl as a precipitation salt. After stirring for a few minutes at room temperature, the brownish solution was flooded with diethyl ether. The mixture was left at 3 ºC overnight. The orange precipitate was

filtered off, and washed with isopropanol, ethanol, water, methanol and diethyl ether. An orange powder, soluble in acetonitrile, was obtained. Yield: 107 mg (71 %).

^{1}H-NMR (d_6-DMSO, 300 MHz): δ = 1.16 (t, 24H), 3.11 (q, 16H), 8.02 ppm (s, 4H).

^{13}C-NMR (d_6-DMSO, 300 MHz): δ = 7.03, 51.39, 136.50, 165 ppm.

ESI(-) MS (CH_3CN, 20V): m/z = 389.7 $[M]^{2-}$.

Elemental analysis (%) calcd. for $C_{24}H_{44}N_6S_8W_2$: C, 27.69; H, 4.26; N, 8.07; found: C, 26.13; H, 4.07; N, 7.85.

$(PPN)_2[W_2O_2S_2(pdt)_2]$, $((PPN)_2$[9])

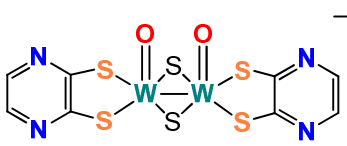

Compound $(PPN)_2[W_2S_4(pdt)_2]$ (50 mg, 0.027 mmol) and 1.1 equivalents of $Co_2(CO)_8$ (10 mg, 0.030 mmol) were mixed with dry CH_2Cl_2, and stirred overnight at room temperature. The solution turned dark brown, and a dark precipitate was observed. The precipitated solid was removed by filtration, and the filtrate was concentrated up to *ca.* 5 mL by rotary evaporation. Then diethyl ether was slowly added while stirring to afford the complete precipitation of a brown solid. The product was filtered off and washed with toluene and diethyl ether to afford a brown powder, soluble in dichloromethane. Yield: 32 mg (66 %).

^{1}H-NMR (d_6-DMSO, 300 MHz): δ = 7.50 – 7.74 (m, 60H), 7.95 ppm (s, 4H).

^{31}P-NMR (d_6-DMSO, 300 MHz): δ = 20.56 ppm.

ESI(-) MS (CH_2Cl_2/CH_3CN, 15V): m/z = 374.1 $[M]^{2-}$.

Elemental analysis (%) calcd. for $C_{80}H_{64}N_6O_2P_4S_6W_2$: C, 52.64; H, 3.53; N, 4.60; S, 10.54; found: C, 52.75; H, 3.25; N, 4.10; S, 10.92.

7.1.4. TRINUCLAR TRIS(DITHIOLENE) MOLYBDENUM CLUSTERS

The synthesis and characterization of molybdenum trinuclear clusters containing dithiolene ligands is described herein. These clusters were prepared by transmetalation using a bis(dithiolene) zinc complex. The thiocluster $(Bu_4N)_2[Mo_3S_7Br_6]$ was employed as a molybdenum cluster source.

$(PPN)_2[Mo_3S_7(met)_3]$, $((PPN)_2[10])$

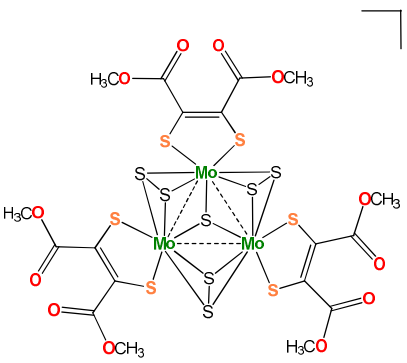

The cluster complex $(Bu_4N)_2[Mo_3S_7Br_6]$ (200 mg, 0.135 mmol) was dissolved in acetonitrile (30 mL), and then solid $(Bu_4N)_2[Zn(met)_2]$ (196 mg, 0.204 mmol) was added all at once. The mixture was stirred overnight at room temperature. The dark solution was taken to dryness by rotary evaporation, and the sticky solid residue was redissolved in warm methanol (60 – 70 mL). An excess of PPNCl was dissolved in methanol and added dropwise to the latter solution under vigorous stirring. A brown solid precipitated from the solution. After stirring for 1h at room temperature, the solid was filtered off and washed with methanol and diethyl ether. Crystals were grown by slow diffusion CH_3CN/Et_2O. Yield: 228 mg (76 %).

^{1}H-NMR (CD_2Cl_2, 300 MHz): δ = 3.62 (dd, 18H), 7.45 – 7.75 ppm (m, 60H).

^{31}P-NMR (CD_2Cl_2, 300 MHz): δ = 21.07 ppm.

ESI(-) MS (CH_3CN, 20V): m/z = 565.2 $[M]^{2-}$.

Elemental analysis (%) calcd. for $C_{90}H_{78}Mo_3N_2O_{12}P_4S_{13}$: C, 48.95; H, 3.56; N, 1.27; S, 18.88; found: C, 48.48; H, 3.24; N, 1.21; S, 18.98.

CV (in CH_2Cl_2, vs Ag/AgCl): $E_{1/2}$ = 0.38 (q. rev.), 0.70 (q. rev.), 1.04 V (q. rev.).

$(Bu_4N)_2[Mo_3S_7(Cl_2bdt)_3]$, ($(Bu_4N)_2$[11])

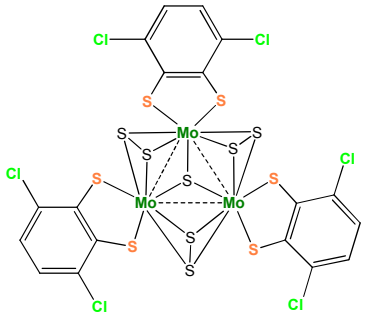

The cluster species $(Bu_4N)_2[Mo_3S_7Br_6]$ (100 mg, 0.068 mmol) and $(Bu_4N)_2[Zn(Cl_2bdt)_2]$ (105 mg, 0.11 mmol) were mixed with acetonitrile (15 mL), and stirred overnight at room temperature. The mixture turned reddish-brown. The solution was filtered, and the filtrate taken to dryness by rotary evaporation. The brown solid residue was suspended in methanol (*ca.* 20 mL) and sonicated. The precipitate was filtered off and washed with methanol, water, again with methanol, and finally with diethyl ether. A brown powder, soluble in acetonitrile and dichloromethane, was obtained. Crystals were grown by gas diffusion Et_2O/CH_2Cl_2. Yield: 73 mg (66 %).

^{1}H-NMR (CD_3CN, 300 MHz): δ = 0.95 (t, 24H), 1.35 (m, 16H), 1.60 (m, 16H), 3.08 (m, 16H), 6.82 ppm (m, 6H).

ESI(-) MS (CH_3CN, 20V): m/z = 569.81 $[M]^{2-}$.

Elemental analysis (%) calcd. for $C_{50}H_{78}Cl_6Mo_3N_2S_{13}$: C, 36.97; H, 4.84; N, 1.72; S, 25.66; found: C, 36.49; H, 4.64; N, 1.58; S, 25.53.

CV (in CH_3CN, vs Ag/AgCl): $E_{1/2}$ = 0.547 V (q. rev.), E_a = 1.412 (irrev.).

7.1.5. HETEROLEPTIC MOLYBDENUM CLUSTERS CONTAINING DIIMINE LIGANDS

A series of Mo_3S_7 complexes functionalized with halides (chloride or bromide) and diimine ligands (bipyridine or phenanthroline derivatives) were prepared. Their general synthetic procedures starting from the $(Bu_4N)_2[Mo_3S_7X_6]$ species (X = Cl or Br) are described below.

General Synthetic Method for $Mo_3S_7X_4$(diimine) Complexes, (X = Cl or Br)

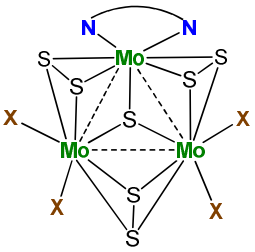

X = Cl or Br

The cluster complex $(Bu_4N)_2[Mo_3S_7X_6]$ (X = Cl or Br) and an excess of a diimine ligand (3 – 5 eq.) were mixed with CH_2Cl_2, and stirred at room temperature (X = Br), or refluxed (X = Cl). The reddish solution was filtered and taken to dryness by rotary evaporation. Unless otherwise stated, the sticky solid residue was thoroughly washed with methanol, acetonitrile (until the filtrate became colorless), dichloromethane and diethyl ether to afford an orange or a reddish powder in high yields.

$Mo_3S_7Br_4$(IPDOP), (12)

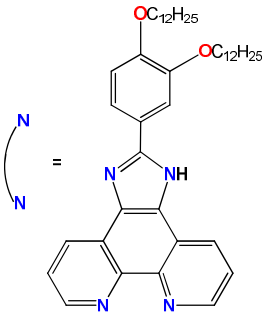

The cluster $(Bu_4N)_2[Mo_3S_7Br_6]$ (100 mg, 0.068 mmol) and the ligand IPDOP (136 mg, 0.20 mmol) were mixed with CH_2Cl_2 (30 mL), and stirred overnight at room temperature. The product was washed with methanol, acetonitrile and diethyl ether to afford a red solid which was dried in a vacuum oven at 50 ºC. Yield: 100 mg (98 %).

^{1}H-NMR ($CDCl_3$, 300 MHz): δ = 0.85 (m, 6H, CH_3-), 1.10-2.00 (m, 40H, -CH_2-), 3.10 (m, 2H, -CH_2-O-), 3.92 (m, 2H, -CH_2-O-), 6.84 (br s, 1H, Ar-H), 7.51 (br s, 2H, Ar-H), 7.92 (m, 2H, Ar-H), 8.83 (br s, 2H, Ar-H), 9.14 ppm (br s, 2H, Ar-H).

Elemental analysis (%) calcd. for $C_{43}H_{60}Br_4Mo_3N_4O_2S_7$: C, 34.50; H, 4.04; N, 3.74; found: C, 34.2; H, 3.7; N, 3.4.

UV/Vis (CH_2Cl_2): λ_{max} (ε) = 282 (104 488), 330 sh (45 600), 484 (2 400) nm ($M^{-1}cm^{-1}$).

$Mo_3S_7Cl_4$(IPDOP), (13)

The cluster $(Bu_4N)_2[Mo_3S_7Cl_6]$ (100 mg, 0.083 mmol) and the ligand IPDOP (165 mg, 0.25 mmol) were dissolved in CH_2Cl_2 (20 mL) and refluxed overnight. Purification was achieved by washing with methanol, acetonitrile and diethyl ether. The red powder obtained was dried in a vacuum oven at 50 ºC. Yield: 105 mg (96 %).

^{1}H-NMR ($CDCl_3$, 300 MHz): δ = 0.83 (m, 6H, CH_3-), 0.90-1.90 (m, 40H, -CH_2-), 3.06 (m, 2H, -CH_2-O-), 3.89 (m, 2H, -CH_2-O-), 6.81 (br s, 1H, Ar-H), 7.47 (br s, 2H, Ar-H), 7.95 (m, 2H, Ar-H), 8.83 (br s, 2H, Ar-H), 9.13 ppm (br s, 2H, Ar-H).

Elemental analysis (%) calcd. for $C_{43}H_{60}Cl_4Mo_3N_4O_2S_7$: C, 39.15; H, 4.58; N, 4.25; found: C, 39.4; H, 4.3; N, 4.2.

UV/Vis (CH_2Cl_2): λ_{max} (ε) = 282 (66 312), 330 sh (33 868), 489 (2 680) nm ($M^{-1}cm^{-1}$).

$Mo_3S_7Br_4$(BPhen), (14)

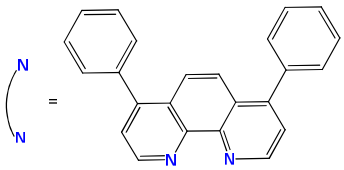

The cluster $(Bu_4N)_2[Mo_3S_7Br_6]$ (100 mg, 0.068 mmol) and commercial 4,7-diphenyl-1,10-phenanthroline (90 mg, 0.27 mmol) were mixed with CH_2Cl_2 (30 mL) and stirred overnight at room temperature. The solid was rinsed with methanol, acetonitrile and diethyl ether. A red powder was obtained. Yield: 73 mg (92 %).

^{1}H-NMR (d_6-DMSO, 300 MHz): δ = 7.59 (s, 3H), 7.62-7.77 (m, 5H), 7.82 (d, 1H), 7.91 (s, 1H), 8.17 (m, 2H), 8.23 (d, 1H), 9.20 (d, 1H), 9.85 (d, 1H), 10.19 ppm (d, 1H).

ESI(-) MS (CH_2Cl_2/CH_3CN, 20V): m/z = 1243.0 $[MBr]^-$.

Elemental analysis (%) calcd. for $C_{24}H_{16}Br_4Mo_3N_2S_7$: C, 24.76; H, 1.39; N, 2.41; found: C, 25.0; H, 1.6; N, 2.7.

UV/Vis (DMSO): λ_{max} (ε) = 389 sh (7632), 467 (3853) nm ($M^{-1}cm^{-1}$).

$Mo_3S_7Cl_4$(BPhen), (15)

The cluster compound $(Bu_4N)_2[Mo_3S_7Cl_6]$ (100 mg, 0.083) was treated with 4,7-diphenyl-1,10-phenanthroline (138 mg, 0.42 mmol) in the presence of CH_2Cl_2 (20 mL). The mixture was refluxed for 6.5 h. After washing with methanol, acetonitrile and diethyl ether, a reddish-orange powder was obtained. Yield: 77 mg (94 %).

^{1}H-NMR (d_6-DMSO, 300 MHz): δ = 7.59 (s, 3H), 7.62-7.78 (m, 5H), 7.87 (s, 1H), 8.19 (s, 2H), 8.22 (d, 2H), 9.17 (d, 1H), 9.87 (d, 1H), 10.09 ppm (d, 1H) ppm.

ESI(-) MS (CH_2Cl_2/CH_3CN, 20V): m/z = 1020.4 $[MCl]^-$.

Elemental analysis (%) calcd. for $C_{24}H_{16}Cl_4Mo_3N_2S_7$: C, 29.22; H, 1.63; N, 2.84; found: C, 29.4; H, 1.9; N, 3.1.

UV/Vis (DMSO): λ_{max} (ε) = 382 sh (4546), 462 (2484) nm ($M^{-1}cm^{-1}$).

$Mo_3S_7Br_4$(tmphen), (16)

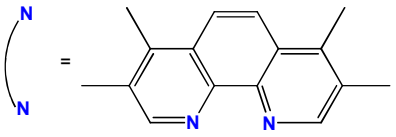

The cluster $(Bu_4N)_2[Mo_3S_7Br_6]$ (100 mg, 0.068 mmol) and commercial 3,4,7,8-tetramethyl-1,10-phenanthroline (64 mg, 0.27 mmol) were mixed with CH_2Cl_2 (30 mL), and stirred overnight at room temperature. Washing with hot

methanol, acetonitrile and diethyl ether afforded an orangish powder. Yield: 67 mg (92 %).

^{1}H-NMR (d_6-DMSO, 300 MHz): δ = 2.60 (m, 6H), 2.87 (m, 6H), 8.48 (m, 2H), 9.30 (s, 1H), 10.02 (m, 1H) ppm.

ESI(-) MS (CH_2Cl_2/CH_3CN, 20V): m/z = 1148.1 $[MBr]^-$, 1102.2 $[MCl]^-$.

Elemental analysis (%) calcd. for $C_{16}H_{16}Br_4Mo_3N_2S_7$: C, 17.99; H, 1.51; N, 2.62; found: C, 17.70; H, 1.35; N, 2.85.

UV/Vis (DMSO): λ_{max} (ε) = 375 sh (6075), 442 (3339) nm ($M^{-1}cm^{-1}$).

$Mo_3S_7Cl_4$(tmphen), (17)

The cluster species $(Bu_4N)_2[Mo_3S_7Cl_6]$ (100 mg, 0.083 mmol) and the ligand 3,4,7,8-tetramethyl-1,10-phenanthroline (78 mg, 0.33 mmol) were mixed with CH_2Cl_2 (20 mL). The mixture was refluxed overnight. Rinsing with hot methanol, acetonitrile, and diethyl ether afforded the title compound as an orangish powder. Yield: 59 mg (97 %).

^{1}H-NMR (d_6-DMSO, 300 MHz): δ = 2.57 (d, 6H), 2.87 (d, 6H), 8.49 (m, 2H), 9.40 (s, 1H), 9.86 (s, 1H) ppm.

ESI(-) MS (CH_2Cl_2/CH_3CN, 20V): m/z = 924.4 $[MCl]^-$, 970.4 $[MBr]^-$.

Elemental analysis (%) calcd. for $C_{16}H_{16}Cl_4Mo_3N_2S_7$: C, 21.58; H, 1.82; N, 3.15; found: C, 21.8; H, 2.1; N, 2.9.

UV/Vis (DMSO): λ_{max} (ε) = 370 sh (4211), 441 (2674) nm ($M^{-1}cm^{-1}$).

$Mo_3S_7Cl_4$(dmbpy), (18)

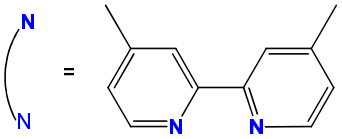

The cluster $(Bu_4N)_2[Mo_3S_7Cl_6]$ (100 mg, 0.083 mmol) and 4 equivalents of commercial 4,4'-dimethyl-2,2'-bipyridine (62 mg, 0.33 mmol) were mixed with CH_2Cl_2 (20 mL) and heated to reflux for 1 day. Purification afforded an orange powder. Yield: 67 mg (96 %).

ESI(-) MS (CH_2Cl_2/CH_3CN, 20V): m/z = 874.3 $[MCl]^-$.

Elemental analysis (%) calcd. for $C_{12}H_{12}Cl_4Mo_3N_2S_7$: C, 17.19; H, 1.44; N, 3.34; found: C, 17.5; H, 1.76; N, 3.45.

UV/Vis (DMSO): λ_{max} (ε) = 381 (1654), 447 (1056) nm ($M^{-1}cm^{-1}$).

$Mo_3S_7Br_4$(dmbpy), (19)

The starting material $(Bu_4N)_2[Mo_3S_7Br_6]$ (100 mg, 0.068 mmol) and an excess of 4,4'-dimethyl-2,2'-bipyridine (50 mg, 0.27 mmol) were mixed with CH_2Cl_2 (30 mL) and stirred overnight at room temperature. After purification, an orange powder was obtained. Yield: 57 mg (82 %).

^{1}H-NMR (d_6-DMSO, 300 MHz): δ = 2.59 (s, 6H), 7.73 (m, 2H), 8.78 (m, 2H), 9.19 (d, 1H), 9.57 ppm (m, 1H).

ESI(-) MS (CH_2Cl_2/CH_3CN, 20V): m/z = 1096.0 $[MBr]^-$, 1052.3 $[MCl]^-$, 1006.3 [M - Br + 2Cl].

Elemental analysis (%) calcd. for $C_{12}H_{12}Br_4Mo_3N_2S_7$: C, 14.18; H, 1.19; N, 2.76; found C, 14.3; H, 1.4; N, 2.4.

UV/Vis (DMSO): λ_{max} (ε) = 450 (2389) nm ($M^{-1}cm^{-1}$).

$Mo_3S_7Br_4$(bpy), (20)

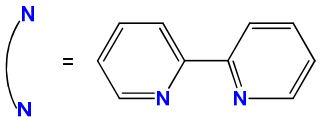

The complex $(Bu_4N)_2[Mo_3S_7Br_6]$ (100 mg, 0.068 mmol) and an excess of 2,2'-bipyridine (0.34 mmol, 53 mg) were stirred overnight at room temperature using CH_2Cl_2 (30 mL) as a solvent. Purification afforded an orange solid. Yield: 45 mg (67 %).

^{1}H-NMR (d_6-DMSO, 300 MHz): δ = 7.91 (m, 2H), 8.48 (q, 2H), 8.91 (m, 2H), 9.36 (d, 1H), 9.81 ppm (d, 1H).

ESI(-) MS (CH_2Cl_2/CH_3CN, 20V): m/z = 1068.0 $[MBr]^-$, 1024.0 $[MCl]^-$, 979.1 [M – Br + 2Cl]$^-$.

Elemental analysis (%) calcd. for $C_{10}H_8Br_4Mo_3N_2S_7$: C, 12.16; H, 0.82; N, 2.84; found: C, 12.40; H, 1.10; N, 2.85.

UV/Vis (DMSO): λ_{max} (ε) = 458 (2258) nm ($M^{-1}cm^{-1}$).

$Mo_3S_7Br_4$(phen), (21)

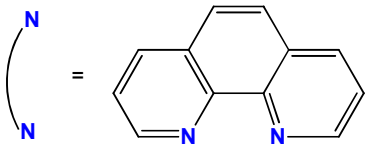

The cluster species $(Bu_4N)_2[Mo_3S_7Br_6]$ (100 mg, 0.068 mmol) and 5 equivalents of commercially available 1,10-phenanthroline (62 mg, 0.34 mmol) were mixed with CH_2Cl_2 (30 mL), and allowed to stir overnight at room temperature. The product was purified, and a reddish-orange solid was obtained. Yield: 55 mg (69 %).

^{1}H-NMR (d_6-DMSO, 300 MHz): δ = 8.27 (m, 2H), 8.41 (s, 2H), 9.13 (m, 2H), 9.65-9.80 (m, 1H), 10.12 ppm (m, 1H).

ESI(-) MS (CH_2Cl_2/CH_3CN, 20V): m/z = 1092.0 $[MBr]^-$, 1048.0 $[MCl]^-$.

Elemental analysis (%) calcd. for $C_{12}H_8Br_4Mo_3N_2S_7$: C, 14.24; H, 0.80; N, 2.77; found: C, 14.55; H, 1.30; N, 2.65.

UV/Vis (DMSO): λ_{max} (ε) = 453 (3149) nm ($M^{-1}cm^{-1}$).

$Mo_3S_7Br_4$(dcmbpy), (22)

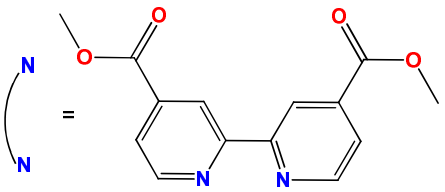

The cluster complex $(Bu_4N)_2[Mo_3S_7Br_6]$ (1 g, 0.68 mmol) and the ligand 4,4'-dicarbomethoxy-2,2'-bipyridine (1 g, 3.68 mmol) were mixed with CH_3CN (60 mL). The mixture was heated to reflux overnight. After cooling to room temperature, the precipitated ligand was filtered off. To afford the complete precipitation, the filtrate was then taken up to *ca.* 5 mL by rotary evaporation, cooled to -30 ºC, and filtered again. The filtrate was taken to dryness by rotary evaporation and washed with methanol, a few mL of acetonitrile, and finally with diethyl ether. To afford the complete precipitation, the mixture was concentrated by rotary evaporation and cooled to -30 ºC for 2 – 3 h. After filtration, an excess of diethyl ether was added to afford the precipitation of a red powder. The solid was collected by filtration and washed with methanol, a few mL of acetonitrile and diethyl ether. Yield: 0.69 g (92 %).

^{1}H-NMR (CD_3CN, 300 MHz): δ = 4.04 (d, 6H), 8.16 (m, 2H), 9.02 (s, 2H), 9.68 (d, 1H), 10.18 ppm (d, 1H).

ESI(-) MS (CH_3CN, 20V): m/z = 1183.5 $[MBr]^-$.

Elemental analysis (from the crystals, %) calcd. for $C_{14}H_{12}Br_4Mo_3N_2O_4S_7 \cdot Bu_4NBr$: C, 25.26; H, 3.39; N, 2.95; S, 15.7; found: C, 25.80; H, 3.50; N, 3.0; S, 15.7.

UV/Vis (DMSO): λ_{max} (ε) = 499 (2822) nm ($M^{-1}cm^{-1}$).

CV (in CH_3CN, vs Ag/AgCl): E_a = 0.92 V (irrev.), E_{c1} = - 0.58 V (q. rev.) and E_{c2} = - 0.83 V (irrev.).

$Mo_3S_7Br_4$(dnbpy), (23)

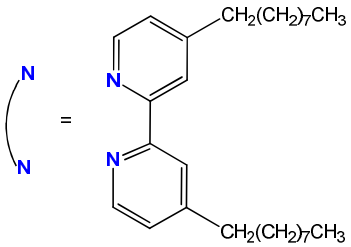

The cluster $(Bu_4N)_2[Mo_3S_7Br_6]$ (100 mg, 0.068 mmol) and 4,4'-dinonyl-2,2'-bipyridine (110 mg, 0.27 mmol) were mixed with CH_2Cl_2 (30 mL), and allowed to stir for 5 hours at room temperature. The solid residue that resulted from the evaporation of the solvent was washed with methanol, acetonitrile and diethyl ether to afford an orange powder. Yield: 71 mg (84 %).

^{1}H NMR (CH_2Cl_2, 300 MHz): δ = 0.88 (m, 4H), 1.04, (t, 6H), 1.20 – 1.80 (m, 20H), 2.90 (m, 4H), 3.22 (m, 4H), 7.45 (d, 1H), 7.52 (d, 1H), 8.20 (d, 2H), 9.37 (d, 1H), 9.84 ppm (d, 1H).

Elemental analysis (%) calcd for $C_{28}H_{44}Br_4Mo_3N_2S_7$: C, 27.11; H, 3.57; N, 2.26; found: C, 26.9; H, 3.65; N, 2.15.

IR (KBr, cm^{-1}): 2922 (s, Csp^3-H), 2850 (m, Csp^3-H), 1614 (s, C=C), 1542 (w, C=C), 1457 (m, C=C), 1419 (m, C=C), 540 (m, S_{eq}-S_{ax}), 419 (w, Mo-μS_3).

UV/Vis (CH_2Cl_2): λ_{max} (ε) = 445 (2921) nm ($M^{-1}cm^{-1}$).

CV (in CH_2Cl_2, vs Ag/AgCl): E_c = -1.06 V.

$Mo_3S_7Br_4$(dcmphen), (24)

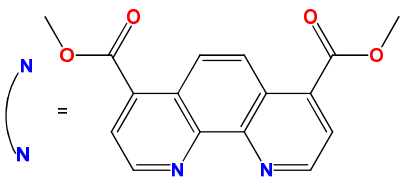

The complex $(Bu_4N)_2[Mo_3S_7Br_6]$ (500 mg, 0.34 mmol) and the same amount of 4,7-dicarbomethoxy-1,10-phenanthroline (500 mg,

1.7 mmol) were mixed with CH_2Cl_2 (130 mL). Purification was carried out as usual to afford a red powder. Yield: 320 mg (84 %).

^{1}H-NMR (CD_2Cl_2, 300 MHz): δ = 4.16 (d, 6H), 8.48 (d, 2H), 9.19 (d, 2H), 10.17 (d, 1H), 10.72 ppm (d, 1H).

ESI(-) MS (CH_2Cl_2/CH_3CN, 20V): m/z = 1208.0 $[MBr]^-$, 1163.1 $[MCl]^-$.

Elemental analysis (%) calcd. for $C_{16}H_{12}Br_4Mo_3N_2O_4S_7$: C, 17.03; H, 1.07; N, 2.48; found: C, 16.65; H, 1.4; N, 2.1.

UV/Vis (DMSO): λ_{max} (ε) = 497 (2926) nm ($M^{-1}cm^{-1}$).

$Mo_3S_7Cl_4$(ppl), (25)

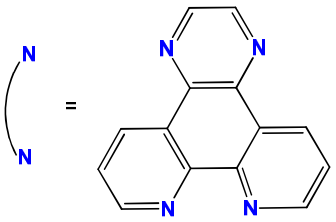

The cluster complex $(Bu_4N)_2[Mo_3S_7Cl_6]$ (100 mg, 0.083) and the ligand pyrazino[2,3-f][1,10]phenanthroline (100 mg, 0.43 mmol) were mixed with CH_2Cl_2 (20 mL). The mixture was heated to reflux for 8.5 h. Purification afforded a reddish solid. Yield: 50 mg (68 %).

^{1}H-NMR (d_6-DMSO, 300 MHz): δ = 8.40 (m, 2H), 9.35 (s, 2H), 9.75 – 10.15 ppm (m, 4H).

ESI(-) MS (CH_2Cl_2/CH_3CN, 20V): m/z = 922.2 $[MCl]^-$, 966.1 $[MBr]^-$.

Elemental analysis (%) calcd. for $C_{14}H_8Cl_4Mo_3N_4S_7$: C, 18.97; H, 0.91; N, 6.32; found: C, 18.65; H, 1.30; N, 6.20.

UV/Vis (DMSO): λ_{max} (ε) = 448 (2552) nm ($M^{-1}cm^{-1}$).

$Mo_3S_7Br_4$(ppl), (26)

The cluster complex $(Bu_4N)_2[Mo_3S_7Br_6]$ (100 mg, 0.068 mmol) and the ligand pyrazino[2,3-f][1,10]phenanthroline (63 mg, 0.27 mmol) were mixed with CH_2Cl_2 (30 mL). The mixture was stirred overnight at room temperature. The usual purification method was carried out. A reddish solid was obtained. Yield: 60 mg (83 %).

^{1}H-NMR (d_6-DMSO, 300 MHz): δ = 8.41 (m, 2H), 9.38 (s, 2H), 9.88 (m, 3H), 10.22 ppm (d, 1H).

ESI(-) MS (CH_2Cl_2/CH_3CN, 20V): m/z = 1142.2 $[MBr]^-$, 1099.6 $[MCl]^-$.

Elemental analysis (%) calcd. for $C_{14}H_8Br_4Mo_3N_4S_7$: C, 15.80; H, 0.76; N, 5.27; found: C, 16.15; H, 1.15; N, 5.0.

UV/Vis (DMSO): λ_{max} (ε) = 460 (2657) nm ($M^{-1}cm^{-1}$).

$Mo_3S_7Cl_4$(mphen), (27)

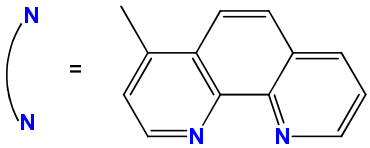

The cluster complex $(Bu_4N)_2[Mo_3S_7Cl_6]$ (100 mg, 0.083) and the ligand 4-methyl-1,10-phenanthroline (50 mg, 0.25 mmol) were mixed with CH_2Cl_2 (20 mL). Reflux overnight followed by purification afforded an orange powder. Yield: 70 mg (99 %).

^{1}H-NMR (d_6-DMSO, 300 MHz): δ = 2.98 (s, 3H), 8.10 (d, 1H), 8.25 (t, 1H), 8.45 (m, 2H), 9.10 (t, 1H), 9.60 – 10.10 ppm (m, 2H).

ESI(-) MS (CH_2Cl_2/CH_3CN, 20V): m/z = 883.4 $[MCl]^-$, 927.4 $[MBr]^-$.

$Mo_3S_7Br_4((COOMe)_2ppl)$, (28)

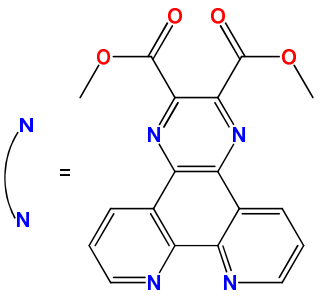

The complex $(Bu_4N)_2[Mo_3S_7Br_6]$ (50 mg, 0.034 mmol) and an excess of 2,3-dimethoxycarbonylpyrazino[2,3-f][1,10]phenanthroline (36 mg, 0.10 mmol) were mixed with CH_2Cl_2 (15 mL). The mixture was stirred overnight at room temperature. After taking to dryness, the solid residue was washed with methanol, acetonitrile, dichloromethane and diethyl ether to afford a reddish powder. Yield: 28 mg (70 %).

^{1}H-NMR (d_6-DMSO, 300 MHz): δ = 4.07 (d, 6H), 8.01 (dd, 1H), 8.45 (m, 2H), 9.29 (d), 9.40 (d), 9.80 (m), 9.90 (d), 10.27 ppm (d, 1H).

ESI(-) MS (CH_2Cl_2/CH_3CN, 20V): m/z = 1260.2 $[MBr]^-$, 1216.1 $[MCl]^-$, 1170.1 [M – Br + 2Cl]$^-$.

UV/Vis (DMSO): λ_{max} (ε) = 460 sh (1593) nm ($M^{-1}cm^{-1}$).

7.1.6. HETEROLEPTIC MOLYBDENUM CLUSTERS WITH DIIMINE AND SULFUR DONOR LIGANDS

Reaction between heteroleptic molybdenum cluster complexes of general formula $Mo_3S_7Br_4$(diimine) and stoichiometric amounts of $[Zn(dmit)_2]^{2-}$ or diethyldithiocarbamate (dtc^-) afforded complexes of formulae $[Mo_3S_7(diimine)L]^{0,\,2+}$ (L = dmit or dtc) by substitution of the halide ligands. The synthetic procedure, as well as the characterization of such compounds is described below.

$Mo_3S_7(dnbpy)(dmit)_2$, (29)

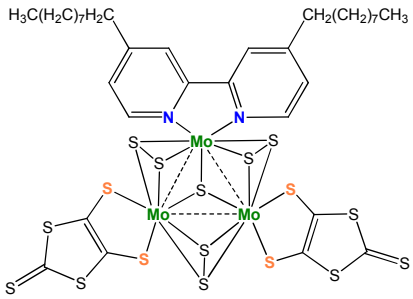

To a solution of $Mo_3S_7Br_4$(dnbpy) (300 mg, 0.24 mmol) in CH_2Cl_2 (75 mL), 1.1 equivalents of $(Bu_4N)_2[Zn(dmit)_2]$ (252 mg, 0.27 mmol) were added. The solution was stirred for 6 h at room temperature. The dark red mixture was filtered, and the filtrate was taken to dryness by rotary evaporation. The sticky dark residue was thoroughly washed with methanol, water, acetonitrile, and diethyl ether. A dark powder was obtained. The reaction is almost quantitative. Yield: 315 mg (99 %).

Elemental analysis (%) calcd. for $C_{34}H_{44}Mo_3N_2S_{17}$: C, 31.09; H, 3.38; N, 2.13; S, 41.50; found C, 31.3; H, 3.7; N, 2.1; S, 41.2.

IR (KBr, cm^{-1}): 2920 (s, Csp^3-H), 2849 (s, Csp^3-H), 1613 (m, C=C), 1542 (w, C=C), 1457 (m, C=C), 1417 (m, C=C), 1053 (s, C=S), 1023 (s, C-S), 516 (w, S_{eq}-S_{ax}), 420 (w, Mo-μ_3S).

UV/Vis (DMSO): λ_{max} (ε) = 326 sh (17 550), 492 (11 665) nm ($M^{-1}cm^{-1}$).

$Mo_3S_7(dcmbpy)(dmit)_2$, (30)

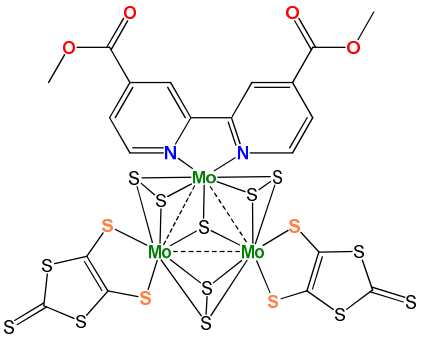

To a solution of $(Bu_4N)[Mo_3S_7Br_5(dcmbpy)]$ (360 mg, 0.25 mmol) in CH_2Cl_2 (60 mL), solid $(Bu_4N)_2[Zn(dmit)_2]$ (240 mg, 0.25 mmol) was added in one portion. The dark purple mixture was stirred for 6.5 h at room temperature. After filtration, the solution was taken to dryness by rotary evaporation. The sticky dark residue was thoroughly washed with methanol, water, hot acetonitrile (until colorless filtrate), and diethyl ether. A dark powder, insoluble in common organic solvents, was obtained. Yield: 240 mg (82 %).

Elemental analysis (%) calcd. for $C_{20}H_{12}Mo_3N_2O_4S_{17}$: C, 20.40; H, 1.03; N, 2.38; found: C, 20.4; H, 1.3; N, 2.4.

IR (KBr, cm^{-1}): 1732 (s, C=O), 1617 (m, C=C), 1542 (w, C=C), 1437 (m, C=C), 1267 (m, C-O), 1053 (s, C=S), 1029 (s, C-S), 517 (w, S_{eq}-S_{ax}), 420 (w, Mo-μ_3S).

UV/Vis (DMSO): λ_{max} (ε) = 326 sh (6730), 490 (4513) nm ($M^{-1}cm^{-1}$).

$Mo_3S_7(dcbpy)(dmit)_2$, (31)

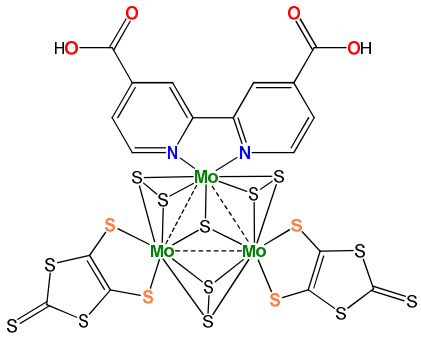

The synthesis of the title compound was carried out in two steps. The cluster complex $(Bu_4N)_2[Mo_3S_7Br_6]$ (500 mg, 0.34 mmol) and 5.5 equivalents of 2,2'-bipyridine-4,4'-dicarboxylic acid (460 mg, 1.88 mmol) were mixed with degassed DMF (100 mL). The mixture was heated to 125-130 °C for 20 h. The red solution, presumably containing the species $(Bu_4N)[Mo_3S_7Br_4(dcbpy)\cdot Br]$, was allowed to cool to room temperature. The excess of ligand precipitated as a white

crystalline solid, which was not removed. To this suspension, 1.1 equivalents of solid $(Bu_4N)_2[Zn(dmit)_2]$ (353 mg, 0.37 mmol) were added. The deep purple mixture was stirred overnight at room temperature. The white solid was removed by filtration, and the filtrate was concentrated by rotary evaporation. The solution was cooled to -30 ºC to allow the complete precipitation of the excess of the ligand. After filtration, the solution was taken to dryness by rotary evaporation. Then the dark residue was thoroughly washed with methanol, water, hot acetonitrile and diethyl ether to afford a dark powder, insoluble in common organic solvents. Yield: 290 mg (74 %).

Elemental analysis (%) calcd. for $C_{18}H_8Mo_3N_2O_4S_{17}$: C, 18.81; H, 0.70; N, 2.44; found: C, 18.5; H, 1.0; N, 2.5.

IR (KBr, cm^{-1}): 3446 (br, OH), 1716 (m, C=O), 1542 (m, C=C), 1458 (m, C=C), 1053 (s, C=S), 516 (w, S_{eq}-S_{ax}), 416 (m, Mo-μ_3S).

UV/Vis (DMSO): λ_{max} (ε) = 336 sh (12 181), 484 (5475) nm ($M^{-1}cm^{-1}$).

$[Mo_3S_7(dmphen)(dtc)_2 \cdot Br](PF_6)$, ([32·Br]($PF_6$))

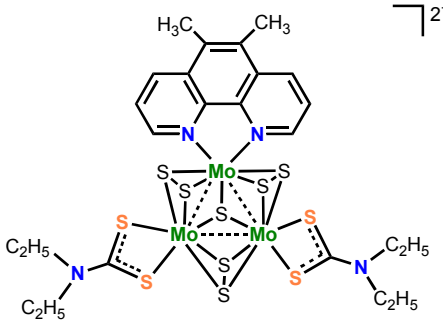

The cluster $(Bu_4N)_2[Mo_3S_7Br_6]$ (50 mg, 0.034 mmol) and 5,6-dimethyl-1,10-phenanthroline (38 mg, 0.18 mmol) were dissolved in 10 ml of CH_2Cl_2. The mixture was refluxed for 1 h. Then solid $Na(dtc)\cdot 3H_2O$ (16 mg, 0.071 mmol) was added to the red solution. The mixture was refluxed for further 1 h. The solution was filtered and evaporated to dryness. The solid was washed with CH_3OH and Et_2O, and dissolved in the minimum amount of CH_2Cl_2. This solution was loaded on a silica gel column and washed with CH_2Cl_2. After that, a red fraction was eluted with a saturated solution of KPF_6 in acetone, and evaporated to dryness. The product was dissolved in CH_2Cl_2. The

KPF_6 and KBr salts were filtered off, the solution was concentrated, and the product was precipitated with diethyl ether. The precipitate was successively washed with H_2O, EtOH, iPrOH and Et_2O. Yield: 30 mg (70 %).

ESI(-) MS (CH_2Cl_2/CH_3CN, 20V): m/z = 1096 $[MBr]^+$, 1052 $[MCl]^+$.

Elemental analysis (%) calcd. for $C_{24}H_{32}N_4BrF_6PMo_3S_{11}$: C, 23.2; H, 2.6; N, 4.5; S, 28.4; found: C, 23.4; H, 3.2; N, 4.1; S, 28.5.

IR (KBr, cm^{-1}): 2963 (m), 2927 (m), 2862 (w), 1512 (s), 1435 (s), 1355 (m), 1274 (s), 1205 (m), 1148 (w), 1077 (m), 1039 (w), 913 (w), 805 (s), 721 (m), 524 (m), 400 (w).

7.2. STRUCTURAL DETERMINATION

7.2.1. GENERAL REMARKS

The methods used for the diffraction data collection, as well as the solution and the refinement of the structures are described in this section. The solid structure of the compounds was determined by X-ray diffraction. In virtually all cases diffraction data were collected at 200 K on an Agilent Supernova diffractometer equipped with an Atlas CCD detector. Data were integrated with the CrysAlisPro program.[15] Mo-Kα radiation (λ = 0.71073 Å) or Cu-Kα radiation (λ = 1.54180 Å) were employed. No instrument or crystal instabilities were observed during data collection. Absorption corrections based on the multi-scan method were applied.[16] In general, structures were solved by charge-flipping methods using Superflip,[17] and refined by the least squares method using SHELXL-2013.[18] Olex2 1.2 software package was used for both the solution and the refinement of the structures.[19] For structures (Bu_4N)[**22**·Br] and [**32**·Br](PF_6), diffraction data were collected on a Bruker CCD diffractometer. These structures were solved by the Patterson method or direct methods, respectively using SHELXS-97, and refined by least squares using SHELXL-97. The SHELXTL software package was used for both the solution and the refinement of the latter structures.[18]

The crystallographic data and structure refinement parameters are given for each compound. Unless otherwise stated, the non-hydrogen atoms were refined anisotropically. The hydrogen atoms bonded to carbon were included at their idealized positions and refined as riders with isotropic displacement parameters assigned as 1.2 times the U_{eq} value of the corresponding bonding partner (1.5 for the methyl groups). Disordering was modelled by expressing the occupation factors of the atoms in terms of a "free variable" so that their sum was contrained to 1, and their Uij parameters were equated using the EADP constraint. The structural figures were drawn by using ORTEP3 v2.02.[20] For trinuclear clusters, the axial sulfide ligands (S_{ax}) are designated by S(3), S(5) and S(7), whereas those which lie in the equatorial

plane (S_{eq}) are designated by S(2), S(4) and S(6). The apical sulfurs (S_{ap}) are labeled as S(1).

7.2.2. STRUCTURE OF BIS(DITHIOLENE) MOLYBDENUM AND TUNGSTEN CLUSTERS

7.2.2.1. STRUCTURE OF $(Et_4N)_2[Mo_2O_2S_2(BPyDTS_2)_2]$, $((Et_4N)_2[4])$

Brown needle-like single crystals of compound $(Et_4N)_2$[**4**] were obtained by slow diffusion of diethyl ether into a sample solution in DMF, and the solid structure was determined by X-ray diffraction. The structure of $(Et_4N)_2$[**4**] was refined in the monoclinic space group C2/c. All non-hydrogen atoms were refined anisotropically. Figure 7.1 shows its ORTEP representation with the atom numbering scheme. No cocrystallized solvents were found. The equivalent positions were generated by symmetry, applying the rule (1-x, y, 3/2 - z). The crystallographic data collection parameters are given in Table 7.1.1.

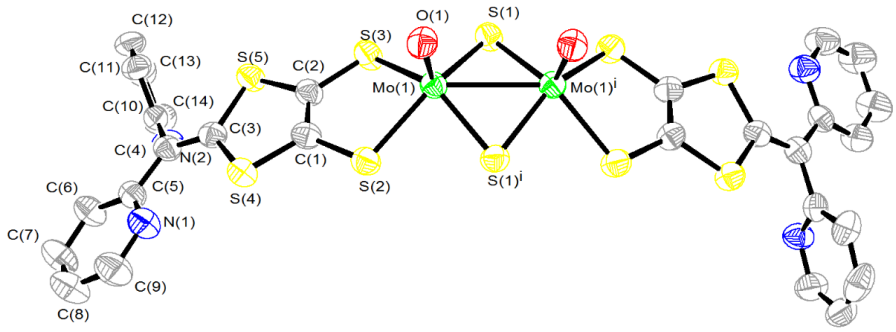

Figure 7.1. ORTEP representation (50 % probability ellipsoids) of the anionic dinuclear cluster [**4**]$^{2-}$ with the atom numbering scheme. Average distances (Å): Mo-Mo, 2.8435(9); Mo-(μ-S), 2.3273(14); Mo=O, 1.687(3); Mo-S_{ligand}, 2.4315(14).

Table 7.1.1. Crystal Structure Data

Crystal Data			
Species	$(Et_4N)_2[Mo_2O_2S_2(BPyDTS_2)_2]$		
Formula	$C_{44}H_{56}Mo_2N_6O_2S_{10}$	**Crystal system**	monoclinic
Space group	C2/c	**Formula weight**	1213.43
a (Å)	29.411(2)	**α** (º)	90
b (Å)	9.4996(4)	**β** (º)	114.965
c (Å)	21.3574(15)	**γ** (º)	90
Z	4	**Vol** (Å^3)	5409.7(6)
Colour	brown	**Crystal size (mm)**	0.4411 × 0.0638 × 0.0272
$\mathbf{d_{calc}}$ (mg/mm^3)	1.490	**λ** (Å)	0.71073
Absorption coefficient (mm^{-1})	0.891	**F (000)**	2488.0

Experimental Data			
Temperature (K)	220	**R(int)**	0.0795
Time per frame (s)	22	**R (σ)**	0.0792
2θ Range (º)	5.74 to 58.82	**Index ranges**	-38 ≤ h ≤ 40 -12 -≤ k ≤ 12 -27 -≤ l ≤ 28
Collected reflections	31083	**Independent reflections**	6874

Solution and Refinement			
Parameters	293	**GooF on F²**	1.059
Restraints	0		
Final R1 ([I>2sigma(I)])	0.0598	**Final R1 (all data)**	0.1168
Final wR2 ([I>2sigma(I)])	0.1194	**Final wR2 (all data)**	0.1512
Max/Min peak (e·Å^{-3})	1.56 / -0.59	**Max. shift/σ**	0.002

$$\boldsymbol{R1} = \sum\big||\boldsymbol{F_0}| - |\boldsymbol{F_1}|\big| / \sum \boldsymbol{F_0} \qquad \boldsymbol{wR2} = \left[\sum\left[\boldsymbol{w}(\boldsymbol{F_0^2} - \boldsymbol{F_c^2})^2\right] / \sum\left[\boldsymbol{w}(\boldsymbol{F_0^2})^2\right]\right]^{1/2}$$

Table 7.1.2. Bond Distances

Atom	Atom	Length/Å	Atom	Atom	Length/Å
Mo1	Mo1[i]	2.8436(9)	S3	C2	1.747(5)
Mo1	S1[i]	2.3250(13)	C4	C5	1.458(7)
Mo1	S1	2.3298(14)	C4	C3	1.343(7)
Mo1	S2	2.4401(14)	N1	C5	1.354(6)
Mo1	S3	2.4224(14)	N1	C9	1.329(7)
Mo1	O1	1.687(3)	C5	C6	1.397(7)
S5	C3	1.771(5)	C2	C1	1.321(7)
S5	C2	1.756(5)	C8	C7	1.363(8)
S4	C3	1.773(5)	C9	C8	1.378(8)
S4	C1	1.763(5)	C6	C7	1.369(8)
S1	Mo1[i]	2.3250(13)	C10	C4	1.509(7)
S2	C1	1.759(5)			

[i] Equivalent positions generated by symmetry, applying the rule (1-x, y, 3/2-z)

Table 7.1.3. Bond Angles

Atom	Atom	Atom	Angle/°	Atom	Atom	Atom	Angle/°
S1	Mo1	Mo1[i]	52.27(3)	C8	C7	C6	120.5(6)
S1[1]	Mo1	Mo1[i]	52.42(3)	C5	C4	C10	118.0(4)
S1[1]	Mo1	S1	99.46(5)	C3	C4	C10	118.2(4)
S1	Mo1	S2	148.12(5)	C3	C4	C5	123.6(5)
S1[1]	Mo1	S2	79.77(5)	C9	N1	C5	117.9(5)
S1[1]	Mo1	S3	142.93(5)	N1	C5	C4	115.8(4)
S1	Mo1	S3	78.43(5)	N1	C5	C6	121.0(5)
S2	Mo1	Mo1[i]	131.61(4)	C6	C5	C4	123.2(5)
S3	Mo1	Mo1[i]	129.16(4)	S5	C3	S4	113.1(3)
S3	Mo1	S2	83.39(5)	C4	C3	S5	120.4(4)
O1	Mo1	Mo1[i]	100.99(12)	C4	C3	S4	126.4(4)
O1	Mo1	S1	107.91(13)	S3	C2	S5	118.9(3)
O1	Mo1	S1[i]	109.89(12)	C1	C2	S5	117.0(4)
O1	Mo1	S2	102.12(13)	C1	C2	S3	123.9(4)
O1	Mo1	S3	105.80(12)	S2	C1	S4	119.2(3)
C2	S5	C3	95.7(2)	C2	C1	S4	118.4(4)
C1	S4	C3	94.7(2)	C2	C1	S2	122.2(4)
Mo1[i]	S1	Mo1	75.31(4)	N1	C9	C8	124.1(6)
C1	S2	Mo1	103.39(17)	C7	C6	C5	118.8(5)
C2	S3	Mo1	103.60(17)	C7	C8	C9	117.5(6)

[i] Equivalent positions generated by symmetry, applying the rule (1-x, y, 3/2-z)

7.2.2.2. STRUCTURE OF $(PPN)_2[Mo_2S_4(pdt)_2]$, $((PPN)_2[6])$

Single crystals of compound $(PPN)_2$[**6**] were obtained by slow diffusion of dichloromethane into a toluene solution of the sample. The structure of $(PPN)_2$[**6**] was refined in the triclinic space group P-1. All non-hydrogen atoms were refined anisotropically. Figure 7.2 shows its ORTEP representation with the atom numbering scheme. Dichloromethane was found cocrystallized with the cluster complex. In addition, the crystal structure contains disordered solvent molecules. In spite of several attempts, the electronic density in this area could not be resolved satisfactorily. Therefore the contribution of the disordered solvent species was subtracted from the structure factor calculations by using the solvent mask[21] instruction in the program Olex2 1.2. The crystallographic data collection parameters are given in Table 7.2.1.

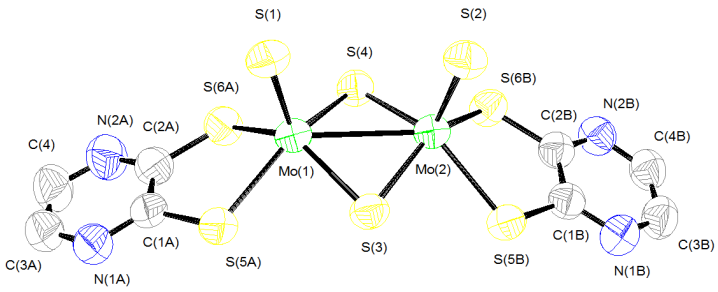

Figure 7.2. ORTEP representation (50 % probability ellipsoids) of the anionic dinuclear cluster $[\mathbf{6}]^{2-}$ with the atom numbering scheme. Average distances (Å): Mo-Mo, 2.8531(4); Mo-(μ-S), 2.3204(10); Mo=S, 2.1198(2); Mo-S_{ligand}, 2.4139(10).

Table 7.2.1. Crystal Structure Data

Crystal Data			
Species	$(PPN)_2[Mo_2S_4(pdt)_2]\cdot CH_2Cl_2$		
Formula	$C_{81}H_{68}Cl_2Mo_2N_6P_4S_8$	**Crystal system**	triclinic
Space group	P-1	**Formula weight**	1766.53
a (Å)	12.2417(2)	**α** (º)	74.0845
b (Å)	17.5979(3)	**β** (º)	79.6296
c (Å)	20.8957(3)	**γ** (º)	71.4901
Z	2	**Vol** (Å^3)	4083.64(11)
Colour	dark red	**Crystal size** (mm)	0.593 × 0.081 × 0.055
$\mathbf{d_{calc}}$ (g/cm^3)	1.437	**λ** (Å)	1.54184
Absorption coefficient (mm^{-1})	6.138	**F (000)**	1800

Experimental Data			
Temperature (K)	200	**R(int)**	0.0478
Time per frame (s)	5	**R (σ)**	0.0255
2θ Range (º)	6.16 to 129.32	**Index ranges**	-14 ≤ h ≤ 14 -20 ≤ k ≤ 20 -24 ≤ l ≤ 24
Collected reflections	64062	**Independent reflections**	13580

Solution and Refinement			
Parameters	928	**GooF on F²**	1.083
Restraints	0		
Final R1 ([I>2sigma(I)])	0.0598	**Final R1 (all data)**	0.1599
Final wR2 ([I>2sigma(I)])	0.0648	**Final wR2 (all data)**	0.1684
Max/Min peak (e·Å^{-3})	1.34 / -0.54	**Max. shift/σ**	0.001

$$\boldsymbol{R1} = \sum\big||\boldsymbol{F_0}| - |\boldsymbol{F_1}|\big| / \sum \boldsymbol{F_0} \qquad \boldsymbol{wR2} = \left[\sum\left[\boldsymbol{w}(\boldsymbol{F_0^2} - \boldsymbol{F_c^2})^2\right] / \sum\left[\boldsymbol{w}(\boldsymbol{F_0^2})^2\right]\right]^{1/2}$$

Table 7.2.2. Bond Distances

Atom	Atom	Length/Å	Atom	Atom	Length/Å
Mo1	Mo2	2.8531(4)	S5A	C1A	1.747(4)
Mo1	S6A	2.3951(10)	N1B	C1B	1.324(5)
Mo1	S3	2.3187(9)	N1B	C3B	1.336(6)
Mo1	S1	2.1145(10)	C2B	C1B	1.423(6)
Mo1	S4	2.3258(10)	C2B	N2B	1.333(5)
Mo1	S5A	2.4283(10)	N2B	C4B	1.338(6)
Mo2	S6B	2.4233(10)	N2A	C2A	1.337(6)
Mo2	S3	2.3232(10)	N2A	C4A	1.338(7)
Mo2	S2	2.1250(10)	C2A	C1A	1.405(7)
Mo2	S4	2.3138(10)	C4A	C3A	1.359(9)
Mo2	S5B	2.4083(9)	N1A	C1A	1.330(6)
S6A	C2A	1.741(5)	N1A	C3A	1.343(7)
S6B	C2B	1.743(4)	C3B	C4B	1.376(7)
S5B	C1B	1.738(4)			

Table 7.2.3. Bond Angles

Atom	Atom	Atom	Angle/˚	Atom	Atom	Atom	Angle/˚
S6A	Mo1	Mo2	126.08(3)	S5B	Mo2	Mo1	127.32(3)
S6A	Mo1	S5A	82.02(4)	S5B	Mo2	S6B	82.03(3)
S3	Mo1	Mo2	52.15(2)	C2A	S6A	Mo1	106.67(15)
S3	Mo1	S6A	140.09(4)	C2B	S6B	Mo2	106.24(14)
S3	Mo1	S4	100.46(3)	Mo1	S3	Mo2	75.85(3)
S3	Mo1	S5A	79.86(3)	Mo2	S4	Mo1	75.90(3)
S1	Mo1	Mo2	104.33(3)	C1B	S5B	Mo2	107.07(14)
S1	Mo1	S6A	108.12(4)	C1A	S5A	Mo1	106.05(15)
S1	Mo1	S3	110.35(4)	C1B	N1B	C3B	116.3(4)
S1	Mo1	S4	107.08(4)	C1B	C2B	S6B	120.6(3)
S1	Mo1	S5A	102.39(4)	N2B	C2B	S6B	117.9(3)
S4	Mo1	Mo2	51.86(2)	N2B	C2B	C1B	121.5(4)
S4	Mo1	S6A	77.75(4)	N1B	C1B	S5B	119.0(3)
S4	Mo1	S5A	148.19(4)	N1B	C1B	C2B	121.3(4)
S5A	Mo1	Mo2	130.67(3)	C2B	C1B	S5B	119.7(3)
S6B	Mo2	Mo1	128.78(3)	C2B	N2B	C4B	116.1(4)
S3	Mo2	Mo1	52.00(2)	C2A	N2A	C4A	115.6(5)
S3	Mo2	S6B	146.71(4)	N2A	C2A	S6A	117.9(4)
S3	Mo2	S5B	78.58(3)	N2A	C2A	C1A	121.1(4)
S2	Mo2	Mo1	103.14(3)	C1A	C2A	S6A	121.0(3)
S2	Mo2	S6B	105.75(4)	N2A	C4A	C3A	123.3(5)
S2	Mo2	S3	105.72(4)	C1A	N1A	C3A	115.9(5)
S2	Mo2	S4	110.31(4)	C2A	C1A	S5A	119.6(3)
S2	Mo2	S5B	107.24(4)	N1A	C1A	S5A	118.2(4)
S4	Mo2	Mo1	52.24(3)	N1A	C1A	C2A	122.1(4)
S4	Mo2	S6B	78.18(4)	N1A	C3A	C4A	121.9(5)
S4	Mo2	S3	100.68(4)				
S4	Mo2	S5B	141.02(4)				

7.2.2.3. STRUCTURE OF $(Et_4N)_2[Mo_2O_2S_2(pdt)_2]$, $((Et_4N)_2[7])$

Single crystals of compound $(Et_4N)_2$[**7**] were obtained by slow diffusion Et_2O/DMF. The structure of $(Et_4N)_2$[**7**] was refined in the orthorhombic space group $P2_12_12_1$. All non-hydrogen atoms were refined anisotropically. Figure 7.3 shows its ORTEP representation with the atom numbering scheme. Owing to disorder, the exclusion of the hydrogen atoms for the CH_2/CH_3 groups in the most disordered alkyl chains in the tetraethylammonium counterion (those centered at N(300) and N(400)) was considered as justified. The crystallographic data collection parameters are given in Table 7.3.1.

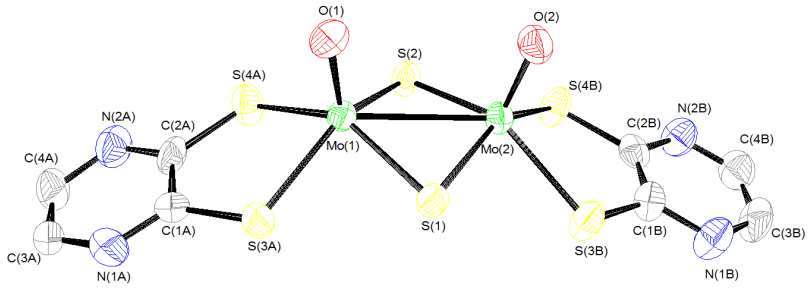

Figure 7.3. ORTEP representation (50 % probability ellipsoids) of the anionic dinuclear cluster $[7]^{2-}$ with the atom numbering scheme. Average distances (Å): Mo-Mo, 2.8622(9); Mo-(μ-S), 2.3258(2); Mo=O, 1.680(6); Mo-S_{ligand}, 2.4283(2).

Table 7.3.1. Crystal Structure Data

Crystal Data			
Species	$(Et_4N)_2[Mo_2O_2S_2(pdt)_2]$		
Formula	$C_{24}H_{44}Mo_2N_6O_2S_6$	**Crystal system**	orthorhombic
Space group	$P2_12_12_1$	**Formula weight**	832.89
a (Å)	25.2807(5)	**α** (º)	90.00
b (Å)	16.3588(3)	**β** (º)	90.00
c (Å)	16.7295(2)	**γ** (º)	90.00
Z	8	**Vol** (Å^3)	6918.7(2)
Colour	yellow	**Crystal size** (mm)	0.171 × 0.139 × 0.0747
$\mathbf{d_{calc}}$ (mg/mm^3)	1.599	**λ** (Å)	0.71073
Absorption coefficient (mm^{-1})	1.119	**F (000)**	3408.0

Experimental Data			
Temperature (K)	220	**R(int)**	0.0455
Time per frame (s)	130	**R (σ)**	0.0539
2θ Range (º)	5.84 to 50	**Index ranges**	-37 ≤ h ≤ 29 -23 ≤ k ≤ 23 -24 ≤ l ≤ 25
Collected reflections	39128	**Independent reflections**	12130

Solution and Refinement			
Parameters	729	**GooF on F²**	1.066
Restraints	0		
Final R1 ([I>2sigma(I)])	0.0484	**R1 (all data)**	0.0733
Final wR2 ([I>2sigma(I)])	0.1108	**wR2 (all data)**	0.1251
Max/Min peak (e·Å^{-3})	0.98 / -0.51	**Max. shift/σ**	0.003

$$\boldsymbol{R1} = \sum\big||\boldsymbol{F_0}| - |\boldsymbol{F_1}|\big| / \sum \boldsymbol{F_0} \qquad \boldsymbol{wR2} = \left[\sum\left[\boldsymbol{w}(\boldsymbol{F_0^2} - \boldsymbol{F_c^2})^2\right] / \sum\left[\boldsymbol{w}(\boldsymbol{F_0^2})^2\right]\right]^{1/2}$$

Table 7.3.2. Bond Distances

Atom	Atom	Length/Å	Atom	Atom	Length/Å
Mo1	Mo2	2.8641(11)	N1A	C1A	1.318(13)
Mo1	S2	2.328(2)	N1A	C3A	1.332(13)
Mo1	S1	2.332(2)	C2B	C1B	1.371(13)
Mo1	S4A	2.426(2)	C4A	C3A	1.361(15)
Mo1	S3A	2.429(3)	N1B	C3B	1.384(14)
Mo1	O1	1.680(6)	N1B	C1B	1.330(12)
Mo2	S2	2.333(2)	N2B	C2B	1.348(12)
Mo2	S1	2.321(2)	N2B	C4B	1.343(14)
Mo2	S4B	2.428(3)	C3B	C4B	1.333(16)
Mo2	S3B	2.421(3)	C2A	C1A	1.422(13)
Mo2	O2	1.675(6)	S3A	C1A	1.743(9)
S4A	C2A	1.748(10)	N2A	C2A	1.343(12)
S4B	C2B	1.745(10)	N2A	C4A	1.351(13)
S3B	C1B	1.779(10)			

Table 7.3.3. Bond Angles

Atom	Atom	Atom	Angle/°	Atom	Atom	Atom	Angle/°
S2	Mo1	Mo2	52.17(6)	O2	Mo2	S4B	107.1(2)
S2	Mo1	S1	100.01(9)	O2	Mo2	S3B	103.6(2)
S2	Mo1	S4A	78.45(8)	Mo1	S2	Mo2	75.82(7)
S2	Mo1	S3A	144.76(10)	Mo2	S1	Mo1	75.98(8)
S1	Mo1	Mo2	51.84(6)	C2A	S4A	Mo1	106.2(3)
S1	Mo1	S4A	143.45(10)	C2B	S4B	Mo2	105.9(3)
S1	Mo1	S3A	78.86(9)	C1B	S3B	Mo2	105.3(3)
S4A	Mo1	Mo2	128.43(7)	C1A	S3A	Mo1	107.3(4)
S4A	Mo1	S3A	82.16(9)	C2A	N2A	C4A	116.7(9)
S3A	Mo1	Mo2	128.89(7)	C1B	N1B	C3B	114.3(10)
O1	Mo1	Mo2	103.1(2)	C4B	N2B	C2B	116.9(10)
O1	Mo1	S2	108.3(2)	C4B	C3B	N1B	122.6(10)
O1	Mo1	S1	108.9(2)	N2A	C2A	S4A	117.7(8)
O1	Mo1	S4A	106.1(2)	N2A	C2A	C1A	120.8(9)
O1	Mo1	S3A	105.2(2)	C1A	C2A	S4A	121.4(7)
S2	Mo2	Mo1	52.01(6)	C1A	N1A	C3A	115.6(10)
S2	Mo2	S4B	78.69(8)	N2B	C2B	S4B	117.8(8)
S2	Mo2	S3B	146.79(10)	N2B	C2B	C1B	120.5(9)
S1	Mo2	Mo1	52.18(6)	C1B	C2B	S4B	121.7(7)
S1	Mo2	S2	100.19(8)	N1B	C1B	S3B	116.4(8)
S1	Mo2	S4B	141.85(11)	N1B	C1B	C2B	123.6(10)
S1	Mo2	S3B	79.17(9)	C2B	C1B	S3B	119.9(7)
S4B	Mo2	Mo1	128.08(7)	N2A	C4A	C3A	120.4(10)
S3B	Mo2	Mo1	129.99(8)	C2A	C1A	S3A	119.4(7)
S3B	Mo2	S4B	81.89(9)	N1A	C1A	S3A	118.8(8)
O2	Mo2	Mo1	103.0(2)	N1A	C1A	C2A	121.8(8)
O2	Mo2	S2	107.7(2)	C3B	C4B	N2B	122.1(12)
O2	Mo2	S1	109.4(2)	N1A	C3A	C4A	124.7(11)

7.2.2.4. STRUCTURE OF $(PPN)_2[W_2S_4(pdt)_2]$, $((PPN)_2[8])$

Single crystals of compound $(PPN)_2$[**8**] were obtained by gas diffusion Et_2O/ CH_2Cl_2. The structure of $(PPN)_2$[**8**] was refined in the triclinic space group P-1. Figure 7.4 shows its ORTEP representation with the atom numbering scheme. All non-hydrogen atoms were refined anisotropically. Dichloromethane was found cocrystallized with the cluster complex. In addition, the crystal structure contains disordered solvent molecules. In spite of several attempts, the electronic density in this area could not be resolved satisfactorily. Therefore the contribution of the disordered solvent species was subtracted from the structure factor calculations by using the solvent mask[21] instruction in the program Olex2 1.2. The crystallographic data collection parameters are given in Table 7.4.1.

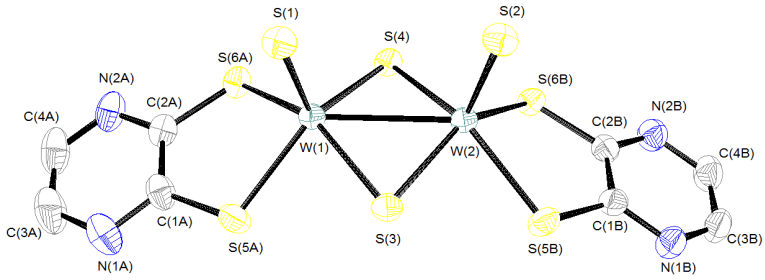

Figure 7.4. ORTEP representation (50 % probability ellipsoids) of the anionic dinuclear cluster [**8**]$^{2-}$ with the atom numbering scheme. Average distances (Å): W-W, 2.8504(2); W-(μ-S), 2.3278(9); W=S, 2.1344(9); W-S_{ligand}, 2.4115(9).

Table 7.4.1. Crystal Structure Data

Crystal Data			
Species	$(PPN)_2[W_2S_4(pdt)_2]\cdot CH_2Cl_2$		
Formula	$C_{81}H_{66}Cl_2N_6P_4S_8W_2$	**Crystal system**	triclinic
Space group	P-1	**Formula weight**	1942.35
a (Å)	12.2682(5)	**α** (º)	74.054(3)
b (Å)	17.6185(8)	**β** (º)	79.548(3)
c (Å)	20.8938(7)	**γ** (º)	71.173(4)
Z	2	**Vol** (Å^3)	4088.6(3)
Colour	orange	**Crystal size** (mm)	0.7533 × 0.0757 × 0.0732
$\mathbf{d_{calc}}$ (g/cm^3)	1.578	**λ** (Å)	1.54184
Absorption coefficient (mm^{-1})	8.742	**F (000)**	1928.0

Experimental Data			
Temperature (K)	200	**R(int)**	0.0567
Time per frame (s)	8	**R (σ)**	0.0328
2θ Range (º)	6.16 to 144.16	**Index ranges**	-14 ≤ h ≤ 15 -21 ≤ k ≤ 21 -25 ≤ l ≤ 25
Collected reflections	71375	**Independent reflections**	15803

Solution and Refinement			
Parameters	928	**GooF on F²**	1.061
Restraints	0		
Final R1 ([I>2sigma(I)])	0.0338	**Final R1 (all data)**	0.0398
Final wR2 ([I>2sigma(I)])	0.0901	**Final wR2 (all data)**	0.0937
Max/Min peak (e·Å^{-3})	1.33 / -1.40	**Max. shift/σ**	0.001

$$\boldsymbol{R1} = \sum\big||\boldsymbol{F_0}| - |\boldsymbol{F_1}|\big| / \sum \boldsymbol{F_0} \qquad \boldsymbol{wR2} = \left[\sum\left[\boldsymbol{w}(\boldsymbol{F_0^2} - \boldsymbol{F_c^2})^2\right] / \sum\left[\boldsymbol{w}(\boldsymbol{F_0^2})^2\right]\right]^{1/2}$$

Table 7.4.2. Bond Distances

Atom	Atom	Length/Å	Atom	Atom	Length/Å
W1	W2	2.8504(2)	S6A	C2A	1.742(4)
W1	S4	2.3261(9)	Cl12	C10	1.757(8)
W1	S1	2.1283(9)	N2B	C2B	1.332(5)
W1	S5A	2.3960(10)	N2B	C4B	1.352(6)
W1	S3	2.3316(9)	N2A	C2A	1.334(5)
W1	S6A	2.4247(9)	N2A	C4A	1.346(6)
W2	S4	2.3293(8)	C1B	N1B	1.329(5)
W2	S6B	2.4077(9)	C1B	C2B	1.417(6)
W2	S5B	2.4175(9)	N1B	C3B	1.339(6)
W2	S2	2.1404(9)	N1A	C3A	1.353(7)
W2	S3	2.3242(10)	N1A	C1A	1.338(6)
S6B	C2B	1.745(4)	C2A	C1A	1.414(6)
S5B	C1B	1.741(4)	C4B	C3B	1.368(7)
S5A	C1A	1.739(4)	C3A	C4A	1.359(8)

Table 7.4.3. Bond Angles

Atom	Atom	Atom	Angle/˚	Atom	Atom	Atom	Angle/˚
S4	W1	W2	52.30(2)	S3	W2	S6B	141.10(3)
S4	W1	S5A	139.96(4)	S3	W2	S5B	78.01(3)
S4	W1	S3	101.05(3)	W1	S4	W2	75.51(3)
S4	W1	S6A	79.56(3)	C2B	S6B	W2	106.72(14)
S1	W1	W2	104.69(3)	C1B	S5B	W2	106.45(13)
S1	W1	S4	110.37(4)	C1A	S5A	W1	106.64(15)
S1	W1	S5A	108.16(4)	W2	S3	W1	75.50(3)
S1	W1	S3	106.89(4)	C2A	S6A	W1	106.03(13)
S1	W1	S6A	102.30(4)	C2B	N2B	C4B	115.8(4)
S5A	W1	W2	125.90(3)	C2A	N2A	C4A	116.1(4)
S5A	W1	S6A	82.06(3)	N1B	C1B	S5B	118.5(3)
S3	W1	W2	52.13(2)	N1B	C1B	C2B	121.2(4)
S3	W1	S5A	77.54(3)	C2B	C1B	S5B	120.3(3)
S3	W1	S6A	148.36(3)	C1B	N1B	C3B	116.0(4)
S6A	W1	W2	130.45(2)	N2B	C2B	S6B	117.9(3)
S4	W2	W1	52.19(2)	N2B	C2B	C1B	122.0(4)
S4	W2	S6B	78.45(3)	C1B	C2B	S6B	120.1(3)
S4	W2	S5B	146.92(3)	C1A	N1A	C3A	115.6(5)
S6B	W2	W1	127.22(2)	N2A	C2A	S6A	118.9(3)
S6B	W2	S5B	82.08(3)	N2A	C2A	C1A	121.5(4)
S5B	W2	W1	128.65(3)	C1A	C2A	S6A	119.5(3)
S2	W2	W1	103.89(3)	N2B	C4B	C3B	121.6(4)
S2	W2	S4	105.94(4)	N1A	C3A	C4A	122.7(5)
S2	W2	S6B	106.92(4)	N1A	C1A	S5A	117.7(4)
S2	W2	S5B	105.19(4)	N1A	C1A	C2A	121.5(4)
S2	W2	S3	110.38(4)	C2A	C1A	S5A	120.8(3)
S3	W2	W1	52.37(2)	N2A	C4A	C3A	122.5(4)
S3	W2	S4	101.17(3)	N1B	C3B	C4B	123.3(4)

7.2.2.5. STRUCTURE OF $(PPN)_2[W_2O_2S_2(pdt)_2]$, $((PPN)_2[9])$

Single crystals of compound $(PPN)_2$[**9**] were obtained by slow diffusion Et_2O/CH_3CN. The structure of $(PPN)_2$[**9**] was refined in the triclinic space group P-1. Figure 7.5 shows its ORTEP representation with the atom numbering scheme. All non-hydrogen atoms were refined anisotropically. Acetonitrile was found cocrystallized with the cluster complex. A relatively high residual density peak (3.74 electrons per $Å^3$) can be found nearby a tungsten atom, which is considered as justified. The crystallographic data collection parameters are given in Table 7.5.1.

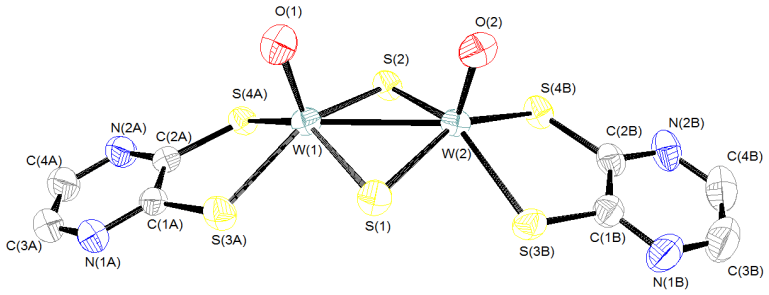

Figure 7.5. ORTEP representation (50 % probability ellipsoids) of the anionic dinuclear cluster $[\mathbf{9}]^{2-}$ with the atom numbering scheme. Average distances (Å): W-W, 2.84137(19); W-(μ-S), 2.3315(8); W=O, 1.737(3); $W\text{-}S_{ligand}$, 2.4183(8).

Table 7.5.1. Crystal Structure Data

Crystal Data			
Species	$(PPN)_2[W_2O_2S_2(pdt)_2]\cdot 2CH_3CN$		
Formula	$C_{84}H_{71}N_8O_2P_4S_6W_2$	**Crystal system**	triclinic
Space group	P-1	**Formula weight**	1908.42
a (Å)	12.0249(3)	**α** (º)	73.616(2)
b (Å)	17.7279(5)	**β** (º)	79.331(2)
c (Å)	20.7210(5)	**γ** (º)	71.884(3)
Z	2	**Vol** (Å^3)	4004.7(2)
Colour	brown	**Crystal size** (mm)	0.391 × 0.303 × 0.162
$\mathbf{d_{calc}}$ (g/cm^3)	1.5	**λ** (Å)	0.71073
Absorption coefficient (mm^{-1})	3.159	**F (000)**	1902.0

Experimental Data			
Temperature (K)	200	**R(int)**	0.0487
Time per frame (s)	5	**R (σ)**	0.0224
2θ Range (º)	5.66 to 53.0	**Index ranges**	-15 ≤ h ≤ 15 -22 ≤ k ≤ 22 -26 ≤ l ≤ 26
Collected reflections	164803	**Independent reflections**	16575

Solution and Refinement			
Parameters	957	**GooF on F²**	1.073
Restraints	0		
Final R1 ([I>2sigma(I)])	0.0243	**Final R1 (all data)**	0.0332
Final wR2 ([I>2sigma(I)])	0.0561	**Final wR2 (all data)**	0.0626
Max/Min peak (e·Å^{-3})	3.74 / -0.90	**Max. shift/σ**	0.002

$$\boldsymbol{R1} = \sum\big||\boldsymbol{F_0}| - |\boldsymbol{F_1}|\big| / \sum \boldsymbol{F_0} \qquad \boldsymbol{wR2} = \left[\sum\left[\boldsymbol{w}(\boldsymbol{F_0^2} - \boldsymbol{F_c^2})^2\right] / \sum\left[\boldsymbol{w}(\boldsymbol{F_0^2})^2\right]\right]^{1/2}$$

Table 7.5.2. Bond Distances

Atom	Atom	Length/Å	Atom	Atom	Length/Å
W2	W1	2.84137(19)	N1A	C1A	1.323(4)
W2	S1	2.3306(8)	N1A	C3A	1.339(5)
W2	S2	2.3331(8)	N2A	C2A	1.328(4)
W2	S4B	2.4341(8)	N2A	C4A	1.345(5)
W2	S3B	2.3990(8)	C2A	C1A	1.423(5)
W2	O2	1.738(2)	N2B	C2B	1.333(4)
W1	S3A	2.4228(9)	N2B	C4B	1.338(5)
W1	S1	2.3277(8)	C1B	N1B	1.329(5)
W1	S2	2.3353(8)	C1B	C2B	1.407(5)
W1	S4A	2.4172(8)	N1B	C3B	1.337(6)
W1	O1	1.736(3)	C11	N10	1.116(6)
S3A	C1A	1.744(3)	C11	C12	1.410(6)
S4A	C2A	1.743(3)	C3B	C4B	1.373(7)
S4B	C2B	1.751(4)	C21	N20	1.109(6)
S3B	C1B	1.740(4)	C21	C22	1.433(7)

Table 7.5.3. Bond Angles

Atom	Atom	Atom	Angle/°	Atom	Atom	Atom	Angle/°
S1	W2	W1	52.37(2)	O1	W1	S4A	105.89(8)
S1	W2	S2	101.49(3)	C1A	S3A	W1	106.32(11)
S1	W2	S4B	148.36(3)	W1	S1	W2	75.17(2)
S1	W2	S3B	76.95(3)	W2	S2	W1	74.98(2)
S2	W2	W1	52.54(2)	C2A	S4A	W1	106.50(11)
S2	W2	S4B	80.18(3)	C2B	S4B	W2	105.95(12)
S2	W2	S3B	140.52(3)	C1B	S3B	W2	106.83(12)
S4B	W2	W1	131.33(2)	C2A	N2A	C4A	115.5(3)
S3B	W2	W1	125.78(2)	N2A	C2A	S4A	118.3(3)
S3B	W2	S4B	82.06(3)	N2A	C2A	C1A	121.5(3)
O2	W2	W1	104.01(8)	C1A	C2A	S4A	120.2(2)
O2	W2	S1	106.19(9)	C2B	N2B	C4B	116.0(4)
O2	W2	S2	110.31(8)	N1A	C1A	S3A	117.7(3)
O2	W2	S4B	102.61(9)	N1A	C1A	C2A	121.9(3)
O2	W2	S3B	107.85(8)	C2A	C1A	S3A	120.3(2)
S3A	W1	W2	128.38(2)	N1B	C1B	S3B	117.1(3)
S1	W1	W2	52.46(2)	N1B	C1B	C2B	121.8(3)
S1	W1	S3A	77.48(3)	C2B	C1B	S3B	121.1(3)
S1	W1	S2	101.51(3)	C1B	N1B	C3B	116.1(4)
S1	W1	S4A	142.65(3)	N2B	C2B	S4B	118.9(3)
S2	W1	W2	52.474(19)	N2B	C2B	C1B	121.4(3)
S2	W1	S3A	147.41(3)	C1B	C2B	S4B	119.7(3)
S2	W1	S4A	79.73(3)	N1A	C3A	C4A	122.9(4)
S4A	W1	W2	129.26(2)	N2A	C4A	C3A	122.6(4)
S4A	W1	S3A	82.16(3)	N10	C11	C12	179.5(6)
O1	W1	W2	103.19(8)	N1B	C3B	C4B	122.2(4)
O1	W1	S3A	104.77(9)	N2B	C4B	C3B	122.4(4)
O1	W1	S1	109.40(9)	N20	C21	C22	176.3(6)
O1	W1	S2	106.14(9)				

7.2.3. STRUCTURE OF TRIS(DITHIOLENE) MOLYBDENUM CLUSTERS

7.2.3.1. STRUCTURE OF $(PPN)_2[Mo_3S_7(met)_3]$, $((PPN)_2[10])$

Single crystals of compound $(PPN)_2$[**10**] were obtained by slow diffusion Et_2O/CH_3CN. The structure of $(PPN)_2$[**10**] was refined in the triclinic space group P-1. All non-hydrogen atoms were refined anisotropically. Figure 7.6 shows its ORTEP representation with the atom numbering scheme. The bond distances of the atoms C(18), C(19), O(11) and C(12) contained in the dithiolene ligand coordinated to Mo(1) were restrained to a fixed value. The oxygen atoms O(9), O(10), O(11) and O(12), as well as the carbon atoms C(16) and C(19), contained in the latter dithiolate were refined with a partial occupancy of 0.66, 0.82, 0.33, 0.60, 0.80 and 0.91, respectively. In the dithiolene ligand coordinated to Mo(2), the methyl group close to O(2) was found disordered over two positions with partial occupations of 0.38 and 0.62. In the PPN^+ counterion, the phenyl groups close to P(100) and P(300) were refined with a partial occupancy of 0.75. Relatively high residual peaks whose density lies between 3.49 and 2.24 electrons per $Å^3$ can be found nearby the metal atoms of the cluster core. This is considered as justified. The crystallographic data collection parameters are given in Table 7.6.1.

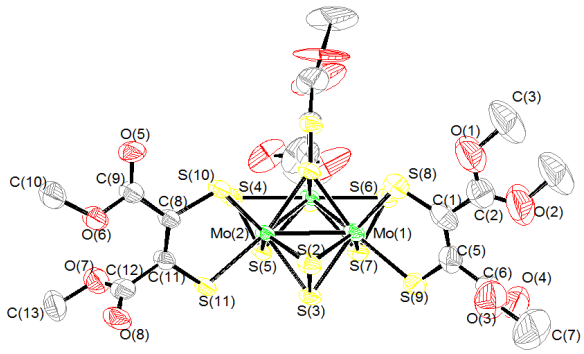

Figure 7.6. ORTEP representation (50 % probability ellipsoids) of the anionic trinuclear cluster $[\mathbf{10}]^{2-}$ with the atom numbering scheme. Average distances (Å): Mo-Mo, 2.7744(10); Mo-(μ_3-S), 2.372(2); Mo-S_{ax}, 2.404(2); Mo-S_{eq}, 2.529(2); Mo-S_{ligand}, 2.461(2).

Table 7.6.1. Crystal Structure Data

Crystal Data			
Species	$(PPN)_2[Mo_3S_7(met)_3]$		
Formula	$C_{85.2}H_{57.8}Mo_3N_2O_{10.4}P_4S_{13}$	**Crystal system**	triclinic
Space group	P-1	**Formula weight**	2104.62
a (Å)	14.3667(3)	**α** (º)	100.9205(18)
b (Å)	17.4281(4)	**β** (º)	103.1263(18)
c (Å)	21.4529(4)	**γ** (º)	91.3941
Z	2	**Vol** ($Å^3$)	5123.61(19)
Colour	dark red	**Crystal size** (mm)	0.3242 × 0.199 × 0.1033
$\mathbf{d_{calc}}$ (g/cm^3)	1.364	**λ** (Å)	0.71073
Absorption coefficient (mm^{-1})	0.740	**F (000)**	2121.0

Experimental Data			
Temperature (K)	200	**R(int)**	0.0527
Time per frame (s)	50	**R (σ)**	0.0550
2θ Range (º)	5.56 to 50	**Index ranges**	- 19 ≤ h ≤ 19 - 22 ≤ k ≤ 24 - 29 ≤ l ≤ 28
Collected reflections	90383	**Independent reflections**	18020

Solution and Refinement			
Parameters	1123	**GooF on F^2**	1.079
Restraints	22		
Final R1 ([I>2sigma(I)])	0.0887	**Final R1 (all data)**	0.1137
Final wR2 ([I>2sigma(I)])	0.2536	**Final wR2 (all data)**	0.2900
Max/Min peak ($e \cdot Å^{-3}$)	3.48 / -0.89	**Max. shift/σ**	<0.001

$$\boldsymbol{R1} = \sum\big||\boldsymbol{F_0}| - |\boldsymbol{F_1}|\big| / \sum \boldsymbol{F_0} \qquad \boldsymbol{wR2} = \left[\sum\left[\boldsymbol{w}(\boldsymbol{F_0^2} - \boldsymbol{F_c^2})^2\right] / \sum\left[\boldsymbol{w}(\boldsymbol{F_0^2})^2\right]\right]^{1/2}$$

Table 7.6.2. Bond Distances

Atom	Atom	Length/Å	Atom	Atom	Length/Å
Mo3	Mo1	2.7807(9)	Mo1	S6	2.525(2)
Mo3	Mo2	2.7713(10)	Mo1	S13	2.483(2)
Mo3	S10	2.432(2)	Mo2	S1	2.365(2)
Mo3	S11	2.501(2)	Mo2	S3	2.405(2)
Mo3	S5	2.409(2)	Mo2	S7	2.406(2)
Mo3	S1	2.377(2)	Mo2	S6	2.531(2)
Mo3	S3	2.409(2)	Mo2	S2	2.525(2)
Mo3	S4	2.534(2)	Mo2	S9	2.491(3)
Mo3	S2	2.521(2)	Mo2	S8	2.420(3)
Mo1	Mo2	2.7711(10)	S10	C8	1.767(8)
Mo1	S5	2.398(2)	S11	C11	1.748(8)
Mo1	S1	2.374(2)	S5	S4	2.040(3)
Mo1	S4	2.537(2)	S3	S2	2.041(3)
Mo1	S7	2.397(2)	S7	S6	2.036(3)
S13	C17	1.746(11)	S12	C14	1.769(10)
Mo1	S12	2.441(2)	S9	C5	1.724(12)

Table 7.6.3. Bond Angles

Atom	Atom	Atom	Angle/°	Atom	Atom	Atom	Angle/°
Mo2	Mo3	Mo1	59.88(2)	S7	Mo2	Mo1	54.62(6)
S10	Mo3	Mo1	121.25(6)	S7	Mo2	S6	48.62(7)
S10	Mo3	Mo2	122.50(6)	S7	Mo2	S2	132.09(8)
S10	Mo3	S11	81.97(7)	S7	Mo2	S9	85.47(9)
S10	Mo3	S4	89.25(8)	S7	Mo2	S8	135.78(8)
S10	Mo3	S2	91.01(8)	S6	Mo2	Mo3	116.87(6)
S11	Mo3	Mo1	139.95(7)	S6	Mo2	Mo1	56.65(6)
S11	Mo3	Mo2	137.95(6)	S2	Mo2	Mo3	56.63(6)
S11	Mo3	S4	95.23(8)	S2	Mo2	Mo1	116.78(6)
S11	Mo3	S2	92.88(8)	S2	Mo2	S6	172.57(8)
S5	Mo3	Mo1	54.48(5)	S9	Mo2	Mo3	138.43(6)
S5	Mo3	Mo2	95.11(6)	S9	Mo2	Mo1	139.64(7)
S5	Mo3	S10	134.70(9)	S9	Mo2	S6	94.06(8)
S5	Mo3	S11	85.72(8)	S9	Mo2	S2	93.37(8)
S5	Mo3	S4	48.68(7)	S8	Mo2	Mo3	121.42(7)
S5	Mo3	S2	133.17(8)	S8	Mo2	Mo1	119.77(7)
S1	Mo3	Mo1	54.12(5)	S8	Mo2	S6	89.77(8)
S1	Mo3	Mo2	54.05(6)	S8	Mo2	S2	91.22(8)
S1	Mo3	S10	80.16(7)	S8	Mo2	S9	83.16(10)
S1	Mo3	S11	162.05(7)	C8	S10	Mo3	106.9(3)
S1	Mo3	S5	108.22(7)	C11	S11	Mo3	105.5(3)
S1	Mo3	S3	108.40(8)	Mo1	S5	Mo3	70.68(6)
S1	Mo3	S4	86.26(8)	S4	S5	Mo3	68.86(9)
S1	Mo3	S2	85.74(8)	S4	S5	Mo1	69.18(9)
S3	Mo3	Mo1	95.61(5)	Mo1	S1	Mo3	71.66(6)
S3	Mo3	Mo2	54.80(5)	Mo2	S1	Mo3	71.53(6)
S3	Mo3	S10	136.30(8)	Mo2	S1	Mo1	71.57(6)
S3	Mo3	S11	83.59(8)	Mo2	S3	Mo3	70.30(6)
S3	Mo3	S5	84.64(8)	S2	S3	Mo3	68.47(9)
S3	Mo3	S4	133.11(8)	S2	S3	Mo2	68.65(9)
S3	Mo3	S2	48.84(8)	Mo3	S4	Mo1	66.51(6)
S4	Mo3	Mo1	56.80(5)	S5	S4	Mo3	62.46(9)
S4	Mo3	Mo2	116.63(5)	S5	S4	Mo1	62.08(8)
S2	Mo3	Mo1	116.57(6)	Mo1	S7	Mo2	70.47(6)
S2	Mo3	Mo2	56.76(5)	S6	S7	Mo1	68.87(9)

Table 7.6.3. [cont.] Bond Angles

Atom	Atom	Atom	Angle/˚	Atom	Atom	Atom	Angle/˚
S2	Mo3	S4	171.84(7)	S13	Mo1	Mo3	137.89(7)
Mo2	Mo1	Mo3	59.89(2)	S13	Mo1	Mo2	139.62(7)
S5	Mo1	Mo3	54.84(5)	S13	Mo1	S4	92.86(8)
S5	Mo1	Mo2	95.36(6)	S13	Mo1	S6	94.34(8)
S5	Mo1	S4	48.74(7)	Mo1	Mo2	Mo3	60.23(2)
S5	Mo1	S12	136.82(9)	S1	Mo2	Mo3	54.43(5)
S5	Mo1	S6	131.65(7)	S1	Mo2	Mo1	54.36(5)
S5	Mo1	S13	83.49(8)	S1	Mo2	S3	108.88(7)
S1	Mo1	Mo3	54.22(5)	S1	Mo2	S7	108.70(8)
S1	Mo1	Mo2	54.07(6)	S1	Mo2	S6	87.10(7)
S1	Mo1	S5	108.67(7)	S1	Mo2	S2	85.89(7)
S1	Mo1	S4	86.26(8)	S1	Mo2	S9	161.48(9)
S1	Mo1	S7	108.70(8)	S1	Mo2	S8	78.36(9)
S1	Mo1	S12	79.93(8)	S3	Mo2	Mo3	54.91(5)
S1	Mo1	S6	87.07(8)	S3	Mo2	Mo1	95.93(6)
S1	Mo1	S13	162.30(8)	S3	Mo2	S7	83.59(8)
S4	Mo1	Mo3	56.70(5)	S3	Mo2	S6	132.07(8)
S4	Mo1	Mo2	116.54(6)	S3	Mo2	S2	48.82(7)
S7	Mo1	Mo3	94.55(5)	S3	Mo2	S9	83.96(8)
S7	Mo1	Mo2	54.92(6)	S3	Mo2	S8	136.92(9)
S7	Mo1	S5	83.03(8)	S7	Mo2	Mo3	94.59(6)
S7	Mo1	S4	131.51(7)	S6	S7	Mo2	68.91(9)
S7	Mo1	S12	135.69(8)	C14	S12	Mo1	106.1(4)
S7	Mo1	S6	48.78(7)	Mo1	S6	Mo2	66.47(6)
S7	Mo1	S13	85.05(9)	S7	S6	Mo1	62.34(9)
S12	Mo1	Mo3	122.44(6)	S7	S6	Mo2	62.47(8)
S12	Mo1	Mo2	121.06(7)	Mo3	S2	Mo2	66.62(6)
S12	Mo1	S4	91.53(8)	S3	S2	Mo3	62.69(9)
S12	Mo1	S6	90.04(8)	S3	S2	Mo2	62.52(8)
S12	Mo1	S13	82.42(9)	C5	S9	Mo2	104.5(4)
S6	Mo1	Mo3	116.76(6)	C17	S13	Mo1	105.2(4)
S6	Mo1	Mo2	56.88(5)	C1	S8	Mo2	106.0(4)
S6	Mo1	S4	172.77(8)				

7.2.3.2. STRUCTURE OF $(Bu_4N)_2[Mo_3S_7(Cl_2bdt)_3]$, $((Bu_4N)_2[\mathbf{11}])$

Single crystals of compound $(Bu_4N)_2$[**11**] were obtained by gas diffusion Et_2O/CH_2Cl_2. The structure of $(Bu_4N)_2$[**11**] was refined in the monoclinic space group Cc. Figure 7.7 shows its ORTEP representation with the atom numbering scheme. Owing to disorder, the hydrogen atoms in the Bu_4N^+ counterion centred at N(200) were not included. Their atoms were refined isotropically due to the same reason. In this molecule, the bond distances between atoms N(200), C(209), C(210), C(211) and C(212) were restrained to fixed values. The carbon atoms C(202) and C(217) in the same molecule were refined with a partial occupancy of 0.75 and 0.50, respectively. Additionally, the atom C(215) was found to be disordered over two positions, with a 0.70/0.30 occupancy ratio. A dichloromethane molecule was found co-crystallized with the cluster complex. In this molecule the carbon atom C(10) was defined as a free variable, refined, and then constrained to a fixed value. The crystallographic data collection parameters are given in Table 7.7.1.

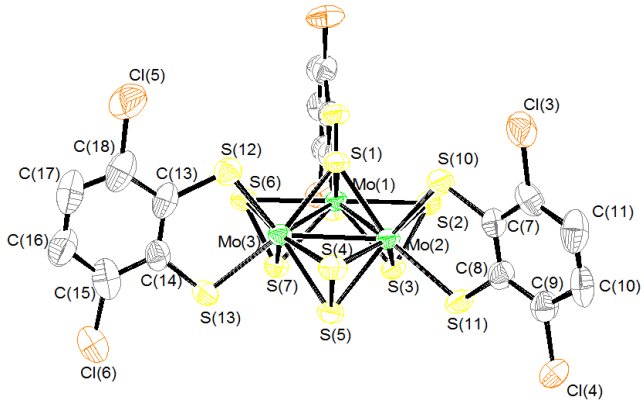

Figure 7.7. ORTEP representation (50 % probability ellipsoids) of the anionic trinuclear cluster $[\mathbf{11}]^{2-}$ with the atom numbering scheme. Average distances (Å): Mo-Mo, 2.7797(14); Mo-(μ_3-S), 2.368(4); Mo-S_{ax}, 2.407(4); Mo-S_{eq}, 2.523(4); Mo-S_{ligand}, 2.447(4).

Table 7.7.1. Crystal Structure Data

Crystal Data			
Species	$(Bu_4N)_2[Mo_3S_7(Cl_2bdt)_3]\cdot CH_2Cl_2$		
Formula	$C_{50.1}H_{43.7}Cl_8Mo_3N_2S_{13}$	**Crystal system**	monoclinic
Space group	Cc	**Formula weight**	1662.93
a (Å)	17.4843(3)	**α** (º)	90
b (Å)	20.0823(4)	**β** (º)	104.793(2)
c (Å)	20.5113(5)	**γ** (º)	90
Z	4	**Vol** (Å^3)	6963.3(2)
Colour	brown	**Crystal size** (mm)	0.4841 × 0.2284 × 0.0371
$\mathbf{d_{calc}}$ (g/cm^3)	1.586	**λ** (Å)	1.54184
Absorption coefficient (mm^{-1})	11.099	**F (000)**	3315.0

Experimental Data			
Temperature (K)	293	**R(int)**	0.0877
Time per frame (s)	25	**R (σ)**	0.0594
2θ Range (º)	6.84 to 145.36	**Index ranges**	-21 ≤ h ≤ 21 -24 ≤ k ≤ 24 -25 ≤ l ≤ 19
Collected reflections	31545	**Independent reflections**	11505

Solution and Refinement			
Parameters	616	**GooF on F²**	1.045
Restraints	10		
Final R1 ([I>2sigma(I)])	0.0737	**Final R1 (all data)**	0.0822
Final wR2 ([I>2sigma(I)])	0.1981	**Final wR2 (all data)**	0.2116
Max/Min peak (e·Å^{-3})	1.85 / -1.14	**Max. shift/σ**	0.001

$$\boldsymbol{R1} = \sum\big||\boldsymbol{F_0}| - |\boldsymbol{F_1}|\big| / \sum \boldsymbol{F_0} \qquad \boldsymbol{wR2} = \left[\sum\left[\boldsymbol{w}(\boldsymbol{F_0^2} - \boldsymbol{F_c^2})^2\right] / \sum\left[\boldsymbol{w}(\boldsymbol{F_0^2})^2\right]\right]^{1/2}$$

Table 7.7.2. Bond Distances

Atom	Atom	Length/Å	Atom	Atom	Length/Å
Mo2	Mo1	2.7829(14)	Mo1	S6	2.512(4)
Mo2	Mo3	2.7900(14)	Mo3	S1	2.371(4)
Mo2	S11	2.474(4)	Mo3	S13	2.469(4)
Mo2	S1	2.370(4)	Mo3	S12	2.412(4)
Mo2	S2	2.527(4)	Mo3	S7	2.400(4)
Mo2	S3	2.420(4)	Mo3	S5	2.401(4)
Mo2	S10	2.435(4)	Mo3	S6	2.498(4)
Mo2	S5	2.404(4)	Mo3	S4	2.546(4)
Mo2	S4	2.516(4)	S11	C8	1.753(16)
Mo1	Mo3	2.7662(15)	S8	C1	1.742(16)
Mo1	S8	2.428(4)	S9	C2	1.769(18)
Mo1	S1	2.363(4)	S2	S3	2.030(5)
Mo1	S9	2.471(4)	S13	C14	1.721(18)
Mo1	S2	2.536(4)	S12	C13	1.745(18)
Mo1	S3	2.410(3)	Cl3	C12	1.73(2)
Mo1	S7	2.407(4)	S10	C7	1.788(17)

Table 7.7.3. Bond Angles

Atom	Atom	Atom	Angle/˚	Atom	Atom	Atom	Angle/˚
Mo1	Mo2	Mo3	59.52(4)	S12	Mo3	S4	94.56(14)
S11	Mo2	Mo1	139.76(11)	S7	Mo3	Mo2	94.37(9)
S11	Mo2	Mo3	139.65(12)	S7	Mo3	Mo1	54.99(9)
S11	Mo2	S2	94.27(15)	S7	Mo3	S13	85.16(13)
S11	Mo2	S4	93.93(15)	S7	Mo3	S12	133.44(13)
S1	Mo2	Mo1	53.87(9)	S7	Mo3	S5	83.06(13)
S1	Mo2	Mo3	53.95(9)	S7	Mo3	S6	48.63(12)
S1	Mo2	S11	161.25(13)	S7	Mo3	S4	131.10(13)
S1	Mo2	S2	85.81(13)	S5	Mo3	Mo2	54.56(9)
S1	Mo2	S3	108.04(13)	S5	Mo3	Mo1	95.63(10)
S1	Mo2	S10	79.42(13)	S5	Mo3	S13	84.03(13)
S1	Mo2	S5	107.97(13)	S5	Mo3	S12	139.58(14)
S1	Mo2	S4	86.06(13)	S5	Mo3	S6	131.54(13)
S2	Mo2	Mo1	56.80(8)	S5	Mo3	S4	48.37(12)
S2	Mo2	Mo3	116.26(9)	S6	Mo3	Mo2	116.84(10)
S3	Mo2	Mo1	54.65(9)	S6	Mo3	Mo1	56.73(9)
S3	Mo2	Mo3	95.40(9)	S6	Mo3	S4	172.33(13)
S3	Mo2	S11	85.47(13)	S4	Mo3	Mo2	56.03(9)
S3	Mo2	S2	48.40(13)	S4	Mo3	Mo1	116.08(10)
S3	Mo2	S10	136.15(14)	C8	S11	Mo2	107.2(6)
S3	Mo2	S4	133.63(13)	C1	S8	Mo1	106.9(6)
S10	Mo2	Mo1	121.68(11)	Mo2	S1	Mo3	72.10(11)
S10	Mo2	Mo3	120.81(10)	Mo1	S1	Mo2	72.02(10)
S10	Mo2	S11	81.83(13)	Mo1	S1	Mo3	71.51(10)
S10	Mo2	S2	90.89(14)	C2	S9	Mo1	106.8(6)
S10	Mo2	S4	89.15(14)	Mo2	S2	Mo1	66.69(10)
S5	Mo2	Mo1	95.13(9)	S3	S2	Mo2	63.06(15)
S5	Mo2	Mo3	54.46(9)	S3	S2	Mo1	62.57(13)
S5	Mo2	S11	85.59(14)	C14	S13	Mo3	105.5(6)
S5	Mo2	S2	133.25(13)	Mo1	S3	Mo2	70.36(10)
S5	Mo2	S3	85.15(13)	S2	S3	Mo2	68.55(15)
S5	Mo2	S10	134.93(14)	S2	S3	Mo1	69.04(15)
S5	Mo2	S4	48.71(13)	C13	S12	Mo3	106.9(6)
S4	Mo2	Mo1	116.54(9)	C7	S10	Mo2	106.9(6)
S4	Mo2	Mo3	57.08(9)	Mo3	S7	Mo1	70.27(10)

Table 7.7.3. [cont.] Bond Angles

Atom	Atom	Atom	Angle/˚	Atom	Atom	Atom	Angle/˚
S4	Mo2	S2	171.72(13)	S7	Mo1	S6	48.40(12)
Mo3	Mo1	Mo2	60.37(4)	S6	Mo1	Mo2	116.61(9)
S8	Mo1	Mo2	121.56(10)	S6	Mo1	Mo3	56.24(9)
S8	Mo1	Mo3	119.29(10)	S6	Mo1	S2	172.59(13)
S8	Mo1	S9	82.74(13)	Mo1	Mo3	Mo2	60.11(4)
S8	Mo1	S2	91.96(13)	S1	Mo3	Mo2	53.95(9)
S8	Mo1	S6	89.94(13)	S1	Mo3	Mo1	54.12(9)
S1	Mo1	Mo2	54.11(9)	S1	Mo3	S13	162.11(14)
S1	Mo1	Mo3	54.37(9)	S1	Mo3	S12	79.25(13)
S1	Mo1	S8	78.43(13)	S1	Mo3	S7	108.91(13)
S1	Mo1	S9	161.16(14)	S1	Mo3	S5	108.07(13)
S1	Mo1	S2	85.76(12)	S1	Mo3	S6	87.77(13)
S1	Mo1	S3	108.62(13)	S1	Mo3	S4	85.36(13)
S1	Mo1	S7	108.92(13)	S13	Mo3	Mo2	138.18(11)
S1	Mo1	S6	87.60(12)	S13	Mo3	Mo1	139.69(11)
S9	Mo1	Mo2	140.34(10)	S13	Mo3	S6	93.91(13)
S9	Mo1	Mo3	138.31(11)	S13	Mo3	S4	93.67(14)
S9	Mo1	S2	95.40(13)	S12	Mo3	Mo2	123.37(11)
S9	Mo1	S6	91.94(13)	S12	Mo3	Mo1	118.45(12)
S2	Mo1	Mo2	56.50(9)	S12	Mo3	S13	83.02(15)
S2	Mo1	Mo3	116.81(10)	S12	Mo3	S6	87.49(13)
S3	Mo1	Mo2	54.99(9)	S6	S7	Mo1	68.52(15)
S3	Mo1	Mo3	96.25(10)	S6	S7	Mo3	68.22(15)
S3	Mo1	S8	137.22(13)	Mo3	S5	Mo2	70.98(11)
S3	Mo1	S9	85.63(13)	S4	S5	Mo2	68.50(16)
S3	Mo1	S2	48.39(13)	S4	S5	Mo3	69.55(16)
S3	Mo1	S6	131.58(13)	Mo3	S6	Mo1	67.03(9)
S7	Mo1	Mo2	94.40(9)	S7	S6	Mo1	63.08(14)
S7	Mo1	Mo3	54.75(9)	S7	S6	Mo3	63.14(14)
S7	Mo1	S8	135.75(13)	Mo2	S4	Mo3	66.89(10)
S7	Mo1	S9	84.39(13)	S5	S4	Mo2	62.79(15)
S7	Mo1	S2	131.38(13)	S5	S4	Mo3	62.08(14)
S7	Mo1	S3	83.31(13)				

7.2.4. STRUCTURE OF HETEROLEPTIC MOLYBDENUM CLUSTERS CONTAINING DIIMINE LIGANDS

7.2.4.1. STRUCTURE OF $(Bu_4N)[Mo_3S_7Br_4(BPhen)\cdot Br]$, $(Bu_4N)[\mathbf{14}\cdot Br]$

In order to obtain single crystals of compound $(Bu_4N)[\mathbf{14}\cdot Br]$, the neutral cluster **14** was suspended in CH_2Cl_2 in the presence of a large excess of Bu_4NBr. After sonicating for a few minutes, the cluster dissolved. Toluene was layered on the top of the resulting solution to afford reddish needle-like crystals after few days. The structure of $(Bu_4N)[\mathbf{14}\cdot Br]$ was refined in the triclinic space group P-1. All non-hydrogen atoms were refined anisotropically. Figure 7.8 shows its ORTEP representation with the atom numbering scheme. Dichloromethane and toluene were found cocrystallized with the cluster complex. In the dichloromethane molecule one chlorine atom was found disordered over two positions with an occupancy ratio of 0.75/0.25, and therefore the hydrogen atoms were not included. The crystallographic data collection parameters are given in Table 7.8.1.

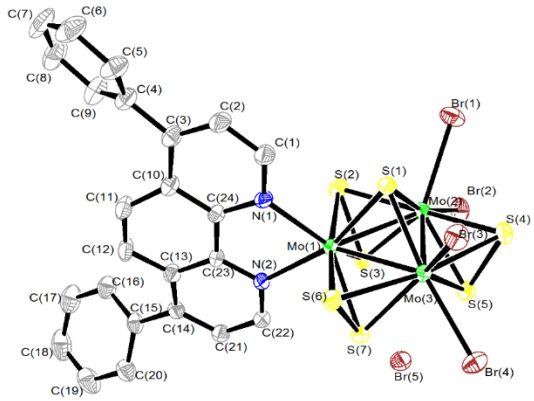

Figure 7.8. ORTEP representation (50 % probability ellipsoids) of the anionic trinuclear cluster $[\mathbf{14}\cdot Br]^-$ with the atom numbering scheme. Average distances (Å): Mo-Mo, 2.7478(4); Mo-(μ_3-S), 2.3593(10); Mo-S_{ax}, 2.3912(10); Mo-S_{eq}, 2.4837(10); Mo-N, 2.218(3); Mo-Br, 2.6277(5); S_{ax}-Br, 2.98(4).

Table 7.8.1. Crystal Structure Data

Crystal Data			
Species	$(Bu_4N)[Mo_3S_7Br_4(BPhen)\cdot Br]\cdot CH_3C_6H_5\cdot CH_2Cl_2$		
Formula	$C_{48}H_{60}Br_5Cl_2Mo_3N_3S_7$	**Crystal system**	triclinic
Space group	P-1	**Formula weight**	1661.68
a (Å)	12.4004(3)	**α** (º)	65.333(2)
b (Å)	15.8574(3)	**β** (º)	85.9821(17)
c (Å)	17.2858(4)	**γ** (º)	75.2290(18)
Z	2	**Vol** (Å^3)	2984.23(11)
Colour	reddish	**Crystal size** (mm)	0.4198 × 0.0829 × 0.0362
$\mathbf{d_{calc}}$ (g/cm^3)	1.849	**λ** (Å)	1.54180
Absorption coefficient (mm^{-1})	12.395	**F (000)**	1652.0
Experimental Data			
Temperature (K)	200	**R(int)**	0.0487
Time per frame (s)	1.50	**R (σ)**	0.0343
2θ Range (º)	6.34 to 145.58	**Index ranges**	-14 ≤ h ≤ 15 -19 ≤ k ≤ 19 -21 ≤ l ≤ 21
Collected reflections	55474	**Independent reflections**	11682
Solution and Refinement			
Parameters	621	**GooF on F²**	1.053
Restraints	0		
Final R1 ([I>2sigma(I)])	0.0341	**Final R1 (all data)**	0.0442
Final wR2 ([I>2sigma(I)])	0.0838	**Final wR2 (all data)**	0.0911
Max/Min peak (e·Å^{-3})	1.25 / -1.05	**Max. shift/σ**	<0.001

$$\boldsymbol{R1} = \sum\big||\boldsymbol{F_0}| - |\boldsymbol{F_1}|\big| / \sum \boldsymbol{F_0} \qquad \boldsymbol{wR2} = \left[\sum\left[\boldsymbol{w}(\boldsymbol{F_0^2} - \boldsymbol{F_c^2})^2\right] / \sum\left[\boldsymbol{w}(\boldsymbol{F_0^2})^2\right]\right]^{\boldsymbol{1/2}}$$

Table 7.8.2. Bond Distances

Atom	Atom	Length/Å	Atom	Atom	Length/Å
Mo1	Mo3	2.7436(4)	N1	C24	1.366(5)
Mo1	Mo2	2.7465(4)	N1	C1	1.331(5)
Mo1	S1	2.3652(10)	Mo3	S4	2.4791(10)
Mo1	S7	2.3993(9)	Mo2	Br2	2.6735(5)
Mo1	S3	2.3942(10)	Mo2	Br1	2.5937(5)
Mo1	S6	2.4846(10)	Mo2	S1	2.3595(10)
Mo1	S2	2.4737(10)	Mo2	S3	2.3825(10)
Mo1	N2	2.218(3)	Mo2	S5	2.3943(9)
Mo1	N1	2.218(3)	Mo2	S4	2.4816(10)
Mo3	Mo2	2.7533(4)	Mo2	S2	2.4926(10)
Mo3	Br3	2.6215(6)	S7	S6	2.0471(14)
Mo3	Br4	2.6222(5)	S3	S2	2.0646(14)
Mo3	S1	2.3532(9)	S5	S4	2.0430(15)
Mo3	S7	2.3917(10)	N2	C23	1.363(5)
Mo3	S5	2.3997(10)	N2	C22	1.334(5)
Mo3	S6	2.4907(10)			

Table 7.8.3. Bond Angles

Atom	Atom	Atom	Angle/°	Atom	Atom	Atom	Angle/°
Mo3	Mo1	Mo2	60.199(11)	S3	Mo2	Br2	79.84(3)
S1	Mo1	Mo3	54.24(2)	S3	Mo2	Br1	137.16(3)
S1	Mo1	Mo2	54.36(3)	S3	Mo2	S5	83.71(3)
S1	Mo1	S7	108.70(3)	S3	Mo2	S4	132.94(4)
S1	Mo1	S3	108.61(3)	S3	Mo2	S2	50.05(3)
S1	Mo1	S6	85.06(3)	S5	Mo2	Mo1	94.83(2)
S1	Mo1	S2	84.84(3)	S5	Mo2	Mo3	55.04(2)
S7	Mo1	Mo3	54.94(2)	S5	Mo2	Br2	84.75(3)
S7	Mo1	Mo2	96.05(2)	S5	Mo2	Br1	133.04(3)
S7	Mo1	S6	49.52(3)	S5	Mo2	S4	49.50(3)
S7	Mo1	S2	135.17(4)	S5	Mo2	S2	133.28(4)
S3	Mo1	Mo3	95.84(2)	S4	Mo2	Mo1	116.05(3)
S3	Mo1	Mo2	54.70(2)	S4	Mo2	Mo3	56.24(2)
S3	Mo1	S7	85.32(3)	S4	Mo2	Br2	97.94(3)
S3	Mo1	S6	134.51(3)	S4	Mo2	Br1	87.94(3)
S3	Mo1	S2	50.16(3)	S4	Mo2	S2	169.88(4)
S6	Mo1	Mo3	56.64(2)	S2	Mo2	Mo1	56.10(2)
S6	Mo1	Mo2	116.71(3)	S2	Mo2	Mo3	115.77(3)
S2	Mo1	Mo3	116.78(3)	S2	Mo2	Br2	92.12(3)
S2	Mo1	Mo2	56.75(2)	S2	Mo2	Br1	92.30(3)
S2	Mo1	S6	169.89(4)	Mo3	S1	Mo1	71.11(3)
N2	Mo1	Mo3	141.46(8)	Mo3	S1	Mo2	71.50(3)
N2	Mo1	Mo2	137.43(9)	Mo2	S1	Mo1	71.09(3)
N2	Mo1	S1	160.78(9)	Mo3	S7	Mo1	69.87(3)
N2	Mo1	S7	86.72(8)	S6	S7	Mo1	67.41(4)
N2	Mo1	S3	83.41(9)	S6	S7	Mo3	67.75(4)
N2	Mo1	S6	97.22(9)	Mo2	S3	Mo1	70.20(3)
N2	Mo1	S2	92.22(9)	S2	S3	Mo1	66.92(4)
N1	Mo1	Mo3	128.05(9)	S2	S3	Mo2	67.74(4)
N1	Mo1	Mo2	127.05(8)	Mo2	S5	Mo3	70.11(3)
N1	Mo1	S1	87.20(9)	S4	S5	Mo3	67.29(4)
N1	Mo1	S7	133.26(9)	S4	S5	Mo2	67.47(4)
N1	Mo1	S3	131.96(9)	Mo1	S6	Mo3	66.93(3)
N1	Mo1	S6	90.63(9)	S7	S6	Mo1	63.07(4)
N1	Mo1	S2	88.54(9)	S7	S6	Mo3	62.72(4)

Table 7.8.3. [cont.] Bond Angles

Atom	Atom	Atom	Angle/˚	Atom	Atom	Atom	Angle/˚
N1	Mo1	N2	73.72(12)	S4	Mo3	Br4	94.28(3)
Mo1	Mo3	Mo2	59.953(11)	S4	Mo3	S6	170.69(3)
Br3	Mo3	Mo1	124.141(16)	Mo1	Mo2	Mo3	59.848(11)
Br3	Mo3	Mo2	122.705(17)	Br2	Mo2	Mo1	134.567(17)
Br3	Mo3	Br4	81.260(17)	Br2	Mo2	Mo3	139.741(17)
Br4	Mo3	Mo1	138.127(17)	Br1	Mo2	Mo1	125.390(17)
Br4	Mo3	Mo2	138.095(17)	Br1	Mo2	Mo3	121.942(18)
S1	Mo3	Mo1	54.65(2)	Br1	Mo2	Br2	82.546(18)
S1	Mo3	Mo2	54.36(3)	S1	Mo2	Mo1	54.55(2)
S1	Mo3	Br3	81.58(3)	S1	Mo2	Mo3	54.15(2)
S1	Mo3	Br4	162.84(3)	S1	Mo2	Br2	164.09(3)
S1	Mo3	S7	109.36(3)	S1	Mo2	Br1	82.06(3)
S1	Mo3	S5	108.86(3)	S1	Mo2	S3	109.20(3)
S1	Mo3	S6	85.17(3)	S1	Mo2	S5	108.83(3)
S1	Mo3	S4	85.67(3)	S1	Mo2	S4	85.48(3)
S7	Mo3	Mo1	55.19(2)	S1	Mo2	S2	84.53(3)
S7	Mo3	Mo2	96.05(3)	S3	Mo2	Mo1	55.10(2)
S7	Mo3	Br3	135.56(3)	S3	Mo2	Mo3	95.86(3)
S7	Mo3	Br4	83.14(3)	Mo3	S4	Mo2	67.42(3)
S7	Mo3	S5	83.84(3)	S5	S4	Mo3	63.24(4)
S7	Mo3	S6	49.53(3)	S5	S4	Mo2	63.03(4)
S7	Mo3	S4	133.09(4)	Mo1	S2	Mo2	67.15(3)
S5	Mo3	Mo1	94.78(3)	S3	S2	Mo1	62.92(4)
S5	Mo3	Mo2	54.86(2)	S3	S2	Mo2	62.21(4)
S5	Mo3	Br3	134.74(3)	C23	N2	Mo1	116.3(3)
S5	Mo3	Br4	83.58(3)	C22	N2	Mo1	125.7(3)
S5	Mo3	S6	132.95(4)	C22	N2	C23	117.8(3)
S5	Mo3	S4	49.48(3)	C24	N1	Mo1	116.3(3)
S6	Mo3	Mo1	56.43(2)	C1	N1	Mo1	126.9(3)
S6	Mo3	Mo2	116.26(3)	C1	N1	C24	116.7(3)
S6	Mo3	Br3	90.81(3)	N1	C24	C23	116.7(3)
S6	Mo3	Br4	94.97(3)	N1	C24	C10	123.2(4)
S4	Mo3	Mo1	116.24(3)	C10	C24	C23	120.1(4)
S4	Mo3	Mo2	56.33(2)	N2	C23	C24	116.8(3)
S4	Mo3	Br3	89.50(3)	N2	C23	C13	122.6(4)

7.2.4.2. STRUCTURE OF $(Bu_4N)[Mo_3S_7Cl_4(BPhen)\cdot Cl]$, $(Bu_4N)[\mathbf{15}\cdot Cl]$

Single crystals of compound $(Bu_4N)[\mathbf{15}\cdot Cl]$ were obtained by dissolving the neutral compound **15** in CH_2Cl_2 in the presence of Bu_4NCl. Toluene was layered on the top of the solution, and reddish crystals grew from the mixture after few days. The structure of $(Bu_4N)[\mathbf{15}\cdot Cl]$ was refined in the monoclinic space group $P2_1/n$. All non-hydrogen atoms were refined anisotropically. Figure 7.9 shows its ORTEP representation with the atom numbering scheme. A toluene molecule was found cocrystallized with the cluster complex. The atom C19A in the bathophenanthroline ligand was refined isotropically in order to improve the Atom Displacement Parameters (ADP). In addition, the crystal structure contains disordered toluene as solvate molecules. In spite of several attempts, the electronic density in this area could not be resolved satisfactory. Therefore the contribution of the disordered solvent species was subtracted from the structure factor calculations by using the solvent mask instruction[21] in the program Olex2 1.2. A relatively high residual density peak (3.37 electrons per $Å^3$) can be found nearby a molybdenum atom, which is considered as justified. The crystallographic data collection parameters are given in Table 7.9.1.

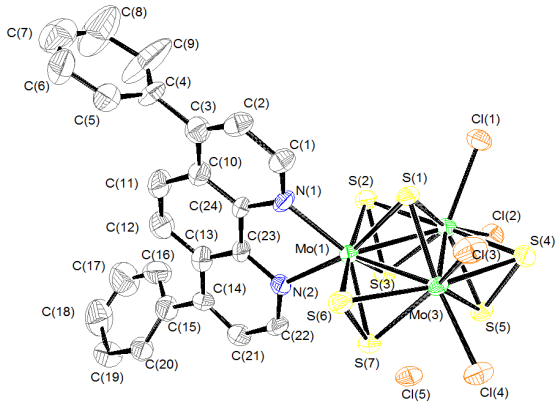

Figure 7.9. ORTEP representation (50 % probability ellipsoids) of the anionic trinuclear cluster $[\mathbf{15}\cdot Cl]^-$ with the atom numbering scheme. Average distances (Å): Mo-Mo, 2.7452(13); Mo-(μ_3-S), 2.3597(3); Mo-S_{ax}, 2.3895(3); Mo-S_{eq}, 2.4867(3); Mo-N, 2.2145(10); Mo-Cl, 2.4708(3); S_{ax}-Cl, 2.91(7).

Table 7.9.1. Crystal Structure Data

Crystal Data			
Species	$(Bu_4N)[Mo_3S_7Cl_4(BPhen)\cdot Cl]$		
Formula	$C_{42.3}H_{54.7}Cl_5Mo_3N_3S_7$	**Crystal system**	monoclinic
Space group	$P2_1/n$	**Formula weight**	1295.04
a (Å)	12.8628(2)	**α** (º)	90
b (Å)	27.4873(6)	**β** (º)	91.4164(16)
c (Å)	48.7034(9)	**γ** (º)	90
Z	12	**Vol** (Å^3)	17214.5(6)
Colour	reddish	**Crystal size** (mm)	0.041 × 0.057 × 0.563
$\mathbf{d_{calc}}$ (g/cm^3)	1.499	**λ** (Å)	1.54184
Absorption coefficient (mm^{-1})	10.049	**F (000)**	7832.0

Experimental Data			
Temperature (K)	211	**R(int)**	0.0533
Time per frame (s)	100	**R (σ)**	0.0644
2θ Range (º)	6.32 to 144.26	**Index ranges**	-10 ≤ h ≤ 15, -32 ≤ k ≤ 33, -59 ≤ l ≤ 58
Collected reflections	65295	**Independent reflections**	32767

Solution and Refinement			
Parameters	1633	**GooF on F²**	1.119
Restraints	1		
Final R1 ([I>2σ(I)])	0.0894	**Final R1 (all data)**	0.1087
Final wR2 ([I>2σ(I)])	0.2118	**Final wR2 (all data)**	0.2177
Max/Min peak (e·Å^{-3})	3.36/-1.57	**Max. shift/σ**	< 0.001

$$\boldsymbol{R1} = \sum\big||\boldsymbol{F_0}| - |\boldsymbol{F_1}|\big| / \sum \boldsymbol{F_0} \qquad \boldsymbol{wR2} = \left[\sum\left[\boldsymbol{w}(\boldsymbol{F_0^2} - \boldsymbol{F_c^2})^2\right] / \sum\left[\boldsymbol{w}(\boldsymbol{F_0^2})^2\right]\right]^{1/2}$$

Table 7.9.2. Bond Distances

Atom	Atom	Length/Å	Atom	Atom	Length/Å
Mo3	Mo2	2.7502(13)	N1	C1	1.332(16)
Mo3	Mo1	2.7394(13)	N1	C24	1.385(16)
Mo3	S5	2.392(3)	Mo2	S2	2.490(3)
Mo3	S1	2.355(3)	Mo1	S1	2.359(3)
Mo3	S4	2.476(3)	Mo1	S3	2.394(3)
Mo3	S7	2.393(3)	Mo1	S7	2.392(3)
Mo3	Cl4	2.479(3)	Mo1	S2	2.485(3)
Mo3	Cl3	2.433(3)	Mo1	S6	2.483(3)
Mo3	S6	2.504(3)	Mo1	N2	2.221(10)
Mo2	Mo1	2.7460(13)	Mo1	N1	2.208(9)
Mo2	S5	2.382(3)	S5	S4	2.035(4)
Mo2	S1	2.365(3)	S3	S2	2.061(4)
Mo2	S3	2.384(3)	S7	S6	2.048(4)
Mo2	S4	2.482(3)	N2	C22	1.322(15)
Mo2	Cl2	2.516(3)	N2	C23	1.388(15)
Mo2	Cl1	2.455(3)			

Table 7.9.3. Bond Angles

Atom	Atom	Atom	Angle/˚	Atom	Atom	Atom	Angle/˚
Mo1	Mo2	Mo3	59.79(3)	S2	Mo2	Cl2	95.85(11)
S5	Mo2	Mo3	55.00(7)	Mo3	Mo1	Mo2	60.18(3)
S5	Mo2	Mo1	93.93(8)	S1	Mo1	Mo3	54.39(7)
S5	Mo2	S3	82.51(10)	S1	Mo1	Mo2	54.57(7)
S5	Mo2	S4	49.40(10)	S1	Mo1	S3	108.87(10)
S5	Mo2	Cl2	82.03(10)	S1	Mo1	S7	108.85(11)
S5	Mo2	Cl1	136.21(11)	S1	Mo1	S2	84.98(10)
S5	Mo2	S2	132.05(11)	S1	Mo1	S6	84.62(11)
S1	Mo2	Mo3	54.18(7)	S3	Mo1	Mo3	95.79(8)
S1	Mo2	Mo1	54.35(7)	S3	Mo1	Mo2	54.76(7)
S1	Mo2	S5	108.95(10)	S3	Mo1	S2	49.94(10)
S1	Mo2	S3	108.98(10)	S3	Mo1	S6	135.33(11)
S1	Mo2	S4	86.53(10)	S7	Mo1	Mo3	55.10(8)
S1	Mo2	Cl2	164.65(10)	S7	Mo1	Mo2	96.79(8)
S1	Mo2	Cl1	82.51(10)	S7	Mo1	S3	86.05(11)
S1	Mo2	S2	84.75(10)	S7	Mo1	S2	135.70(11)
S3	Mo2	Mo3	95.73(8)	S7	Mo1	S6	49.65(10)
S3	Mo2	Mo1	55.08(7)	S2	Mo1	Mo3	116.61(8)
S3	Mo2	S4	131.72(11)	S2	Mo1	Mo2	56.58(8)
S3	Mo2	Cl2	82.56(10)	S6	Mo1	Mo3	57.05(8)
S3	Mo2	Cl1	134.99(12)	S6	Mo1	Mo2	117.04(8)
S3	Mo2	S2	49.98(10)	S6	Mo1	S2	169.58(11)
S4	Mo2	Mo3	56.20(7)	N2	Mo1	Mo3	141.6(3)
S4	Mo2	Mo1	115.98(8)	N2	Mo1	Mo2	135.2(3)
S4	Mo2	Cl2	93.20(10)	N2	Mo1	S1	161.8(3)
S4	Mo2	S2	170.94(11)	N2	Mo1	S3	81.2(3)
Cl2	Mo2	Mo3	136.66(8)	N2	Mo1	S7	86.6(3)
Cl2	Mo2	Mo1	137.55(8)	N2	Mo1	S2	90.7(3)
Cl1	Mo2	Mo3	123.65(9)	N2	Mo1	S6	99.0(3)
Cl1	Mo2	Mo1	124.34(8)	N1	Mo1	Mo3	128.7(3)
Cl1	Mo2	S4	91.22(11)	N1	Mo1	Mo2	128.0(3)
Cl1	Mo2	Cl2	82.15(10)	N1	Mo1	S1	88.0(3)
Cl1	Mo2	S2	90.05(11)	N1	Mo1	S3	131.8(3)
S2	Mo2	Mo3	116.06(8)	N1	Mo1	S7	131.8(3)
S2	Mo2	Mo1	56.42(7)	N1	Mo1	S2	89.2(3)

Table 7.9.3. [cont.] Bond Angles

Atom	Atom	Atom	Angle/˚	Atom	Atom	Atom	Angle/˚
N1	Mo1	S6	89.6(3)	S6	S7	Mo1	67.50(12)
N1	Mo1	N2	74.2(4)	Mo1	S6	Mo3	66.63(8)
Mo2	S5	Mo3	70.34(8)	S7	S6	Mo3	62.48(11)
S4	S5	Mo3	67.46(12)	S7	S6	Mo1	62.86(12)
S4	S5	Mo2	67.86(12)	C22	N2	Mo1	128.4(8)
Mo3	S1	Mo2	71.28(8)	C22	N2	C23	117.7(11)
Mo3	S1	Mo1	71.06(8)	C23	N2	Mo1	113.1(7)
Mo1	S1	Mo2	71.08(8)	C1	N1	Mo1	128.4(9)
Mo2	S3	Mo1	70.16(8)	C1	N1	C24	116.6(11)
S2	S3	Mo2	67.67(12)	C24	N1	Mo1	114.8(8)
S2	S3	Mo1	67.34(12)	N1	C1	C2	123.3(13)
Mo3	S4	Mo2	67.37(8)	N1	C24	C10	123.3(12)
S5	S4	Mo3	63.16(11)	N1	C24	C23	116.3(11)
S5	S4	Mo2	62.74(11)	N2	C23	C24	118.0(11)
Mo1	S7	Mo3	69.85(8)	N2	C23	C13	121.2(12)
S6	S7	Mo3	68.13(12)				

7.2.4.3. STRUCTURE OF $(Bu_4N)[Mo_3S_7Br_4(tmphen)\cdot Br]$, $(Bu_4N)[\mathbf{16}\cdot Br]$

Single crystals of compound $(Bu_4N)[\mathbf{16}\cdot Br]$ were obtained by dissolving the neutral compound **16** in CH_2Cl_2 in the presence of Bu_4NBr. Toluene was slowly added to afford single crystals after few days. The structure of $(Bu_4N)[\mathbf{16}\cdot Br]$ was refined in the triclinic space group P-1. All non-hydrogen atoms were refined anisotropically. Figure 7.10 shows its ORTEP representation with the atom numbering scheme. Dichloromethane was found cocrystallized with the cluster complex. In the tetrabutylammonium counterion centered at N(200), a terminal carbon atom was found disordered over two positions with an occupancy ratio of 0.60/0.40, and therefore the hydrogen atoms were not included. The crystallographic data collection parameters are given in Table 7.10.1.

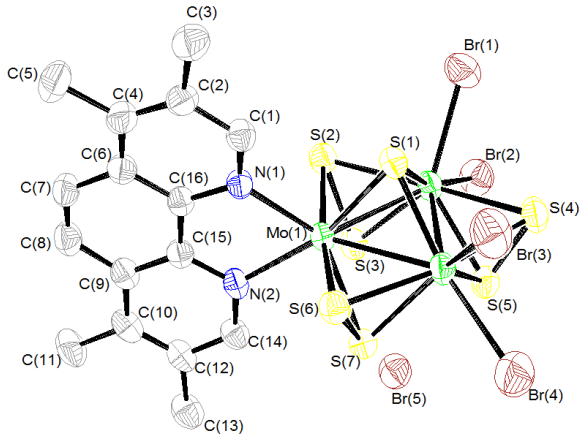

Figure 7.10. ORTEP representation (50 % probability ellipsoids) of the anionic trinuclear cluster $[\mathbf{16}\cdot Br]^-$ with the atom numbering scheme. Average distances (Å): Mo-Mo, 2.7480(8); Mo-(μ_3-S), 2.3601(18); Mo-S_{ax}, 2.3811(16); Mo-S_{eq}, 2.4848(16); Mo-N, 2.222(6); Mo-Br, 2.5814(12); S_{ax}-Br, 3.05(9).

Table 7.10.1. Crystal Structure Data

Crystal Data			
Species	$(Bu_4N)[Mo_3S_7Br_4(tmphen)\cdot Br]\cdot 1.5CH_3C_6H_5$		
Formula	$C_{42.5}H_{49.2}Br_5Mo_3N_3S_7$	**Crystal system**	triclinic
Space group	P-1	**Formula weight**	1513.84
a (Å)	14.6617(3)	**α** (º)	83.8100(14)
b (Å)	17.5340(3)	**β** (º)	80.5709(15)
c (Å)	23.8551(4)	**γ** (º)	67.1680(17)
Z	4	**Vol** (Å^3)	5569.14(18)
Colour	reddish	**Crystal size** (mm)	0.1729 × 0.1333 × 0.0537
$\mathbf{d_{calc}}$ (g/cm^3)	1.806	**λ** (Å)	1.54180
Absorption coefficient (mm^{-1})	12.351	**F (000)**	2953.0

Experimental Data			
Temperature (K)	200	**R(int)**	0.0367
Time per frame (s)	4	**R (σ)**	0.0271
2θ Range (º)	6.50 to 145.6	**Index ranges**	-17 ≤ h ≤ 18, -21 ≤ k ≤ 21, -29 ≤ l ≤ 27
Collected reflections	102370	**Independent reflections**	21820

Solution and Refinement			
Parameters	1108	**GooF on F²**	1.093
Restraints	1		
Final R1 ([I>2sigma(I)])	0.0561	**Final R1 (all data)**	0.0746
Final wR2 ([I>2sigma(I)])	0.1672	**Final wR2 (all data)**	0.1833
Max/Min peak (e·Å^{-3})	1.85/-2.84	**Max. shift/σ**	< 0.001

$$\boldsymbol{R1} = \sum\big||\boldsymbol{F_0}| - |\boldsymbol{F_1}|\big| / \sum \boldsymbol{F_0} \qquad \boldsymbol{wR2} = \left[\sum\left[\boldsymbol{w}(\boldsymbol{F_0^2} - \boldsymbol{F_c^2})^2\right] / \sum\left[\boldsymbol{w}(\boldsymbol{F_0^2})^2\right]\right]^{1/2}$$

Table 7.10.2. Bond Distances

Atom	Atom	Length/Å	Atom	Atom	Length/Å
Mo1	Mo2	2.7479(7)	Mo2	S4	2.476(2)
Mo1	Mo3	2.7434(8)	Mo3	Br3	2.5677(12)
Mo1	S1	2.3656(17)	Mo3	Br4	2.5785(14)
Mo1	S7	2.3956(19)	Mo3	S1	2.3579(19)
Mo1	S3	2.3943(18)	Mo3	S7	2.3940(18)
Mo1	S2	2.4882(19)	Mo3	S6	2.4946(18)
Mo1	S6	2.4795(19)	Mo3	S5	2.386(2)
Mo1	N2	2.226(5)	Mo3	S4	2.4707(19)
Mo1	N1	2.217(6)	S7	S6	2.053(3)
Mo2	Mo3	2.7527(8)	S3	S2	2.055(3)
Mo2	Br2	2.6186(11)	S5	S4	2.034(3)
Mo2	Br1	2.5608(11)	N2	C15	1.365(9)
Mo2	S1	2.3567(18)	N2	C14	1.345(9)
Mo2	S3	2.3961(18)	N1	C16	1.371(8)
Mo2	S2	2.4995(19)	N1	C1	1.326(9)
Mo2	S5	2.388(2)			

Table 7.10.3. Bond Angles

Atom	Atom	Atom	Angle/°	Atom	Atom	Atom	Angle/°
Mo3	Mo1	Mo2	60.17(2)	S1	Mo3	S7	86.01(7)
S1	Mo1	Mo2	54.27(4)	S1	Mo3	S6	135.37(8)
S1	Mo1	Mo3	54.36(5)	S1	Mo3	S5	56.67(4)
S1	Mo1	S7	108.83(6)	S1	Mo3	S4	116.66(5)
S1	Mo1	S3	108.74(6)	S7	Mo3	Mo1	96.12(5)
S1	Mo1	S2	84.66(6)	S7	Mo3	Mo2	55.02(5)
S1	Mo1	S6	84.69(6)	S7	Mo3	Br3	135.31(7)
S7	Mo1	Mo2	96.55(5)	S7	Mo3	Br4	49.65(8)
S7	Mo1	Mo3	55.03(4)	S7	Mo3	S6	116.79(5)
S7	Mo1	S2	135.79(7)	S7	Mo3	S4	56.74(5)
S7	Mo1	S6	49.76(6)	S6	Mo3	Mo1	169.66(7)
S3	Mo1	Mo2	55.03(4)	S6	Mo3	Mo2	140.74(17)
S3	Mo1	Mo3	96.43(5)	S6	Mo3	Br3	137.67(17)
S3	Mo1	S7	86.39(7)	S6	Mo3	Br4	161.37(18)
S3	Mo1	S2	49.73(6)	S5	Mo3	Mo1	85.84(18)
S3	Mo1	S6	135.81(7)	S5	Mo3	Mo2	97.02(17)
S2	Mo1	Mo2	56.77(4)	S5	Mo3	Br3	83.19(17)
S2	Mo1	Mo3	116.76(5)	S5	Mo3	Br4	92.59(17)
S6	Mo1	Mo2	116.77(5)	S5	Mo3	S7	74.1(2)
S6	Mo1	Mo3	56.79(4)	S5	Mo3	S6	128.75(18)
S6	Mo1	S2	169.30(6)	S5	Mo3	S4	126.30(16)
N2	Mo1	Mo2	138.91(15)	S4	Mo3	Mo1	87.29(18)
N2	Mo1	Mo3	139.47(16)	S4	Mo3	Mo2	133.64(17)
N2	Mo1	S1	161.37(16)	S4	Mo3	Br3	91.20(17)
N2	Mo1	S7	84.72(16)	S4	Mo3	Br4	130.70(18)
N2	Mo1	S3	84.22(15)	S4	Mo3	S6	87.78(17)
N2	Mo1	S2	94.48(16)	Mo2	S1	Mo1	71.17(5)
N2	Mo1	S6	95.30(16)	Mo2	S1	Mo3	71.44(5)
N1	Mo1	Mo2	127.33(15)	Mo3	S1	Mo1	71.01(5)
N1	Mo1	Mo3	128.12(15)	Mo3	S7	Mo1	69.89(5)
N1	Mo1	S1	87.39(15)	S6	S7	Mo1	67.24(7)
N1	Mo1	S7	132.41(16)	S6	S7	Mo3	67.75(7)
N1	Mo1	S3	131.41(16)	Mo1	S3	Mo2	70.01(5)
N1	Mo1	S2	88.73(16)	S2	S3	Mo1	67.51(7)
N1	Mo1	S6	89.83(16)	S2	S3	Mo2	67.83(7)

Table 7.10.3. [cont.] Bond Angles

Atom	Atom	Atom	Angle/°	Atom	Atom	Atom	Angle/°
N1	Mo1	N2	74.0(2)	S4	Mo2	Br1	88.96(6)
Mo1	Mo2	Mo3	59.84(2)	S4	Mo2	S2	170.46(7)
Br2	Mo2	Mo1	138.97(3)	Mo1	Mo3	Mo2	60.19(2)
Br2	Mo2	Mo3	136.48(4)	Br3	Mo3	Mo1	54.14(5)
Br1	Mo2	Mo1	125.13(3)	Br3	Mo3	Mo2	54.28(5)
Br1	Mo2	Mo3	122.07(4)	Br3	Mo3	Br4	108.63(7)
Br1	Mo2	Br2	81.59(4)	Br4	Mo3	Mo1	84.43(7)
S1	Mo2	Mo1	54.57(4)	Br4	Mo3	Mo2	108.85(7)
S1	Mo2	Mo3	54.30(5)	S1	Mo3	Mo1	85.25(7)
S1	Mo2	Br2	163.41(6)	S1	Mo3	Mo2	55.06(5)
S1	Mo2	Br1	81.86(5)	S1	Mo3	Br3	96.62(5)
S1	Mo2	S3	108.98(6)	S1	Mo3	Br4	49.67(7)
S1	Mo2	S2	84.59(6)	Mo1	S2	Mo2	66.86(5)
S1	Mo2	S5	108.79(7)	S3	S2	Mo1	62.76(7)
S1	Mo2	S4	86.10(7)	S3	S2	Mo2	62.59(7)
S3	Mo2	Mo1	54.97(4)	Mo1	S6	Mo3	66.94(5)
S3	Mo2	Mo3	96.15(5)	S7	S6	Mo1	62.99(7)
S3	Mo2	Br2	84.06(5)	S7	S6	Mo3	62.65(7)
S3	Mo2	Br1	136.41(6)	Mo3	S5	Mo2	70.43(6)
S3	Mo2	S2	49.58(6)	S4	S5	Mo2	67.57(8)
S3	Mo2	S4	132.70(7)	S4	S5	Mo3	67.43(8)
S2	Mo2	Mo1	56.37(4)	Mo3	S4	Mo2	67.62(5)
S2	Mo2	Mo3	116.03(5)	S5	S4	Mo2	63.03(8)
S2	Mo2	Br2	97.08(5)	S5	S4	Mo3	63.09(7)
S2	Mo2	Br1	91.79(5)	C15	N2	Mo1	115.4(5)
S5	Mo2	Mo1	94.01(5)	C14	N2	Mo1	126.4(5)
S5	Mo2	Mo3	54.75(5)	C14	N2	C15	118.1(6)
S5	Mo2	Br2	82.25(5)	C16	N1	Mo1	115.1(4)
S5	Mo2	Br1	134.24(6)	C1	N1	Mo1	127.3(5)
S5	Mo2	S3	83.52(7)	C1	N1	C16	117.7(6)
S5	Mo2	S2	132.61(7)	N2	C15	C16	116.7(6)
S5	Mo2	S4	49.40(7)	N2	C15	C9	122.1(7)
S4	Mo2	Mo1	115.91(5)	N1	C16	C15	117.6(6)
S4	Mo2	Mo3	56.09(5)	N1	C16	C6	122.2(6)
S4	Mo2	Br2	92.44(6)	N1	C1	C2	123.8(7)

7.2.4.4. STRUCTURE OF $(Bu_4N)[Mo_3S_7Cl_4(tmphen)\cdot Cl]$, $(Bu_4N)[\mathbf{17}\cdot Cl]$

Single crystals of compound $(Bu_4N)[\mathbf{17}\cdot Cl]$ were obtained by slowly diffusing toluene into a solution of **17** in CH_2Cl_2, in the presence of a large excess of Bu_4NCl. The structure of $(Bu_4N)[\mathbf{17}\cdot Cl]$ was refined in the monoclinic space group $P2_1$. All non-hydrogen atoms were refined anisotropically. Figure 7.11 shows its ORTEP representation with the atom numbering scheme. Dichloromethane was found cocrystallized with the cluster complex. The crystallographic data collection parameters are given in Table 7.11.1.

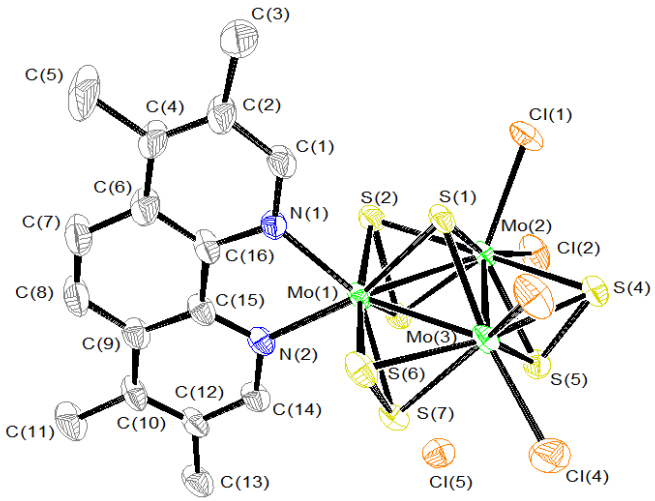

Figure 7.11. ORTEP representation (50 % probability ellipsoids) of the anionic trinuclear cluster $[\mathbf{17}\cdot Cl]^-$ with the atom numbering scheme. Average distances (Å): Mo-Mo, 2.7465(10); Mo-(μ_3-S), 2.3517(2); Mo-S_{ax}, 2.3922(2); Mo-S_{eq}, 2.4872(2); Mo-N, 2.209(7); Mo-Cl, 2.4605(2); S_{ax}-Cl, 2.89(4).

Table 7.11.1. Crystal Structure Data

Crystal Data			
Species	$(Bu_4N)[Mo_3S_7Cl_4(tmphen)\cdot Cl]\cdot 3CH_2Cl_2$		
Formula	$C_{35}H_{58}Cl_{11}Mo_3N_3S_7$	**Crystal system**	monoclinic
Space group	$P2_1$	**Formula weight**	1423.03
a (Å)	11.8749(3)	**α** (º)	90.00
b (Å)	19.5703(3)	**β** (º)	108.810(2)
c (Å)	12.5826(3)	**γ** (º)	90.00
Z	2	**Vol** (Å^3)	2767.97(10)
Colour	reddish	**Crystal size** (mm)	0.3267 × 0.221 × 0.0469
$\mathbf{d_{calc}}$ (g/cm^3)	1.707	**λ** (Å)	0.71070
Absorption coefficient (mm^{-1})	1.494	**F (000)**	1428.0

Experimental Data			
Temperature (K)	200	**R(int)**	0.0435
Time per frame (s)	18	**R (σ)**	0.0429
2θ Range (º)	5.6 to 50	**Index ranges**	-14 ≤ h ≤ 13, -23 ≤ k ≤ 23, -14 ≤ l ≤ 14
Collected reflections	26486	**Independent reflections**	9629

Solution and Refinement			
Parameters	540	**GooF on F²**	1.076
Restraints	1		
Final R1 ([I>2sigma(I)])	0.0431	**Final R1 (all data)**	0.0464
Final wR2 ([I>2sigma(I)])	0.1192	**Final wR2 (all data)**	0.1237
Max/Min peak (e·Å^{-3})	0.93/-0.91	**Max. shift/σ**	<0.001

$$\boldsymbol{R1} = \sum\big||\boldsymbol{F_0}| - |\boldsymbol{F_1}|\big| / \sum \boldsymbol{F_0} \qquad \boldsymbol{wR2} = \left[\sum\left[\boldsymbol{w}(\boldsymbol{F_0^2} - \boldsymbol{F_c^2})^2\right] / \sum\left[\boldsymbol{w}(\boldsymbol{F_0^2})^2\right]\right]^{\mathbf{1/2}}$$

Table 7.11.2. Bond Distances

Atom	Atom	Length/Å	Atom	Atom	Length/Å
Mo1	Mo2	2.7368(9)	Mo2	S2	2.489(2)
Mo1	Mo3	2.7504(10)	Mo3	S1	2.346(2)
Mo1	S1	2.357(2)	Mo3	S4	2.479(2)
Mo1	S3	2.392(2)	Mo3	S5	2.387(2)
Mo1	S7	2.398(2)	Mo3	S7	2.397(2)
Mo1	S2	2.483(2)	Mo3	S6	2.498(2)
Mo1	S6	2.491(2)	Mo3	Cl3	2.452(2)
Mo1	N2	2.198(7)	Mo3	Cl4	2.475(3)
Mo1	N1	2.220(7)	S3	S2	2.045(3)
Mo2	Mo3	2.7524(10)	S4	S5	2.040(3)
Mo2	S1	2.352(2)	S7	S6	2.053(3)
Mo2	S3	2.400(2)	N2	C15	1.350(13)
Mo2	Cl1	2.441(2)	N2	C14	1.364(11)
Mo2	S4	2.483(2)	N1	C1	1.320(12)
Mo2	S5	2.379(2)	N1	C16	1.356(12)
Mo2	Cl2	2.474(2)			

Table 7.11.3. Bond Angles

Atom	Atom	Atom	Angle/°	Atom	Atom	Atom	Angle/°
Mo2	Mo1	Mo3	60.21(3)	S4	Mo3	Mo2	56.37(6)
S1	Mo1	Mo2	54.37(6)	S4	Mo3	S6	170.73(9)
S1	Mo1	Mo3	54.03(6)	S5	Mo3	Mo1	93.98(7)
S1	Mo1	S3	109.27(8)	S5	Mo3	Mo2	54.60(6)
S1	Mo1	S7	108.52(8)	S5	Mo3	S4	49.52(8)
S1	Mo1	S2	85.73(8)	S5	Mo3	S7	83.22(9)
S1	Mo1	S6	84.87(8)	S5	Mo3	S6	132.31(9)
S3	Mo1	Mo2	55.31(5)	S5	Mo3	Cl3	135.98(10)
S3	Mo1	Mo3	96.15(6)	S5	Mo3	Cl4	83.24(10)
S3	Mo1	S7	85.01(8)	S7	Mo3	Mo1	55.01(6)
S3	Mo1	S2	49.57(8)	S7	Mo3	Mo2	95.67(6)
S3	Mo1	S6	134.35(9)	S7	Mo3	S4	132.54(8)
S7	Mo1	Mo2	96.05(6)	S7	Mo3	S6	49.55(8)
S7	Mo1	Mo3	54.98(6)	S7	Mo3	Cl3	135.30(9)
S7	Mo1	S2	134.27(8)	S7	Mo3	Cl4	84.45(9)
S7	Mo1	S6	49.62(8)	S6	Mo3	Mo1	56.43(6)
S2	Mo1	Mo2	56.71(6)	S6	Mo3	Mo2	115.95(7)
S2	Mo1	Mo3	116.82(6)	Cl3	Mo3	Mo1	123.74(8)
S2	Mo1	S6	170.60(8)	Cl3	Mo3	Mo2	122.94(7)
S6	Mo1	Mo2	116.75(6)	Cl3	Mo3	S4	90.43(8)
S6	Mo1	Mo3	56.67(6)	Cl3	Mo3	S6	90.35(9)
N2	Mo1	Mo2	141.4(2)	Cl3	Mo3	Cl4	81.25(10)
N2	Mo1	Mo3	138.9(2)	Cl4	Mo3	Mo1	139.32(7)
N2	Mo1	S1	159.9(2)	Cl4	Mo3	Mo2	137.31(9)
N2	Mo1	S3	86.5(2)	Cl4	Mo3	S4	92.81(9)
N2	Mo1	S7	84.6(2)	Cl4	Mo3	S6	96.43(10)
N2	Mo1	S2	95.9(2)	Mo2	S1	Mo1	71.07(6)
N2	Mo1	S6	93.0(2)	Mo3	S1	Mo1	71.58(7)
N2	Mo1	N1	73.4(3)	Mo3	S1	Mo2	71.74(7)
N1	Mo1	Mo2	125.6(2)	Mo1	S3	Mo2	69.66(6)

Table 7.11.3. [cont.] Bond Angles

Atom	Atom	Atom	Angle/˚	Atom	Atom	Atom	Angle/˚
N1	Mo1	S1	86.7(2)	S5	Mo2	S3	83.17(8)
N1	Mo1	S3	130.8(2)	S5	Mo2	Cl1	134.44(9)
N1	Mo1	S7	134.8(2)	S5	Mo2	S4	49.55(8)
N1	Mo1	S2	87.7(2)	S5	Mo2	Cl2	83.86(10)
N1	Mo1	S6	92.0(2)	S5	Mo2	S2	132.23(8)
Mo1	Mo2	Mo3	60.14(3)	Cl2	Mo2	Mo1	138.16(7)
S1	Mo2	Mo1	54.56(5)	Cl2	Mo2	Mo3	138.30(8)
S1	Mo2	Mo3	54.04(6)	Cl2	Mo2	S4	94.15(9)
S1	Mo2	S3	109.18(8)	Cl2	Mo2	S2	94.53(9)
S1	Mo2	Cl1	81.25(9)	S2	Mo2	Mo1	56.50(6)
S1	Mo2	S4	85.83(8)	S2	Mo2	Mo3	116.54(6)
S1	Mo2	S5	108.62(9)	Mo1	Mo3	Mo2	59.65(2)
S1	Mo2	Cl2	162.87(9)	S1	Mo3	Mo1	54.40(6)
S1	Mo2	S2	85.71(8)	S1	Mo3	Mo2	54.22(6)
S3	Mo2	Mo1	55.02(5)	S1	Mo3	S4	86.02(8)
S3	Mo2	Mo3	95.90(6)	S1	Mo3	S5	108.54(9)
S3	Mo2	Cl1	136.94(8)	S1	Mo3	S7	108.92(8)
S3	Mo2	S4	132.51(8)	S1	Mo3	S6	84.95(8)
S3	Mo2	Cl2	83.40(8)	S1	Mo3	Cl3	81.57(9)
S3	Mo2	S2	49.42(8)	S1	Mo3	Cl4	162.77(9)
Cl1	Mo2	Mo1	124.20(7)	S4	Mo3	Mo1	115.99(6)
Cl1	Mo2	Mo3	121.54(7)	S2	S3	Mo2	67.57(9)
Cl1	Mo2	S4	88.77(8)	Mo3	S4	Mo2	67.39(6)
Cl1	Mo2	Cl2	81.62(10)	S5	S4	Mo2	62.59(9)
Cl1	Mo2	S2	91.92(8)	S5	S4	Mo3	62.90(9)
S4	Mo2	Mo1	116.36(6)	Mo2	S5	Mo3	70.54(7)
S4	Mo2	Mo3	56.25(6)	S4	S5	Mo2	67.86(10)
S4	Mo2	S2	171.31(8)	S4	S5	Mo3	67.59(9)
S5	Mo2	Mo1	94.50(6)	Mo3	S7	Mo1	70.01(6)
S5	Mo2	Mo3	54.86(6)	S6	S7	Mo1	67.56(10)

Table 7.11.3. [cont.] Bond Angles

Atom	Atom	Atom	Angle/°	Atom	Atom	Atom	Angle/°
S6	S7	Mo3	67.80(9)	C1	N1	Mo1	126.1(7)
Mo1	S2	Mo2	66.78(6)	C1	N1	C16	118.1(8)
S3	S2	Mo1	62.88(9)	C16	N1	Mo1	115.8(6)
S3	S2	Mo2	63.01(9)	N1	C1	C2	124.0(9)
Mo1	S6	Mo3	66.90(6)	N2	C15	C16	116.2(8)
S7	S6	Mo1	62.82(9)	N2	C15	C9	123.9(9)
S7	S6	Mo3	62.66(9)	N1	C16	C15	117.1(9)
C15	N2	Mo1	117.4(6)	N1	C16	C6	122.0(9)
C15	N2	C14	116.2(8)	N2	C14	C12	124.1(9)
C14	N2	Mo1	126.4(6)				

7.2.4.5. STRUCTURE OF $(Bu_4N)[Mo_3S_7Cl_4(dmbpy)\cdot Cl]$, $(Bu_4N)[\mathbf{18}\cdot Cl]$

Reddish single crystals of compound $(Bu_4N)[\mathbf{18}\cdot Cl]$ were obtained in a similar fashion to compound $(Bu_4N)[\mathbf{15}\cdot Cl]$. The structure of $(Bu_4N)[\mathbf{18}\cdot Cl]$ was refined in the monoclinic space group $P2_1/n$. All non-hydrogen atoms were refined anisotropically. Figure 7.12 shows its ORTEP representation with the atom numbering scheme. Three molecules of dichloromethane were found cocrystallized with the cluster complex. In the dichloromethane molecule centered at C(20) one chlorine atom was refined with a free occupancy and then constrained to the optimum occupancy value. The crystallographic data collection parameters are given in Table 7.12.1.

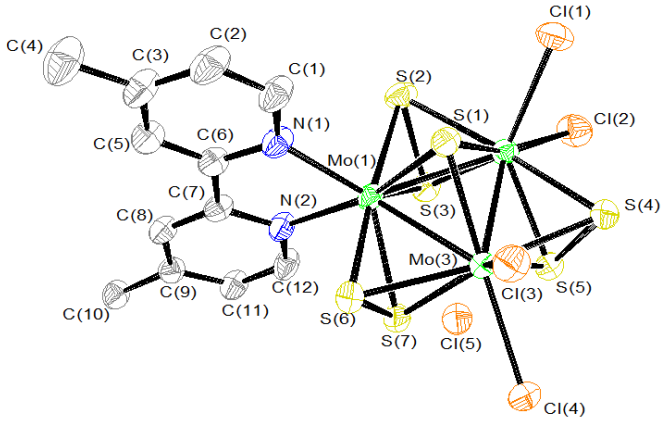

Figure 7.12. ORTEP representation (50 % probability ellipsoids) of the anionic trinuclear cluster $[\mathbf{18}\cdot Cl]^-$ with the atom numbering scheme. Average distances (Å): Mo-Mo, 2.7502(6); Mo-(μ_3-S), 2.3531(12); Mo-S_{ax}, 2.3852(13); Mo-S_{eq}, 2.4861(14); Mo-N, 2.211(4); Mo-Cl, 2.4644(13); S_{ax}-Cl, 2.93(4).

Table 7.12.1. Crystal Structure Data

Crystal Data			
Species	$(Bu_4N)[Mo_3S_7Cl_4(dmbpy)\cdot Cl]\cdot 3CH_2Cl_2$		
Formula	$C_{31}H_{53}Cl_{11}Mo_3N_3S_7$	**Crystal system**	monoclinic
Space group	$P2_1/n$	**Formula weight**	1369.95
a (Å)	13.8174(2)	**α** (º)	90
b (Å)	19.3711(3)	**β** (º)	103.4323(15)
c (Å)	20.0877(3)	**γ** (º)	90
Z	4	**Vol** (Å^3)	5229.55(14)
Colour	reddish	**Crystal size** (mm)	0.4689 × 0.1936 × 0.0702
$\mathbf{d_{calc}}$ (g/cm^3)	1.740	**λ** (Å)	0.71070
Absorption coefficient (mm^{-1})	1.578	**F (000)**	2740.0

Experimental Data			
Temperature (K)	200	**R(int)**	0.0332
Time per frame (s)	28	**R (σ)**	0.0229
2θ Range (º)	5.86 to 50	**Index ranges**	$-16 \le h \le 16$, $-22 \le k \le 23$, $-23 \le l \le 23$
Collected reflections	50572	**Independent reflections**	9195

Solution and Refinement			
Parameters	502	**GooF on F²**	1.088
Restraints	0		
Final R1 ([I>2sigma(I)])	0.0426	**Final R1 (all data)**	0.0541
Final wR2 ([I>2sigma(I)])	0.1056	**Final wR2 (all data)**	0.1188
Max/Min peak (e·Å^{-3})	1.54/-0.90	**Max. shift/σ**	< 0.001

$$\boldsymbol{R1} = \sum\big||\boldsymbol{F_0}| - |\boldsymbol{F_1}|\big| / \sum \boldsymbol{F_0} \qquad \boldsymbol{wR2} = \left[\sum\left[\boldsymbol{w}(\boldsymbol{F_0^2} - \boldsymbol{F_c^2})^2\right] / \sum\left[\boldsymbol{w}(\boldsymbol{F_0^2})^2\right]\right]^{\mathbf{1/2}}$$

Table 7.12.2. Bond Distances

Atom	Atom	Length/Å	Atom	Atom	Length/Å
Mo3	Mo1	2.7371(6)	Mo1	N2	2.210(4)
Mo3	Mo2	2.7599(6)	Mo2	S1	2.3519(13)
Mo3	Cl3	2.4419(13)	Mo2	S5	2.3947(13)
Mo3	S1	2.3527(12)	Mo2	S4	2.4768(13)
Mo3	Cl4	2.4858(12)	Mo2	Cl1	2.4512(13)
Mo3	S5	2.3939(13)	Mo2	S3	2.3912(13)
Mo3	S4	2.4843(13)	Mo2	Cl2	2.4785(14)
Mo3	S7	2.3859(13)	Mo2	S2	2.4987(13)
Mo3	S6	2.4884(13)	S5	S4	2.0347(18)
Mo1	Mo2	2.7537(6)	S7	S6	2.0458(18)
Mo1	S1	2.3548(12)	S3	S2	2.0460(18)
Mo1	S7	2.3891(13)	N1	C6	1.366(6)
Mo1	S3	2.3991(13)	N1	C1	1.343(7)
Mo1	S6	2.4768(14)	N2	C12	1.341(6)
Mo1	S2	2.4918(14)	N2	C7	1.361(6)
Mo1	N1	2.212(4)			

Table 7.12.3. Bond Angles

Atom	Atom	Atom	Angle/°	Atom	Atom	Atom	Angle/°
Mo1	Mo3	Mo2	60.124(15)	S5	Mo2	S2	133.06(5)
Cl3	Mo3	Mo1	123.82(4)	S1	Mo2	Cl1	82.02(5)
Cl3	Mo3	Mo2	122.56(4)	S1	Mo2	S3	108.63(4)
Cl3	Mo3	Cl4	81.07(5)	S1	Mo2	Cl2	163.15(5)
Cl3	Mo3	S4	90.38(4)	S1	Mo2	S2	83.99(4)
Cl3	Mo3	S6	90.98(4)	S5	Mo2	Mo3	54.79(3)
S1	Mo3	Mo1	54.49(3)	S5	Mo2	Mo1	93.91(3)
S1	Mo3	Mo2	54.07(3)	S5	Mo2	S4	49.34(4)
S1	Mo3	Cl3	81.66(4)	S5	Mo2	Cl1	135.19(5)
S1	Mo3	Cl4	162.62(5)	S5	Mo2	Cl2	83.03(5)
S1	Mo3	S5	108.63(4)	S4	Mo2	Mo3	56.33(3)
S1	Mo3	S4	86.08(4)	S4	Mo2	Mo1	115.84(3)
S1	Mo3	S7	109.19(4)	S4	Mo2	Cl2	92.84(5)
S1	Mo3	S6	85.62(4)	S4	Mo2	S2	170.09(5)
Cl4	Mo3	Mo1	136.95(4)	Cl1	Mo2	Mo3	122.67(4)
Cl4	Mo3	Mo2	139.78(4)	Cl1	Mo2	Mo1	124.52(4)
Cl4	Mo3	S6	92.81(4)	Cl1	Mo2	S4	89.93(4)
S5	Mo3	Mo1	94.35(3)	Cl1	Mo2	Cl2	81.16(5)
S5	Mo3	Mo2	54.82(3)	Cl1	Mo2	S2	90.46(5)
S5	Mo3	Cl3	135.60(5)	S3	Mo2	Mo3	96.51(4)
S5	Mo3	Cl4	85.25(4)	S3	Mo2	Mo1	55.05(3)
S5	Mo3	S4	49.26(4)	S3	Mo2	S5	84.23(5)
S5	Mo3	S6	131.90(5)	S3	Mo2	S4	133.38(5)
S4	Mo3	Mo1	116.18(3)	S3	Mo2	Cl1	134.85(5)
S4	Mo3	Mo2	56.07(3)	S3	Mo2	Cl2	84.12(5)
S4	Mo3	Cl4	95.89(4)	S3	Mo2	S2	49.41(4)
S4	Mo3	S6	171.30(4)	Cl2	Mo2	Mo3	137.32(4)
S7	Mo3	Mo1	55.08(3)	Cl2	Mo2	Mo1	139.10(4)
S7	Mo3	Mo2	95.69(4)	Cl2	Mo2	S2	97.00(5)
S7	Mo3	Cl3	136.02(5)	S2	Mo2	Mo3	115.70(4)
S7	Mo3	Cl4	82.33(5)	S2	Mo2	Mo1	56.39(3)

Table 7.12.3. [cont.] Bond Angles

Atom	Atom	Atom	Angle/°	Atom	Atom	Atom	Angle/°
S7	Mo3	S5	82.69(4)	Mo3	S1	Mo1	71.10(4)
S7	Mo3	S4	131.75(5)	Mo2	S1	Mo3	71.84(4)
S7	Mo3	S6	49.58(4)	Mo2	S1	Mo1	71.61(4)
S6	Mo3	Mo1	56.35(3)	Mo3	S5	Mo2	70.39(4)
S6	Mo3	Mo2	116.37(3)	S4	S5	Mo3	67.68(5)
Mo3	Mo1	Mo2	60.349(14)	S4	S5	Mo2	67.43(5)
S1	Mo1	Mo3	54.41(3)	Mo2	S4	Mo3	67.60(3)
S1	Mo1	Mo2	54.14(3)	S5	S4	Mo3	63.06(5)
S1	Mo1	S7	109.01(4)	S5	S4	Mo2	63.23(5)
S1	Mo1	S3	108.27(5)	Mo3	S7	Mo1	69.95(4)
S1	Mo1	S6	85.84(4)	S6	S7	Mo3	67.82(5)
S1	Mo1	S2	84.08(4)	S6	S7	Mo1	67.39(5)
S7	Mo1	Mo3	54.97(3)	Mo2	S3	Mo1	70.18(4)
S7	Mo1	Mo2	95.77(3)	S2	S3	Mo1	67.65(5)
S7	Mo1	S3	86.07(5)	S2	S3	Mo2	68.03(5)
S7	Mo1	S6	49.68(4)	Mo1	S6	Mo3	66.90(3)
S7	Mo1	S2	135.09(5)	S7	S6	Mo3	62.60(5)
S3	Mo1	Mo3	96.93(3)	S7	S6	Mo1	62.93(5)
S3	Mo1	Mo2	54.78(3)	Mo1	S2	Mo2	66.98(3)
S3	Mo1	S6	135.50(5)	S3	S2	Mo1	62.93(5)
S3	Mo1	S2	49.41(5)	S3	S2	Mo2	62.56(5)
S6	Mo1	Mo3	56.75(3)	C6	N1	Mo1	116.5(3)
S6	Mo1	Mo2	117.00(3)	C1	N1	Mo1	126.4(3)
S6	Mo1	S2	169.90(5)	C1	N1	C6	116.7(4)
S2	Mo1	Mo3	116.75(3)	C12	N2	Mo1	124.9(3)
S2	Mo1	Mo2	56.63(3)	C12	N2	C7	117.9(4)
N1	Mo1	Mo3	125.48(11)	C7	N2	Mo1	117.0(3)
N1	Mo1	Mo2	130.09(11)	N2	C12	C11	123.0(5)
N1	Mo1	S1	87.70(11)	N2	C7	C8	121.5(4)
N1	Mo1	S7	129.49(12)	N2	C7	C6	115.7(4)
N1	Mo1	S3	134.59(12)	N1	C6	C7	116.0(4)

Table 7.12.3. [cont.] Bond Angles

Atom	Atom	Atom	Angle/°	Atom	Atom	Atom	Angle/°
N1	Mo1	S6	86.43(12)	N2	Mo1	N1	73.95(14)
N1	Mo1	S2	92.66(12)	Mo1	Mo2	Mo3	59.527(14)
N2	Mo1	Mo3	137.20(11)	S1	Mo2	Mo3	54.10(3)
N2	Mo1	Mo2	140.68(11)	S1	Mo2	Mo1	54.24(3)
N2	Mo1	S1	161.62(11)	S1	Mo2	S5	108.63(4)
N2	Mo1	S7	82.86(11)	S1	Mo2	S4	86.26(4)
N2	Mo1	S3	86.00(11)	N1	C6	C5	121.5(5)
N2	Mo1	S6	91.96(12)	N1	C1	C2	123.8(5)
N2	Mo1	S2	97.46(12)				

7.2.4.6. STRUCTURE OF $(Bu_4N)[Mo_3S_7Br_4(dmbpy)\cdot Br]$, $(Bu_4N)[\mathbf{19}\cdot Br]$

Single crystals of compound $(Bu_4N)[\mathbf{19}\cdot Br]$ were obtained by slow diffusion toluene/CH_2Cl_2, in a similar fashion to compound $(Bu_4N)[\mathbf{14}\cdot Br]$. The structure of $(Bu_4N)[\mathbf{19}\cdot Br]$ was refined in the triclinic space group P-1. All non-hydrogen atoms were refined anisotropically. Figure 7.13 shows its ORTEP representation with the atom numbering scheme. One terminal carbon atom in the tetrabutylammonium counterion centered at N(400) was found to be disordered over two positions with a 0.55/0.45 partial occupancy ratio. Dichloromethane and toluene were found co-crystallized with the cluster complex. In the dichloromethane molecule centered at C(40), one chlorine atom was found disordered between two positions with partial occupancies of 0.60 and 0.40, and therefore the hydrogen atoms were not included. The bond distances in the dichloromethane molecule centered at C(30) were restrained to fixed values, and all the atoms in this molecule were refined isotropically. The crystallographic data collection parameters are given in Table 7.13.1.

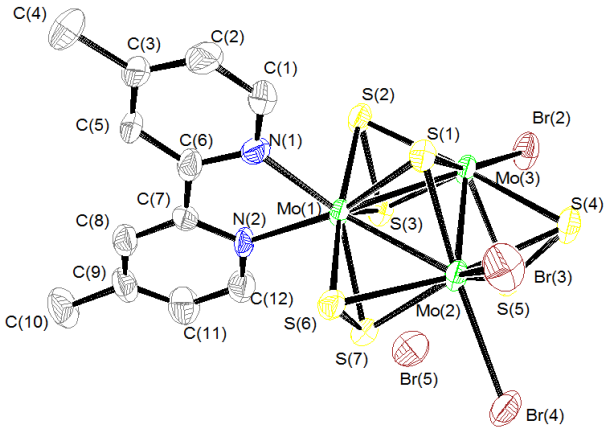

Figure 7.13. ORTEP representation (50 % probability ellipsoids) of the anionic trinuclear cluster $[\mathbf{19}\cdot Br]^-$ with the atom numbering scheme. Average distances (Å): Mo-Mo, 2.7502(11); Mo-(μ_3-S), 2.359(3); Mo-S_{ax}, 2.393(3); Mo-S_{eq}, 2.481(3); Mo-N, 2.211(8); Mo-Br, 2.6172(14); S_{ax}-Br, 3.05(5).

Table 7.13.1. Crystal Structure Data

Crystal Data			
Species	$(Bu_4N)[Mo_3S_7Br_4(dmbpy)\cdot Br]\cdot(1/6)CH_3C_6H_5\cdot(1/2)CH_2Cl_2$		
Formula	$C_{29.7}H_{49.2}Br_5ClMo_3N_3S_7$	**Crystal system**	triclinic
Space group	P-1	**Formula weight**	1395.96
a (Å)	19.3605(3)	**α** (º)	71.8853(15)
b (Å)	25.9644(4)	**β** (º)	76.3237(14)
c (Å)	34.7600(5)	**γ** (º)	70.0386(15)
Z	12	**Vol** (Å^3)	15442.7(5)
Colour	reddish	**Crystal size** (mm)	0.4007 × 0.2194 × 0.0933
$\mathbf{d_{calc}}$ (g/cm^3)	1.797	**λ** (Å)	0.71073
Absorption coefficient (mm^{-1})	4.957	**F (000)**	8124.0

Experimental Data			
Temperature (K)	200	**R(int)**	0.0725
Time per frame (s)	38	**R (σ)**	0.0684
2θ Range (º)	5.58 to 52	**Index ranges**	$-23 \le h \le 23$ $-32 \le k \le 32$ $-42 \le l \le 42$
Collected reflections	331374	**Independent reflections**	60352

Solution and Refinement			
Parameters	2663	**GooF on F²**	1.029
Restraints	2		
Final R1 ([I>2sigma(I)])	0.0647	**Final R1 (all data)**	0.1153
Final wR2 ([I>2sigma(I)])	0.1675	**Final wR2 (all data)**	0.2012
Max/Min peak (e·Å^{-3})	3.08 / -1.57	**Max. shift/σ**	< 0.001

$$\boldsymbol{R1} = \sum\big||\boldsymbol{F_0}| - |\boldsymbol{F_1}|\big| / \sum \boldsymbol{F_0} \qquad \boldsymbol{wR2} = \left[\sum\left[\boldsymbol{w}(\boldsymbol{F_0^2} - \boldsymbol{F_c^2})^2\right] / \sum\left[\boldsymbol{w}(\boldsymbol{F_0^2})^2\right]\right]^{1/2}$$

Table 7.13.2. Bond Distances

Atom	Atom	Length/Å	Atom	Atom	Length/Å
Mo3	Mo2	2.7598(12)	Mo2	S5	2.395(3)
Mo3	Br2	2.6373(13)	Mo2	S4	2.481(3)
Mo3	Br1	2.5971(15)	Mo2	Mo1	2.7456(11)
Mo3	S3	2.394(3)	S7	Mo1	2.390(3)
Mo3	S1	2.357(3)	S6	Mo1	2.473(3)
Mo3	S2	2.489(2)	S3	S2	2.048(4)
Mo3	S5	2.394(3)	S3	Mo1	2.391(3)
Mo3	S4	2.477(3)	S1	Mo1	2.367(3)
Mo3	Mo1	2.7453(11)	S2	Mo1	2.474(3)
Mo2	Br4	2.6537(14)	N2	C7	1.343(12)
Mo2	Br3	2.5777(14)	N2	C12	1.354(14)
Mo2	S7	2.391(3)	N2	Mo1	2.210(8)
Mo2	S6	2.491(3)	N1	C6	1.368(13)
Mo2	S1	2.354(3)	N1	Mo1	2.212(8)

Table 7.13.3. Bond Angles

Atom	Atom	Atom	Angle/°	Atom	Atom	Atom	Angle/°
Br2	Mo3	Mo2	137.30(5)	S4	Mo2	Mo1	115.88(7)
Br2	Mo3	Mo1	139.17(5)	Mo1	Mo2	Mo3	59.82(3)
Br1	Mo3	Mo2	123.51(5)	S6	S7	Mo2	67.66(11)
Br1	Mo3	Br2	81.67(5)	S6	S7	Mo1	67.11(10)
Br1	Mo3	Mo1	122.55(4)	Mo1	S7	Mo2	70.10(8)
S3	Mo3	Mo2	95.62(7)	S7	S6	Mo2	62.57(10)
S3	Mo3	Br2	84.38(7)	S7	S6	Mo1	62.90(10)
S3	Mo3	Br1	134.14(8)	Mo1	S6	Mo2	67.15(7)
S3	Mo3	S2	49.53(9)	S2	S3	Mo3	67.66(11)
S3	Mo3	S4	132.83(10)	S2	S3	Mo1	67.24(10)
S3	Mo3	Mo1	54.94(6)	Mo1	S3	Mo3	70.02(8)
S1	Mo3	Mo2	54.09(7)	Mo3	S1	Mo1	71.06(8)
S1	Mo3	Br2	162.76(8)	Mo2	S1	Mo3	71.73(8)
S1	Mo3	Br1	81.21(8)	Mo2	S1	Mo1	71.12(8)
S1	Mo3	S3	109.17(9)	S3	S2	Mo3	62.81(10)
S1	Mo3	S2	85.21(9)	S3	S2	Mo1	63.02(10)
S1	Mo3	S5	108.54(10)	Mo1	S2	Mo3	67.15(7)
S1	Mo3	S4	85.31(9)	Mo3	S5	Mo2	70.39(8)
S1	Mo3	Mo1	54.65(7)	S4	S5	Mo3	67.44(11)
S2	Mo3	Mo2	115.87(7)	S4	S5	Mo2	67.53(11)
S2	Mo3	Br2	96.44(7)	Mo3	S4	Mo2	67.65(7)
S2	Mo3	Br1	89.02(7)	S5	S4	Mo3	63.18(10)
S2	Mo3	Mo1	56.16(6)	S5	S4	Mo2	63.13(10)
S5	Mo3	Mo2	54.82(7)	C7	N2	C12	117.4(9)
S5	Mo3	Br2	82.92(7)	C7	N2	Mo1	118.2(7)
S5	Mo3	Br1	136.76(8)	C12	N2	Mo1	124.2(7)
S5	Mo3	S3	83.71(10)	C6	N1	Mo1	116.6(7)
S5	Mo3	S2	132.82(10)	C1	N1	C6	117.4(9)
S5	Mo3	S4	49.39(10)	C1	N1	Mo1	126.0(7)
S5	Mo3	Mo1	94.74(7)	N2	C7	C6	115.3(9)
S4	Mo3	Mo2	56.23(7)	N2	C7	C8	122.1(10)
S4	Mo3	Br2	93.20(7)	N1	C6	C7	116.6(9)
S4	Mo3	Br1	91.53(8)	N1	C6	C5	119.9(11)

Table 7.13.3. [cont.] Bond Angles

Atom	Atom	Atom	Angle/°	Atom	Atom	Atom	Angle/°
S4	Mo3	S2	170.31(9)	N1	C1	C2	123.3(11)
S4	Mo3	Mo1	116.02(7)	Mo3	Mo1	Mo2	60.35(3)
Mo1	Mo3	Mo2	59.83(3)	S7	Mo1	Mo3	96.34(7)
Br4	Mo2	Mo3	138.30(5)	S7	Mo1	Mo2	54.96(7)
Br4	Mo2	Mo1	136.95(5)	S7	Mo1	S6	49.99(9)
Br3	Mo2	Mo3	123.25(5)	S7	Mo1	S3	85.37(9)
Br3	Mo2	Br4	81.58(5)	S7	Mo1	S2	134.82(9)
Br3	Mo2	Mo1	124.43(5)	S6	Mo1	Mo3	116.91(7)
S7	Mo2	Mo3	95.93(7)	S6	Mo1	Mo2	56.74(6)
S7	Mo2	Br4	82.21(7)	S6	Mo1	S2	170.01(10)
S7	Mo2	Br3	135.10(8)	S3	Mo1	Mo3	55.04(7)
S7	Mo2	S6	49.76(9)	S3	Mo1	Mo2	96.06(7)
S7	Mo2	S5	84.16(10)	S3	Mo1	S6	135.03(9)
S7	Mo2	S4	133.21(10)	S3	Mo1	S2	49.74(9)
S7	Mo2	Mo1	54.93(6)	S1	Mo1	Mo3	54.29(6)
S6	Mo2	Mo3	115.75(7)	S1	Mo1	Mo2	54.22(7)
S6	Mo2	Br4	94.74(7)	S1	Mo1	S7	108.69(9)
S6	Mo2	Br3	90.41(7)	S1	Mo1	S6	84.69(9)
S6	Mo2	Mo1	56.11(6)	S1	Mo1	S3	108.91(9)
S1	Mo2	Mo3	54.18(7)	S1	Mo1	S2	85.33(9)
S1	Mo2	Br4	163.69(8)	S2	Mo1	Mo3	56.69(6)
S1	Mo2	Br3	82.13(8)	S2	Mo1	Mo2	116.91(6)
S1	Mo2	S7	109.10(9)	N2	Mo1	Mo3	140.3(2)
S1	Mo2	S6	84.56(9)	N2	Mo1	Mo2	138.6(2)
S1	Mo2	S5	108.60(10)	N2	Mo1	S7	84.1(2)
S1	Mo2	S4	85.29(9)	N2	Mo1	S6	93.7(2)
S1	Mo2	Mo1	54.66(7)	N2	Mo1	S3	85.6(2)
S5	Mo2	Mo3	54.79(7)	N2	Mo1	S1	161.0(2)
S5	Mo2	Br4	83.70(7)	N2	Mo1	S2	95.6(2)
S5	Mo2	Br3	134.75(8)	N2	Mo1	N1	72.9(3)
S5	Mo2	S6	133.41(10)	N1	Mo1	Mo3	127.7(2)
S5	Mo2	S4	49.34(10)	N1	Mo1	Mo2	128.6(2)
S5	Mo2	Mo1	94.71(7)	N1	Mo1	S7	132.6(2)
S4	Mo2	Mo3	56.11(6)	N1	Mo1	S6	90.1(2)

7.2.4.7. STRUCTURE OF $(Bu_4N)[Mo_3S_7Br_4(bpy)\cdot Br]$, $(Bu_4N)[\mathbf{20}\cdot Br]$

Single crystals of compound $(Bu_4N)[\mathbf{20}\cdot Br]$ were obtained in a similar fashion to cluster $(Bu_4N)[\mathbf{14}\cdot Br]$. The structure of $(Bu_4N)[\mathbf{20}\cdot Br]$ was refined in the monoclinic space group $P2_1$. Figure 7.14 shows its ORTEP representation with the atom numbering scheme. Dichloromethane and toluene were found cocrystallized with the cluster complex. In the tetrabutylammonium anion centered at N(200), the terminal carbon C(116) was found to be disordered over two positions with a partial occupancy ratio of 0.6/0.4. Owing to disorder, we considered as justified the omission of the hydrogen atoms in this molecule. The crystallographic data collection parameters are given in Table 7.14.1.

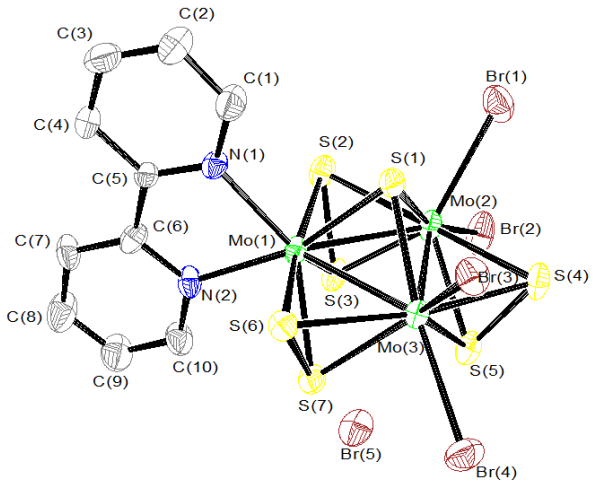

Figure 7.14. ORTEP representation (50 % probability ellipsoids) of the anionic trinuclear cluster $[\mathbf{20}\cdot Br]^-$ with the atom numbering scheme. Average distances (Å): Mo-Mo, 2.7438(14); Mo-(μ_3-S), 2.3583(3); Mo-S_{ax}, 2.391(3); Mo-S_{eq}, 2.485(3); Mo-N, 2.225(10); Mo-Br, 2.6212(17); S_{ax}-Br, 3.043(14).

Table 7.14.1. Crystal Structure Data

Crystal Data			
Species	$(Bu_4N)[Mo_3S_7Br_4(bpy)\cdot Br]\cdot CH_2Cl_2\cdot CH_3C_6H_5$		
Formula	$C_{30}H_{30.5}Br_5ClMo_3N_3S_7$	**Crystal system**	monoclinic
Space group	$P2_1$	**Formula weight**	1380.31
a (Å)	11.19024(19)	**α** (º)	90
b (Å)	32.5907(6)	**β** (º)	108.499(2)
c (Å)	14.5892(3)	**γ** (º)	90
Z	4	**Vol** (Å^3)	5045.73(16)
Colour	reddish	**Crystal size** (mm)	0.063 × 0.189 × 0.296
$\mathbf{d_{calc}}$ (g/cm^3)	1.817	**λ** (Å)	0.71070
Absorption coefficient (mm^{-1})	5.060	**F (000)**	2646.0

Experimental Data			
Temperature (K)	200	**R(int)**	0.0338
Time per frame (s)	28	**R (σ)**	0.0409
2θ Range (º)	5.68 to 50	**Index ranges**	-13 ≤ h ≤ 13, -38 ≤ k ≤ 38, -17 ≤ l ≤ 17
Collected reflections	48304	**Independent reflections**	17681

Solution and Refinement			
Parameters	891	**GooF on F²**	1.068
Restraints	6		
Final R1 ([I>2sigma(I)])	0.0429	**Final R1 (all data)**	0.0470
Final wR2 ([I>2sigma(I)])	0.1225	**Final wR2 (all data)**	0.1256
Max/Min peak (e·Å^{-3})	3.29/-0.58	**Max. shift/σ**	<0.001

$$\boldsymbol{R1} = \sum\big||\boldsymbol{F_0}| - |\boldsymbol{F_1}|\big| / \sum \boldsymbol{F_0} \qquad \boldsymbol{wR2} = \left[\sum\left[\boldsymbol{w}(\boldsymbol{F_0^2} - \boldsymbol{F_c^2})^2\right] / \sum\left[\boldsymbol{w}(\boldsymbol{F_0^2})^2\right]\right]^{1/2}$$

Table 7.14.2. Bond Distances

Atom	Atom	Length/Å	Atom	Atom	Length/Å
Mo1	Mo3	2.7359(13)	Mo2	S3	2.387(3)
Mo1	Mo2	2.7405(14)	Mo2	S4	2.493(3)
Mo1	S1	2.366(3)	Mo2	S2	2.488(3)
Mo1	S3	2.393(3)	Mo2	S5	2.398(3)
Mo1	S7	2.390(3)	S3	S2	2.047(5)
Mo1	S6	2.476(3)	S7	S6	2.048(4)
Mo1	S2	2.489(3)	S4	S5	2.047(5)
Mo1	N2	2.214(10)	N2	C10	1.348(17)
Mo1	N1	2.236(9)	N2	C6	1.339(16)
Mo3	Mo2	2.7549(15)	C10	C9	1.38(2)
Mo3	Br3	2.5847(16)	C3	C4	1.37(2)
Mo3	Br4	2.6381(17)	C3	C2	1.36(2)
Mo3	S1	2.354(3)	N1	C1	1.337(18)
Mo3	S7	2.379(3)	N1	C5	1.321(15)
Mo3	S6	2.491(3)	C6	C7	1.379(18)
Mo3	S4	2.471(3)	C6	C5	1.462(18)
Mo3	S5	2.397(3)	C4	C5	1.434(17)
Mo2	Br2	2.6394(18)	C1	C2	1.408(19)
Mo2	Br1	2.6226(18)	C7	C8	1.40(2)
Mo2	S1	2.355(3)	C9	C8	1.34(2)

Table 7.14.3. Bond Angles

Atom	Atom	Atom	Angle/°	Atom	Atom	Atom	Angle/°
Mo3	Mo1	Mo2	60.40(4)	S1	Mo2	Br2	163.60(10)
S1	Mo1	Mo3	54.37(8)	S1	Mo2	Br1	81.94(9)
S1	Mo1	Mo2	54.33(8)	S1	Mo2	S3	109.37(11)
S1	Mo1	S3	108.79(12)	S1	Mo2	S4	85.00(11)
S1	Mo1	S7	108.71(11)	S1	Mo2	S2	85.45(11)
S1	Mo1	S6	85.29(11)	S1	Mo2	S5	108.71(12)
S1	Mo1	S2	85.19(11)	S3	Mo2	Mo1	55.13(8)
S3	Mo1	Mo3	96.11(8)	S3	Mo2	Mo3	95.75(9)
S3	Mo1	Mo2	54.92(8)	S3	Mo2	Br2	80.71(9)
S3	Mo1	S6	134.75(12)	S3	Mo2	Br1	136.62(10)
S3	Mo1	S2	49.54(12)	S3	Mo2	S4	132.83(13)
S7	Mo1	Mo3	54.80(8)	S3	Mo2	S2	49.61(12)
S7	Mo1	Mo2	96.04(8)	S3	Mo2	S5	83.71(12)
S7	Mo1	S3	85.27(12)	S4	Mo2	Mo1	115.57(9)
S7	Mo1	S6	49.75(11)	S4	Mo2	Mo3	55.91(8)
S7	Mo1	S2	134.49(12)	S4	Mo2	Br2	97.63(9)
S6	Mo1	Mo3	56.85(7)	S4	Mo2	Br1	88.73(10)
S6	Mo1	Mo2	117.12(8)	S2	Mo2	Mo1	56.61(8)
S6	Mo1	S2	170.48(11)	S2	Mo2	Mo3	116.20(9)
S2	Mo1	Mo3	116.85(8)	S2	Mo2	Br2	92.08(9)
S2	Mo1	Mo2	56.56(8)	S2	Mo2	Br1	91.87(9)
N2	Mo1	Mo3	138.6(3)	S2	Mo2	S4	170.25(12)
N2	Mo1	Mo2	139.8(3)	S5	Mo2	Mo1	94.70(9)
N2	Mo1	S1	161.2(3)	S5	Mo2	Mo3	54.93(8)
N2	Mo1	S3	85.2(3)	S5	Mo2	Br2	84.77(9)
N2	Mo1	S7	84.3(3)	S5	Mo2	Br1	133.64(9)
N2	Mo1	S6	93.6(3)	S5	Mo2	S4	49.44(12)
N2	Mo1	S2	95.3(3)	S5	Mo2	S2	132.94(12)
N2	Mo1	N1	73.4(4)	Mo3	S1	Mo1	70.85(9)
N1	Mo1	Mo3	128.7(3)	Mo3	S1	Mo2	71.61(9)
N1	Mo1	Mo2	127.4(3)	Mo2	S1	Mo1	70.96(9)

Table 7.14.3. [cont.] Bond Angles

Atom	Atom	Atom	Angle/°	Atom	Atom	Atom	Angle/°
N1	Mo1	S1	87.9(3)	Mo2	S3	Mo1	69.96(9)
N1	Mo1	S3	131.3(3)	S2	S3	Mo1	67.66(13)
N1	Mo1	S7	133.3(3)	S2	S3	Mo2	67.75(13)
N1	Mo1	S6	90.7(3)	Mo3	S7	Mo1	70.01(9)
N1	Mo1	S2	88.9(3)	S6	S7	Mo1	67.30(12)
Mo1	Mo3	Mo2	59.88(4)	S6	S7	Mo3	68.02(12)
Br3	Mo3	Mo1	122.98(5)	Mo1	S6	Mo3	66.84(8)
Br3	Mo3	Mo2	123.21(5)	S7	S6	Mo1	62.95(12)
Br3	Mo3	Br4	81.89(5)	S7	S6	Mo3	62.30(12)
Br4	Mo3	Mo1	138.34(6)	Mo3	S4	Mo2	67.41(8)
Br4	Mo3	Mo2	137.65(6)	S5	S4	Mo3	63.27(13)
S1	Mo3	Mo1	54.78(8)	S5	S4	Mo2	62.85(13)
S1	Mo3	Mo2	54.22(8)	Mo2	S2	Mo1	66.83(9)
S1	Mo3	Br3	81.14(9)	S3	S2	Mo1	62.80(13)
S1	Mo3	Br4	163.01(9)	S3	S2	Mo2	62.64(12)
S1	Mo3	S7	109.52(11)	Mo3	S5	Mo2	70.13(9)
S1	Mo3	S6	85.21(10)	S4	S5	Mo3	67.02(14)
S1	Mo3	S4	85.53(11)	S4	S5	Mo2	67.71(14)
S1	Mo3	S5	108.78(12)	C10	N2	Mo1	124.7(9)
S7	Mo3	Mo1	55.19(8)	C6	N2	Mo1	117.2(8)
S7	Mo3	Mo2	95.93(9)	C6	N2	C10	118.0(11)
S7	Mo3	Br3	134.48(9)	N2	C10	C9	122.9(14)
S7	Mo3	Br4	83.32(9)	C1	N1	Mo1	124.8(8)
S7	Mo3	S6	49.68(10)	C5	N1	Mo1	115.8(8)
S7	Mo3	S4	133.27(12)	C5	N1	C1	119.4(11)
S7	Mo3	S5	83.77(11)	N2	C6	C7	121.6(12)
S6	Mo3	Mo1	56.32(8)	N2	C6	C5	115.4(11)
S6	Mo3	Mo2	116.06(8)	C10	N2	Mo1	124.7(9)
S6	Mo3	Br3	89.40(8)	C6	N2	Mo1	117.2(8)
S6	Mo3	Br4	95.60(9)	C6	N2	C10	118.0(11)
S4	Mo3	Mo1	116.51(9)	N2	C10	C9	122.9(14)

Table 7.14.3. [cont.] Bond Angles

Atom	Atom	Atom	Angle/°	Atom	Atom	Atom	Angle/°
S4	Mo3	Mo2	56.68(8)	Br1	Mo2	Mo1	125.07(6)
S4	Mo3	Br3	90.54(9)	Br1	Mo2	Mo3	122.39(6)
S4	Mo3	Br4	93.65(9)	Br1	Mo2	Br2	81.94(6)
S4	Mo3	S6	170.64(12)	S1	Mo2	Mo1	54.70(8)
S5	Mo3	Mo1	94.83(9)	S1	Mo2	Mo3	54.17(8)
S5	Mo3	Mo2	54.95(9)	C1	N1	Mo1	124.8(8)
S5	Mo3	Br3	136.13(9)	C5	N1	Mo1	115.8(8)
S5	Mo3	Br4	83.05(9)	C5	N1	C1	119.4(11)
S5	Mo3	S6	133.02(11)	N2	C6	C7	121.6(12)
S5	Mo3	S4	49.71(12)	N2	C6	C5	115.4(11)
Mo1	Mo2	Mo3	59.72(4)	N1	C1	C2	122.6(13)
Br2	Mo2	Mo1	135.49(6)	N1	C5	C6	118.1(10)
Br2	Mo2	Mo3	139.62(6)	N1	C5	C4	121.0(11)

7.2.4.8. STRUCTURE OF $(Bu_4N)[Mo_3S_7Br_4(phen)\cdot Br]$, $(Bu_4N)[\mathbf{21}\cdot Br]$

Single crystals of compound $(Bu_4N)[\mathbf{21}\cdot Br]$ were obtained in a similar fashion to compound $(Bu_4N)[\mathbf{14}\cdot Br]$. Reddish needle-like crystals grew from the mixture after few days. The structure of $(Bu_4N)[\mathbf{21}\cdot Br]$ was refined in the triclinic space group P-1. All non-hydrogen atoms were refined anisotropically. Figure 7.15 shows its ORTEP representation with the atom numbering scheme. In the tetrabutylammonium counterion, three terminal carbons (C104, C108 and C112) were refined with a partial occupancy (0.5, 0.5 and 0.75, respectively). Additionally, the bond distances between three pairs of terminal atoms (C103-C104, C107-C108 and C111-C112) were restrained to fixed values. The crystallographic data collection parameters are given in Table 7.15.1.

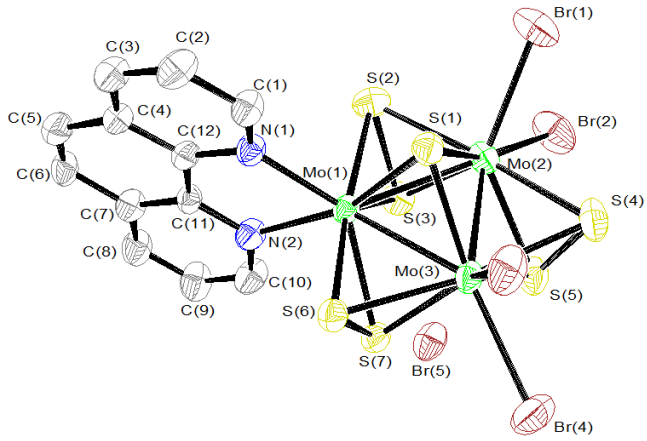

Figure 7.15. ORTEP representation (50 % probability ellipsoids) of the anionic trinuclear cluster $[\mathbf{21}\cdot Br]^-$ with the atom numbering scheme. Average distances (Å): Mo-Mo, 2.7414(7); Mo-(μ_3-S), 2.3553(15); Mo-S_{ax}, 2.3958(16); Mo-S_{eq}, 2.4852(17); Mo-N, 2.216(5); Mo-Br, 2.6083(9); S_{ax}-Br, 3.04(8).

Table 7.15.1. Crystal Structure Data

Crystal Data			
Species	$(Bu_4N)[Mo_3S_7Br_4(phen)\cdot Br]$		
Formula	$C_{26.8}H_{36.3}Br_5Mo_3N_3S_7$	**Crystal system**	triclinic
Space group	P-1	**Formula weight**	1311.63
a (Å)	11.9690(3)	**α** (º)	71.325(3)
b (Å)	12.7039(4)	**β** (º)	79.119(2)
c (Å)	16.6526(5)	**γ** (º)	65.163(3)
Z	2	**Vol** (Å^3)	2172.55(12)
Colour	reddish	**Crystal size** (mm)	0.5229 × 0.2075 × 0.034
$\mathbf{d_{calc}}$ (g/cm^3)	2.005	**λ** (Å)	1.54180
Absorption coefficient (mm^{-1})	15.699	**F (000)**	1262.0

Experimental Data			
Temperature (K)	200	**R(int)**	0.0712
Time per frame (s)	1	**R (σ)**	0.0430
2θ Range (º)	5.16 to 144	**Index ranges**	-14 ≤ h ≤ 14, -14 ≤ k ≤ 15, -20 ≤ l ≤ 20
Collected reflections	31156	**Independent reflections**	8395

Solution and Refinement			
Parameters	419	**GooF on F²**	1.027
Restraints	3		
Final R1 ([I>2sigma(I)])	0.0538	**Final R1 (all data)**	0.0612
Final wR2 ([I>2sigma(I)])	0.1534	**Final wR2 (all data)**	0.1654
Max/Min peak (e·Å^{-3})	1.75 / -1.46	**Max. shift./σ**	0.306

$$\boldsymbol{R1} = \sum\big||\boldsymbol{F_0}| - |\boldsymbol{F_1}|\big| / \sum \boldsymbol{F_0} \qquad \boldsymbol{wR2} = \left[\sum\left[\boldsymbol{w}(\boldsymbol{F_0^2} - \boldsymbol{F_c^2})^2\right] / \sum\left[\boldsymbol{w}(\boldsymbol{F_0^2})^2\right]\right]^{1/2}$$

Table 7.15.2. Bond Distances

Atom	Atom	Length/Å	Atom	Atom	Length/Å
Mo1	Mo3	2.7283(6)	Mo3	S4	2.4804(17)
Mo1	Mo2	2.7454(7)	Mo2	Br1	2.6119(9)
Mo1	S1	2.3568(15)	Mo2	Br2	2.6210(9)
Mo1	S7	2.4021(14)	Mo2	S1	2.3566(15)
Mo1	S6	2.4900(15)	Mo2	S5	2.3880(17)
Mo1	S3	2.4005(16)	Mo2	S3	2.3882(18)
Mo1	S2	2.4892(16)	Mo2	S2	2.4890(18)
Mo1	N2	2.218(5)	Mo2	S4	2.4780(19)
Mo1	N1	2.213(5)	S7	S6	2.047(2)
Mo3	Mo2	2.7506(7)	S5	S4	2.034(3)
Mo3	Br3	2.5976(9)	S3	S2	2.051(2)
Mo3	Br4	2.6025(9)	N2	C11	1.357(7)
Mo3	S1	2.3526(15)	N2	C10	1.350(8)
Mo3	S7	2.4018(15)	N1	C12	1.384(8)
Mo3	S6	2.4843(15)	N1	C1	1.334(8)
Mo3	S5	2.3943(17)			

Table 7.15.3. [cont.] Bond Angles

Atom	Atom	Atom	Angle/˚	Atom	Atom	Atom	Angle/˚
Mo3	Mo1	Mo2	60.333(18)	S1	Mo2	Mo1	54.38(4)
S1	Mo1	Mo3	54.53(4)	S1	Mo2	Mo3	54.19(4)
S1	Mo1	Mo2	54.37(4)	S1	Mo2	Br1	80.60(4)
S1	Mo1	S7	109.40(5)	S1	Mo2	Br2	163.14(5)
S1	Mo1	S6	85.22(5)	S1	Mo2	S5	108.91(6)
S1	Mo1	S3	108.60(6)	S1	Mo2	S3	109.01(5)
S1	Mo1	S2	84.38(6)	S1	Mo2	S2	84.39(6)
S7	Mo1	Mo3	55.39(4)	S1	Mo2	S4	86.22(6)
S7	Mo1	Mo2	96.72(4)	S5	Mo2	Mo1	94.10(4)
S7	Mo1	S6	49.43(5)	S5	Mo2	Mo3	55.00(4)
S7	Mo1	S2	135.60(6)	S5	Mo2	Br1	135.48(5)
S6	Mo1	Mo3	56.64(4)	S5	Mo2	Br2	82.85(5)
S6	Mo1	Mo2	116.84(4)	S5	Mo2	S3	83.70(6)
S3	Mo1	Mo3	96.55(4)	S5	Mo2	S2	132.87(6)
S3	Mo1	Mo2	54.81(4)	S5	Mo2	S4	49.38(6)
S3	Mo1	S7	86.36(6)	S3	Mo2	Mo1	55.23(4)
S3	Mo1	S6	135.42(5)	S3	Mo2	Mo3	96.25(4)
S3	Mo1	S2	49.55(6)	S3	Mo2	Br1	135.69(5)
S2	Mo1	Mo3	116.67(5)	S3	Mo2	Br2	83.74(5)
S2	Mo1	Mo2	56.53(4)	S3	Mo2	S2	49.68(6)
S2	Mo1	S6	169.60(6)	S3	Mo2	S4	132.88(6)
N2	Mo1	Mo3	141.87(13)	S2	Mo2	Mo1	56.53(4)
N2	Mo1	Mo2	136.95(14)	S2	Mo2	Mo3	115.87(4)
N2	Mo1	S1	160.48(14)	S2	Mo2	Br1	90.50(5)
N2	Mo1	S7	86.62(14)	S2	Mo2	Br2	96.48(5)
N2	Mo1	S6	97.80(14)	S4	Mo2	Mo1	115.86(5)
N2	Mo1	S3	82.79(14)	S4	Mo2	Mo3	56.35(4)
N2	Mo1	S2	91.88(14)	S4	Mo2	Br1	89.82(5)
N1	Mo1	Mo3	125.93(13)	S4	Mo2	Br2	93.05(5)
N1	Mo1	Mo2	127.92(13)	S4	Mo2	S2	170.42(6)
N1	Mo1	S1	86.29(13)	Mo3	S1	Mo1	70.81(4)

Table 7.15.3. [cont.] Bond Angles

Atom	Atom	Atom	Angle/°	Atom	Atom	Atom	Angle/°
N1	Mo1	S7	130.83(13)	Mo3	S1	Mo2	71.48(4)
N1	Mo1	S6	88.07(13)	Mo2	S1	Mo1	71.25(4)
N1	Mo1	S3	133.65(13)	Mo3	S7	Mo1	69.21(4)
N1	Mo1	S2	90.83(13)	S6	S7	Mo1	67.52(6)
N1	Mo1	N2	74.59(18)	S6	S7	Mo3	67.35(6)
Mo1	Mo3	Mo2	60.142(18)	Mo3	S6	Mo1	66.52(4)
Br3	Mo3	Mo1	122.29(3)	S7	S6	Mo1	63.05(6)
Br3	Mo3	Mo2	121.69(3)	S7	S6	Mo3	63.15(6)
Br3	Mo3	Br4	81.42(3)	Mo2	S5	Mo3	70.22(5)
Br4	Mo3	Mo1	141.09(3)	S4	S5	Mo3	67.56(7)
Br4	Mo3	Mo2	137.01(3)	S4	S5	Mo2	67.61(7)
S1	Mo3	Mo1	54.67(4)	Mo2	S3	Mo1	69.96(5)
S1	Mo3	Mo2	54.33(4)	S2	S3	Mo1	67.47(6)
S1	Mo3	Br3	79.89(4)	S2	S3	Mo2	67.72(7)
S1	Mo3	Br4	161.10(5)	Mo2	S2	Mo1	66.94(4)
S1	Mo3	S7	109.54(5)	S3	S2	Mo1	62.97(6)
S1	Mo3	S6	85.44(5)	S3	S2	Mo2	62.61(7)
S1	Mo3	S5	108.83(6)	Mo2	S4	Mo3	67.39(4)
S1	Mo3	S4	86.25(6)	S5	S4	Mo3	63.15(7)
S7	Mo3	Mo1	55.40(4)	S5	S4	Mo2	63.00(7)
S7	Mo3	Mo2	96.58(4)	C11	N2	Mo1	115.1(4)
S7	Mo3	Br3	134.99(5)	C10	N2	Mo1	126.3(4)
S7	Mo3	Br4	85.82(4)	C10	N2	C11	118.6(5)
S7	Mo3	S6	49.50(5)	C12	N1	Mo1	114.6(4)
S7	Mo3	S4	132.76(6)	C1	N1	Mo1	128.6(4)
S6	Mo3	Mo1	56.84(4)	C1	N1	C12	116.8(5)
S6	Mo3	Mo2	116.84(4)	N1	C12	C11	117.4(5)
S6	Mo3	Br3	89.55(4)	N1	C12	C4	122.0(6)
S6	Mo3	Br4	97.21(4)	N2	C11	C12	117.8(5)
S5	Mo3	Mo1	94.39(5)	N2	C11	C7	121.6(5)
S5	Mo3	Mo2	54.78(4)	N1	C1	C2	123.5(6)

7.2.4.9. STRUCTURE OF $(Bu_4N)[Mo_3S_7Br_4(dcmbpy)\cdot Br]$, $(Bu_4N)[\mathbf{22}\cdot Br]$

Single crystals of compound $(Bu_4N)[\mathbf{22}\cdot Br]$ were obtained by slow diffusion Et_2O/CH_3CN by following the procedure described herein. The reaction mixture was cooled to -30 ºC, and the excess ligand was removed by filtration. Then diethyl ether was layered on the top of the acetonitrile solution. Dark red crystals were obtained. The structure of $(Bu_4N)[\mathbf{22}\cdot Br]$ was refined in the triclinic space group P-1. All non-hydrogen atoms were refined anisotropically. Figure 7.16 shows its ORTEP representation with the atom numbering scheme. Toluene and dichloromethane were found cocrystallized with the cluster complex. The toluene molecule was found to be disordered over two close positions with a 0.4/0.3 occupancy ratio. The dichloromethane molecule has also disordering over three positions with a 0.3/0.2/0.2 ratio. Since the solvent molecules are highly disordered with small occupancies, their carbon atoms were refined isotropically. The crystallographic data collection parameters are given in Table 7.16.1.

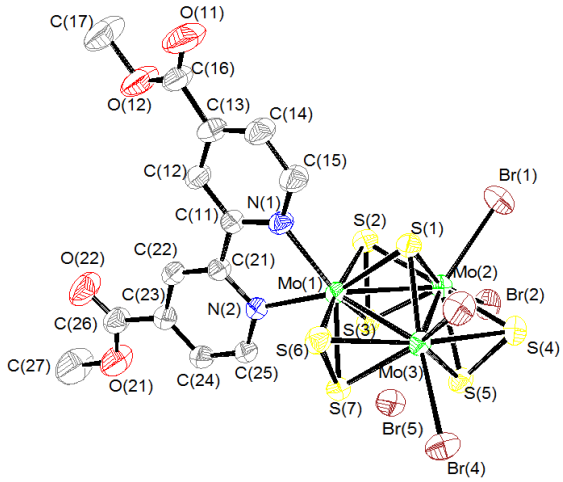

Figure 7.16. ORTEP representation (50 % probability ellipsoids) of the anionic trinuclear cluster $[\mathbf{22}\cdot Br]^-$ with the atom numbering scheme. Average distances (Å): Mo-Mo, 2.7531(4); Mo-(μ_3-S), 2.3607(9); Mo-S_{ax}, 2.3948(9); Mo-S_{eq}, 2.4881(10); Mo-N, 2.229(3); Mo-Br, 2.6259(5); S_{ax}-Br, 2.990(2).

Table 7.16.1. Crystal Structure Data

Crystal Data			
Species	$(Bu_4N)[Mo_3S_7Br_4(dcmbpy)\cdot Br]\cdot 0.7CH_3C_6H_5\cdot 0.7CH_2Cl_2$		
Formula	$C_{35.6}H_{55}Br_5Cl_{1.4}Mo_3N_3O_4S_7$	**Crystal system**	triclinic
Space group	P-1	**Formula weight**	1550.45
a (Å)	12.3010(3)	**α** (º)	64.2000(10)
b (Å)	15.2101(4)	**β** (º)	80.5140(10)
c (Å)	17.2369(4)	**γ** (º)	78.0520(10)
Z	2	**Vol** (Å^3)	2830.40(12)
Colour	dark red	**Crystal size** (mm)	0.20 × 0.12 × 0.08
$\mathbf{d_{calc}}$ (g/cm^3)	1.819	**λ** (Å)	0.71073
Absorption coefficient (mm^{-1})	4.544	**F (000)**	1517.0

Experimental Data			
Temperature (K)	296	**R(int)**	0.0400
Time per frame (s)	25	**R (σ)**	0.0420
2θ Range (º)	4.04 to 75.28	**Index ranges**	-20 ≤ h ≤ 18, -25 ≤ k ≤ 26, -29 ≤ l ≤ 27
Collected reflections	63649	**Independent reflections**	26635

Solution and Refinement			
Parameters	546	**GooF on F²**	0.961
Restraints	12		
Final R1 ([I>2sigma(I)])	0.0495	**Final R1 (all data)**	0.1478
Final wR2 ([I>2sigma(I)])	0.1223	**Final wR2 (all data)**	0.1543
Max/Min peak (e·Å^{-3})	1.08 / -0.84	**Max. shift./σ**	0.001

$$\boldsymbol{R1} = \sum\big||\boldsymbol{F_0}| - |\boldsymbol{F_1}|\big| / \sum \boldsymbol{F_0} \qquad \boldsymbol{wR2} = \left[\sum\left[\boldsymbol{w}(\boldsymbol{F_0^2} - \boldsymbol{F_c^2})^2\right] / \sum\left[\boldsymbol{w}(\boldsymbol{F_0^2})^2\right]\right]^{\boldsymbol{1/2}}$$

Table 7.16.2. Bond Distances

Atom	Atom	Length/Å	Atom	Atom	Length/Å
Mo2	S1	2.3604(9)	Mo1	Mo3	2.7494(4)
Mo2	S3	2.3862(9)	Mo3	S1	2.3565(9)
Mo2	S5	2.3909(9)	Mo3	S5	2.3920(9)
Mo2	S4	2.4811(10)	Mo3	S7	2.3955(9)
Mo2	S2	2.4918(10)	Mo3	S4	2.4869(10)
Mo2	Br1	2.6004(5)	Mo3	S6	2.4938(9)
Mo2	Br2	2.6612(5)	Mo3	Br3	2.6210(5)
Mo2	Mo3	2.7506(4)	Mo3	Br4	2.6212(5)
Mo2	Mo1	2.7591(4)	S6	S7	2.0534(12)
Mo1	N1	2.227(3)	S3	S2	2.0606(12)
Mo1	N2	2.231(3)	S4	S5	2.0438(13)
Mo1	S1	2.3651(9)	N1	C15	1.351(4)
Mo1	S3	2.3995(9)	N1	C11	1.354(4)
Mo1	S7	2.4043(9)	N2	C25	1.354(4)
Mo1	S2	2.4864(10)	N2	C21	1.363(4)
Mo1	S6	2.4891(10)			

Table 7.16.3. Bond Angles

Atom	Atom	Atom	Angle/°	Atom	Atom	Atom	Angle/°
S1	Mo2	S3	108.89(3)	S4	Mo3	S6	170.94(3)
S1	Mo2	S5	108.89(3)	S1	Mo3	Br3	81.35(2)
S3	Mo2	S5	83.45(3)	S5	Mo3	Br3	134.66(3)
S1	Mo2	S4	86.16(3)	S7	Mo3	Br3	135.93(3)
S3	Mo2	S4	132.80(3)	S4	Mo3	Br3	89.20(3)
S5	Mo2	S4	49.56(3)	S6	Mo3	Br3	91.02(3)
S1	Mo2	S2	84.47(3)	S1	Mo3	Br4	163.40(3)
S3	Mo2	S2	49.92(3)	S5	Mo3	Br4	82.99(3)
S5	Mo2	S2	132.91(3)	S7	Mo3	Br4	82.93(3)
S4	Mo2	S2	170.49(3)	S4	Mo3	Br4	93.72(3)
S1	Mo2	Br1	81.87(2)	S6	Mo3	Br4	95.28(3)
S3	Mo2	Br1	136.70(3)	Br3	Mo3	Br4	82.048(16)
S5	Mo2	Br1	134.01(3)	S1	Mo3	Mo1	54.53(2)
S4	Mo2	Br1	88.56(3)	S5	Mo3	Mo1	94.71(3)
S2	Mo2	Br1	91.71(3)	S7	Mo3	Mo1	55.20(2)
S1	Mo2	Br1	164.10(3)	S4	Mo3	Mo1	116.47(3)
S3	Mo2	Br2	81.53(2)	S6	Mo3	Mo1	56.43(2)
S5	Mo2	Br2	83.74(3)	Br3	Mo3	Mo1	124.096(15)
S4	Mo2	Br2	95.48(3)	Br4	Mo3	Mo1	137.969(16)
S2	Mo2	Br2	93.98(3)	S1	Mo3	Mo2	54.40(2)
Br1	Mo2	Br2	82.360(17)	S5	Mo3	Mo2	54.87(2)
S1	Mo2	Mo3	54.26(2)	S7	Mo3	Mo2	96.34(3)
S3	Mo2	Mo3	95.85(2)	S4	Mo3	Mo2	56.28(2)
S5	Mo2	Mo3	54.91(2)	S6	Mo3	Mo2	116.51(3)
S4	Mo2	Mo3	56.48(2)	Br3	Mo3	Mo2	122.079(15)
S2	Mo2	Mo3	115.95(2)	Br4	Mo3	Mo2	137.490(16)
Br1	Mo1	Mo3	122.076(16)	Mo1	Mo3	Mo2	60.219(11)
Br2	Mo2	Mo3	138.475(16)	S7	S6	Mo1	63.06(4)
S1	Mo2	Mo1	54.36(2)	S7	S6	Mo3	62.70(3)
S3	Mo2	Mo1	55.02(2)	Mo1	S6	Mo3	66.98(2)
S5	Mo2	Mo1	94.49(2)	Mo3	S1	Mo2	71.34(3)
S4	Mo2	Mo1	116.32(3)	Mo3	S1	Mo1	71.23(2)
S2	Mo2	Mo1	56.25(2)	Mo2	S1	Mo1	71.45(3)
Br1	Mo2	Mo1	124.870(16)	S2	S3	Mo2	67.70(4)
Br2	Mo2	Mo1	136.317(16)	S2	Mo1	Mo2	56.44(2)

Table 7.16.3. [cont.] Bond Angles

Atom	Atom	Atom	Angle/°	Atom	Atom	Atom	Angle/°
Mo3	Mo2	Mo1	59.869(10)	Mo3	Mo1	Mo2	59.912(11)
N1	Mo1	N2	73.08(10)	S1	Mo3	S5	108.98(3)
N1	Mo1	S1	87.54(8)	S1	Mo3	S7	109.24(3)
N2	Mo1	S1	160.40(7)	S5	Mo3	S7	83.70(3)
N1	Mo1	S3	131.87(8)	S1	Mo3	S4	86.11(3)
N2	Mo1	S3	83.59(8)	S5	Mo3	S4	49.48(3)
S1	Mo1	S3	108.29(3)	S7	Mo3	S4	132.99(3)
N1	Mo1	S7	133.19(8)	S1	Mo3	S6	84.97(3)
N2	Mo1	S7	87.35(7)	S5	Mo3	S6	132.89(3)
S1	Mo1	S7	108.65(3)	S7	Mo3	S6	49.62(3)
S3	Mo1	S7	85.42(3)	S2	S3	Mo1	67.27(4)
N1	Mo1	S2	88.91(8)	Mo2	S3	Mo1	70.41(2)
N2	Mo1	S2	92.14(8)	S3	S2	Mo1	62.88(4)
S1	Mo1	S2	84.49(3)	S3	S2	Mo2	62.38(4)
S3	Mo1	S2	49.85(3)	Mo1	S2	Mo2	67.32(3)
S7	Mo1	S2	134.92(3)	S5	S4	Mo2	62.92(4)
N1	Mo1	S6	90.71(8)	S5	S4	Mo3	62.84(4)
N2	Mo1	S6	97.90(8)	Mo2	S4	Mo3	67.24(3)
S1	Mo1	S6	84.89(3)	S4	S5	Mo2	67.52(4)
S3	Mo1	S6	134.61(3)	S4	S5	Mo3	67.67(4)
S7	Mo1	S6	49.58(3)	Mo2	S5	Mo3	70.21(3)
S2	Mo1	S6	169.39(3)	S6	S7	Mo3	67.68(4)
N1	Mo1	Mo3	128.40(8)	S6	S7	Mo1	67.36(4)
N2	Mo1	Mo3	142.08(7)	Mo3	S7	Mo1	69.89(2)
S1	Mo1	Mo3	54.24(2)	C15	N1	C11	117.4(3)
S3	Mo1	Mo3	95.57(2)	C15	N1	Mo1	125.4(2)
S7	Mo1	Mo3	54.90(2)	C11	N1	Mo1	117.0(2)
S2	Mo1	Mo3	116.18(2)	C25	N2	C21	117.8(3)
S6	Mo1	Mo3	56.59(2)	C25	N2	Mo1	124.6(2)
N1	Mo1	Mo2	127.31(7)	C21	N2	Mo1	117.4(2)
N2	Mo1	Mo2	137.41(7)	N2	C21	C22	121.7(3)
S1	Mo1	Mo2	54.20(2)	N2	C21	C11	115.1(3)
S3	Mo1	Mo2	54.57(2)	N1	C11	C12	122.2(3)
S7	Mo1	Mo2	95.91(2)	N1	C11	C21	116.5(3)
S6	Mo1	Mo2	116.36(2)	N2	C25	C24	123.3(3)

7.2.4.10. STRUCTURE OF $(Bu_4N)[Mo_3S_7Br_4(dcmphen)\cdot Br]$, $(Bu_4N)[\mathbf{24}\cdot Br]$

Single crystals of compound $(Bu_4N)[\mathbf{24}\cdot Br]$ were obtained in a similar fashion to $(Bu_4N)[\mathbf{14}\cdot Br]$. The structure of $(Bu_4N)[\mathbf{24}\cdot Br]$ was refined in the monoclinic space group C2/c. All non-hydrogen atoms were refined anisotropically. Figure 7.17 shows its ORTEP representation with the atom numbering scheme. The bond distances of some adjacent carbon atoms in the Bu_4N^+ counterion (C107 – C108 and C115 – C116) were restrained to fixed values. A remaining high electronic density peak was modelled as an oxygen atom with a factor occupancy of 0.50. The crystallographic data collection parameters are given in Table 7.17.1.

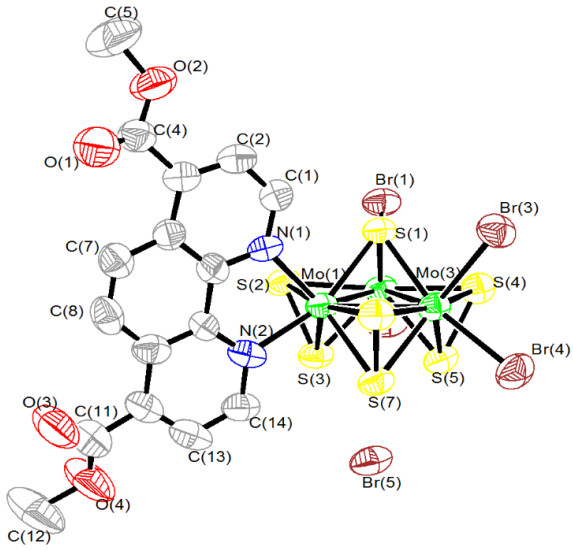

Figure 7.17. ORTEP representation (50 % probability ellipsoids) of the anionic trinuclear cluster $[\mathbf{24}\cdot Br]^-$ with the atom numbering scheme. Average distances (Å): Mo-Mo, 2.7507(17); Mo-(μ_3-S), 2.358(3); Mo-S_{ax}, 2.398(4); Mo-S_{eq}, 2.486(4); Mo-N, 2.221(11); Mo-Br, 2.6155(19); S_{ax}-Br, 3.06(9).

Table 7.17.1. Crystal Structure Data

Crystal Data			
Species	$(Bu_4N)[Mo_3S_7Br_4(dcmphen)\cdot Br]\cdot H_2O$		
Formula	$C_{32}H_{50}Br_5Mo_3N_3O_{4.5}S_7$	**Crystal system**	monoclinic
Space group	C2/c	**Formula weight**	1460.54
a (Å)	36.5632(14)	**α** (º)	90.00
b (Å)	13.1724(4)	**β** (º)	105.689
c (Å)	24.2562(12)	**γ** (º)	90.00
Z	8	**Vol** ($Å^3$)	11247.2(8)
Colour	red	**Crystal size** (mm)	0.3237 × 0.1727 × 0.0758
$\mathbf{d_{calc}}$ (mg/mm^3)	1.725	**λ** (Å)	0.71070
Absorption coefficient (mm^{-1})	4.504	**F (000)**	5696.0

Experimental Data			
Temperature (K)	298	**R(int)**	0.0596
Time per frame (s)	55	**R (σ)**	0.0784
2θ Range (º)	6.26 to 50	**Index ranges**	-42 ≤ h ≤ 43 -15 ≤ k ≤ 11 -28 ≤ l ≤ 28
Collected reflections	26951	**Independent reflections**	9880

Solution and Refinement			
Parameters	498	**GooF on F^2**	1.047
Restraints	2		
Final R1 ([I>2sigma(I)])	0.0766	**Final R1 (all data)**	0.1348
Final wR2 ([I>2sigma(I)])	0.2061	**Final wR2 (all data)**	0.2566
Max/Min peak ($e\cdot Å^{-3}$)	1.82 / -0.60	**Max. shift/σ**	0.001

$$\boldsymbol{R1} = \sum\big||\boldsymbol{F_0}| - |\boldsymbol{F_1}|\big| / \sum \boldsymbol{F_0} \qquad \boldsymbol{wR2} = \left[\sum\left[\boldsymbol{w}(\boldsymbol{F_0^2} - \boldsymbol{F_c^2})^2\right] / \sum\left[\boldsymbol{w}(\boldsymbol{F_0^2})^2\right]\right]^{\boldsymbol{1/2}}$$

Table 7.17.2. Bond Distances

Atom	Atom	Length/Å	Atom	Atom	Length/Å
Mo1	Mo2	2.7551(17)	Mo2	S4	2.480(4)
Mo1	Mo3	2.7393(17)	Mo3	Br3	2.6098(19)
Mo1	S1	2.364(4)	Mo3	Br4	2.6205(18)
Mo1	S7	2.398(3)	Mo3	S1	2.355(3)
Mo1	S3	2.406(4)	Mo3	S7	2.409(4)
Mo1	S2	2.480(4)	Mo3	S6	2.474(4)
Mo1	S6	2.488(4)	Mo3	S5	2.392(4)
Mo1	N2	2.230(12)	Mo3	S4	2.498(4)
Mo1	N1	2.211(10)	S7	S6	2.058(5)
Mo2	Mo3	2.7558(16)	S3	S2	2.052(5)
Mo2	Br1	2.6029(18)	S5	S4	2.043(5)
Mo2	Br2	2.6286(19)	N2	C14	1.323(17)
Mo2	S1	2.345(3)	N2	C15	1.359(16)
Mo2	S3	2.381(4)	N1	C16	1.378(17)
Mo2	S2	2.498(4)	N1	C1	1.330(17)
Mo2	S5	2.399(3)			

Table 7.17.3. Bond Angles

Atom	Atom	Atom	Angle/˚	Atom	Atom	Atom	Angle/˚
Mo3	Mo1	Mo2	60.21(4)	S1	Mo3	S5	108.67(12)
S1	Mo1	Mo2	53.87(9)	S1	Mo3	S4	85.91(13)
S1	Mo1	Mo3	54.37(9)	S7	Mo3	Mo1	55.08(9)
S1	Mo1	S7	109.34(13)	S7	Mo3	Mo2	96.51(10)
S1	Mo1	S3	107.76(13)	S7	Mo3	Br3	134.58(11)
S1	Mo1	S2	84.31(12)	S7	Mo3	Br4	82.98(10)
S1	Mo1	S6	84.72(12)	S7	Mo3	S6	49.82(12)
S7	Mo1	Mo2	96.80(10)	S7	Mo3	S4	132.76(13)
S7	Mo1	Mo3	55.46(10)	S6	Mo3	Mo1	56.72(9)
S7	Mo1	S3	86.27(12)	S6	Mo3	Mo2	116.72(10)
S7	Mo1	S2	135.66(13)	S6	Mo3	Br3	89.58(10)
S7	Mo1	S6	49.77(12)	S6	Mo3	Br4	94.71(10)
S3	Mo1	Mo2	54.43(10)	S6	Mo3	S4	170.99(13)
S3	Mo1	Mo3	96.00(11)	S5	Mo3	Mo1	94.43(10)
S3	Mo1	S2	49.63(11)	S5	Mo3	Mo2	55.00(9)
S3	Mo1	S6	135.49(12)	S5	Mo3	Br3	135.77(12)
S2	Mo1	Mo2	56.72(10)	S5	Mo3	Br4	83.73(10)
S2	Mo1	Mo3	116.75(11)	S5	Mo3	S7	83.63(13)
S2	Mo1	S6	169.01(13)	S5	Mo3	S6	133.04(14)
S6	Mo1	Mo2	116.28(10)	S5	Mo3	S4	49.33(13)
S6	Mo1	Mo3	56.26(10)	S4	Mo3	Mo1	116.24(10)
N2	Mo1	Mo2	136.4(3)	S4	Mo3	Mo2	56.07(10)
N2	Mo1	Mo3	143.0(3)	S4	Mo3	Br3	90.73(11)
N2	Mo1	S1	160.2(3)	S4	Mo3	Br4	94.24(10)
N2	Mo1	S7	87.6(3)	Mo2	S1	Mo1	71.61(10)
N2	Mo1	S3	82.8(3)	Mo2	S1	Mo3	71.79(10)
N2	Mo1	S2	90.6(3)	Mo3	S1	Mo1	70.95(9)
N2	Mo1	S6	99.5(3)	Mo1	S7	Mo3	69.46(10)
N1	Mo1	Mo2	129.0(3)	S6	S7	Mo1	67.37(14)
N1	Mo1	Mo3	126.7(3)	S6	S7	Mo3	66.73(15)
N1	Mo1	S1	87.8(3)	Mo2	S3	Mo1	70.27(10)
N1	Mo1	S7	130.0(3)	S2	S3	Mo1	67.05(15)
N1	Mo1	S3	133.9(3)	S2	S3	Mo2	68.15(15)
N1	Mo1	S2	91.2(3)	Mo1	S2	Mo2	67.21(10)

Table 7.17.3. [cont.] Bond Angles

Atom	Atom	Atom	Angle/˚	Atom	Atom	Atom	Angle/˚
N1	Mo1	S6	87.8(3)	S4	Mo2	Br1	91.69(10)
N1	Mo1	N2	73.1(4)	S4	Mo2	Br2	91.06(11)
Mo1	Mo2	Mo3	59.61(4)	S4	Mo2	S2	170.60(14)
Br1	Mo2	Mo1	123.51(6)	Mo1	Mo3	Mo2	60.18(4)
Br1	Mo2	Mo3	123.97(6)	Br3	Mo3	Mo1	123.98(6)
Br1	Mo2	Br2	80.80(6)	Br3	Mo3	Mo2	123.02(6)
Br2	Mo2	Mo1	140.23(7)	Br3	Mo3	Br4	81.04(6)
Br2	Mo2	Mo3	136.38(6)	Br4	Mo3	Mo1	137.86(7)
S1	Mo2	Mo1	54.53(9)	Br4	Mo3	Mo2	138.33(7)
S1	Mo2	Mo3	54.28(8)	S1	Mo3	Mo1	54.68(9)
S1	Mo2	Br1	81.94(9)	S1	Mo3	Mo2	53.93(9)
S1	Mo2	Br2	162.49(10)	S1	Mo3	Br3	82.03(9)
S1	Mo2	S3	109.27(14)	S1	Mo3	Br4	163.07(10)
S1	Mo2	S2	84.30(13)	S1	Mo3	S7	109.27(13)
S1	Mo2	S5	108.77(12)	S1	Mo3	S6	85.21(12)
S1	Mo2	S4	86.55(13)	S3	S2	Mo1	63.32(14)
S3	Mo2	Mo1	55.30(10)	S3	S2	Mo2	62.19(15)
S3	Mo2	Mo3	96.17(10)	Mo3	S6	Mo1	67.01(10)
S3	Mo2	Br1	133.64(10)	S7	S6	Mo1	62.86(13)
S3	Mo2	Br2	84.99(11)	S7	S6	Mo3	63.45(15)
S3	Mo2	S2	49.66(12)	Mo3	S5	Mo2	70.23(10)
S3	Mo2	S5	83.31(13)	S4	S5	Mo2	67.33(15)
S3	Mo2	S4	132.65(13)	S4	S5	Mo3	68.04(15)
S2	Mo2	Mo1	56.08(9)	Mo2	S4	Mo3	67.23(11)
S2	Mo2	Mo3	115.52(10)	S5	S4	Mo2	63.20(15)
S2	Mo2	Br1	89.13(9)	S5	S4	Mo3	62.63(15)
S2	Mo2	Br2	98.31(11)	C14	N2	Mo1	125.5(11)
S5	Mo2	Mo1	93.86(10)	C14	N2	C15	117.9(13)
S5	Mo2	Mo3	54.76(9)	C15	N2	Mo1	116.6(8)
S5	Mo2	Br1	137.06(12)	C16	N1	Mo1	116.4(8)
S5	Mo2	Br2	82.32(10)	C1	N1	Mo1	125.9(10)
S5	Mo2	S2	132.37(13)	C1	N1	C16	117.7(11)
S5	Mo2	S4	49.47(13)	N1	C16	C6	122.2(12)
S4	Mo2	Mo1	116.29(10)	N1	C16	C15	116.7(12)
S4	Mo2	Mo3	56.70(10)	N2	C14	C13	122.5(15)

7.2.4.11. STRUCTURE OF $(Bu_4N)[Mo_3S_7Cl_4(ppl)\cdot Cl]$, $(Bu_4N)[\mathbf{25}\cdot Cl]$

Single crystals of compound $(Bu_4N)[\mathbf{25}\cdot Cl]$ were obtained in a similar fashion to compound $(Bu_4N)[\mathbf{15}\cdot Cl]$. The structure of $(Bu_4N)[\mathbf{25}\cdot Cl]$ was refined in the monoclinic space group $P2_1/n$. Figure 7.18 shows its ORTEP representation with the atom numbering scheme. Dichloromethane and toluene were found cocrystallized with the cluster complex. Owing to disorder, the carbon atoms in the cocrystallized toluene molecule centered at C(30) were refined isotroprically. The same was done for two terminal atoms in the tetrabutylammonium counterion centered at N(100), that is, C(111) and C(112). For the latter atoms, hydrogens were not included. Additionally, the carbon atom C(112) was refined with a free occupancy and then constrained to the optimum occupancy value (*ca.* 0.30). With the exception of the atoms mentioned, all non-hydrogen atoms were refined anisotropically. The crystallographic data collection parameters are given in Table 7.18.1.

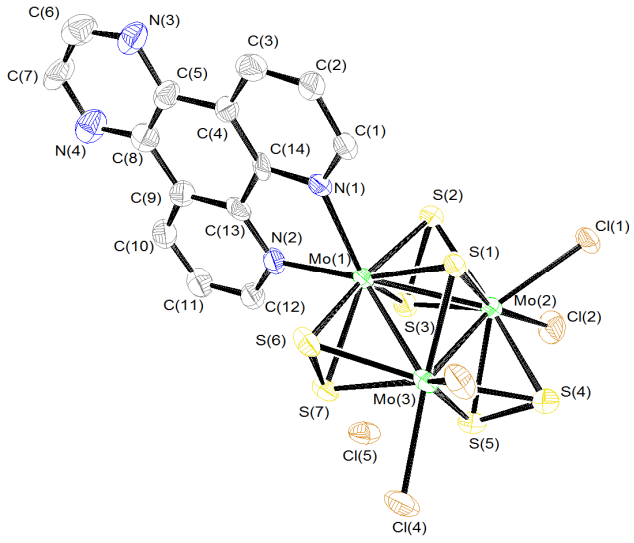

Figure 7.18. ORTEP representation (50 % probability ellipsoids) of the anionic trinuclear cluster **[25**·Cl**]**$^-$ with the atom numbering scheme. Average distances (Å): Mo-Mo, 2.7486(13); Mo-(μ_3-S), 2.357(3); Mo-S_{ax}, 2.395(3); Mo-S_{eq}, 2.485(3); Mo-N, 2.219(10); Mo-Cl, 2.460(3); S_{ax}-Cl, 2.90(4).

Table 7.18.1. Crystal Structure Data

Crystal Data			
Species	$(Bu_4N)[Mo_3S_7Cl_5(ppl)\cdot Cl]\cdot CH_3C_6H_5\cdot(1/2)CH_2Cl_2$		
Formula	$C_{37.2}H_{50.5}Cl_6Mo_3N_2S_7$	**Crystal system**	monoclinic
Space group	$P2_1/n$	**Formula weight**	1292.30
a (Å)	22.0304(4)	**α** (º)	90.00
b (Å)	14.6079(3)	**β** (º)	91.8093(17)
c (Å)	34.2716(8)	**γ** (º)	90.00
Z	8	**Vol** (Å^3)	11023.7(4)
Colour	reddish	**Crystal size** (mm)	0.4598 × 0.1175 × 0.0705
$\mathbf{d_{calc}}$ (g/cm^3)	1.557	**λ** (Å)	0.71070
Absorption coefficient (mm^{-1})	1.259	**F (000)**	2129.0
Experimental Data			
Temperature (K)	150	**R(int)**	0.0425
Time per frame (s)	80	**R (σ)**	0.0310
2θ Range (º)	5.71 to 50	**Index ranges**	-26 ≤ h ≤ 26 -17 ≤ k ≤ 17 -40 ≤ l ≤ 40
Collected reflections	105489	**Independent reflections**	19396
Solution and Refinement			
Parameters	1008	**GooF on F²**	1.195
Restraints	1		
Final R1 ([I>2sigma(I)])	0.0926	**Final R1 (all data)**	0.1022
Final wR2 ([I>2sigma(I)])	0.2196	**wR2 (all data)**	0.2272
Max/Min peak (e·Å^{-3})	2.79 / -1.16	**Max. shift/σ**	0.002

$$\boldsymbol{R1} = \sum\big||\boldsymbol{F_0}| - |\boldsymbol{F_1}|\big| / \sum \boldsymbol{F_0} \qquad \boldsymbol{wR2} = \left[\sum\left[\boldsymbol{w}(\boldsymbol{F_0^2} - \boldsymbol{F_c^2})^2\right] / \sum\left[\boldsymbol{w}(\boldsymbol{F_0^2})^2\right]\right]^{\boldsymbol{1/2}}$$

Table 7.18.2. Bond Distances

Atom	Atom	Length/Å	Atom	Atom	Length/Å
Mo1	Mo2	2.7492(13)	Mo2	S4	2.480(3)
Mo1	Mo3	2.7459(14)	Mo2	S5	2.393(3)
Mo1	S1	2.361(3)	Mo3	S1	2.353(3)
Mo1	S2	2.476(3)	Mo3	S7	2.397(3)
Mo1	S7	2.398(3)	Mo3	Cl3	2.457(3)
Mo1	S3	2.394(3)	Mo3	Cl4	2.461(3)
Mo1	S6	2.486(3)	Mo3	S4	2.493(3)
Mo1	N1	2.228(9)	Mo3	S5	2.396(3)
Mo1	N2	2.210(10)	Mo3	S6	2.484(3)
Mo2	Mo3	2.7506(13)	S2	S3	2.053(4)
Mo2	Cl1	2.450(3)	S7	S6	2.056(4)
Mo2	S1	2.357(3)	S4	S5	2.046(4)
Mo2	S2	2.491(3)	N3	C6	1.309(18)
Mo2	S3	2.392(3)	N3	C5	1.362(16)
Mo2	Cl2	2.472(3)	N1	C14	1.364(15)
Mo2	S4	2.480(3)	N1	C1	1.344(15)
Mo2	S5	2.393(3)	N4	C7	1.321(17)
Mo3	S1	2.353(3)	N4	C8	1.362(17)
Mo3	S7	2.397(3)	N2	C13	1.360(15)
Mo3	Cl3	2.457(3)	N2	C12	1.334(15)

Table 7.18.3. Bond Angles

Atom	Atom	Atom	Angle/°	Atom	Atom	Atom	Angle/°
Mo3	Mo1	Mo2	60.07(3)	S7	Mo3	Mo2	95.87(8)
S1	Mo1	Mo2	54.28(7)	S7	Mo3	Cl3	136.43(11)
S1	Mo1	Mo3	54.24(7)	S7	Mo3	Cl4	83.43(11)
S1	Mo1	S2	84.24(10)	S7	Mo3	S4	131.66(11)
S1	Mo1	S7	108.85(11)	S7	Mo3	S6	49.78(10)
S1	Mo1	S3	108.59(10)	Cl3	Mo3	Mo1	124.07(9)
S1	Mo1	S6	84.88(10)	Cl3	Mo3	Mo2	121.99(8)
S2	Mo1	Mo2	56.65(7)	Cl3	Mo3	Cl4	80.64(11)
S2	Mo1	Mo3	116.50(8)	Cl3	Mo3	S4	90.02(11)
S2	Mo1	S6	169.12(11)	Cl3	Mo3	S6	91.19(11)
S7	Mo1	Mo2	95.89(8)	Cl4	Mo3	Mo1	138.10(9)
S7	Mo1	Mo3	55.06(8)	Cl4	Mo3	Mo2	139.55(10)
S7	Mo1	S2	135.33(11)	Cl4	Mo3	S4	94.65(11)
S7	Mo1	S6	49.75(10)	Cl4	Mo3	S6	93.92(11)
S3	Mo1	Mo2	54.90(8)	S4	Mo3	Mo1	116.21(8)
S3	Mo1	Mo3	96.54(8)	S4	Mo3	Mo2	56.20(8)
S3	Mo1	S2	49.82(10)	S5	Mo3	Mo1	93.86(8)
S3	Mo1	S7	85.91(10)	S5	Mo3	Mo2	54.88(7)
S3	Mo1	S6	135.30(11)	S5	Mo3	S7	82.38(11)
S6	Mo1	Mo2	116.36(9)	S5	Mo3	Cl3	135.63(12)
S6	Mo1	Mo3	56.42(8)	S5	Mo3	Cl4	85.16(12)
N1	Mo1	Mo2	129.0(2)	S5	Mo3	S4	49.44(10)
N1	Mo1	Mo3	127.0(3)	S5	Mo3	S6	131.75(11)
N1	Mo1	S1	87.8(3)	S6	Mo3	Mo1	56.49(8)
N1	Mo1	S2	90.7(2)	S6	Mo3	Mo2	116.38(8)
N1	Mo1	S7	131.1(2)	S6	Mo3	S4	171.42(11)
N1	Mo1	S3	133.0(3)	Mo2	S1	Mo1	71.29(8)
N1	Mo1	S6	88.5(2)	Mo3	S1	Mo1	71.24(8)
N2	Mo1	Mo2	138.7(2)	Mo3	S1	Mo2	71.47(8)
N2	Mo1	Mo3	139.1(3)	Mo1	S2	Mo2	67.20(8)
N2	Mo1	S1	161.9(3)	S3	S2	Mo1	63.00(11)

Table 7.18.3. [cont.] Bond Angles

Atom	Atom	Atom	Angle/°	Atom	Atom	Atom	Angle/°
N2	Mo1	S2	95.1(3)	Cl2	Mo2	S4	94.46(12)
N2	Mo1	S7	84.3(3)	S4	Mo2	Mo1	116.54(8)
N2	Mo1	S3	84.1(3)	S4	Mo2	Mo3	56.64(8)
N2	Mo1	S6	95.1(3)	S4	Mo2	S2	170.76(11)
N2	Mo1	N1	74.1(4)	S5	Mo2	Mo1	93.85(8)
Mo1	Mo2	Mo3	59.90(3)	S5	Mo2	Mo3	55.00(8)
Cl1	Mo2	Mo1	124.98(8)	S5	Mo2	Cl1	134.39(11)
Cl1	Mo2	Mo3	121.40(8)	S5	Mo2	S2	132.48(11)
Cl1	Mo2	S2	91.90(10)	S5	Mo2	Cl2	84.24(11)
Cl1	Mo2	Cl2	81.71(11)	S5	Mo2	S4	49.62(10)
Cl1	Mo2	S4	88.53(10)	Mo1	Mo3	Mo2	60.02(3)
S1	Mo2	Mo1	54.44(7)	S1	Mo3	Mo1	54.51(7)
S1	Mo2	Mo3	54.21(7)	S1	Mo3	Mo2	54.32(7)
S1	Mo2	Cl1	81.53(10)	S1	Mo3	S7	109.14(10)
S1	Mo2	S2	84.02(10)	S1	Mo3	Cl3	81.24(10)
S1	Mo2	S3	108.83(10)	S1	Mo3	Cl4	161.82(12)
S1	Mo2	Cl2	163.15(11)	S1	Mo3	S4	86.69(10)
S1	Mo2	S4	86.92(10)	S1	Mo3	S5	109.00(10)
S1	Mo2	S5	109.00(11)	S1	Mo3	S6	85.10(10)
S2	Mo2	Mo1	56.14(7)	S7	Mo3	Mo1	55.08(7)
S2	Mo2	Mo3	115.83(8)	S3	S2	Mo2	62.65(12)
S3	Mo2	Mo1	54.98(7)	Mo3	S7	Mo1	69.86(8)
S3	Mo2	Mo3	96.47(8)	S6	S7	Mo1	67.34(12)
S3	Mo2	Cl1	136.61(11)	S6	S7	Mo3	67.29(12)
S3	Mo2	S2	49.67(10)	Mo2	S3	Mo1	70.12(9)
S3	Mo2	Cl2	82.44(11)	S2	S3	Mo1	67.18(12)
S3	Mo2	S4	132.85(10)	S2	S3	Mo2	67.68(12)
S3	Mo2	S5	83.36(11)	Mo2	S4	Mo3	67.16(8)
Cl2	Mo2	Mo1	137.21(9)	S5	S4	Mo2	62.96(12)
Cl2	Mo2	Mo3	138.88(9)	S5	S4	Mo3	62.81(12)
Cl2	Mo2	S2	94.74(11)	Mo2	S5	Mo3	70.12(8)

Table 7.18.3. [cont.] Bond Angles

Atom	Atom	Atom	Angle/˚	Atom	Atom	Atom	Angle/˚
S4	S5	Mo2	67.41(12)	N1	C14	C4	122.7(10)
S4	S5	Mo3	67.75(13)	N1	C14	C13	116.4(10)
Mo3	S6	Mo1	67.09(8)	N4	C7	C6	122.5(13)
S7	S6	Mo1	62.91(11)	N3	C6	C7	123.9(13)
S7	S6	Mo3	62.93(12)	N2	C13	C14	116.7(11)
C6	N3	C5	115.2(12)	N2	C13	C9	123.6(11)
C14	N1	Mo1	116.1(7)	N1	C1	C2	122.1(12)
C1	N1	Mo1	125.9(8)	N2	C12	C11	123.3(12)
C1	N1	C14	117.9(10)	N4	C8	C9	118.4(12)
C7	N4	C8	115.1(13)	N4	C8	C5	122.0(12)
C13	N2	Mo1	116.7(8)	N3	C5	C4	118.0(12)
C12	N2	Mo1	127.0(8)	N3	C5	C8	121.3(12)

7.2.4.12. STRUCTURE OF $(Bu_4N)[Mo_3S_7Cl_4(mphen)\cdot Cl]$, $(Bu_4N)[\mathbf{27}\cdot Cl]$

Single crystals of compound $(Bu_4N)[\mathbf{27}\cdot Cl]$ were grown by slow diffusion methods, by following the same approach used for cluster $(Bu_4N)[\mathbf{15}\cdot Cl]$. The structure of $(Bu_4N)[\mathbf{27}\cdot Cl]$ was refined in the orthorhombic space group Pbna. All non-hydrogen atoms were refined anisotropically. Figure 7.19 shows its ORTEP representation with the atom numbering scheme. In the tetrabutylammonium anion centered at N(100), one terminal carbon was found to be disordered over two positions with a 0.58/0.42 partial occupancy ratio. Owing to disorder, the omission of the hydrogen atoms in the carbon atoms C(115), C(116) and C(117) in this molecule was considered as justified. Furthermore the carbon atom C(112) was refined with a partial occupancy of 0.75. The crystal structure contains disordered solvent molecules. In spite of several attempts, the electronic density in this area could not be resolved satisfactorily. Therefore the contribution of the disordered solvent species was subtracted from the structure factor calculations by using the solvent mask[21] instruction in the program Olex2 1.2. The crystallographic data collection parameters are given in Table 7.19.1.

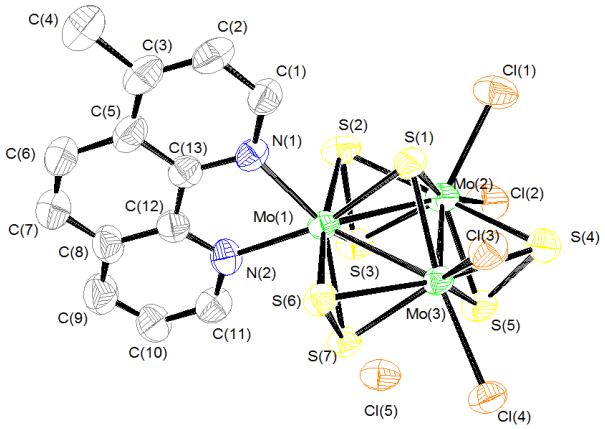

Figure 7.19. ORTEP representation (50 % probability ellipsoids) of the anionic trinuclear cluster $[\mathbf{27}\cdot Cl]^-$ with the atom numbering scheme. Average distances (Å): Mo-Mo, 2.7461(10); Mo-(μ_3-S), 2.354(3); Mo-S_{ax}, 2.388(2); Mo-S_{eq}, 2.494(2); Mo-N, 2.213(7); Mo-Cl, 2.463(2); S_{ax}-Cl, 2.920(11).

Table 7.19.1. Crystal Structure Data

Crystal Data			
Species	$(Bu_4N)[Mo_3S_7Cl_4(mphen)\cdot Cl]$		
Formula	$C_{28.8}H_{40.3}Cl_5Mo_3N_3S_7$	**Crystal system**	orthorhombic
Space group	Pbna	**Formula weight**	1117.38
a (Å)	12.7736(2)	**α** (º)	90
b (Å)	23.3575(5)	**β** (º)	90
c (Å)	36.7215	**γ** (º)	90
Z	8	**Vol** (Å^3)	10956.2(3)
Colour	reddish	**Crystal size** (mm)	0.224 × 0.138 × 0.124
$\mathbf{d_{calc}}$ (g/cm^3)	1.355	**λ** (Å)	0.71073
Absorption coefficient (mm^{-1})	1.207	**F (000)**	4454.0

Experimental Data			
Temperature (K)	200	**R(int)**	0.0548
Time per frame (s)	66	**R (σ)**	0.0367
2θ Range (º)	5.74 to 52	**Index ranges**	-16 ≤ h ≤ 16 -32 ≤ k ≤ 29 -48 ≤ l ≤ 48
Collected reflections	122345	**Independent reflections**	10753

Solution and Refinement			
Parameters	437	**GooF on F²**	1.087
Restraints	0		
Final R1 ([I>2sigma(I)])	0.0781	**Final R1 (all data)**	0.1855
Final wR2 ([I>2sigma(I)])	0.1855	**Final wR2 (all data)**	0.1944
Max/Min peak (e·Å^{-3})	1.83 / -0.75	**Max. shift/σ**	0.001

$$\boldsymbol{R1} = \sum\big||\boldsymbol{F_0}| - |\boldsymbol{F_1}|\big| / \sum \boldsymbol{F_0} \qquad \boldsymbol{wR2} = \left[\sum\left[\boldsymbol{w}(\boldsymbol{F_0^2} - \boldsymbol{F_c^2})^2\right] / \sum\left[\boldsymbol{w}(\boldsymbol{F_0^2})^2\right]\right]^{1/2}$$

Table 7.19.2. Bond Distances

Atom	Atom	Length/Å	Atom	Atom	Length/Å
Mo3	Mo1	2.7368(10)	Mo1	S6	2.485(2)
Mo3	Mo2	2.7534(10)	Mo2	Cl1	2.451(3)
Mo3	Cl3	2.436(2)	Mo2	Cl2	2.488(2)
Mo3	Cl4	2.475(2)	Mo2	S5	2.382(2)
Mo3	S5	2.380(2)	Mo2	S1	2.354(2)
Mo3	S7	2.382(2)	Mo2	S4	2.491(3)
Mo3	S1	2.357(2)	Mo2	S2	2.496(3)
Mo3	S4	2.487(2)	Mo2	S3	2.399(3)
Mo3	S6	2.500(2)	S5	S4	2.050(3)
Mo1	Mo2	2.7480(10)	S7	S6	2.051(3)
Mo1	S7	2.397(2)	S2	S3	2.051(3)
Mo1	S1	2.352(2)	N2	C11	1.336(11)
Mo1	S2	2.497(2)	N2	C12	1.374(11)
Mo1	S3	2.396(2)	N1	C13	1.372(11)
Mo1	N2	2.212(7)	N1	C1	1.344(11)
Mo1	N1	2.213(6)			

Table 7.19.3. Bond Angles

Atom	Atom	Atom	Angle/°	Atom	Atom	Atom	Angle/°
Mo1	Mo3	Mo2	60.07(3)	S5	Mo2	S3	83.38(9)
Cl3	Mo3	Mo1	122.36(6)	S1	Mo2	Mo3	54.28(5)
Cl3	Mo3	Mo2	123.36(6)	S1	Mo2	Mo1	54.25(5)
Cl3	Mo3	Cl4	81.68(8)	S1	Mo2	Cl1	82.30(8)
Cl3	Mo3	S4	91.46(8)	S1	Mo2	Cl2	163.98(9)
Cl3	Mo3	S6	89.43(7)	S1	Mo2	S5	108.63(8)
Cl4	Mo3	Mo1	139.79(6)	S1	Mo2	S4	85.96(8)
Cl4	Mo3	Mo2	136.72(6)	S1	Mo2	S2	84.96(8)
Cl4	Mo3	S4	92.00(8)	S1	Mo2	S3	108.72(8)
Cl4	Mo3	S6	96.39(8)	S4	Mo2	Mo3	56.36(6)
S5	Mo3	Mo1	94.45(6)	S4	Mo2	Mo1	115.98(6)
S5	Mo3	Mo2	54.73(6)	S4	Mo2	S2	170.74(8)
S5	Mo3	Cl3	137.31(8)	S2	Mo2	Mo3	116.16(6)
S5	Mo3	Cl4	82.61(8)	S2	Mo2	Mo1	56.62(6)
S5	Mo3	S7	82.45(8)	S3	Mo2	Mo3	95.68(6)
S5	Mo3	S4	49.77(8)	S3	Mo2	Mo1	54.97(5)
S5	Mo3	S6	131.70(8)	S3	Mo2	Cl1	136.34(10)
S7	Mo3	Mo1	55.32(5)	S3	Mo2	Cl2	83.48(9)
S7	Mo3	Mo2	95.47(6)	S3	Mo2	S4	132.86(8)
S7	Mo3	Cl3	134.76(8)	S3	Mo2	S2	49.50(8)
S7	Mo3	Cl4	84.65(8)	Mo3	S5	Mo2	70.65(6)
S7	Mo3	S4	132.05(8)	S4	S5	Mo3	67.84(9)
S7	Mo3	S6	49.60(7)	S4	S5	Mo2	67.90(9)
S1	Mo3	Mo1	54.39(6)	Mo3	S7	Mo1	69.87(6)
S1	Mo3	Mo2	54.18(5)	S6	S7	Mo3	68.20(8)
S1	Mo3	Cl3	81.22(7)	S6	S7	Mo1	67.42(8)
S1	Mo3	Cl4	162.71(8)	Mo1	S1	Mo3	71.07(6)
S1	Mo3	S5	108.63(8)	Mo1	S1	Mo2	71.46(6)
S1	Mo3	S7	109.37(8)	Mo2	S1	Mo3	71.54(6)
S1	Mo3	S4	85.97(8)	Mo3	S4	Mo2	67.16(6)
S1	Mo3	S6	85.92(7)	S5	S4	Mo3	62.38(8)
S4	Mo3	Mo1	116.51(7)	S5	S4	Mo2	62.40(9)
S4	Mo3	Mo2	56.48(6)	Mo2	S2	Mo1	66.79(6)
S4	Mo3	S6	171.61(8)	S3	S2	Mo1	62.67(9)
S6	Mo3	Mo1	56.44(5)	S3	S2	Mo2	62.80(10)

Table 7.19.3. [cont.] Bond Angles

Atom	Atom	Atom	Angle/°	Atom	Atom	Atom	Angle/°
S6	Mo3	Mo2	116.45(6)	Mo1	S6	Mo3	66.59(5)
Mo3	Mo1	Mo2	60.26(3)	S7	S6	Mo3	62.20(8)
S7	Mo1	Mo3	54.81(6)	S7	S6	Mo1	62.95(8)
S7	Mo1	Mo2	95.26(6)	S6	Mo1	Mo2	117.17(5)
S7	Mo1	S2	133.53(8)	S6	Mo1	S2	171.30(9)
S7	Mo1	S6	49.63(7)	Mo1	Mo2	Mo3	59.67(2)
S1	Mo1	Mo3	54.54(5)	Cl1	Mo2	Mo3	122.64(7)
S1	Mo1	Mo2	54.29(5)	Cl1	Mo2	Mo1	125.07(7)
S1	Mo1	S7	109.01(8)	Cl1	Mo2	Cl2	81.69(9)
S1	Mo1	S2	84.96(8)	Cl1	Mo2	S4	88.89(9)
S1	Mo1	S3	108.88(8)	Cl1	Mo2	S2	91.67(9)
S1	Mo1	S6	86.36(7)	Cl2	Mo2	Mo3	136.77(7)
S2	Mo1	Mo3	116.73(7)	Cl2	Mo2	Mo1	138.36(8)
S2	Mo1	Mo2	56.59(7)	Cl2	Mo2	S4	93.24(9)
S3	Mo1	Mo3	96.20(6)	Cl2	Mo2	S2	95.98(9)
S3	Mo1	Mo2	55.09(6)	S5	Mo2	Mo3	54.63(5)
S3	Mo1	S7	84.37(8)	S5	Mo2	Mo1	94.09(6)
S3	Mo1	S2	49.53(8)	S5	Mo2	Cl1	134.37(10)
S3	Mo1	S6	133.82(8)	S5	Mo2	Cl2	82.53(8)
N2	Mo1	Mo3	138.0(2)	S5	Mo2	S4	49.70(8)
N2	Mo1	Mo2	141.79(19)	S5	Mo2	S2	132.46(9)
N2	Mo1	S7	84.1(2)	Mo1	S3	Mo2	69.94(6)
N2	Mo1	S1	159.9(2)	S2	S3	Mo1	67.81(9)
N2	Mo1	S2	97.0(2)	S2	S3	Mo2	67.70(10)
N2	Mo1	S3	87.0(2)	C11	N2	Mo1	127.3(6)
N2	Mo1	N1	74.0(3)	C11	N2	C12	117.2(8)
N2	Mo1	S6	91.3(2)	C12	N2	Mo1	115.1(6)
N1	Mo1	Mo3	125.36(17)	N2	C11	C10	123.5(9)
N1	Mo1	Mo2	128.03(19)	C13	N1	Mo1	115.8(5)
N1	Mo1	S7	131.94(19)	C1	N1	Mo1	128.1(6)
N1	Mo1	S1	86.02(18)	C1	N1	C13	116.0(7)
N1	Mo1	S2	91.92(18)	N1	C13	C5	122.3(8)
N1	Mo1	S3	134.84(18)	N1	C13	C12	116.5(8)
N1	Mo1	S6	88.07(18)	N2	C12	C8	122.8(8)
S6	Mo1	Mo3	56.97(5)	N2	C12	C13	117.8(8)

7.2.4.13. STRUCTURE OF $(Bu_4N)[Mo_3S_7Br_4((COOMe)ppl)\cdot Br]$, $(Bu_4N)[\mathbf{28}\cdot Br]$

Single crystals of compound $(Bu_4N)[\mathbf{28}\cdot Br]$ were grown in a similar fashion to cluster $(Bu_4N)[\mathbf{14}\cdot Br]$. The structure of $(Bu_4N)[\mathbf{28}\cdot Br]$ was refined in the triclinic space group P-1. All non-hydrogen atoms were refined anisotropically. Figure 7.20 shows its ORTEP representation with the atom numbering scheme. In the terminal groups of the ligand coordinated to Mo(1B), disordering was observed. The oxygen atom O(1B), close to C(7B) was found to be disordered over two positions with partial occupancies of 0.52 and 0.48. The same situation was observed for O(2B), which is also connected to C(7B). In the latter case, the occupation factors of O(2B1) and O(2B2) resulted to be 0.48 and 0.52, respectively. The terminal methyl group C(8B) was found to be in two positions with a 0.55/0.45 occupancy ratio. Finally, the oxygen atom connected to C(10B) was also refined with two partial occupancies: 0.51 and 0.49. The crystallographic data collection parameters are given in Table 7.20.1.

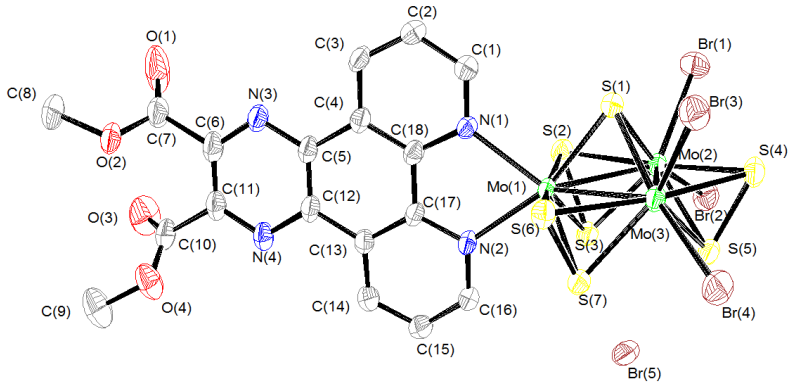

Figure 7.20. ORTEP representation (50 % probability ellipsoids) of the anionic trinuclear cluster $[\mathbf{28}\cdot Br]^-$ with the atom numbering scheme. Average distances (Å): Mo-Mo, 2.7448(4); Mo-(μ_3-S), 2.3628(10); Mo-S_{ax}, 2.3908(11); Mo-S_{eq}, 2.4831(11); Mo-N, 2.226(3); Mo-Br, 2.6114(6); S_{ax}-Br, 3.02(6).

Table 7.20.1. Crystal Structure Data

Crystal Data			
Species	$(Bu_4N)[Mo_3S_7Br_4((COOMe)_2ppl)\cdot Br]$		
Formula	$C_{34}H_{45.5}Br_5Mo_3N_5O_4S_7$	**Crystal system**	triclinic
Space group	P-1	**Formula weight**	1500.04
a (Å)	12.73580(10)	**α** (º)	84.9513(6)
b (Å)	19.92427(15)	**β** (º)	84.4925(7)
c (Å)	21.54206(14)	**γ** (º)	74.3313(7)
Z	4	**Vol** (Å^3)	5227.90(7)
Colour	red	**Crystal size** (mm)	0.2158 × 0.1827 × 0.1453
$\mathbf{d_{calc}}$ (g/cm^3)	1.906	**λ** (Å)	0.71073
Absorption coefficient (mm^{-1})	4.849	**F (000)**	2918.0

Experimental Data			
Temperature (K)	200	**R(int)**	0.0315
Time per frame (s)	24	**R (σ)**	0.0282
2θ Range (º)	5.68 to 59.09	**Index ranges**	- 17 ≤ h ≤ 17 - 25 ≤ k ≤ 26 - 29 ≤ l ≤ 29
Collected reflections	115507	**Independent reflections**	26425

Solution and Refinement			
Parameters	1068	**GooF on F²**	1.075
Restraints	0		
Final R1 ([I>2sigma(I)])	0.0417	**Final R1 (all data)**	0.0595
Final wR2 ([I>2sigma(I)])	0.1089	**Final wR2 (all data)**	0.1171
Max/Min peak (e·Å^{-3})	1.67 / -2.31	**Máx. shift./σ**	< 0.001

$$\boldsymbol{R1} = \sum||\boldsymbol{F_0}| - |\boldsymbol{F_c}||/\sum \boldsymbol{F_0} \qquad \boldsymbol{wR2} = \left[\sum\left[\boldsymbol{w}(\boldsymbol{F_0^2} - \boldsymbol{F_c^2})^2\right]/\sum\left[\boldsymbol{w}(\boldsymbol{F_0^2})^2\right]\right]^{1/2}$$

Table 7.20.2. Bond Distances

Atom	Atom	Length/Å	Atom	Atom	Length/Å
Mo1	Mo2	2.7448(4)	Mo2	S1	2.3610(11)
Mo1	Mo3	2.7494(4)	Mo3	Br3	2.6063(6)
Mo1	S2	2.4815(11)	Mo3	Br4	2.6224(6)
Mo1	S6	2.4857(11)	Mo3	S4	2.4798(11)
Mo1	S3	2.3854(11)	Mo3	S6	2.4842(10)
Mo1	S7	2.3991(10)	Mo3	S7	2.3948(10)
Mo1	S1	2.3660(10)	Mo3	S5	2.3917(11)
Mo1	N1	2.227(3)	Mo3	S1	2.3613(10)
Mo1	N2	2.224(3)	S2	S3	2.0529(14)
Mo2	Mo3	2.7402(5)	S4	S5	2.0328(16)
Mo2	Br1	2.5800(6)	S6	S7	2.0485(15)
Mo2	Br2	2.6370(6)	N1	C18	1.363(5)
Mo2	S2	2.4858(10)	N1	C1	1.333(5)
Mo2	S4	2.4818(11)	N2	C17	1.358(4)
Mo2	S3	2.3817(11)	N2	C16	1.347(5)
Mo2	S5	2.3921(10)			

Table 7.20.3. Bond Angles

Atom	Atom	Atom	Angle/°	Atom	Atom	Atom	Angle/°
Mo2	Mo1	Mo3	59.834(12)	S7	Mo3	Mo1	55.08(2)
S2	Mo1	Mo2	56.53(2)	S7	Mo3	Mo2	95.95(3)
S2	Mo1	Mo3	116.10(3)	S7	Mo3	Br3	137.60(3)
S2	Mo1	S6	168.51(4)	S7	Mo3	Br4	83.07(3)
S6	Mo1	Mo2	116.09(3)	S7	Mo3	S4	131.87(4)
S6	Mo1	Mo3	56.39(2)	S7	Mo3	S6	49.61(4)
S3	Mo1	Mo2	54.78(3)	S5	Mo3	Mo1	94.17(3)
S3	Mo1	Mo3	96.54(3)	S5	Mo3	Mo2	55.06(3)
S3	Mo1	S2	49.85(4)	S5	Mo3	Br3	134.22(3)
S3	Mo1	S6	135.52(4)	S5	Mo3	Br4	83.89(3)
S3	Mo1	S7	86.35(4)	S5	Mo3	S4	49.29(4)
S7	Mo1	Mo2	95.73(3)	S5	Mo3	S6	131.95(4)
S7	Mo1	Mo3	54.93(3)	S5	Mo3	S7	82.74(4)
S7	Mo1	S2	135.72(4)	S1	Mo3	Mo1	54.52(3)
S7	Mo1	S6	49.55(4)	S1	Mo3	Mo2	54.53(3)
S1	Mo1	Mo2	54.42(3)	S1	Mo3	Br3	80.84(3)
S1	Mo1	Mo3	54.36(3)	S1	Mo3	Br4	162.66(3)
S1	Mo1	S2	83.73(4)	S1	Mo3	S4	87.10(4)
S1	Mo1	S6	84.78(4)	S1	Mo3	S6	84.92(4)
S1	Mo1	S3	108.53(4)	S1	Mo3	S7	109.09(3)
S1	Mo1	S7	108.79(4)	S1	Mo3	S5	109.36(4)
N1	Mo1	Mo2	129.00(8)	Mo1	S2	Mo2	67.09(3)
N1	Mo1	Mo3	128.71(9)	S3	S2	Mo1	62.64(4)
N1	Mo1	S2	89.33(9)	S3	S2	Mo2	62.45(4)
N1	Mo1	S6	90.04(9)	Mo3	S4	Mo2	67.05(3)
N1	Mo1	S3	131.19(9)	S5	S4	Mo2	63.07(4)
N1	Mo1	S7	131.88(9)	S5	S4	Mo3	63.10(4)
N1	Mo1	S1	88.58(9)	Mo3	S6	Mo1	67.17(3)
N2	Mo1	Mo2	137.61(9)	S7	S6	Mo1	63.02(4)
N2	Mo1	Mo3	139.25(8)	S7	S6	Mo3	62.93(4)
N2	Mo1	S2	94.71(9)	Mo2	S3	Mo1	70.31(3)
N2	Mo1	S6	96.14(9)	S2	S3	Mo1	67.51(4)
N2	Mo1	S3	83.05(9)	S2	S3	Mo2	67.72(4)
N2	Mo1	S7	84.49(9)	Mo3	S7	Mo1	69.99(3)
N2	Mo1	S1	162.49(8)	S6	S7	Mo1	67.43(4)

Table 7.20.3. [cont.] Bond Angles

Atom	Atom	Atom	Angle/°	Atom	Atom	Atom	Angle/°
N2	Mo1	N1	73.95(11)	S1	Mo2	S3	108.82(4)
Mo3	Mo2	Mo1	60.166(12)	S1	Mo2	S5	109.36(4)
Br1	Mo2	Mo1	127.047(18)	Mo2	Mo3	Mo1	60.001(12)
Br1	Mo2	Mo3	122.007(19)	Br3	Mo3	Mo1	124.579(17)
Br1	Mo2	Br2	81.099(19)	Br3	Mo3	Mo2	121.000(18)
Br2	Mo2	Mo1	135.577(19)	Br3	Mo3	Br4	81.867(19)
Br2	Mo2	Mo3	138.919(18)	Br4	Mo3	Mo1	137.887(19)
S2	Mo2	Mo1	56.38(3)	Br4	Mo3	Mo2	138.53(2)
S2	Mo2	Mo3	116.28(3)	S4	Mo3	Mo1	116.51(3)
S2	Mo2	Br1	92.64(3)	S4	Mo3	Mo2	56.51(3)
S2	Mo2	Br2	93.59(3)	S4	Mo3	Br3	88.58(3)
S4	Mo2	Mo1	116.60(3)	S4	Mo3	Br4	93.82(3)
S4	Mo2	Mo3	56.44(3)	S4	Mo3	S6	171.67(4)
S4	Mo2	Br1	87.57(3)	S6	Mo3	Mo1	56.44(3)
S4	Mo2	Br2	95.62(3)	S6	Mo3	Mo2	116.31(3)
S4	Mo2	S2	170.71(4)	S6	Mo3	Br3	92.49(3)
S3	Mo2	Mo1	54.91(3)	S6	Mo3	Br4	94.51(3)
S3	Mo2	Mo3	96.87(3)	S6	S7	Mo3	67.46(4)
S3	Mo2	Br1	136.69(3)	Mo3	S5	Mo2	69.89(3)
S3	Mo2	Br2	80.86(3)	S4	S5	Mo2	67.67(4)
S3	Mo2	S2	49.83(3)	S4	S5	Mo3	67.61(5)
S3	Mo2	S4	133.19(4)	Mo2	S1	Mo1	70.99(3)
S3	Mo2	S5	84.08(4)	Mo2	S1	Mo3	70.94(3)
S5	Mo2	Mo1	94.28(3)	Mo3	S1	Mo1	71.12(3)
S5	Mo2	Mo3	55.05(3)	C18	N1	Mo1	115.6(2)
S5	Mo2	Br1	132.38(3)	C1	N1	Mo1	127.0(3)
S5	Mo2	Br2	84.05(3)	C1	N1	C18	117.4(3)
S5	Mo2	S2	133.40(4)	C17	N2	Mo1	116.3(3)
S5	Mo2	S4	49.26(4)	C16	N2	Mo1	126.0(2)
S1	Mo2	Mo1	54.59(3)	C16	N2	C17	117.6(3)
S1	Mo2	Mo3	54.54(3)	N1	C18	C4	122.4(4)
S1	Mo2	Br1	83.09(3)	N1	C18	C17	117.5(3)
S1	Mo2	Br2	163.83(3)	N1	C1	C2	123.3(4)
S1	Mo2	S2	83.74(4)	N2	C17	C18	116.6(3)
S1	Mo2	S4	87.06(4)	N2	C17	C13	122.1(4)

7.2.5. STRUCTURE OF HETEROLEPTIC MOLYBDENUM CLUSTERS WITH DIIMINE AND SULFUR DONOR LIGANDS

7.2.5.1. STRUCTURE OF $[Mo_3S_7(dmphen)(dtc)_2 \cdot Br](PF_6)$, ($[32 \cdot Br](PF_6)$)

Single crystals of compound [**32**·Br](PF_6) were obtained by the slow evaporation of a $CHCl_3$ solution of the sample. The structure of [**32**·Br](PF_6) was refined in the monoclinic space group $P2_1/n$. All non-hydrogen atoms were refined anisotropically. Figure 7.21 shows its ORTEP representation with the atom numbering scheme. The terminal carbon atoms of the dtc^- ligand coordinated to Mo(3) were found to be disordered over two positions with relative occupancies of 0.70 and 0.30. The PF_6^- anion was also found to be disordered over two close positions with a 0.5/0.5 occupancy ratio. Chloroform was found cocrystallized with the cluster complex. This solvent molecule has disordering over two positions with a 0.7/0.3 ratio. The crystallographic data collection parameters are given in Table 7.21.1.

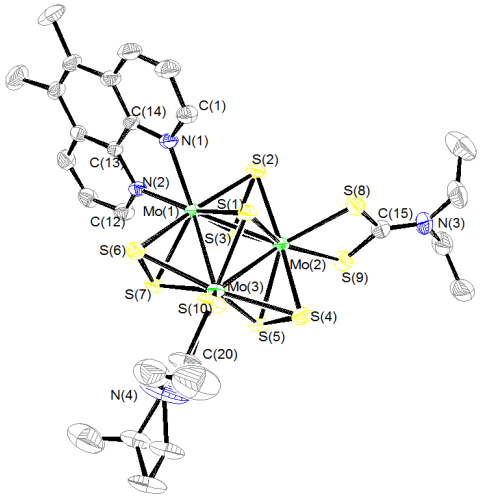

Figure 7.21. ORTEP representation (50 % probability ellipsoids) of the anionic trinuclear cluster $[\mathbf{32}]^{2+}$ with the atom numbering scheme. The bromide anion has been omitted for clarity. Average distances (Å): Mo-Mo, 2.7248(7); Mo-(μ_3-S), 2.3735(16); Mo-S_{ax}, 2.4021(16); Mo-S_{eq}, 2.4869(17); Mo-N, 2.216(5); Mo-S_{ligand}, 2.4933(17); S_{ax}-Br, 2.98(4).

Table 7.21.1. Crystal Structure Data

Crystal Data			
Species	$[Mo_3S_7(dtc)_2(dmphen)\cdot Br](PF_6)\cdot CHCl_3$		
Formula	$C_{27}H_{35}BrCl_9F_6Mo_3N_4PS_{11}$	**Crystal system**	monoclinic
Space group	$P2_1/n$	**Formula weight**	1600.00
a (Å)	19.779	**α** (º)	90.0
b (Å)	14.7004(19)	**β** (º)	111.490(4)
c (Å)	19.957(3)	**γ** (º)	90.0
Z	4	**Vol** (Å^3)	5399.3
Colour	yellowish	**Crystal size** (mm)	0.29 × 0.18 × 0.07
$\mathbf{d_{calc}}$ (g/cm^3)	1.968	**λ** (Å)	0.71073
Absorption coefficient (mm^{-1})	2.377	**F (000)**	3136.0
Experimental Data			
Temperature (K)	243	**R(int)**	0.0585
Time per frame (s)	25	**R (σ)**	0.0725
2θ Range (º)	3.54 to 56.56	**Index ranges**	- 26 ≤ h ≤ 26 - 19 ≤ k ≤ 16 - 26 ≤ l ≤ 18
Collected reflections	38102	**Independent reflections**	13399
Solution and Refinement			
Parameters	717	**GooF on F²**	1.051
Restraints	216		
Final R1 ([I>2sigma(I)])	0.0560	**Final R1 (all data)**	0.0970
Final wR2 ([I>2sigma(I)])	0.1378	**Final wR2 (all data)**	0.1563
Max/Min peak (e·Å^{-3})	1.85 / -1.12	**Máx. shift./σ**	0.001

$$R1 = \sum||F_0| - |F_c||/\sum F_0 \qquad wR2 = \left[\sum[w(F_0^2 - F_c^2)^2]/\sum[w(F_0^2)^2]\right]^{1/2}$$

Table 7.21.2. Bond Distances

Atom	Atom	Length/Å	Atom	Atom	Length/Å
Mo1	Mo3	2.7297(7)	Mo2	S2	2.4991(16)
Mo1	Mo2	2.7226(7)	Mo2	S3	2.3912(16)
Mo1	S1	2.3896(16)	Mo2	S4	2.4907(17)
Mo1	S2	2.4818(16)	Mo2	S5	2.4083(16)
Mo1	S3	2.4072(16)	Mo2	S8	2.4780(18)
Mo1	S7	2.4112(16)	S9	C15	1.723(7)
Mo1	S6	2.4703(17)	S2	S3	2.052(2)
Mo1	N1	2.221(5)	S11	C20	1.708(7)
Mo1	N2	2.211(5)	S4	S5	2.056(2)
Mo3	Mo2	2.7222(7)	S7	S6	2.055(2)
Mo3	S1	2.3652(16)	S10	C20	1.725(7)
Mo3	S11	2.5117(17)	S8	C15	1.725(7)
Mo3	S4	2.4910(17)	N1	C14	1.374(8)
Mo3	S7	2.3923(17)	N1	C1	1.330(8)
Mo3	S6	2.4883(17)	N3	C15	1.305(8)
Mo3	S10	2.4756(17)	N2	C12	1.332(8)
Mo3	S5	2.4022(16)	N2	C13	1.370(8)
Mo2	S9	2.5077(17)	N4	C20	1.313(9)
Mo2	S1	2.3657(16)			

Table 7.21.3. Bond Angles

Atom	Atom	Atom	Angle/°	Atom	Atom	Atom	Angle/°
Mo2	Mo1	Mo3	59.904(19)	S3	Mo2	S8	131.77(6)
S1	Mo1	Mo3	54.55(4)	S4	Mo2	Mo1	116.97(4)
S1	Mo1	Mo2	54.66(4)	S4	Mo2	Mo3	56.88(4)
S1	Mo1	S2	85.44(6)	S4	Mo2	S9	93.08(6)
S1	Mo1	S3	109.27(6)	S4	Mo2	S2	170.83(6)
S1	Mo1	S7	109.03(5)	S5	Mo2	Mo1	96.02(4)
S1	Mo1	S6	84.90(6)	S5	Mo2	Mo3	55.43(4)
S2	Mo1	Mo3	116.94(4)	S5	Mo2	S9	86.61(6)
S2	Mo1	Mo2	57.17(4)	S5	Mo2	S2	134.05(6)
S3	Mo1	Mo3	96.15(4)	S5	Mo2	S4	49.60(6)
S3	Mo1	Mo2	55.15(4)	S5	Mo2	S8	133.36(6)
S3	Mo1	S2	49.60(5)	S8	Mo2	Mo1	126.99(5)
S3	Mo1	S7	85.58(6)	S8	Mo2	Mo3	127.56(5)
S3	Mo1	S6	135.05(6)	S8	Mo2	S9	70.44(6)
S7	Mo1	Mo3	55.04(4)	S8	Mo2	S2	89.39(6)
S7	Mo1	Mo2	96.04(4)	S8	Mo2	S4	90.54(6)
S7	Mo1	S2	134.90(6)	C15	S9	Mo2	87.8(2)
S7	Mo1	S6	49.77(5)	Mo3	S1	Mo1	70.07(4)
S6	Mo1	Mo3	56.92(4)	Mo3	S1	Mo2	70.26(4)
S6	Mo1	Mo2	116.67(4)	Mo2	S1	Mo1	69.85(4)
S6	Mo1	S2	170.34(6)	Mo1	S2	Mo2	66.27(4)
N1	Mo1	Mo3	127.76(13)	S3	S2	Mo1	63.31(6)
N1	Mo1	Mo2	127.55(13)	S3	S2	Mo2	62.49(6)
N1	Mo1	S1	86.79(14)	C20	S11	Mo3	87.6(2)
N1	Mo1	S2	89.36(13)	Mo2	S3	Mo1	69.14(4)
N1	Mo1	S3	132.17(13)	S2	S3	Mo1	67.09(6)
N1	Mo1	S7	132.55(14)	S2	S3	Mo2	67.96(6)
N1	Mo1	S6	89.70(13)	Mo2	S4	Mo3	66.25(4)
N2	Mo1	Mo3	137.26(13)	S5	S4	Mo3	62.93(6)
N2	Mo1	Mo2	140.86(13)	S5	S4	Mo2	63.12(6)
N2	Mo1	S1	161.09(14)	Mo3	S7	Mo1	69.26(4)
N2	Mo1	S2	96.69(13)	S6	S7	Mo1	66.61(6)
N2	Mo1	S3	85.85(13)	S6	S7	Mo3	67.56(7)
N2	Mo1	S7	82.74(13)	Mo1	S6	Mo3	66.80(4)
N2	Mo1	S6	92.32(13)	S7	S6	Mo1	63.62(6)

Table 7.21.3. [cont.] Bond Angles

Atom	Atom	Atom	Angle/°	Atom	Atom	Atom	Angle/°
N2	Mo1	N1	74.47(19)	S5	Mo3	S6	134.01(6)
Mo2	Mo3	Mo1	59.920(19)	S5	Mo3	S10	134.83(6)
S1	Mo3	Mo1	55.39(4)	Mo3	Mo2	Mo1	60.176(19)
S1	Mo3	Mo2	54.88(4)	S7	S6	Mo3	62.70(6)
S1	Mo3	S11	156.22(6)	C20	S10	Mo3	88.4(2)
S1	Mo3	S4	85.29(6)	Mo3	S5	Mo2	68.93(4)
S1	Mo3	S7	110.51(5)	S4	S5	Mo3	67.42(7)
S1	Mo3	S6	85.02(5)	S4	S5	Mo2	67.29(7)
S1	Mo3	S10	86.06(6)	C15	S8	Mo2	88.7(2)
S1	Mo3	S5	109.95(6)	C14	N1	Mo1	114.7(4)
S11	Mo3	Mo1	141.84(5)	C1	N1	Mo1	127.3(4)
S11	Mo3	Mo2	141.72(5)	S9	Mo2	Mo1	142.48(5)
S4	Mo3	Mo1	116.71(4)	S9	Mo2	Mo3	140.98(5)
S4	Mo3	Mo2	56.87(4)	S1	Mo2	Mo1	55.49(4)
S4	Mo3	S11	94.06(6)	S1	Mo2	Mo3	54.86(4)
S7	Mo3	Mo1	55.70(4)	S1	Mo2	S9	156.11(6)
S7	Mo3	Mo2	96.50(4)	S1	Mo2	S2	85.56(5)
S7	Mo3	S11	86.93(6)	S1	Mo2	S3	110.63(6)
S7	Mo3	S4	134.09(6)	S1	Mo2	S4	85.29(6)
S7	Mo3	S6	49.75(6)	S1	Mo2	S5	109.73(6)
S7	Mo3	S10	130.16(6)	S1	Mo2	S8	85.73(6)
S7	Mo3	S5	84.68(6)	S2	Mo2	Mo1	56.56(4)
S6	Mo3	Mo1	56.28(4)	S2	Mo2	Mo3	116.61(4)
S6	Mo3	Mo2	116.06(4)	S2	Mo2	S9	95.53(6)
S6	Mo3	S11	95.16(6)	S3	Mo2	Mo1	55.71(4)
S6	Mo3	S4	170.27(6)	S3	Mo2	Mo3	96.73(4)
S10	Mo3	Mo1	126.17(5)	S3	Mo2	S9	87.48(6)
S10	Mo3	Mo2	128.96(5)	S3	Mo2	S2	49.55(5)
S10	Mo3	S11	70.20(6)	S3	Mo2	S4	134.25(6)
S10	Mo3	S4	92.42(6)	S3	Mo2	S5	84.86(6)
S10	Mo3	S6	87.79(6)	C1	N1	C14	118.0(5)
S5	Mo3	Mo1	95.98(4)	C12	N2	C13	118.0(5)
S5	Mo3	Mo2	55.64(4)	C13	N2	Mo1	116.3(4)
S5	Mo3	S11	86.99(6)	S11	C20	S10	113.3(4)
S5	Mo3	S4	49.65(6)	N4	C20	S11	123.7(6)

Table 7.21.3. [cont.] Bond Angles

Atom	Atom	Atom	Angle/°	Atom	Atom	Atom	Angle/°
N3	C15	S8	123.7(6)	N4	C20	S10	122.9(5)
N1	C14	C13	118.3(5)	S9	C15	S8	113.0(4)
N1	C13	C14	116.1(5)	N3	C15	S9	123.3(6)

7.2.6. STRUCTURE OF DIALKYLTIN DITHIOLENE COMPLEXES

7.2.6.1. STRUCTURE OF $Me_2Sn(BPyDTS_2)$, (3)

Single crystals of complex **3** suitable for X-ray diffraction were obtained by slowly diffusing hexane into a solution of the compound in tetrahydrofuran under a N_2 atmosphere. The structure of compound **3** was refined in the monoclinic space group $P2_1$. All non-hydrogen atoms were refined anisotropically. Figure 7.22 shows its ORTEP representation with the atom numbering scheme. Co-crystallized with the tin complex, a tetrahydrofuran molecule was found. The oxygen atom in the THF molecule was found to be disordered, and consequently was modelled over two positions with a constraint to the total occupancy of one. The hydrogen atoms for the CH_2 groups in the solvent molecule were not included owing to disorder. The crystallographic data collection parameters are given in Table 7.22.1.

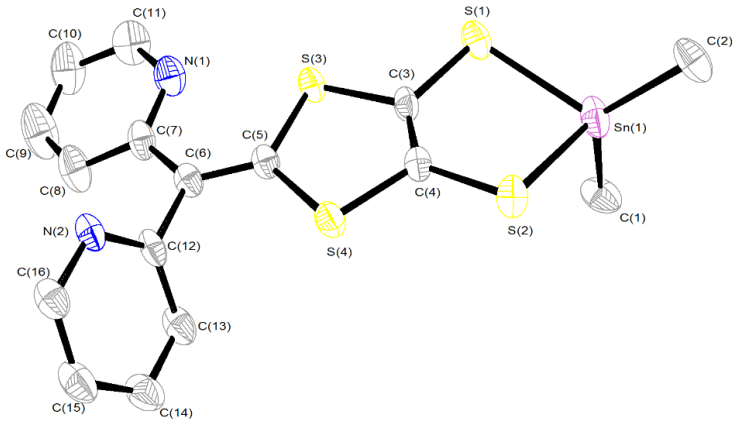

Figure 7.22. ORTEP representation (50 % probability ellipsoids) of the complex **3** with the atom numbering scheme. Average distances (Å): Sn-C, 2.116(5); Sn-S, 2.4881(13).

Table 7.22.1. Crystal Structure Data

Crystal Data			
Species	$Me_2Sn(BpyDTS_2)\cdot THF$		
Formula	$C_{20}H_{15}N_2OS_4Sn$	**Crystal system**	monoclinic
Space group	$P2_1$	**Formula weight**	546.27
a (Å)	6.90185(15)	**α** (º)	90
b (Å)	15.7670(4)	**β** (º)	93.706(2)
c (Å)	10.3916(3)	**γ** (º)	90
Z	2	**Vol** (Å^3)	1128.46(5)
Colour	yellow	**Crystal size** (mm)	0.429 × 0.196 × 0.085
$\mathbf{d_{calc}}$ (mg/mm^3)	1.608	**λ** (Å)	0.71073
Absorption coefficient (mm^{-1})	1.515	**F (000)**	542.0

Experimental Data			
Temperature (K)	200	**R(int)**	0.0316
Time per frame (s)	2	**R (σ)**	0.0417
2θ Range (º)	5.92 to 57.82	**Index ranges**	-9 ≤ h ≤ 9 -21 ≤ k ≤ 21 -13 ≤ l ≤ 12
Collected reflections	12798	**Independent reflections**	5281

Solution and Refinement			
Parameters	264	**GooF on F²**	1.072
Restraints	1		
Final R1 ([I>2sigma(I)])	0.0338	**Final R1 (all data)**	0.0406
Final wR2 ([I>2sigma(I)])	0.0729	**Final wR2 (all data)**	0.0791
Max/Min peak (e·Å^{-3})	0.66 / -0.82	**Max. shift/σ**	<0.001

$$\boldsymbol{R1} = \sum||\boldsymbol{F_0}| - |\boldsymbol{F_c}||/\sum \boldsymbol{F_0} \qquad \boldsymbol{wR2} = \left[\sum\left[\boldsymbol{w}(\boldsymbol{F_0^2} - \boldsymbol{F_c^2})^2\right]/\sum\left[\boldsymbol{w}(\boldsymbol{F_0^2})^2\right]\right]^{1/2}$$

Table 7.22.2. Bond Distances

Atom	Atom	Length/Å	Atom	Atom	Length/Å
Sn1	S2	2.5196(12)	N1	C11	1.346(6)
Sn1	S1	2.4607(11)	C6	C12	1.491(5)
Sn1	C2	2.116(4)	C6	C7	1.461(5)
Sn1	C1	2.120(4)	C13	C12	1.389(6)
S3	C3	1.764(4)	C13	C14	1.371(6)
S3	C5	1.756(4)	C12	N2	1.351(5)
S4	C4	1.762(4)	C7	C8	1.389(6)
S4	C5	1.756(4)	N2	C16	1.336(5)
S2	C4	1.749(4)	C16	C15	1.376(6)
S1	C3	1.753(4)	C11	C10	1.370(7)
C3	C4	1.329(5)	C15	C14	1.377(6)
C5	C6	1.366(5)	C8	C9	1.375(7)
N1	C7	1.350(5)	C10	C9	1.370(8)

Table 7.22.3. Bond Angles

Atom	Atom	Atom	Angle/°	Atom	Atom	Atom	Angle/°
S1	Sn1	S2	87.62(3)	C11	N1	C7	117.9(4)
C2	Sn1	S2	102.41(11)	C5	C6	C12	118.6(3)
C2	Sn1	S1	116.34(13)	C5	C6	C7	122.3(3)
C2	Sn1	C1	130.28(19)	C7	C6	C12	119.1(3)
C1	Sn1	S2	102.55(12)	C14	C13	C12	120.0(4)
C1	Sn1	S1	107.00(15)	C13	C12	C6	121.0(3)
C5	S3	C3	95.48(18)	N2	C12	C6	117.7(3)
C5	S4	C4	96.73(18)	N2	C12	C13	121.3(4)
C4	S2	Sn1	95.28(13)	N1	C7	C6	116.1(3)
C3	S1	Sn1	97.11(13)	N1	C7	C8	121.3(4)
S1	C3	S3	115.1(2)	C8	C7	C6	122.5(4)
C4	C3	S3	118.4(3)	C16	N2	C12	117.6(3)
C4	C3	S1	126.3(3)	N2	C16	C15	123.8(4)
S2	C4	S4	116.0(2)	N1	C11	C10	123.2(5)
C3	C4	S4	115.8(3)	C16	C15	C14	118.4(4)
C3	C4	S2	128.1(3)	C13	C14	C15	118.7(4)
S3	C5	S4	113.5(2)	C9	C8	C7	119.5(5)
C6	C5	S3	125.4(3)	C11	C10	C9	118.7(4)
C6	C5	S4	121.1(3)	C10	C9	C8	119.3(5)

7.3. PHOTOPHYSICAL STUDIES

7.3.1. LUMINESCENT PROPERTIES

The luminescence behavior of compounds **3**, $(Et_4N)_2$[**4**] and $(Et_4N)_2$[**5**] was assessed in collaboration with Dr. K. Brylev and Prof. N. Kitamura at Hokkaido University (Sapporo, Japan). Emission measurements were carried out at 298 K, and acetonitrile solutions were deaerated by purging an Ar-gas stream for 30 min. The samples were excited by 532-nm laser pulses (6 ns duration, LOTIS TII, LS-2137/3). Corrected emission spectra were recorded on a red-sensitive multichannel photodetector (Hamamatsu Photonics, PMA-12). The emission quantum yields (ϕ_{em}) of the samples were estimated by using $[Ru(bpy)_3](PF_6)_2$ as a standard: λ_{em} = 0.095 in deaerated acetonitrile.[22,23]

For clusters $Mo_3S_7X_4$(IPDOP), (X = Br; **12**, or Cl; **13**), the luminescent properties were studied at Universitat Jaume I (Castelló, Spain) in collaboration with Prof. F. Galindo. Emission measurements were carried out at 298 K in air. Steady-state fluorescence spectra were recorded on a Spex Fluorog 3-11 fluorimeter equipped with a 450 W xenon lamp, and the emission spectra were corrected. The emission quantum yields (ϕ_{em}) of the samples were estimated by using quinine sulfate as a standard (ϕ_{em} = 0.546 in 0.5 M H_2SO_4),[24] and using the formula $\phi_s=(\phi_r \cdot A_r \cdot I_s \cdot n_s^2)/(A_s \cdot I_r \cdot n_r^2)$, where A_s and A_r are the absorbance of the sample and the reference; I_s and I_r are the corresponding integrated emissions, and n_s and n_r are the refractive indexes of the solvent of the sample and the reference. Luminescence lifetimes were recorded at 298 K on a single photon counting Jobin Yvon Horiba IBH-5000-U fluorimeter by using a 304 nm LED as a light source (pulsewidth < 1.2 ns). Data were fitted to a monoexponential model using the IBM DAS6 emission decay analysis software.

7.3.2. OPTICAL LIMITING BEHAVIOR

The optical nonlinearities of clusters $(Et_4N)_2$[**4**], **18** – **21** and **29** – **31** were studied at the Research School of Chemistry (RSC), Australian National University (ANU) by the group headed by Prof. M. Humphrey. Optical measurements were performed on dimethylformamide solutions of samples placed in 1 mm glass cells. Linear optical spectra were obtained on a Varian Cary 5 spectrophotometer over the spectral range 270 - 800 nm. The light source used for the determination of power limiting properties was an Opolette (HE) 355 II (Opotek), located at RSC, ANU. This is a single-housing tuneable ns laser system in which a flashlamp-pumped Nd:YAG laser (355 nm pump wavelength, 20 Hz repetition rate, 5 ns pulse length) pumps an OPO (tuning range 410-2200 nm, peak OPO energy 10 mJ, spectral linewidth 4 - 7 cm^{-1}). The optical power limiting experiments were performed on solutions of concentrations 0.07 - 0.35% w/w. The properties were assessed by the open-aperture Z-scan technique at 570 nm at which the samples had low, but non-zero, linear absorption (corresponding to ε values of 307 - 4411 M^{-1} cm^{-1} at the measurement wavelength). The data from the power limiting curves obtained by the open-aperture Z-scan technique were then converted into transmittance-fluence plots assuming a Gaussian character of the beam, the w_0 parameter of the beam being determined from closed-aperture Z-scan results.

7.3.3. PHOTOCATALYSIS

Spectroscopic and electrochemical studies were carried out in collaboration with Prof. R. Gómez and T. Lana at University of Alacant. UV/Vis diffuse reflectance spectra of powdered samples were recorded either on a Shimadzu UV-2450 or a Shimadzu UV-2401 PC spectrophotometer equipped with integrating spheres. The high-resolution XPS spectra were acquired using a K-Alpha spectrometer from Thermo-Scientific.

The electrodes were prepared by the application of an aqueous slurry of TiO_2 Degussa P25 nanoparticles (composed of 1.3 mL water + 30 mL acetylacetone + 30 mL Triton X-100) on FTO substrates (Pilkington) by using the doctor blade method. After drying in air, the electrodes were heated in air at 450 ºC for 1 h. The electrode film thickness was measured by using an AlphaStep D-100 Stylus Profilometer from KLA Tencor. The modification of TiO_2 with (Bu_4N)[**22**·Br] or compound **23** was performed by immersing the electrodes in the corresponding acetone solution in the dark. Figure 7.23 shows the aspect of the TiO_2 electrodes after several experimental conditions.

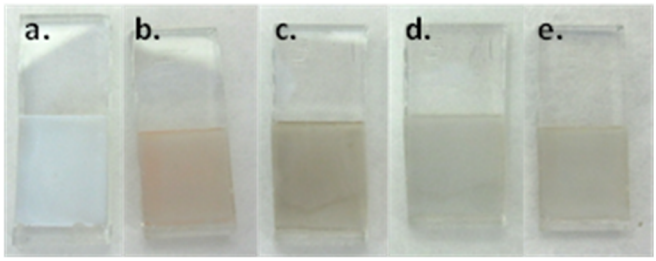

Figure 7.23. Photographs showing the aspect of the TiO_2 electrodes: a) naked; b) after immersion for 1 hour in a 72 μM (Bu_4N)[**22**·Br] acetone solution; c) after immersion of the modified electrode in a N_2-purged 0.1 M Na_2S + 0.02 M Na_2SO_3 aqueous solution; d) after CV experiments in N_2-purged 0.1 M Na_2S + 0.02 M Na_2SO_3; e) after CV experiments in N_2-purged 0.1 M $HClO_4$.

The electrochemical measurements were performed by using an Autolab PGSTAT 30 potentiostat in a three-electrode cell, using a Pt wire as a counter electrode and an Ag/AgCl/KCl electrode as a reference electrode. The electrolyte was either 0.1 M $HClO_4$ or 0.1 M Na_2S + 0.02 M Na_2SO_3 purged with N_2. The illumination for the photoelectrochemical experiments was provided by a 300 W Xe arc lamp (ThermoOriel) coupled with a monochromator (Oriel, model 74100). The light intensity was measured by using an optical power meter (Oriel, model 70310) equipped with a photodetector (ThermoOriel, model 71608).

The photocatalytic hydrogen evolution experiments of (Bu_4N)[**22**·Br]/TiO_2 were carried out by Dr. E.A. Kozlova at Boreskov Institute of Catalysis (Novosibirsk, Russia). The sample was illuminated with a Hg lamp equipped with a visible light filter, and the hydrogen emission was measured by Gas Chromatography. Further details are published in the journal ChemSusChem.[25]

7.3.4. THEORETICAL CALCULATIONS

The electronic structures of complexes **3**, $(Et_4N)_2$[**4**] and $(Et_4N)_2$[**5**] were calculated by M. R. Rhzhikov at the Nikolaev Institute of Inorganic Chemistry (Novosibirsk, Russia). The DFT calculations were performed with the ADF2012 program suite.[26] Geometry optimizations and frequency calculations were done with standard STO's, all electron TZP basis set.[27] VWN and Becke+Perdew functional were used for LDA and GGA parts, respectively. The geometries for excitation energy calculations were taken from the previous steps. QZ4P basis set and the statistical average of orbital potentials (SAOP) model were used for Time-Dependent Density Functional Theory (TDDFT) calculations of excitation energies.[28,29] All calculations were performed with Zero Order Regular Approximation (ZORA) in order to take into account scalar relativistic effects.[30]

7.4. REFERENCES

(1) Coucouvanis, D.; Toupadakis, A.; Hadjikyriacou, A. *Inorg. Chem.* **1988**, *27*, 3272–3273.

(2) Müller, A.; Krickemeyer, E.; Hadjikyriacou, A.; Coucouvanis, D. In *Inorganic Syntheses*; Ginsberg, A. P., Ed.; John Wiley & Sons, Inc., 1990; Vol. 27, pp. 47–51.

(3) Fedin, V. P.; Sokolov, M. N.; Mironov, Y. V.; Kolesov, B. A.; Tkachev, S. V.; Fedorov, V. Y. *Inorganica Chim. Acta* **1990**, *167*, 39–45.

(4) Kumasaki, M.; Tanaka, H.; Kobayashi, A. *J. Mater. Chem.* **1998**, *8*, 301–307.

(5) Hansen, T. K.; Becher, J.; Jørgensen, T.; Varma, K. S.; Rajesh; Khedekar, M. P. C.; Hynes, J.; Smith, A. B. *Org. Synth.* **1996**, *73*, 270.

(6) Liu, W.; Wang, R.; Zhou, X. H.; Zuo, J. L.; You, X. Z. *Organometallics* **2008**, *27*, 126–134.

(7) Ribas, X.; Dias, J. C.; Morgado, J.; Wurst, K.; Molins, E.; Ruiz, E.; Almeida, M.; Veciana, J.; Rovira, C. *Chem. - A Eur. J.* **2004**, *10*, 1691–1704.

(8) Kobayashi, Y.; Jacobs, B.; Allendorf, M. D.; Long, J. R. *Chem. Mater.* **2010**, *22*, 4120–4122.

(9) Schwalbe, M.; Schäfer, B.; Görls, H.; Rau, S.; Tschierlei, S.; Schmitt, M.; Popp, J.; Vaughan, G.; Henry, W.; Vos, J. G. *Eur. J. Inorg. Chem.* **2008**, *2008*, 3310–3319.

(10) Wiederholt, K.; Mclaughlin, L. W. *Nucleic Acids Res.* **1999**, *27*, 2487–2493.

(11) Yanagida, M.; Singh, L. P.; Sayama, K.; Hara, K.; Katoh, R.; Islam, A.; Sugihara, H.; Arakawa, H.; Nazeeruddin, M. K.; Grätzel, M. *J. Chem. Soc. Dalt. Trans.* **2000**, 2817–2822.

(12) Paw, W.; Eisenberg, R.; York, N. *Inorg. Chem.* **1997**, *1669*, 2287–2293.

(13) Myśliwiec, D.; Donnio, B.; Chmielewski, P. J.; Heinrich, B.; Stępień, M. *J. Am. Chem. Soc.* **2012**, *134*, 4822–4833.

(14) Parg, R. P.; Kilburn, J. D.; Petty, M. C.; Pearson, C.; Ryan, T. G. *Synthesis.* **1994**, *1994*, 613–618.

(15) Agilent. *CrysAllis version 171.35.11*.

(16) Blessing, R. H. *Acta Crystallogr. Sect. A Found. Crystallogr.* **1995**, *51*, 33–38.

(17) Palatinus, L.; Chapuis, G. *J. Appl. Crystallogr.* **2007**, *40*, 786–790.

(18) Sheldrick, G. M. *Acta Crystallogr. Sect. A Found. Crystallogr.* **2008**, *64*, 112–122.

(19) Dolomanov, O. V; Bourhis, L. J.; Gildea, R. J.; Howard, J. A. K.; Puschmann, H. *J. Appl. Crystallogr.* **2009**, *42*, 339–341.

(20) Farrugia, L. J. *J. Appl. Crystallogr.* **1997**, *30*, 565.

(21) Rees, B.; Jenner, L.; Yusupov, M. *Acta Crystallogr. Sect. D Biol. Crystallogr.* **2005**, *61*, 1299–1301.

(22) Suzuki, K.; Kobayashi, A.; Kaneko, S.; Takehira, K.; Yoshihara, T.; Ishida, H.; Shiina, Y.; Oishic, S.; Tobita, S. *Phys. Chem. Chem. Phys.* **2009**, *11*, 9850–9860.

(23) Ishida, H.; Tobita, S.; Hasegawa, Y.; Katoh, R.; Nozaki, K. *Coord. Chem. Rev.* **2010**, *254*, 2449–2458.

(24) Brouwer, A. M. *Pure Appl. Chem.* **2011**, *83*, 2213–2228.

(25) Recatalá, D.; Llusar, R.; Gushchin, A. L.; Kozlova, E. A.; Laricheva, Y. A.; Abramov, P. A.; Sokolov, M. N.; Gómez, R.; Lana-villarreal, T. *ChemSusChem* **2015**, *8*, 148–157.

(26) SCM, Theoretical Chemistry, Vrije Universiteit, Amsterdam, T. N. ADF2012. *http://www.scm.com*.

(27) Van Lenthe, E.; Baerends, E. J. *J. Comput. Chem.* **2003**, *24*, 1142–1156.

(28) Van Gisbergen, S. J. A.; Snijders, J. G.; Baerends, E. J. *Comput. Phys. Commun.* **1999**, *118*, 119–138.

(29) Gritsenko, O. V.; Schipper, P. R. T.; Baerends, E. J. *Chem. Phys. Lett.* **1999**, *302*, 199–207.

(30) Vanlenthe, E.; Baerends, E. J.; Snijders, J. G. *J. Chem. Phys.* **1993**, *99*, 4597–4610.

8

CONCLUDING REMARKS

"[…] We live in an ordered universe that can be understood by the application of rational reasoning."

Richard P. Feynman, *The Character of Physical Law*

The following conclusions can be drawn from the results presented in this PhD thesis:

1) A family of $M_2Q_2(\mu\text{-}S)_2$-based clusters, where M = Mo or W, and Q = O, or S, functionalized with dithiolene ligands bearing nitrogen donor atoms have been prepared by diverse synthetic methods. These cluster complexes can be employed as building blocks for the preparation of heterometallic compounds, in which the additional metal fragments are connected through the outer nitrogen atoms of the dithiolene ligands.
2) The reaction of molybdenum and tungsten cluster anions of formulae $[M_2S_2(\mu\text{-}S)_2(pdt)_2]^{2-}$ (pdt = 2,3-pyrazinedithiolate) with metal carbonyls affords the substitution of the terminal sulfur atoms in the cluster unit by oxygen, resulting in the formation of M=O bonds.
3) Triangular heteroleptic $Mo_3S_7X_4$(diimine) clusters (X = Cl, or Br) bearing a diversity of bipyridine- or phenanthroline- derivatives can be conveniently prepared under mild reaction conditions by partial ligand substitutions in the $[Mo_3S_7X_6]^{2-}$ cluster precursors. The use of a large excess of diimine ligand equally leads to the same monosubstituted neutral products.
4) Heteroleptic $Mo_3S_7X_4$(diimine) clusters (X = Cl, or Br) exhibit an anomalous solubility behavior. These complexes are soluble in the reaction mixture. However, after purification they become extremely insoluble in common organic solvents, and their redissolution in CH_2Cl_2 requires sonication in the presence of tetrabutylammonium halide salts, due to the formation of $[Mo_3S_7X_4(diimine)\cdot X]^-$ aggregates.
5) In $Mo_3S_7X_4$(diimine) clusters (X = Cl, or Br), the two nitrogen atoms of the diimine ligand are coordinated to one of the molybdenum atoms in a chelating mode, and the plane defined by the ligand is oriented almost perpendicular to the trimetallic plane. The structure of $[Mo_3S_7X_4(diimine)\cdot X]^-$ cluster aggregates present non-bonding interactions

between the halide anions and the axial sulfur atoms in these cluster units. These anionic adducts are readily soluble in common organic solvents. Additional interactions between equatorial sulfur atoms and halide ligands connect adjacent aggregates, resulting in the formation of $\{[Mo_3S_7X_4(diimine)\cdot X]_2\}^{2-}$ dimers.

6) The reaction between $Mo_3S_7X_4(diimine)$ clusters (X = Cl, or Br) and sulfur donor ligands, such as 1,3-dithiole-2-thione-4,5-dithiolate (dmit) or diethyldithiocarbamate (dtc) affords the substitution of the halides by the sulfur atoms of the bidentate ligand, resulting in complexes of formulae $[Mo_3S_7(diimine)L_2]^{0,\,2+}$, where L = dmit or dtc. The dmit derivatives exhibit poor solubility in common organic solvents, which limits the number of techniques available for their characterization.

7) The dinuclear cluster complex $(Et_4N)_2[Mo_2O_2(\mu\text{-}S)_2(BPyDTS_2)_2]$ exhibits emission in acetonitrile solution at 628 nm, with a quantum yield of *ca.* 0.10. This emission band has been ascribed by TDDFT calculations to an ILCT from the dithiolene (π) to the pyridyl (π^*) orbitals. Insertion of two terminal $Re(CO)_3Cl$ fragments in the aforementioned cluster decreases the quantum yield by a factor of around 4.6, presumably due to fast charge separation in the excited state.

8) Two heteroleptic Mo_3S_7 complexes bearing the IPDOP imidazophenanthroline ligand, namely $Mo_3S_7X_4(IPDOP)$, (X = Cl, or Br), exhibit luminescence in the 375 nm – 600 nm region in both dichloromethane and dimethylformamide. The maximum quantum yield and emission lifetime have been registered for the bromide derivative in DMF, with values of 0.15 and 7.5 ns, respectively. Addition of proton-abstractor anions (F^-, OH^- and AcO^-) to sample solutions of these complexes leads to a striking shift in their emission spectra of around 92 nm towards longer emission wavelengths.

9) Correlations between molecular structures and nonlinear optical functions have been obtained by comparing the optical power limiting of a series of mixed-ligand diimine-halide and diimine-dithiolene Mo_3S_7 cluster complexes to that of a dithiolene dinuclear cluster possessing the $Mo_2O_2S_2$ core. All trinuclear clusters are efficient optical limiters, and the optical limiting merit increases on increasing the metal nuclearity, and upon extending the π-conjugated system with dithiolene ligands.
10) Functionalization of Mo_3S_7 clusters with diimine ligands facilitate their adsorption over TiO_2 nanoparticles supported on FTO. These complexes can be electrochemically reduced to generate molybdenum(IV) sulfide species. The as-generated species exhibit significantly superior electrocatalytic activity in the hydrogen evolution reaction to bare TiO_2, with a decrease in the hydrogen reduction overpotential by 0.3 – 0.4 V, depending on the media (0.1 M Na_2S/0.02 M Na_2SO_3 mixtures, or 0.1 M $HClO_4$, respectively). In agreement with the electrochemical results, the modified TiO_2 nanoparticles show photocatalytic activity (TOF = 8×10^{-5} s^{-1}) for hydrogen generation in the presence of Na_2S/Na_2SO_3 as a sacrificial electron donor system.

(CATALAN VERSION)

A partir dels resultats presentats en aquesta Tesi Doctoral, es poden obtindre les següents conclusions:

1) Una família de clústers del tipus $M_2Q_2(\mu\text{-}S)_2$, on M = Mo, ó W, i Q = O, ó S, funcionalitzats amb lligams ditiolè que contenen àtoms de nitrogen donadors, han sigut preparats mitjançant diversos mètodes sintètics. Aquests complexos clúster poden ser utilitzats com a blocs de construcció per a la preparació de compostos heterometàl·lics, en els quals els fragments metàl·lics addicionals es connecten a través dels àtoms de nitrogen externs dels lligams ditiolè.
2) La reacció entre els anions clúster de molibdè i tungstè de fórmula $[M_2S_2(\mu\text{-}S)_2(pdt)_2]$ (pdt = 2,3-pirazinaditiol) i carbonils metàl·lics resulta en la substitució dels àtoms de sofre terminals de la unitat clúster per oxigen, amb la conseqüent formació d'enllaços M=O.
3) Els clústers heterolèptics triangulars de fórmula general $Mo_3S_7X_4$(diimina), (X = Cl, ó Br), funcionalitzats amb un gran nombre de derivats de la bipiridina o de la fenantrolina, poden ser convenientment preparats sota condicions suaus de reacció, mitjançant la substitució parcial de lligams en el precursor $[Mo_3S_7X_6]^{2-}$. L'ús d'un gran excés de lligam diimina condueix igualment als mateixos productes neutres monosubstituïts.
4) Els clústers del tipus $Mo_3S_7X_4$(diimina), (X = Cl, ó Br) presenten un anòmal comportament de solubilitat. Aquests complexos són solubles en el medi de reacció. No obstant, després de la purificació es tornen completament insolubles en dissolvents orgànics comuns, i la seua redissolució en CH_2Cl_2 requereix sonicació en presència d'halurs de tetrabutilammoni, ja que així es formen agregats del tipus $[Mo_3S_7X_4(\text{diimina})\cdot X]^-$.
5) En clústers del tipus $Mo_3S_7X_4$(diimina), (X = Cl, ó Br), els dos àtoms de nitrogen es coordinen al mateix àtom de molibdè, i el plànol definit pel lligam

és quasi perpendicular al pla trimetàl·lic. L'estructura dels agregats clúster del tipus $[Mo_3S_7X_4(diimina)\cdot X]^-$ presenta interaccions no enllaçants entre els anions halur i els àtoms de sofre axials de la unitat clúster. Aquests adductes aniònics són solubles en dissolvents orgànics comuns. Interaccions addicionals entre els àtoms de sofre equatorials i els lligams halur connecten agregats contigus, resultant en la formació de dímers de fórmula $\{[Mo_3S_7X_4(diimine)\cdot X]_2\}^{2-}$.

6) La reacció entre els clústers $Mo_3S_7X_4(diimina)$, (X = Cl, ó Br) i lligams amb àtoms de sofre donadors, tals com 1,3-ditiol-2-tiona-4,5-ditiolat (dmit) o dietilditiocarbamat (dtc), resulta en la substitució dels halurs pels àtoms de sofre del lligam bidentat, amb la conseqüent formació de complexos de fórmula $[Mo_3S_7(diimina)L_2]^{0,2+}$, en què L = dmit ó dtc. Els derivats de dmit presenten baixa solubilitat en dissolvents orgànics comuns, la qual cosa limita el nombre de tècniques disponibles per a la seua caracterització.
7) El clúster dinuclear de fórmula $(Et_4N)_2[Mo_2O_2(\mu\text{-}S)_2(BPyDTS_2)_2]$ presenta emissió en acetonitril a 628 nm, amb un rendiment quàntic de *ca.* 0.10. Aquesta banda d'emissió ha sigut identificada mitjançant càlculs TDDFT amb una ILCT des dels orbitals del ditiolè (π) fins als dels grups piridil (π^*). La inserció de dos fragments terminals, $Re(CO)_3Cl$, en el clúster esmentat anteriorment disminueix el rendiment quàntic un factor d'aproximadament 4.6, probablement degut a una ràpida separació de càrrega en l'estat excitat.
8) Dos complexes heterolèptics del tipus Mo_3S_7 que contenen el lligam imidazofenantrolina IPDOP, és a dir $Mo_3S_7X_4(IPDOP)$, amb X = Cl, ó Br, presenten luminiscència en la regió compresa entre 375 i 600 nm, tant en diclorometà com en dimetilformamida. El màxim rendiment quàntic i el màxim temps de vida d'emissió han sigut registrats per al derivat bromat en DMF, que presenta uns valors de 0.15 i 7.5 ns, respectivament. L'addició d'anions abstractors de protons (F^-, OH^- i AcO^-) a dissolucions d'aquests

complexos condueix a un desplaçament de l'espectre d'emissió de vora 92 nm cap a longituds d'ona més llargues.

9) La comparació entre el poder òptic limitant d'una sèrie de clústers Mo_3S_7 funcionalitzats amb lligams mixtes (diimina-halur o diimina-ditiolè) i el d'un clúster dinuclear basat en el nucli $Mo_2O_2S_2$ i lligams ditiolè, ha permès obtindré correlacions entre estructures moleculars i funcions d'òptica no lineal. Tota la sèrie de clústers trinuclears són limitadors òptics eficients, i el mèrit de limitació òptica augmenta en augmentar la nuclearitzat, i en estendre el sistema π conjugat mitjançant lligams ditiolè.

10) La funcionalització de clústers Mo_3S_7 amb lligams diimina facilita la seua adsorpció sobre nanopartícules de TiO_2 suportades sobre FTO. Aquests complexos poden ser reduïts electroquímicament per generar sulfurs de molibdè(IV). Les espècies generades d'aquesta manera presenten activitat electrocatalítica superior a la del TiO_2 sense modificar, amb un sobrepotencial de reducció d'hidrogen de 0.3 – 0.4 V en funció del medi (Na_2S 0.1M/Na_2SO_3 0.02M, ó $HClO_4$ 0.1 M). En concordança amb els resultats electroquímics, les nanopartícules de TiO_2 modificades mostren activitat fotocatalítica (TOF = 8×10^{-5} s^{-1}) per a la generació d'hidrogen en presència del sistema Na_2S/Na_2SO_3 com a agent de sacrifici.

9

PUBLICATIONS

"La patience, c'est comme le chocolat…
On n'en a jamais assez!"

Christelle Heurtault

The results presented in this PhD Thesis are included in the following papers:

1) "First Heteroleptic Mo_3S_7 Clusters Containing Non-Innocent Phenanthroline Ligands." Artem Gushchin, Rosa Llusar, David Recatalá and Pavel Abramov, *Russian Journal of Coordination Chemistry*, **2012**, 38, 173 – 177

2) "Dithiolene Dimetallic Molybdenum(V) Complexes Displaying Intraligand Charge Transfer (ILCT) Emission." David Recatalá, Artem L. Gushchin, Rosa Llusar, Francisco Galindo, Konstantin A. Brylev, Maxim R. Ryzhikov and Noboru Kitamura, *Dalton Transactions*, **2013**, 42, 12947 – 12955

3) "Photogeneration of Hydrogen from Water by Hybrid Molybdenum Sulfide Clusters Immobilized on Titania." David Recatalá, Rosa Llusar, Artem L. Gushchin, Ekaterina A. Kozlova, Yuliya A. Laricheva, Pavel A. Abramov, Maxim N. Sokolov, Roberto Gómez and Teresa Lana-Villarreal, *ChemSusChem*, **2015**, 8, 148 – 157

4) "Heteroleptic Phenanthroline Complexes of Trinuclear Molybdenum Clusters with Luminescent Properties." David Recatalá, Rosa Llusar, Francisco Galindo, Konstantin A. Brylev and Artem L. Gushchin, *European Journal of Inorganic Chemistry*, **2015** (Article in press)

5) "Synthesis and Third-Order Nonlinear Optical Properties of Heteroleptic Mo_3S_7 Clusters." David Recatalá, Rosa Llusar, Adam Barlow, Genmiao Wang, Marek Samoc, Mark G. Humphrey and Artem L. Gushchin, (Submitted to *Dalton Transactions*)

Luminescence

Hydrogen Photogeneration

Nonlinear Optics

Metal Clusters

Molybdenum

Coordination Chemistry